Investigations of Ride Comfort and Control Evaluation of Heavy Commercial Road Vehicle

THESIS

**Submitted in Delhi Technological University
for the Award of the Degree of**

DOCTOR OF PHILOSOPHY

in

ENGINEERING

By

ASHISH GUPTA
(2K14/PH.D/ME/06)

**DEPARTMENT OF MECHANICAL, PRODUCTION &
INDUSTRIAL, AND AUTOMOBILE ENGINEERING
DELHI TECHNOLOGICAL UNIVERSITY
DELHI - 110042 (INDIA)**

MAY 2018

Investigations of Ride Comfort and Control Evaluation of Heavy Commercial Road Vehicle

THESIS

Submitted in Delhi Technological University
for the award of the degree of

DOCTOR OF PHILOSOPHY
in
ENGINEERING

By

ASHISH GUPTA
(2K14/PH.D/ME/06)

Under the Supervision of

Prof. VIKAS RASTOGI
Department of Mechanical, Production & Industrial
and Automobile Engineering

DELHI TECHNOLOGICAL UNIVERSITY
DELHI - 110042 (INDIA)

MAY 2018

Dedicated to

My Late Grand Parents

and

My Beloved Parents

DELHI TECHNOLOGICAL UNIVERSITY
Shahabad Daulatpur, Main Bawana Road
Delhi-110042 (India)

DECLARATION

I hereby declare that the thesis entitled **"Investigations of Ride Comfort and Control Evaluation of Heavy Commercial Road Vehicle"** submitted by me, for the award of the degree of *Doctor of Philosophy* to **Delhi Technological University (Formerly DCE)** is a record of *bona fide* work carried out by me under the guidance of Prof. Vikas Rastogi.

I further declare that the work reported in this thesis has not been submitted and will not be submitted, either in part or in full, for the award of any other degree or diploma in this Institute or any other Institute or University.

Ashish Gupta
Reg No: 2K14/Ph.D/ME/06
Department of Mechanical, Industrial,
Production and Automobile Engineering

Place: New Delhi
Date:

CERTIFICATE

This is to certify that the thesis entitled **"Investigations of Ride Comfort and Control Evaluation of Heavy Commercial Road Vehicle"** submitted by **Mr. Ashish Gupta** to **Delhi Technological University (Formerly DCE)**, for the award of the degree of "*Doctor of Philosophy*" in Mechanical engineering is a record of *bona fide* work carried out by him. Ashish Gupta has worked under my guidance and supervision and has fulfilled the requirements for the submission of this thesis, which to our knowledge has reached requisite standards.

The results contained in this thesis are original and have not been submitted to any other university or institute for an award of any degree or diploma.

Prof. Vikas Rastogi
Professor
Department of Mechanical, Industrial,
Production and Automobile Engineering
Delhi Technological University (DTU)
Bawana, Delhi-110042

ACKNOWLEDGEMENTS

Pawan, Tameshwar, Aditya, Deepak, Vineet, Nahid, Saurabh, Neeraj, Ambrish, Lakhan and Ajay who have always been my guiding light when I didn't believe in myself.

I am greatly indebted to my parents for their love and blessings to see me scaling greater heights of life. One who matters most in my Ph.D work is my younger brother Mr. Abhishsek Gupta without whose motivation and encouragement, pursuit of this Ph.D work would have never been possible.

Above all, I would thanks Almighty for blessing such an affectionate & efficient people playing great asset for me.

(Ashish Gupta)

ABSTRACT

For developing country like India, where the demand of industry is consistently increasing from year to year, which also raises the requirement of the heavy commercial vehicle on roads for dispatching the product from one place to another. In the present scenario of India, freight road transport is the majorly used after railway freight transport. Heavy vehicle transportation is a massive enterprise with substantial direct influence on the economic growth of our country, which shares around 4.2% GDP of our nation. This rapid growth of road transportation increases traffic, and also extends the risk of accidents on roads. As per the report of the ministry of road transport, the heavy vehicle has the most impact on these accidents after two-wheelers. However, the main reason for accidents on roads is the fault of the driver. There are many reports or surveys published in a national or international level shows that whole body vibration is the reason for work-related accidents and causes many work-related diseases.

A heavy vehicle like truck and buses having a large structure to carry their load, ride in all kind of terrains, for thousands of miles without failing structure. Structure (chassis or frame) of the truck must be able to sustain all kind of vibration (i.e., longitudinal, transverse and flexural). Flexural vibration was overlooked for road vehicle in literature whereas it was considered only for rail vehicles. This thesis starts with development of an analytical model with consideration of Rayleigh beam approach, where the rotary inertia of the beam is also considerd. However, very limited studies have reported for modelling a vehicle flexure vibration. This work also examines an structural damping of the chassis, which has been neglected in the past studies specifically for flexural vibration. Further, bond graph model of the flexible

structure of heavy road vehicle is being developed, whereas this model will be derived through modal expansion approach. A computational model of the structure consists non-linear suspension model. The dynamic response of the structure is being analyzed under various random road conditions at different vehicle speed. These random models of the road are also developed according to ISO 8608 standard, whereas four (H1-H4) kind of road category are adopted. Results are being shown the dynamic response of chassis structure under the real road responses so that parameters of the various parts of the structure has been evaluated, which further raised the ride comfort and road holding capability of the structure. Further, this work also investigates the effect of structural damping or internal damping on the dynamics of the system. This formulation is extended to build an extended formulation for flexural vibration of truck chassis through a novel approach of extended Lagrangian mechanics, where the system is asymmetric due to varying nonpotential fields of the chassis. The amplitude and the natural frequency of the vehicle frame are obtained analytically through the proposed methodology.

The next focus of this work is to obtain accelerations at the driver-vehicle interface and then, to process these acceleration signals in order to calculate the human comfort. Vibration due to road irregularities constitutes another significant aspect of the physical environment after flexural vibration that can cause discomfort to the driver. Numerous approaches have been suggested and developed to access this vibration level. Thus, the comfort index calculated is independent of the seat characteristics and human parameters. Bio-dynamics of human subjects has been a topic of interest over the years, and number of mathematical models have been established. However, there are only limited studies incorporating bio-dynamic models in heavy vehicle applications. So, the

present work is an attempt to evaluate the ride comfort level and to calculate root mean square acceleration of different body parts as per ISO 2631 guidelines through bondgraph modeling technique. The frame flexibility is also incorporated in the model using modal expansion of a free-free beam. Physiological effects of the vibration on the human body are also analyzed using the criteria specified in International Organization for Standardization (ISO) 2631.

The next significant vehicle component is the suspension system, which is generally considered as the linkage between the vehicle body and wheels. The design of a better-quality suspension system remains an essential development objective for the automotive industry. An ideal vehicle suspension should have the capability to reduce the displacement and acceleration of the vehicle body, and thus; maximizing the ride comfort. The quarter car model (two degrees of freedom) of heavy vehicle is constructed, which is being created through bondgraphs and well incorporated in semi-active suspension, controlled by skyhook, ground hook and balance logic control algorithms. The 2-DOF model is subjected to road profiles like single half sine bump and random road input. This work also demonstrates various hybrid control strategies for semi-active suspension system. A new hybrid controller is proposed in this work, which consists of three "on-off" control strategies (i.e., skyhook, ground hook and balance logic). Its performance is evaluated in terms of acceleration transmissibility, and also compared with those of other proposed hybrid dampers with a new hybrid controller. The results show that the semi-active system with the proposed hybrid controller provides a better isolation at higher frequencies than previously reported hybrid controllers. Furthermore, two new proposals of hybrid robust control strategies are also studied, where PID controller is implemented along $H\infty$ controller

configuration. In this configuration, first one includes single H∞ along with PID configuration, whereas the second configuration incorporates two H∞ controller along with PID arrangement. The comparative study of all these proposed controllers are being presented and the best-suited configuration for heavy vehicle system over random road condition is evaluated.

The another highlight of this thesis is development of the experimental test rig of quarter car for heavy vehicle system, which is being designed and fabricated. This test rig is able to measure the performance of the heavy vehicle system in a dynamic system. The main objective to develop this test rig is to tune the suspension setting of the heavy vehicle system. The test rig also consists of MR damper, which is mounted parallel to the leaf spring arrangement. Further, the computational model of the test rig is also developed and simulation results are validated with experimental responses. The another task is to optimize the parameters for a quarter car model alongwith MR damper in a real heavy vehicle configuration. Response surface methodology (RSM) technique is profitably used in order to improve the ride comfort level of the driver.

TABLE OF CONTENTS

LIST OF FIGURES

xvii

LIST OF TABLES

LIST OF ABBREVIATIONS

AAP	Average Absorbed Power
ANN	Artificial Area Network
ADAMS	Automated Dynamic Analysis of Mechanical System
ANSYS	Analysis System
ANOVA	Analysis of Variance
BS	British Standard
BioD	Bio-dynamic model
CAD	Compute Aided Design
CAN	Conntroller Area Network
CAE	Computer Aided Engineering
CCD	Central Composite Design
DOF	Degrees of Freedom
DOE	Design of Experiment
DPMI	Driving Point Mechanical Impedance
DQ	Differential Quadrature
DC	Direct Current
FEM	Finite Element Method
FFT	Fast Fourier Transformation
FRFs	Frequency Response Function
HY-SH-GH	Hybrid Skyhook Grounddhook
HY-SH-B	Hybrid Skyhook Balance
HY-GH-B	Hybrid Groundhook Balance
HY-SH-GH-B	Hybrid Skyhook Groundhook Balance
HMMWV	High Mobility Multipurpose Wheeled Vehicle
HP	Horse Power
ICP	Integrated Circuit-Piezoelectric
ISO	International Standard Organization
LTI	Linear Time-Invariant
LFT	Linear Fraction Transformation
MIT	Massachusetts Institute of Technology
PCB	Printed Circuit Board
PLC	Programmable Logic Controller

RMS	Root Mean Square
RPM	Rotation Per Minute
RSM	Response Surface Method
RC	Ride Comfort
STHT	Seat to Head Transmissibility
TTL	Transistor-transistor Logic
MBM	Multi Body Modeling
MR	Magneto-Rheological
HBM	Human Body Model
FFT	Fast Fourier Transform
VDANL	Vehicles Dynamics Analysis Non Linear
VPG	Vertical Providing Ground
ISO	International Standard Organisation
PSD	Power Spectral Denisity
PID	Proportional Integrated Derivative
GDP	Gross Domestic Product
WBV	Whole Body Vibration

NOMENCLATURES

a_n	maximum accelration value
A_{irms}	RMS acceleration value
A	area of cross-section
A_n	slowly varying function of time
a_{wi}	frequency weighted acceleration
C_s^f	damping coefficient of front damper
C_s^r	damping coefficient of rear damper
$C_{skyhook}$	skyhook damping coefficient
C_{on}	on-state damping
C_{max}, C_{min}	maximum and minimum damping coefficient
C_{gnd}	damping coefficient of groundhook damper
μ_I	internal or structural damping
d	desirability index
EI	flexural rigidity
$F_{balance}$	damping force of the balance logic damper
$F_{skyhook}$	skyhook damping force of the skyhook damper
$F_{groundhook}$	damping force of the groundhook damper
G_d	PSD of vertical displacement
G	system
$h(x)$	simple harmonic function of road profile
h	height of bump
I_d	roatrary inertia
I	current
J	pitch inertia
K_I	coefficient for integral term
K_s	suspension stiffness

K_t	tire stiffness
K_i	weighted coefficient
L	Beam length
L_b	length of bump
M	center of mass
M_s	sprung mass
M_{us}	unsprung mass
n	spatial frequency
Δn	frequency band
N_{exp}	total number of experiments
n_{cp}	no of replicates
P	tire pressure
$\hat{T}(.)$	kinetic energy density
u	control force
U	Amplitude of vibration
$\hat{V}(.)$	potential energy density
V	velocity input
$W(x)$	eigen-function
w	transverse displacement
W_k	weighted acceleration
W_d	weighted acceleration for horizontal acceleration (Lognitudinal and lateral)
W_b	weighing factor for vertical acceleration
$x_1, \dot{x}_1, \ddot{x}_1$	vertical displacement, velocity, acceleration of sprung mass
$x_2, \dot{x}_2, \ddot{x}_2$	vertical displacement, velocity, acceleration of unsprung mass
Y	measured controller
y	second order model
y_{max}, y_{min}	upper and lower limit of response
z	reference vector

Greek Symbols

ρ	mass denisity
α	significance level
β	second order regression coefficient
ε	error coefficient
τ	period of vibration
ω	eigenfrequency
η	umbra time
ω_n	natural frequency
δ	dirac delta function
a_i	RMS acceleration
Ω	Angular spatial frequency
Ω_0	Initial angular spatial frequency
θ	Pitch velocity

Bondgraph Elements

0	Common effort junction
1	Common flow junction
I	I-element or Inertial element
C	C-element or compliant element
R	R-element or dissipative element
SE	Source of effort
SF	Source of flow
TF	Transformer
GY	Gyrator
e_i	Generalized effort in i$^{\text{th}}$ bond
f_i	Generalized flow in i$^{\text{th}}$ bond

1.1 Background and motivation

India has a road networks of 54 lakh kilometres, which is one of the most extensive road networks in the world, consisting of national highways, expressways, state highways. About, 65% of the freight and 86.7% passenger traffic is carried by roads. In 2012, the loss to Indian economy due to road traffic accidents was estimated as 3% of GDP. The accident on roads due to high traffic are increasing day-by-day, which is evident from Table 1.1.

Table 1.1: Detail of road accident deaths 2002-2011*(As per data.gov.in* 2011*)*

Year	No. of road accident
2002	407497
2003	406,726
2004	429,910
2005	439,255
2006	460,920
2007	479,216
2008	484,704
2009	486384
2010	499,628
2011	500,686

According to the Road Accident Report (2014) published by the Ministry of Road Transport and Highways, that around 4,726 people have lost their lives in accidents due to humps, 6,672 were killed in crashes caused due to potholes and speed breakers (*Road Accidents in India,* 2012*; The Times of India Report,* 2015).
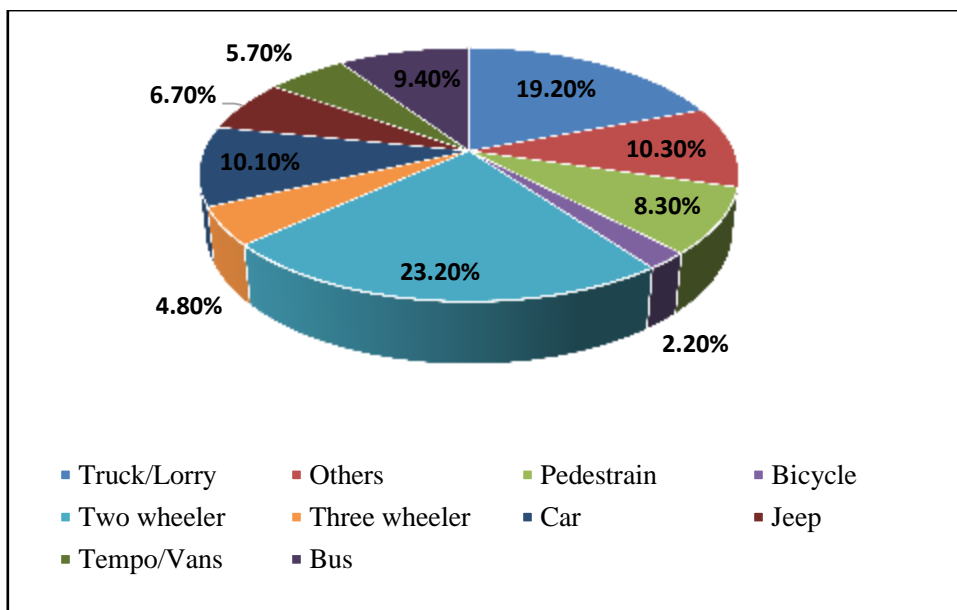
Figure 1.1: Road accident deaths by various modes of transport during 2012
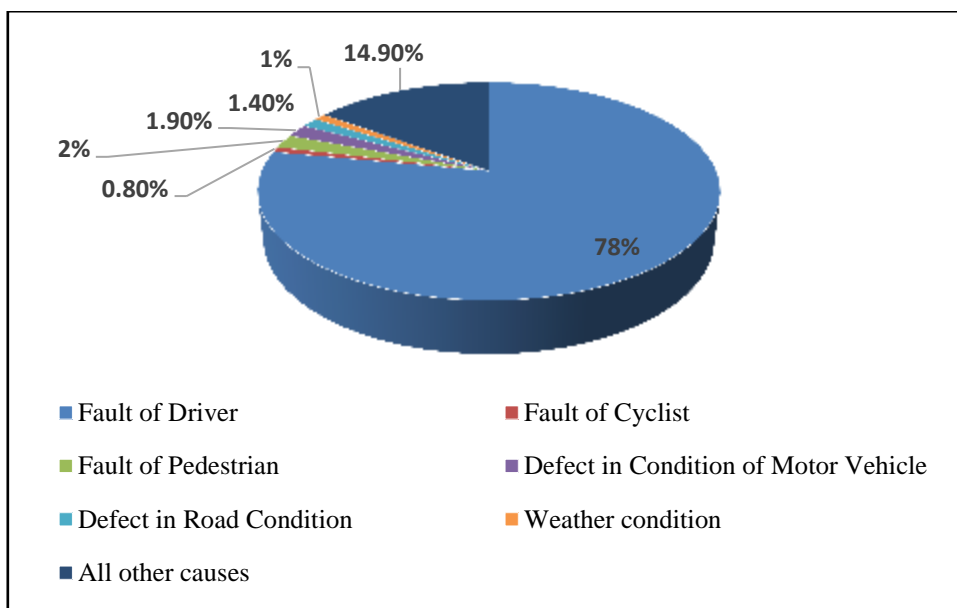
Figure 1.2: Causes of road accidents (Government of India, Ministry of Road Transport and Highways Ttransport Research Wing, New Delhi)

The nature of the surface of roads (Potholes) accounted for 9,699 road accidents and 2,607 road accident fatalities in 2013. The majorly affected vehicle due to these road accidents is heavy road truck after two-wheelers around 19.2 %, which can be seen in Figure 1.1.

As shown in Figure 1.2, the fault of driver accounted for 78% of road accidents in India in the year 2013. Road roughness is a primary source of vibration in vehicles and a well-known cause of wear and damage to sensitive payloads to the vehicle itself, as well as to bridges and pavements. The nature of the surface of roads (Potholes) accounted for 9,699 road accidents and 2,607 road accident fatalities in 2013. As a share, the total road accidents and fatalities, due to potholes constituted 2.0 percent and 1.9 percent respectively (*Road Accidents in India,* 2013). Vehicle vibration, in turn, brings whole-body vibration (WBV) exposure to drivers and passengers. WBV is a cause of work-related accidents and work-related diseases like spinal compression stress, heart disease and musculoskeletal problems (*ROADEX-III report, under National Periphery Program, European Union; Granlund,* 2012). The comfort of the driver is therefore of utmost importance as WBV caused by the unevenness of the road may lead to fatigue of the driver, in turn, degrading driver's performance and concentration.

Thus the motivation for this research work came from aforementioned data or figures and the recent trends of increasing truck traffic on major highways and urban areas influencing the truck dominance in freight movement. Concern for truck vibration problems has increased in recent years as trucks have evolved to fill today's more demanding trucking industry needs. Several current design trends have resulted in trucks that are more susceptible to vibration problems, which increased driver comfort and reduced cargo damage.

Heavy vehicle design is an expensive and time-consuming process that is initiated with an extensive analysis of the vehicle system and observing any faults

related to the design to determine the desired characteristics and efficiency of the vehicle. This is followed by detail design of numerous sub-systems and components to visualize the real model of the vehicle. The main structure of vibration transmission in heavy vehicle system is being presented in Figure 1.3.
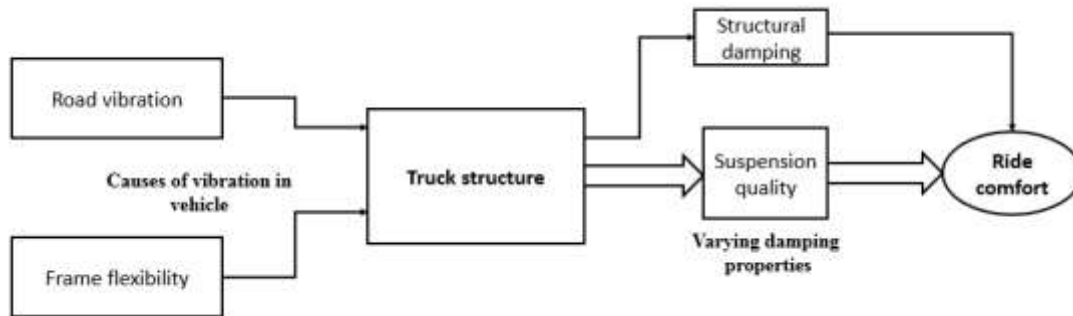
Figure 1.3: Systematic structure of vibration in heavy vehicle system

There is two essential aspects of truck design, i.e., driver comfort or ride quality. Since, drivers spend much time on the road, in their truck cabins, this environment should be as comfortable as possible. Research in the past pointed out that truck drivers are frequent victims of lower back problems (*Deprez et al.,* 2005). The origin of these health problems issues (at least partly) in the cabin vibrations resulting from the unevenness of the road profile. It can able to minimise the vibrations transmitted to the driver, induced by the road and cargo. There are two leading causes of ride vibration (presented in Figure 1.3) in heavy road transport system:

i.   Road input: stochastic road condition directly influence the vibration level of the vibration level of the truck body, which requires optimum suspension setting.

ii.   Frame flexibility: Flexibility of vehicle chassis can be raised the vibration level of the vehicle.

The road profile plays a vital role in vehicle design. In India, it has been noticed that road conditions are very diverse, no specific condition can assume to modelling a road for vehicle simulation.The vertical profile can be measured along two roads sections. The road roughness are expressed in terms of the spectral density function of the measured vertical pavement profile concerning the evenness wave number of the pavement roughness. A frequency response analysis is also applied to obtain the vertical and angular modal vehicle dynamic response with the excitation of the power spectral density (PSD) of the pavement roughness. Frame flexibility can also be influenced by heavy vehicle motion. Previous attempts to incorporate frame flexibility in simulation models consisted of modelling the frame with few rigid parts connected to each other with torsion spring or simplifying the frame by a structure that early described analytically.

Vehicle suspension performs a vital role in vehicle dynamics, contributing to improve the ride comfort and the vehicle stability. The vehicle suspension system design is an active research area, where one of the goals is to alleviate the passenger's comfort through the vibration reduction of the internal engine as well as external road disturbances. Suspension systems can be classified into three basic classes, passive suspensions, semi-active suspensions and active suspensions. There are three types of suspension, which are commonly used in the vehicle system. 1) Passive suspension system 2) Active suspension system, and 3) Semi-active suspension system. A passive suspension system is one, in which the spring stiffness and the damping coefficient are fixed. These characteristics are decided by the designer of the suspension according to the design objectives and the intended application. In an active suspension, force actuator is used instead of the passive damper or both damper and

spring. The force actuator is capable of adding and dissipating energy from the system, whereas a passive damper can only dissipate energy. The force applied by the force actuator does not become dependent on the relative velocity or displacement across the suspension. In semi-active suspension system, the conventional spring element is present, but the damper is substituted with a controllable damper. The advantage of a semi-active suspension is that it allows regular control of the damping force, hence providing a solution to the design strife between ride comfort and the road holding. Moreover, if the controllable damper of a semi-active suspension system fails, it will just convert into a passive damper, which is far safer than active suspension. Hence, the study of semi-active suspension control has gained popularity over the years. The next section will present a brief review of literature, which includes the latest state of art on heavy vehicle dynamics.

1.2 Review of literature

In the last few decades, extensive research has been carried out on various aspects of heavy vehicle dynamics. Keeping in view the scope and objective of the present research the literature study has been broadly divided into three categories, i.e. 1) Issues of frame flexibility for heavy vehicles 2) Ride comfort analysis 3) Control of semi-active suspension in heavy vehicles.

1.2.1 Issues of frame flexibility for heavy vehicle

 The dynamic analysis of trucks requires a mathematical model of the vehicle structure, which includes cab, suspension system, tires and road excitation. Although flexural vibration of chassis can often be neglected in smaller and relatively stiffer automobiles. However, the large trucks and buses can experience significant "beaming mode"

vibration. Margolis (*Margolis et al.* 1989; *Margolis,* 1990) has worked on beaming response of the frame and its modal frequency and suggested that the non-articulated trucks can be sizeable at the center of the frame midway between the steered wheel rear axles. *Michelberger et al.* (1989) have extended the scope of truck frame flexibility and found that flexibility can also disturb vehicle dynamics outputs such as driver vertical acceleration and pitch acceleration for long and heavy trucks.

Cao (2005) has advocated three modeling approaches for the frame flexibility, which were frame flexibility by using a discrete approach, modelling the frame as a regular free-free beam and calculating, estimating or measuring modal masses and stiffness's, and finally modeling the whole vehicle using the FEM approach.

Ibrahim et al. (1995) have studied the ride vibration behaviour of trucks which was mainly focus on the effect of flexible frame. This work mainly focused on ride comfort in the heavy vehicle and Gaussian random excitations. FEM modelling technique was used for modelling a vehicle, and its modal properties have been evaluated. Further, a passive suspension system is used with a half car vehicle model. The results shows comparison between the response of the rigid and flexible body models, which suggested that the frame flexibility strongly affected the driver vertical acceleration, the cab pitch acceleration, the acceleration of a point on the frame under the cab and the acceleration of a point on the frame under the C.G of the truck body respectively.

Rideout et al. (2010) have developed a bondgraph model of flexible truck and investigated the connection between rigid and flexible dynamics. The model of this research was based on a power-based modelling method by using response surface analysis, which further determined the number of required flexible modes, and also the

range of validity of a rigid model. They have not neglected the frame flexibility for outputs such as payload acceleration that was directly related to transverse frame vibration. In their analysis, they have described the first bending mode but excluding the higher modes, which gave acceptable errors regardless of road roughness or load. *Filippini* (2010) investigated the car dynamics by extending the formalism to include three-dimensional rotations. Several elements oriented to multibody systems have been developed, which allowed working with different reference frames and operating with them through the use of translations and general transformations. This toolbox was useful and acceptable in the vehicle dynamics prediction, and it was successfully applied to similar project based on vehicle fault diagnostics.

Kienckeet et al., (2007) have observed the lateral vehicle dynamics and determined the dynamics for the detection of critical driving situations as well as the estimation of adhesion characteristics during cornering of the vehicle. Further, it included the comparison of linear and nonlinear observer.

Li and Sandu (2005) have developed an algorithm to calculate the tractive capacity of an off-road vehicle. They incorporated vehicle parameters (such as suspension stiffness, suspension damping coefficient, tire stiffness and tire inflation pressure) operating on soft soil with an uncertain level of moisture and also on a terrain topology, which was mainly induced by rapidly changing external excitations on the vehicle. This analysis of the vehicle–soil dynamics was performed for the light cargo as well as the heavy cargo scenarios.

Chrstos and Heydinger (1997) have published a study in which the Vehicle Dynamics Analysis Non-Linear (VDANL) and Vehicle Dynamics Models for Roadway

Analysis and Design (VDM Road) software packages were used to predict the dynamics of 1994 Ford Trucks. They had mainly focused on a specific trend of a linear and non-linear range of the vehicle response, which was compared with the experimental data.

Margolis (2001) developed a bondgraph model for incorporating sensors, actuators, and vehicle dynamics for developing controllers for vehicle safety. In this work, he had included 6-DOF model of the human body, front steering, suspension system, and the roadway input. A novel additive steering controller was incorporated as electric brakes at each wheel including controlled suspensions.

Teng et al. (2008) have employed the multi-body dynamics method to explore frontal collision phenomena. A 3D 15-segment model of the hybrid dummy was developed, and the governing equations of motion are obtained from Kane's formulation. The current results were compared with experimental tests and those obtained from LS-DYNA 3D-finite element code, to confirm the accuracy of the proposed numerical procedure. The results of this research have pointed out that the numerical method proposed in this study has considerable potential for evaluating a vehicle's crash safety performance and guiding the future development of safety technologies.

Fischer et al. (2007) have designed a system to aid the driver to prevent the unstable or unpredictable vehicle behaviour and to stabilise the horizontal and vertical motion of the vehicle. It was attained by the integration of actuators, sensors and data processing. However, the attained benefits were paralleled by an increase in the complexity of the system requiring enhanced methods for fault detection and diagnosis.

Margolis and Shim (2001) have developed a four-wheel, nonlinear vehicle dynamic model with electrically controlled brakes and steering, along with controller at each suspension corner. Controllers were exhibited through simulation only. A four-wheel model was the extended form for one-wheel model, but still it was assumed with simple assumptions that allowed the model to expose the essence of the vehicle dynamics. Bondgraphs were used for this model creation. The model has included a suspension at each corner of the vehicle along with an actuator between each vehicle corner and the un-sprung mass at that corner. The model consisted individual electric brake actuators. A steering actuator was included that has a differential in the steering column so that an electric motor could be steer additionally to the command from the driver without forcing the driver's hands to move.

Kiencke and Daib (1997) have presented a comparison of a linear and a nonlinear observer for the vehicle and tire side-slip angles. The first part shows the critical driving condition. Whereas, second part generates the equation for non-linear observation. The final part of this research work develops a linear observer for comparison.

Zhou et al. (2009) have developed an analytical model of passenger car body, where an influence of flexibility on the vertical stiffness of the car body has been studied. They had also involved the effect of structural damping on car body vibration and found that structural damping attenuate the vibration level to some extent. This study introduced geometric filter phenomenon and spotted its impact on resonant vibration level of the car body. *Huong et al.* (2010) have constructed a mathematical model of the vertical vibration for high railway passenger car, where the car was

modelled as a Euler beam with free ends. Numerical results of this work illustrated that the first bending mode of car body occurs near the rigid body mode, where ride comfort was majorly affected.

Tomioka et al. (2006) suggested an analytical method to investigate the 3D flexural vibration of the railway vehicle car bodies in which the car body was modelled as a box-type structure consisting of plates and beams. To investigate the improvement in the ride comfort of lightweight railway vehicles using an active vibration reduction system using piezo-stack actuators, *Schandl et al.* (2007) have used an MBM of the vehicle. *Diana et al.* (2002) have developed a complex FEM of the vehicle which were suitable for reproducing its dynamic behavior in the 0-50 Hz frequency range, especially concerning the ride comfort problem. *Carlbom* (2000) has combined the multi-body system theory with the FE method to examine the flexural response of the railway vehicle.

Further, *Tomioka et al.* (2017) have investigated the effects of damping of a passenger on flexural vibration on railway passenger car. The principal focus of this work was to investigate the damping effect on vertical vehicle vibrations followed by different postures and distributions of the passenger. Running test and stationary excitation tests were also conducted on an actual railway vehicle. The average RMS value was evaluated calculated from the following relation:

$$S_{rms} = \frac{1}{N}\sum_{n=1}^{N} P_{rms} \tag{1.1}$$

Where n and N denotes an acceleration points, P_{rms} is the band-limited RMS value. Results of excitation test included mode shapes and Frequency response function

(FRFs), whereas FRFs were calculated for three different body posture of the passenger. *Dumitui et al.* (2017) have established the computation model of a railway car through FEM along with the flexible model. The results have demonstrated of this work comparison between flexible body responses to the rigid body response.

Carlbom (2000; 2001) has studied the influences of a car body flexibility on ride quality and vehicle dynamics through measurements and simulations. To reduce the finite-element model and make the simulation more efficient, four criteria has been presented, i.e. modal participation factors, mode contribution factors, excitation spectra, and comfort filters, to select which car body eigen modes have the enormous contribution upon ride quality. *Diana* et al. (2002) have also demonstrated that it was essential to consider the car body flexibility to reproduce ride comfort of railway vehicles.

The above literature has included all major contributions of frame flexibility. The next subsection will investigate the archival literature on ride comfort analysis.

1.2.2 Ride comfort

Numerous studies have been conducted to evaluate a ride comfort of the vehicle. Road handling capability of the vehicle directly affects the ride comfort. Thus these two properties of vehicle dynamics are related to each other. Ride comfort for the heavy vehicle is a crucial topic for research, where the driver rides the vehicle for a long time in a single ride. Although, very few studies have conducted to evaluate a ride comfort for a heavy vehicle.

Uys et al. (2007) have investigated the suspension setting for optimal ride comfort of an off-road vehicle travelling on roads with different roughness and speeds.

Optimization has been carried out with the help of DQ algorithm on a car vehicle (Land Rover) model in MSC. For this purpose, ADAMS software has been applied and evaluated different speeds ranges from 10 to 50 kmph. Similarly, in other studies, the ride comfort activity has been optimised with the help of RMS value of vertical acceleration at the driver seat over the periodic road excitation. For this aim, the weighted acceleration has been taken in terms of the BS-6841 filter (*Els and Uys,* 2003), and the RMS vertical acceleration value was evaluated as described for the integrated model of driver along with driver seat (*Els et al.,* 2006).

Eleberg and Karnoop (1996) have considered a broadband stochastic roadway efforts related with the simplified displacement in terms of PSD at various intensity levels to a quarter-car model. However, the best probable isolation has been required subject to the constraint, whereas, RMS value of suspension deflection remained intact. In this quarter-car model, partially and fully active, optimal passive, active and variable damper system was accomodated. They further advocated the policy for acquiring suspension systems based on suspension travel.

Mastinu et al. (2001) have formulated the transfer functions for the standard deviation for vertical force between tire and road, for vertical body acceleration and the relative displacement between wheel and body due to the road input. Further, this work was extended for two different PSD formulations. Analytical expressions for the best trade-off for conflicting performance indices were obtained for the simplified PSD formulations. Therefore, the optimal value of suspension damping and stiffness alongwith tire stiffness were evaluated. For the most significant expression of the PSD formulations, the optimal settings were speed dependent, whereas the suspension

damping and stiffness should be within derived constrains and the tyre stiffness should be minimal. *Lozia* (1991) has investigated the lateral dynamics of vehicle in term of lateral acceleration, velocity, displacement and heading angle. These parametric study was conducted on a full car vehicle model over the different road inputs including smooth road, an average class (D) road and a poor road of the class (E) during a lane change at 80 km/h, resulting into the road unevenness decreases with the lateral displacement by 23% of the lane width. In another study, *Yoon and Hac* (1995) have adopted optimal control for semi-active suspensions of a quarter car vehicle model for various road inputs at different vehicle speeds, whereas, road input is modelled as white noise, in which the covariance was presented in terms of road roughness parameter. The results presented in the form of body acceleration and tyre deflection, which was obtained over the crossing of two large bumps and an asphalt road at 20 m/s.

Furthermore, *Marzaband et al.* (2004) have described the paved road with roughness and formulated by an elevation spectral density and surface irregularity standard deviation with lift of 0.01 m. In this work, optimal suspension settings for ride comfort was obtained for a four DOF half car model. Moreover, *Tamboli and Joshi* (1991) have calculated different values for the spring damping and stiffness coefficient, which was further used for optimisation for the mean square of vertical acceleration in course of vehicle travelling at multi speeds over sinusoidal highways and urban roads. In further study, *Kashyzadeh* et al. (2014) have presented a quarter car models according to road classification ISO 2631-1, which was achieved road roughness as PSD function in a constant speed of the car by using MATLAB$^{®}$ code. They had suggested that the situation of worst conditions was adhesion, when suspension system

vibrations were Max value and the oscillation frequency is equal to the resonance frequency. Moreover, tire adhesion effect to the ground has been investigated.

In a separate study, *Kong et al.* (2014) have investigated the urban bus characteristics through simulation with experimental study. The random vibration of bus model has measured with two parallel tracks of terrain profile. They had also developed a bus frequency modal with embedded modal excitation data to enhance computation efficiency. There have been lots of attempts to model the heavy vehicles by using some popular software's. In this direction, *Ke and Jie* (2010) have proposed Virtual Proving Ground (VPG) to simulate a vehicle ride comfort. The software LS-DYNA obtained the body acceleration time domain and frequency domain power spectrum. The proposed method of analysing a vehicle ride comfort realised on the computer has important practical significance for improving vehicle ride comfort, reducing production costs and shorting development cycle and the feasibility of the integrated CAE analysis methodology was verified. In another research, *Els et al.* (2007) have determined the damper and spring settings that signified the optimal ride comfort of an off-road vehicle for multi road profiles at different speeds. These settings were furthe extended for the formation of a four-stage semi-active hydro-pneumatic spring-damper suspension system (4S4). The optimization study was also conducted with the DQ algorithm on a Land Rover vehicle in MSC. Previously, *Els* (2005) has evaluated a ride comfort of the off-road vehicle through four prescribed standards. These standards were BS-6841, ISO-2631, AAP, and VDI-2057. The vertical responses of body were used in all mentioned cases, while the RMS value is adequate for BS-6841, ISO-2631, and un-weighted values.

The authors (*Griffin*, 1990; *Wu and Rakheja*, 1999; *Boileau and Rakheja*, 1998) have shown that most researchers considered linear one-dimensional models with a limited masses. If the discrete model used elastic-damping elements, they were linear irrespective of the non-linear biodynamic response function. The number of degrees of freedom of presented model ranged from 1-5 (*Frolov*, 1991; *Mansfield and Lunstrog*, 1999), whereas other researchers suggested only one-dimensional linear models with excitation in the vertical direction. *Rakheja et al.* (1998) have developed an apparent mass discrete models with the seated human body exposed to horizontal vibration. Most of the research studies have (*Miwa*, 1967; *Leatherwood*, 1980; *Oborne et al.*, 1981) considered the vertical vibration for evaluating a human comfort. Limited studies have been taken transverse vibration for human ride comfort. Also, many studies have considered sinusoidal steady-state input, but only a few of them considered the influence of random, quasi-random vibration or repeated shocks on human body (*Demicd,* 1986).

Further, *Yang et al.* (2004) have demonstrated the ride comfort inside a railway vehicle represented as a sequence of moving loads and also as two degree-of-freedom systems as it travelled over a simply supported single and three-span bridge. They had used maximum acceleration level as the comfort indicator. *Lin et al.* (2001) have suggested the safety criterion for the irregularity, based on management standards of train safety and passenger comfort. *Demicd et al.* (2002) addressed the issue of ride comfort of road vehicle over the random road conditions. They have included two phase of research. First phase influence of broadband random road condition on the human biodynamic model was examined. *Nisihiyam et al.* (2000), experimented evaluating vibrational characteristics of vehicle subsystem involve with human, seat,

steering wheel and pedals. The whole analysis was done sinusoidal and random excitation. The results showed that arm angle in driving posture significant influence on the human dynamic behaviour while driving. Several other investigations have been reported in past which claimed that the human posture affects the ride comfort level of the driver as well as passenger (*Fairley and Griffin*, 1989; *Wilder et al*, 1994; *Paddan and Griffin*, 1994; *Lewis and Griffin*, 1996; *Fairley and Griffin*, 1988; *Parsons and Griffin*, 1988; *Corbridge and Griffin*, 1986).

In another study, *Kargornovin et al.* (2005) have determined a ride comfort of the high-speed train while it was passing through a bridge. In this work, ride comfort level was evaluated from sparling index and the peak value of the vertical acceleration. *Ataei et al.* (2017) have worked on hybrid electromagnetic suspension system for improving a ride comfort level. This system was integrated with 2 DOF quarter suspension model and results were optimised where ride comfort was taken as a primary objective function. *Park et al.* (2017) have conducted a quantitative analysis for determining the frequency changes and amplitude of beating vibration which directly affects the comfort level of a passenger vehicle. The results of this study which evaluated the discomfort caused by beating vibration. It was also found that the level of discomfort varied with the amplitude ratio of beating vibration and beating frequency.

Mohajer et al. (2017) have suggested digital filters for ISO 2631 and 5349 frequency weighing factor. They had developed a passive 3D MBS based human biodynamic model for seated human inside a road vehicle. Further, this work has been extended with the incorporation of seat foam model in the previous seat-MBS human biodynamic model. The main contribution of this paper has included: the design and

application of equivalent digital filters for ISO 2631 and 5349 frequency weightings and development of a passive 3D MBS based HBM for seated human inside a road vehicle.

Boileau et al. (2001) have performed a synthesis of reported data to define ranges of DPMI and STHT characteristics in the 0.5×10^{20} Hz range under particular conditions applicable to vehicle driving. The conditions included the human subjects sitting erect without back support with feet supported and vibrated, and exposed to vertical vibration with magnitude equal to less than 5 m/s^2. The results of the study were subsequently adopted in the ISO-5982 (2001).

1.2.3 Control evaluation

Many archival studies have been conducted to demonstrate the significances of semi-active systems over conventional passive system. Firstly, *Karnoop et al.* (1974) have investigated the performance of a skyhook controlled semi-active system and they have compared it with the traditional passive system (*Karnopp,* 1990). The controlled semi-active systems may deliver the flexibility, versatility, and greater performance of fully active systems with a miniscule amount of energy while maintaining the reliability of passive systems. *Alanoly and Sankar* (1987;1988) have studied the balance logic for vibration and shock isolation, whereas *Liu et al.* (2005) have studied the "on-off" and "continuous" forms of both skyhook and balance logic and they have compared it to adaptive passive damping control system. *Shamsi and Choupani* (2008) have presented the on-off and continuous skyhook control for half-car roll plane model and compared the frequency and transient responses with that of a passive system.

In this regard, *Strecker et al.* (2015) have presented the comparison between three semi-active control algorithms viz. groundhook, skyhook and modified groundhook

and passive system. The simulation was conducted for three different response time of magneto-rheological (MR) damper; 1.5, 8 and 20ms. The effect of the MR damper response time on the efficiency of semi-active suspension system has been studied. The algorithms are presented below:

Groundhook: $F_{gh} = \begin{cases} c_{max}(\dot{x}_1 - \dot{x}_2), & (\dot{x}_2 - \dot{x}_{in})(\dot{x}_1 - \dot{x}_2) < 0 \\ c_{min}(\dot{x}_1 - \dot{x}_2), & (\dot{x}_2 - \dot{x}_{in})(\dot{x}_1 - \dot{x}_2) \geq 0 \end{cases}$ (1.2)

Skyhook: $F_{sa} = \begin{cases} c_{max}(\dot{x}_1 - \dot{x}_2), & \dot{x}_1(\dot{x}_1 - \dot{x}_2) \geq 0 \\ c_{min}(\dot{x}_1 - \dot{x}_2), & \dot{x}_1(\dot{x}_1 - \dot{x}_2) < 0 \end{cases}$ (1.3)

Modified Groundhook: $F_{ghmod} = \begin{cases} c_{max}(\dot{x}_1 - \dot{x}_2), & \ddot{x}_2(\dot{x}_1 - \dot{x}_2) \geq 0 \\ c_{min}(\dot{x}_1 - \dot{x}_2), & \ddot{x}_2(\dot{x}_1 - \dot{x}_2) < 0 \end{cases}$ (1.4)

Results have shown that the MR damper with modified groundhook shows better grip for the shorter response time of 1.5ms. If the response time is long (20ms), the comfort level achieved is slightly better than that of a passive system. On the contrary, the influence of response time on the suspension quality is less for the skyhook control strategy. Here, better comfort could be achieved even with a longer response time of 20ms. Overall, better performance was shown by the damper with less response time. To enlarge the scope of control algorithms, *Bakar et al.* (2015) have compared skyhook and modified skyhook control algorithms for a validated full car model. The modified skyhook control strategy was adopted to reduce the water hammer effect of the original skyhook control. It includes the effect of both the passive and skyhook dampers. The skyhook logic employed was given below

$If \ v_1 v_{12} \geq 0 \ then \ F_d = c_{sky} v_1$
$If \ v_1 v_{12} < 0 \ then \ F_d = 0$ (1.5)

Where, v_1 is the absolute velocity of the sprung mass, v_{12} is the relative velocity of the sprung mass as compared to the un-sprung mass, F_d is the damping force and c_{sky} is

the skyhook damping constant. The modified skyhook logic has included both the passive damper and the skyhook damper. The logic may be given as,

$$F_d = c_{ms}\big[\alpha(\dot{Z}_u - \dot{Z}_s) + (1 - \alpha)\dot{Z}_s\big] \tag{1.6}$$

where, c_{ms} is the modified skyhook damping, α is the passive to skyhook ratio, $\dot{Z}_u$ and $\dot{Z}_s$ are the unsprung body velocity and the sprung body velocity respectively. In general, the semi-active system performance is better than that of a conventional system. However, the semi-active system performance is dependent on the control algorithm used. The results have been shown that for random road input, the overall performance of the skyhook logic is better than that of modified skyhook by 3.2%. The modified skyhook performs better in case of vertical and roll motion though.

In another study, *Hailong et al.* (2013) have examined the skyhook based semi-active control of full vehicle suspension system incorporated with MR damper. A 7-DOF full vehicle dynamic model was set up by using the modified Bouc-wen hysteretic model of MR damper, and modified skyhook control is proposed to individually control the four MR quarter vehicle sub-systems of the full vehicle. The modified skyhook control proposed is as given below:

$$i_{di} = \begin{cases} k_d |\dot{x}_{si}|^m, & \dot{x}_{si}(\dot{x}_{si} - \dot{x}_{ui}) > 0, \\ 0, & \dot{x}_{si}(\dot{x}_{si} - \dot{x}_{ui}) \leq 0, \end{cases} \quad i = 1, 2, 3, 4, \tag{1.7}$$

where i_{di} are controlled driver currents for four MR dampers, k_d is the controller gain, $m(m \geq 0)$ represents the controller order. $\dot{x}_{si}$ and $\dot{x}_{ui}$ are velocities of sprung and unsprung masses of the four quarter car sub-suspensions. Controller parameters are taken as $m = 2$ and $k_d = 3$. The vertical motion characteristics have been inspected using

harmonic excitations with delay time. The results have showed that the peak value of the vehicle body acceleration decreases by 30% for the suspension incorporated with MR damper in comparison with passive system. However, the un-sprung mass acceleration showed abrupt responses. The pitch angular acceleration and the roll angular acceleration were found to be less in the semi-active MR suspension system. The vehicle dynamic model was also subjected to rounded pulse excitations to assess the vibration diminishment performance of the suspension system. Results have exhibited that the performance of the MR suspension is better than that of a passive system in terms of shock diminishment whereas road handling and ride comfort have been slightly compromised. In case of random road inputs, the semi-active MR suspension has potential of resonance attenuation for low frequency range (0.5-2.0 Hz).

Amin et al. (2015) have studied the skyhook logic for a 7-DOF ride model of an armoured vehicle. The skyhook controller proposed by them consisted of an outer loop and an inner loop. The purpose of the outer loop was to control the body acceleration, pitch acceleration and roll accelerations due to road excitations whereas, the inner loop controlled the damping characteristics. The outer loop has utilised PID control while the inner loop used skyhook logic to control the damping force. The semi-active damping force is given by

$$F_{sa} = -c_{sa}(\dot{x}_2 - \dot{x}_1) = -c_{sky}\dot{x}_1 \tag{1.8}$$

where, F_{sa} is the damping force, c_{sa} is the semi-active damping coefficient, c_{sky} is the skyhook damping coefficient, $\dot{x}_1$ is the velocity of the sprung mass and $\dot{x}_2$ is the velocity of the unsprung mass. High mobility multipurpose wheeled vehicle (HMMWV) was considered in the main focus of the paper. The simulation results show

that the body acceleration, pitch acceleration and roll acceleration have been significantly reduced by the proposed skyhook control as compared to PID control of semi-active the system or passive suspension.

Raj et al. (2015) have adopted a fuzzy logic controller based on skyhook logic to control a semi-active suspension system. The fuzzy logic, which is a multi-valued logic was introduced in 1965 by *Lotfi Zadeh* (1965). The fuzzy controller based on skyhook logic was supposed to operate between a high damping state and a low damping state. There are two inputs to the system, viz. velocity of sprung mass and relative velocity. The output was the damping coefficient of the semi-active damper. The linguistic variables for input are Negative Big (NB), Negative Small (NS), Zero (Z), Positive Small (PS) and Positive Big (PB). The outputs are LV (Large Value), L_{AVG} (Large Average), L (Large), M (Medium), S (Small), S_{AVG} (Small Average) and SS (Small Small). The rules are defined by the Rule Matrix as shown in Table 1.2.

Table 1.2: Rule Matrix

		Velocity				
		NB	NS	Z	PS	PB
	NB	LV	L_{AVG}	M	S_{AVG}	SS
	NS	L_{AVG}	L	M	S	S_{AVG}
Relative Velocity	Z	M	M	S	M	M
	PS	S_{AVG}	S	M	L	L_{AVG}
	PB	SS	S_{AVG}	M	L_{AVG}	LV

A PID controller was also embedded with the fuzzy logic, which will give better ride comfort by smoothing the velocity and the displacement. A sinusoidal road input was provided into the system to evaluate the performance. The results showed considerable improvement in case of the semi-active suspension using continuous

skyhook, fuzzy logic based on skyhook control and fuzzy PID as compared to on-off skyhook or passive system. The fuzzy controller embedded with continuous skyhook logic showed better performance regarding displacement of sprung mass and sprung mass acceleration than simple on-off skyhook or continuous skyhook. However, the inclusion of PID with fuzzy gives better ride comfort by smoothing the velocity.

(i) Hybrid control strategies

Strydom et al., (2014) have investigated the applicability of hybrid control to a small off-road vehicle. The suspension system consists of controllable dampers and passive spring-damper units. Skyhook and ground-hook control are used to control the nonlinear, three-dimensional, 12-DOF dynamic model. The skyhook control provides reduced vehicle body motion, thus improving ride comfort at the expense of un-sprung mass motion. On the contrary, ground-hook control results in decreased un-sprung mass motion, thus better road handling at the expense of ride comfort. Adaptive control has been adopted to incorporate the relative velocity over the damper, which may be given by

$$
\begin{aligned}
\dot{Z}_s \dot{x}_{cl} > 0: & \qquad \sigma_{sky} = \dot{Z}_s \\
\dot{Z}_s \dot{x}_{cl} \leq 0: & \qquad \sigma_{sky} = 0 \\
\dot{Z}_u \dot{x}_{cl} < 0: & \qquad \sigma_{gnd} = -\dot{Z}_u \\
\dot{Z}_u \dot{x}_{cl} \geq 0: & \qquad \sigma_{gnd} = 0
\end{aligned}
\tag{1.8}
$$

where, $\dot{Z}_s$ is the sprung mass velocity, $\dot{Z}_u$ is the unsprung mass velocity, $\dot{x}_{cl}$ is the relative velocity across the damper, σ_{sky} and σ_{gnd} are the skyhook and groundhook control inputs to the semi-active force, $F_{SA,z}$, which is given by

$$
F_{SA,z} = G\big[a\sigma_{sky} + (1 - a)\sigma_{gnd}\big]
\tag{1.9}
$$

where, G is the controller gain and a is the skyhook to groundhook ratio. It is evident from ride comfort that the improvement can be achieved by implementation of skyhook logic with a control gain of 1200Ns/m. The groundhook logic is capable of diminishing the vertical acceleration of the wheels. In case of road holding, an uncontrolled system with low damping gives the best results.

In another study *Kashem et al.* (2015) have introduced a modified continuous skyhook strategy along with adaptive gain that directs the semi-active vehicle suspension. They have scrutinised 11 sets of suspension parameters and considered a set of parameters that demonstrated better performance regarding peak amplitude and settling time. The proposed system first apprehends the road input and determined the best value for skyhook gain (SG). In the meantime, the system is controlled by the new skyhook algorithm which may be presented as

$$f_d = \begin{cases} C_{max}(\dot{z}_2 - \dot{z}_1), & if \ \dfrac{\dot{z}_2}{(\dot{z}_2 - \dot{z}_1)} \geq \dfrac{C_{sky}}{C_{max}} \\ C_{sky}\dot{z}_2, & if \ \dfrac{C_{sky}}{C_{max}} > \dfrac{\dot{z}_2}{(\dot{z}_2 - \dot{z}_1)} > \dfrac{C_{sky}}{C_{min}} \\ C_{min}(\dot{z}_2 - \dot{z}_1), & otherwise \end{cases} \qquad (1.10)$$

Where, C_{max} and C_{min} are the maximum and the minimum damping coefficients of the semi-active damper, C_{sky} is the skyhook damping constant and varied corresponding to the road input, $\dot{z}_2$ and $\dot{z}_1$ are velocities of the sprung and the un-sprung masses. A comparison of the above control strategy is made with three skyhook control strategies proposed by *Karnopp et al.*(1974); *Bessinger et al.* (1995); and *Nguyen, et al.* (2009) respectively. Ride comfort has been found to be enhanced by 38.4% for the modified skyhook logic by *Kashemet et al.* (2015) as compared to a passive system, whereas

improvements of 27.3% for optimal skyhook control by *Nguyen, et al* (2009). In another results, 2.8% improvement has been found for modified skyhook control by *Bessinger et al.* (1995) and 5.9% for continuous skyhook control by *Karnopp et al.* (1974) have been observed. Moreover, the proposed modified skyhook control system provides superior ride comfort as compared to passive or any of the skyhook control implementation.

Espinoza et al. (2014) have studied three hybrid control strategies for semi-active suspension system viz., hybrid sky hook-ground hook, hybrid mix-1-sensor and frequency estimation-based controller. A commercial magneto-rheological damper was designed by using an artificial neural network (ANN) approach. The automotive semi-active suspension was appointed in a commercial controller area network (CAN) system, and the control logic was enforced in a micro-controller system with the goals to optimise comfort and road holding. Results show the usefulness of this approach in commercial utilisation. All control algorithms have better results than default solutions. Using the pseudo-Bode diagram, hybrid solutions exhibited good results in both frequencies range of interest (comfort and road holding); these results were further validated with the RMS index.

The next section will present the research gaps, which has been compiled after a comprehensive literature survey.

1.3 Identified research gap

Various studies have been conducted in this area of vehicle dynamics, in which researchers have made attempts for enhancing the ride comfort and stability of vehicle at maximum speeds. Several computational models are available, but there is a wide gap between a complete framework of computational analysis and experimental

framework. The research gap can be identified in the following two subsections, which are to be addressed in this research work.

1.3.1 Vehicle modelling and frame flexibility

After going through a detailed review on frame flexibility, researchers are more intended for railway passenger car over the track irregularities of the railway, whereas very limited studies have been addressed on this issue of heavy road vehicle accompanied by random road responses. India is the country, where multifarious road conditions are presented, which creates an infirm condition in front of all leading automobile industries to maintain comfort level as per standard on the every road condition. The suspension system of any vehicle majorly affects the ride quality of the vehicle, but it is crippled under the variety of road conditions.

Some studies have mentioned that structural damping is also taking participation in ride quality improvement, whereas few study focused on increased damping by changing the posture of the passenger. Thus frame flexibility is one of the issues for ride comfort of a vehicle. This issue has been investigated through different methodology in the literature. However, the development of an analytical framework through extended Lagrangian formalism is the major highlight, which is not attempted by any other researcher.

1.3.2 Ride comfort and vehicle suspension control

Ride comfort and vehicle suspension control are the one of the main focus of the vehicle dynamics. The following gaps are identified under this subsection:

- It has been noticed that suspension setting and road condition of a vehicle directly influence the ride comfort of a vehicle. Various methods are available to enhance the performance of a suspension system. However, any optimum suspension system is rarely seen in archival literature.

- Comfort level of the driver has been obtained from peak vertical accelerations of a vehicle and compared with some given standards. However, few attempts have been made to create the model for the driver seat along with a cabin for ride comfort analysis.

- It is evident that limited studies are performed to incorporate controllers with the suspension system. Effect of the hybrid controller on the performance of heave of the vehicle is rarely found in the literature.

After going through the detailed literature review, significantly an ample amounts of work have been done on suspension systems. Several researchers have worked on semi-active suspension system and passive suspension system. Different semi-active control strategies have been studied through different practical method and software like MATLAB/Simulink$^{®}$ etc. Comparison of different semi-active control policies with passive suspension has also been carried out. It has been observed that very limited studies are developed on computational model of suspension controller through bondgraph modelling. Although different studies have been carried out through bondgraph modelling of vehicle system. However implementation of semi-active control strategies in bondgraph modelling is a research area which requires further exploration. Moreover, hybrid combination of skyhook and groundhook control logic has been studied by many researchers. But the combination of other control logic for the formulation of different hybrid control logic has not gained popularity. Hence further research and experimental validation is required. The next subsection will present about the uniqueness of bondgraph modeling as a modeling tool.

1.4 Significance of bondgraph modeling

In the 1950s, H.M. Paynter of MIT worked on interdisciplinary engineering projects including hydroelectric plants, analogue and digital computing, nonlinear dynamics, and control (*Elbeheiry and Karnoop*, 1996). He observed that dynamic systems generate similar forms of equations in a wide variety of domain (for example electrical, fluid, and mechanical). *Paynter* (1960) incorporated the notion of an energy port into his methodology, and thus bondgraphs were invented in 1959. Later on, bondgraph theory has further developed by many researchers like *Karnopp et al.* (1990); *Breedveld and Dauphi* (1992); *Gawthrop and Smith* (1996); *Mukherjee and Karmakar* (2000); *Brown* (2006) and many more.

A bondgraph method is a graphical approach to modelling in which component energy parts are connected by bonds that supply the transfer of energy between systems components. The language of bondgraphs aspires to express a general class of physical systems through power interactions. The factors of power, i.e., Effort and Flow, have different interpretations in different physical domains. Power can always be used as a generalised co-ordinate to model coupled systems residing in several energy domains. In bondgraphs, one needs to recognize only four groups of basic symbols, i.e., three basic one port passive elements inertance (I), capacitance (C), and resistance (R); two basic active elements source of effort (SE), and source of flow (SF); two basic two-port elements gyrator (GY), and transformer (TF); and two basic junctions i.e., constant effort junction (0), and constant flow junction (1). The basic variables are effort (e), flow (f), time integral of effort (P) and the time integral of flow (Q).

In this approach, a physical systemcan be symbolised through ports and lines, identifying the power flow paths. The discrete elements of resistance, capacitance, and

inertance are interconnected in an energy conserving way by bonds and junctions resulting in a network structure. From the graphical representation of the bondgraph, the deviation of system equation is so systematic that it can be algorithmized. The whole procedure of modelling and simulation of the system may be performed by some of the existing software, e.g., **ENPORT, Camp- G, SYMBOL-shakti, 20sim, COSMO** etc.

The bondgraph modeling can able to describe the systems with diverse energy in a unified manner. The power conservation property of this tool need to constraint velocity only, whereas the forces will automatically be balanced. This tool provide a useful notation to model a complex physical systems. Bondgraph technique offers flexibility in modelling and formulation of system equations. A very large system may also be modelled in a modular form by creating subsystem models and then joining them together at their interaction port to create an integrated system model. The model may be easily modified making it a powerful tool for system synthesis and consolidation of innovative ideas. Bondgraph equations normally use generalised displacement and generalised moment as state variables. The bondgraph modelling, their simulation and animation are performed using SYMBOLS Sonata® (*Mukherjee and Samantaray,* 2006), a bondgraph modelling software.

1.5 Scope and objectives of research

The present dissertation research work thus aims to develop a comprehensive model of heavy road vehicle consideration of random road excitation, base frame flexibility, human biodynamic characteristics and semi-active vibration control for a heavy road vehicle. Also, a quarter car test rig of the heavy vehicle has been fabricated for validation of simulation model of the heavy vehicle passive suspension system.

After a comprehensive review of the literature, following objectives have been set as the objective of the research work:

i. The analytical framework of rigid frame of chassis of road truck through extended Lagrange formalism.

ii. Creation of a model of road truck vehicle considering lumped and distributed parameter. Simulate this bondgraph model for variable parameters to obtain behaviour of road truck.

iii. Ride comfort analysis of vehicle with a driver on typical Indian road condition.

iv. To develop a control model for the suspension system of a heavy road vehicle.

v. Explore the other possibility to validate the dynamic model of a heavy road vehicle.

1.6 Contribution of the thesis

The contribution of this dissertation to the following areas of heavy road vehicle dynamics.

i. **The issue of frame flexibility:** previously many studies were attempted this issue for road/rail dynamics. However, very few are attempted for heavy vehicle system. In this work, an analytical model of truck frame considering flexible effect with Rayleigh beam approach. Effect of structural damping on dynamics of flexible chassis is separately presented. Further, this work has been extended to create a bondgraph model, which is based on modal superposition theorem. Simulation work is being carried out for three modes of flexible frame. Furthermore, this analytical formulation has been extended to incorporate non-potential and non-conservative fields to the Lagrangian density function and Hamiltonian function, which are conveniently expressed in umbra time.

ii.   **Ride comfort analysis:** A ride comfort analysis for heavy vehicle system combined with the human biodynamic model is presented. The whole body vibration in heavy road vehicle will be examined by using a 7-DOF human biodynamic model. The physiological effect of the human body due to vibration is being analysed as per specified criteria ISO 2631. The RMS weighted value of different body segments is superimposed over ISO curves.

iii.   **Control evaluation for suspension system:** The various semi control logics, i.e., On-off skyhook, continuous skyhook, have been modelled through bondgraphs, and a detailed comparison study is presented through simulation. Further, these logics are combined with each other and make a three different hybrid control logic. In the last H_∞ controller logic combined with PID controller is proposed for the heavy vehicle system. The simulation of this model is being carried for obtaining various parameters of suspension system.

iv.   **Experimental analysis:** Finally, a quarter car suspension test rig is fabricated for conducting the experimental study. This test rig involves controlled MR damper (RD 8040-1), which is mounted parallel to a leaf spring on the axle of the wheel. The experimental results are presented in PSD (Power Spectral Density) form. The bondgraph model of MR damper is also developed considering Bouc-ben approach and combined with quarter car model, whereas simulation results are validated with experimental test results. The response of sprung mass has been captured for different road excitations.

1.7 Outline of the thesis

The thesis consists of seven chapters. *The first chapter* is introductory. It discussed the fundamental goal with all data and figures which motivates the author to persuade this work. It is also more on theory and literature survey that has been done. It will discuss vehicle modelling, frame flexibility and suspension control that work already being done related to car vehicle, railway vehicle and heavy vehicle system. Thus the primary goal of this chapter is to provide the reader basic idea of the thesis. The *second chapter* presents the alternative formulation for frame flexibility of truck chassis under consideration of *Rayleigh beam* approach. Further, this approach is adopted for bondgraph modelling of truck beam structure for simulating the effect of flexibility of chassis under random road conditions as per ISO 8608. In the last, this analytical formulation has been derived with umbra Lagrangian and Hamiltonian approach.

The *third chapter* evaluates the ride comfort for the driver, where the biodynamic model of driver integrated with flexible pitch plane model of truck chassis. Further, this integrated model simulated under various random road condition as per ISO 8608. The *fourth chapter* described the various semi-active control strategies of the vehicle and obtained a hybrid control strategy for a quarter model of heavy truck. One more controller is adapted for simulation of quarter car model and compares the response from previously defined studies. The simulation work has been carried out on Matlab/ Simulink software.

The *fifth chapter* presents the construction of quarter car suspension test rig. In the first part of this chapter, a bondgraph model of MR damper is created with the help of bouc-ben principle. Further, this model is simulated and validated with archival

literature. Then the test rig is constructed with leaf spring and MR damper, where various responses of sprung mass are captured through OROS vibration analyser. In the last section of this chapter, experimental results are validated with simulation results.

The *chapter six* presents the experimental analysis and capturing the responses for the validation of simulation results. *Chapter seven* concludes the thesis and presents the scope for further research.

Chapter 2

Analytical Model of Frame Flexibility for Heavy Vehicle System

2.1 Introduction

Ride vibration is a principal concern for vehicle dynamics, where frame flexibility plays a very significant role. Numerous studies have been conducted on problems of ride vibration, however very few studies have been carried out to study the effect of vibration which includes flexible frame. It has been generally noticed that the flexural vibration can be neglected for smaller vehicles, relatively for stiffer automobiles. However, trucks and the long heavy vehicle experience significant beaming mode vibration. Most of the analyses on the effects of chassis flexibility in vehicle dynamics were based on the use of particular developed models, whereas the FEM (Finite Element Method) and the modal superposition theory have been extensively used to calculate the modal properties of the frame structure. This problem occurs due to beam flexibility of the vehicle, which is termed as 'Beaming response of vehicle' (*Margolis and Edeal,* 1989*; Ibrahim et al.,* 1996). Previously, Euler Bernoulli approach was attempted to introduce beam flexibility in heavy truck chassis modeling (*Rideout,* 2012*; Zhou et al.,* 2012). Heavy long vehicles have a ladder-type chassis structure across the whole length of the vehicle. These structures are stiffer in bending, which can respond bending frequencies more than 20 Hz. When the engine and other elements are mounted on the structure, these bending frequencies are reduced up to 8 Hz, for highly stiffer frames (*Kim and Yim,* 1994; *Huang and Zing*, 2010). It is apparent that beaming

frequency is higher than the rigid frequency of the vehicle (*Tomioko and Takigami,* 2015). However, in large vehicles, beaming frequency is influenced by road inputs.

It is evident in extended review on frame flexibility in chapter *two* researchers are now more intended for railway passenger car over the track irregularities of the railway, whereas limited studies are available raised for a heavy road vehicle accompanied by random road responses. A country like India, where multifarious road conditions are present, which creates an infirm condition before all leading automobile industries to maintain comfort level as per standard on every road conditions. The suspension system of any vehicle affects the ride quality of the vehicle, but it is crippled under the variety of road conditions. Some studies have mentioned that structural damping can participate in ride quality improvement. The Lagrangian approach has been applied to obtain the energy equations of the vehicle system motions which resulted from the well-known rigid body modes and the modal parameters of the frame structure flexibility. The work has involved the importance of structural or internal damping of beam-type chassis structure on flexural vibration over the random road response prescribed by ISO 8608 (*Agostinacchio et al.,* 2014). Beam structure has been modeled with Rayleigh beam approach through bondgraph modeling, where it has been demonstrated a role of internal damping, with or without conditions. Besides, the response of beam, it also presented the various category of the road (as per ISO 8608) at various vehicle speeds.

This chapter begins by deriving Lagrange equation of beam structure for truck flexural response under consideration of Rayleigh beam approach. Then, this formulation is being extended for bondgraph modeling with or without consideration of

structural damping effect. Simulations are also carried out to visualize the beaming mode response over the random road conditions as prescribed by ISO 8608. Further in another section, the dynamic analysis of a continuous flexural beam is derived through extended Lagrangian formulism. The governing equations of motion and boundary conditions for infinitesimal beam are obtained through the variational formulation. An extended Noether's theorem along with an umbra-Hamiltonian is employed to get invariants of motion or possible invariant trajectories of motion. These constants of motions or conserved quantities are identified by applying an extended Noether's theorem (*Bahar and Kwatny,* 1987). The next section will present the analytical for heavy vehicle through classical mechanics approach.

2.2 Analytical framework for heavy vehicle system through classical mechanics

2.2.1 Generalized Lagrange's equation for continuous system

It is well known fact that the Lagrange formulation provides one of the most convenient ways of writing down the equation of motion for a wide range of mechanical systems. The principal advantage of Lagrange's equation is that it is easier to apply to dynamical systems other than the simplest. This formulation is created from scalar quantities of kinetic energy, potential energy, work expressed in terms of generalized coordinates and developed for universal handling of dynamical systems (*Meirovitch,* 1980). The equation is formulated equations of motion from the principle of least action. This density function is a function comprising of time, transverse displacements and transverse velocities, and up to second derivatives of displacements with respect to space coordinates x, which may be expressed as

$$\widehat{L}\big(w(t,x),\dot{w}(t,x),w'(t,x),w''(t,x),\dot{w}'(t,x)\big)=\hat{T}(t,x)-\hat{V}(t,x) \qquad (2.1)$$

Where $\widehat{L}(.)$ is the Lagrangian density function, $\hat{T}(.)$ is the kinetic energy density, which may be expressed as,

$$\widehat{T}(x,t)=\widehat{T}(\dot{w}(x,t),\dot{w}'(x,t)) \qquad (2.2)$$

Moreover, $\hat{V}(t,x)$ is the potential energy density, which has the following functional dependence

$$\widehat{V}(x,t)=\widehat{V}(w'(x,t),w''(x,t)) \qquad (2.3)$$

The next step is used for finding the equation of motion and the boundary conditions for the beam through the variational principle (see *Appendix B*). This formulation yields

$$\delta\int_{t1}^{t2}\widehat{L}\big(w(t,x),\dot{w}(t,x),w'(t,x),w''(t,x),\dot{w}'(t,x)\big)dt=0 \qquad (2.4)$$

Where $\delta(.)$ is infinitesimal variation operator and it is very similar to the total derivative operator, the only difference is that $\delta(.)$ does not vary with time. Another significant property of infinitesimal operator is that it commutes with the differential operator. Using the extremization condition, one may obtain

$$\int_{0}^{L}\int_{t1}^{t2}\delta\widehat{L}\big(w(t,x),\dot{w}(t,x),w'(t,x),w''(t,x),\dot{w}'(t,x)\big)dxdt=0 \qquad (2.5)$$

Or

$$\int_{0}^{L}\int_{t1}^{t2}\left[\frac{\partial\widehat{L}}{\partial w}\delta w+\frac{\partial\widehat{L}}{\partial\dot{w}}\delta\dot{w}+\frac{\partial\widehat{L}}{\partial w'}\delta w'+\frac{\partial\widehat{L}}{\partial\dot{w}'}\delta\dot{w}'+\frac{\partial\widehat{L}}{\partial w''}\delta w''\right]dxdt=0 \qquad (2.6)$$

37

The detailed derivation of the variational formulation is presented in *Appendix B*.

2.2.2 Analytical formulation for flexural behavior of truck chassis structure

Analytical formulation for flexural behavior of truck structure is being attempted in this section. The vehicle base is modeled as a rigid body with a local coordinate reference frame (w, x) attached to the center of mass (M) and aligned with the inertia principal axes as shown in Figure 2.1. It has density (ρ), and *p*itch inertia (J) respect to the body $W_1(t) - W_2(t)$ displacement axis, *EI* flexural rigidity and $\theta(t)$ pitch velocity of the base. It is connected with the suspension system to different elements of the vehicles. The spring and damper in the suspension system are characterized by the spring stiffness k_s and damping coefficient R_s respectively. The various displacements of the vehicle are described $w(x,t)$ with respect to the equilibrium positions. As the vehicle is assumed to be rigid, thus its motion can be described by the vertical displacement (bounce) as $w(x,t)$ and the rotation about the transverse horizontal axis (pitch) as $\dot{\theta}(t)$. The model of the vehicle is being created with the following assumptions:

- The components of the vehicle body act as a rigid body.

- The springs and dampers of the suspension system have linear characteristics.

- The spring damper system is assumed to be massless.

- The tire is assumed to provide stiffness and thus modeled as a spring element.

- The positions of the two ends of the spring connecting two rigid bodies or connecting one rigid body and one contact point are required as input data.

- Each rigid body is connected to each other by the spring-damper system.

- The traveling road is assumed to be straight.

- The road inputs are assumed to be random.
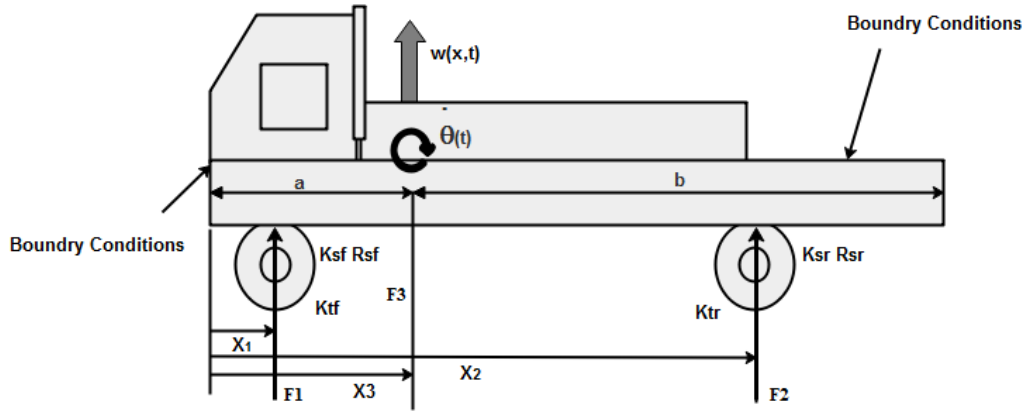
Figure 2.1: Schematic diagram of a continuous frame of vehicle

The analytical framework of truck chassis can be assumed as a free-free beam structure, where Rayleigh beam approach is being adopted. Let us consider a transverse deflection of the beam $w(x,t)$, where x varies from 0 to beam length L. The formalism of beam flexibility is easily obtained through the well-known equation of Lagrangian. Lagrangian density variation may be obtained from the following expression as

$$L = \left[\frac{1}{2}\int_0^L \left(\rho A \dot{w}(x,t)^2 + \rho I \dot{w}'(x,t)^2\right)dx - \frac{1}{2}\int_0^L \left(EIw''(x,t)^2\right)dx\right] \tag{2.7}$$

where, ρ is the mass density, A is the area of cross-section, EI is the rigidity, I is the second moment of area of the cross-section of the beam about the neutral axis. In the Eq. (2.7), the first term represents as kinetic energy of the beam, second term presents as inertial energy and final term is strain energy. The variational formulation presents a refined and classical method of deriving the equation of motion of a dynamical system, where all the boundary conditions of a system can be revealed. However, fundamentals of variational formulation for the continuous system are detailed in *Appendix B*.

The equation of motion is obtained after applying a variational formulation and boundary conditions in free vibration condition, which may be expressed as

$$\rho A \ddot{w}(x,t) - \left(\rho I \ddot{w}''(x,t) \right)' + \left(EI w''(x,t) \right)'' = 0 \tag{2.8}$$

This equation of motion is based on Rayleigh beam model. The term $\left(EI w''(x,t) \right)''$ is usually referred to as the flexural term, where EI is called the flexural stiffness and $\left(\rho I \ddot{w}''(x,t) \right)'$ is known as the rotary inertia term. If this term is zero, then equation (2.8) will become a Euler-beam model. Thus, the term $\left(\rho I \ddot{w}''(x,t) \right)'$ can also be named as a Rayleigh beam term.

Assuming a modal solution for Eq. (2.8) in the form of

$$w(x,t) = W(x) e^{i\omega t} \tag{2.9}$$

where, ω is the eigenfrequency and $W(x)$ is the Eigen-function. The actual solution of the equation may be obtained by taking the real part of the solution. Substituting the modal solution in the field Eq. (2.8) yields after rearrangement as

$$-\omega^2 \left[\rho A W - \left(\rho I W' \right)' \right] + \left(EI W'' \right)'' = 0 \tag{2.10}$$

which along with the corresponding boundary condition represents the Eigenvalue problem for a Rayleigh beam.

2.2.3 Modal analysis for uniform Rayleigh beam

Considering Eq. (2.10) as a uniform beam and substituting in Eq. (2.9) a solution of the form

$$W(x) = Ce^{\lambda x} \tag{2.11}$$

Where, C and λ are constants, Eq. (2.10) can be rewritten as

$$EI\lambda^4 - \omega^2 \rho I \lambda^2 - \omega^2 \rho A = 0 \tag{2.12}$$

Yields

$$\lambda^2 = \frac{1}{2EI} \left[\omega^2 \rho I \pm \sqrt{\omega^4 \rho^2 I^2 + 4\omega^2 EI\rho A} \right]$$

Thus, the spatial equation (real form) of Eq. (2.12) has the general solution, which may be expressed as

$$W(x) = A\cosh \lambda x + B\sinh \lambda x + C\cos \lambda x + D\sin \lambda x \tag{2.13}$$

Here, one may consider a uniform Rayleigh beam for which the free-free boundary conditions are given by

$$W(0) = 0, \ W'(0) = 0, \ W''(l) = 0, \ W'''(l) = 0, \tag{2.14}$$

Using Eq. (2.14) in Eq. (2.13) yields the frequency equation as

$$\cosh \lambda_n l \cos \lambda_n l - 1 = 0 \tag{2.15}$$

The solution of Eq. (2.15) yields

$$\lambda_n = \left(\frac{2n+1}{2} \pi \right) \frac{1}{l}$$

Moreover, the mode shape function may be expressed as

$$W_n(x) = (\cos \lambda_n l - \cosh \lambda_n l)(\sin \lambda_n x + \sinh \lambda_n x) - (\sin \lambda_n l - \sinh \lambda_n l)(\cos \lambda_n x + \cosh \lambda_n x) \tag{2.16}$$

41

Thus, one may obtain the natural frequency of Eq. (2.6), which may be written as

$$\omega_n = \lambda_n^2 \frac{1}{\left[1 + \lambda_n^2 \dfrac{I}{A}\right]^{1/2}} \sqrt{\frac{EI}{\rho A}} \qquad (2.17)$$

It is recognized that conditions are force-free at this point, which permits $\omega_n = 0$ to be a mode frequency. Thus Eq. (2.10) will be written as

$$\frac{d^4 W}{dx^4} = 0 \qquad (2.18)$$

or

$$W = c_1 x^3 + c_2 x^2 + c_1 x + c_4 \qquad (2.19)$$

There are two possible solutions for Eq. (2.13), which satisfied all boundary conditions. They are $W = const$ and $W = ax + b$. These are called rigid-body modes, and it is convenient to assume then as rigid body rotation of the beam about the centrally located center of mass. Thus,

$$W_{00}(x) = 1 \qquad (2.20)$$

and

$$W_0(x) = x - \frac{L}{2} \qquad (2.21)$$

Let us consider an analysis for truck chassis, which is presented in Figure 2.1. In this figure, the half model of the road truck is supported by front and rear suspension, which exerted an external force on the beam over the various road responses. Since equation of motion, Eq. (2.8) will be rewritten as

$$\rho A \ddot{w}(x,t) - \left(\rho I \ddot{w}''(x,t)\right)' + \left(EI w''(x,t)\right)'' = F_1 \delta(x-x_1) + F_2 \delta(x-x_2) + F_3 \delta(x-x_3) \quad (2.22)$$

where, F_1, F_2 are the force exerted by front and rear suspension systems respectively and F_3 is dead weight on the beam, $\delta(.)$ is the Dirac-delta function, x_1 and x_2 are the respective distance from left end to the front and rear suspension of the vehicle respectively x_3 is the distance of dead weight from the left end. One may assume that the solution of Eq. (2.22) is separable in space and time, and the forced solution has the following form,

$$w(x,t) = \sum_{n=0}^{\infty} W_n(x) U_n(t) \qquad (2.23)$$

where $W_n(x)$ depends on the spatial position and $U_n(t)$ depends on time. Introducing, Eq. (2.23) into Eq. (2.22), and multiply each term by $W_m(x)$ and integrate with respect to $x=0, x=l$ one may then use the orthogonal property to the modes and obtain as

$$\int_0^l \rho A W_n^2 dx \ddot{U}(t) + \omega_n^2 (\rho I \lambda_n^2 - \rho A) \int_0^l W_n^2 dx U(t)$$
$$= F_1 W_n(x_1) + F_2 W_n(x_2) + F_3 W_n(x_3) \qquad (2.24)$$

$$\rho A \left(1 - \frac{I}{A}\lambda_n^2\right) \int_0^l W_n^2 dx \ddot{U}(t) + \rho A \left(1 - \frac{I}{A}\lambda_n^2\right) \omega_n^2 \int_0^l W_n^2 dx U(t)$$
$$= F_1 W_n(x_1) + F_2 W_n(x_2) + F_3 W_n(x_3) \qquad (2.25)$$

Eq. (2.25) can be represented in general form as

$$m\ddot{U}(t) + kU(t) = F_1 W_n(x_1) + F_2 W_n(x_2) + F_3 W_n(x_3) \qquad (2.26)$$

where,

$$m = \rho A \left(1 - \frac{I}{A} \lambda_n^2 \right) \int_0^l W_n^2 dx$$

$$k = m\omega_n^2 \int_0^l W_n^2 dx$$

Now one may write the first frequency modes *(Karnopp et al., 2013)*

$$\left[\rho A \int_0^l (1)_n^2 dx \right] \ddot{U}_{00} = F_1 + F_2 + F_3 \text{ or } m\ddot{U}_{00} = F_1 + F_2 + F_3 \tag{2.27}$$

which simply states that the external force accelerates the center of mass of the beam. The other zero frequency mode yields

$$\left[\rho A \int_0^l \left(x - \frac{l}{2} \right)^2 dx \right] \ddot{U}_{00} = F_1 + F_2 + F_3 \tag{2.28}$$

or

$$J\ddot{U}_0 = F_1 + F_2 + F_3$$

This equation states that the moment of the external forces about the center of mass produces angular acceleration $\ddot{U}_{00}$, where J is the centroid moment of inertia of beam. The next subsection will present the formulation, which including structural damping.

2.2.4 Incorporation of structural damping

Now one may consider internal damping (the detailed derivation of internal damping is presented in *Appendix C* for ready reference) of the beam and Eq. (2.22) may be rewritten as

$$\rho A\ddot{w}(x,t)-\left(\rho I\ddot{w}''(x,t)\right)'+\left(EIw''(x,t)\right)''-\mu_I\left(\dot{w}'''\right)'$$
$$=F_1\delta(x-x_1)+F_2\delta(x-x_2)+F_3\delta(x-x_3)$$

$$(2.29)$$

$$\rho A\ddot{w}(x,t)-\left(\rho I\ddot{w}''(x,t)\right)'+\omega^2(\rho I\lambda^2-\rho A)-\mu_I\left(\dot{w}'''\right)'$$
$$=F_1\delta(x-x_1)+F_2\delta(x-x_2)+F_3\delta(x-x_3)$$

$$(2.30)$$

where μ_I is the structural damping coefficient, δ is the Dirac-delta function, x_1 and x_2 are the respective distance from left corner to the front and rear suspension of the vehicle and x_3 is the distance of dead weight from the extreme left corner of the vehicle. F_1 and F_1 are the suspension forces of the front and rear suspension system respectively and F_3 is the dead weight. The front and rear suspension forces of the vehicle may be expressed as

$$F_1=C_s^f(V_f-\dot{w}_1)+K_s^f(\int_0^t V_f dt-w_1)$$

$$(2.31)$$

$$F_2=C_s^r(V_r-\dot{w}_2)+K_s^r(\int_0^t V_r dt-w_2)$$

$$(2.32)$$

where, C_s^f and C_s^r are respective damping coefficient of the front and rear damper; V_f and V_r are the road velocity input at front and rear wheel respectively; K_s^f and K_s^r are the suspension stiffness of front and rear suspension system respectively; $\dot{w}_1$ and w_1 are the velocity and displacement of front sprung mass; $\dot{w}_2$ and w_2 are the velocity and displacement of rear sprung mass.

One may assume solution as similar to Eq. (2.24), applying Eq. (2.23) to Eq. (2.30), one may obtain solution as

$$\int_0^l \rho A W_n^2 dx \ddot{U}(t) + \omega_n^2 (\rho I \lambda_n^2 - \rho A) \int_0^l W_n^2 dx U(t) - \rho I \lambda_n^2 \int_0^l W_n^2 dx \ddot{U}(t)$$

$$- \mu_I I \lambda_n^4 \int_0^l W_n^2 dx \dot{U}(t) = F_1 W_n(x_1) + F_2 W_n(x_2) + F_3 W_n(x_3) \tag{2.33}$$

Rearranging Eq. (2.33), one may obtain

$$\rho A \left(1 - \frac{I}{A} \lambda_n^2\right) \int_0^l W_n^2 dx \ddot{U}(t) + \rho A \left(1 - \frac{I}{A} \lambda_n^2\right) \omega_n^2 \int_0^l W_n^2 dx U(t)$$

$$- \mu_I I \lambda_n^4 \int_0^l W_n^2 dx \dot{U}(t) = F_1 W_n(x_1) + F_2 W_n(x_2) + F_3 W_n(x_3) \tag{2.34}$$

Finally, Eq. (2.34) may be represented as

$$m_n \ddot{U}(t) + R_n \dot{U}(t) + k_n U(t) = F_1 W_n(x_1) + F_2 W_n(x_2) + F_3 W_n(x_3) \tag{2.35}$$

where,

$$m_n = \rho A \left(1 - \frac{I}{A} \lambda_n^2\right) \int_0^l W_n^2 dx, \tag{2.36}$$

$$k_n = m \omega_n^2 \int_0^l W_n^2 dx, \tag{2.37}$$

$$R_n = \mu_I I \lambda_n^4 \int_0^l W_n^2 dx \tag{2.38}$$

It is depicted from the Eqs (2.36-2.38) that the rotary inertia affects the dynamics of the beam, which is not being taken in case of Euler beam. However, in this case, the value of $I/A \cdot \lambda_n^2$ is always less than 1. Generally, distributed elements that one may obtain to involve in almost all the system models are lightly damped. It cannot be precisely

identified the location of structure damping from where it arises. The mechanism of energy dissipation is very typical and complicated; some dissipation takes place because of the plastic deformation, and some of the energy radiation from material surfaces. It is not assured in modeling that individual conventional damper will attach to model for representing the damping of distributed elements. It can happen if the damping includes functionally by incorporating it into individual modes. This is accompanied by merely appending R-elements to the mode oscillators of the modal bondgraph. R-element represented in Eq (2.30), where μ_I is varied from 0.01 to 0.1. The next sub section will present the bondgraph modeling to visualize the simulation for different parameters.

2.3 Bondgraph modeling of truck chassis structure

The physical system of a truck chassis (pitch plane model) with front and rear suspension system driven over the random road is presented in Figure 2.1. The boundary condition of the structure is taken as free-free. The dynamic disturbance in vertical direction of the vehicle due to random road conditions is the main attraction of this modeling. The longitudinal and lateral dynamics are not considered in the modeling. The bondgraph technique is being used as a modeling tool, and the bondgraph of the system is created through formulation, which was developed in the previous section. Figure 2.2 presents the bondgraph model of a flexible infinitesimal beam, whereas Figure 2.3 shows the bondgraph model of a flexible beam with internal damping along with suspension system. The rigid body modes appear as simply as inertia elements with associated modal stiffness and damping. The first inertia

parameter is the beam mass (M) and second is the beam moment of inertia (Jg). The transformer (-TF-) elements connected to the rigid body modes, which correctly apply the forces and moments to these elements. The modal masses are taken from Eq. (2.36), whereas modal stiffness and modal damping can be taken from Eq. (2.37) and Eq. (2.38) respectively.
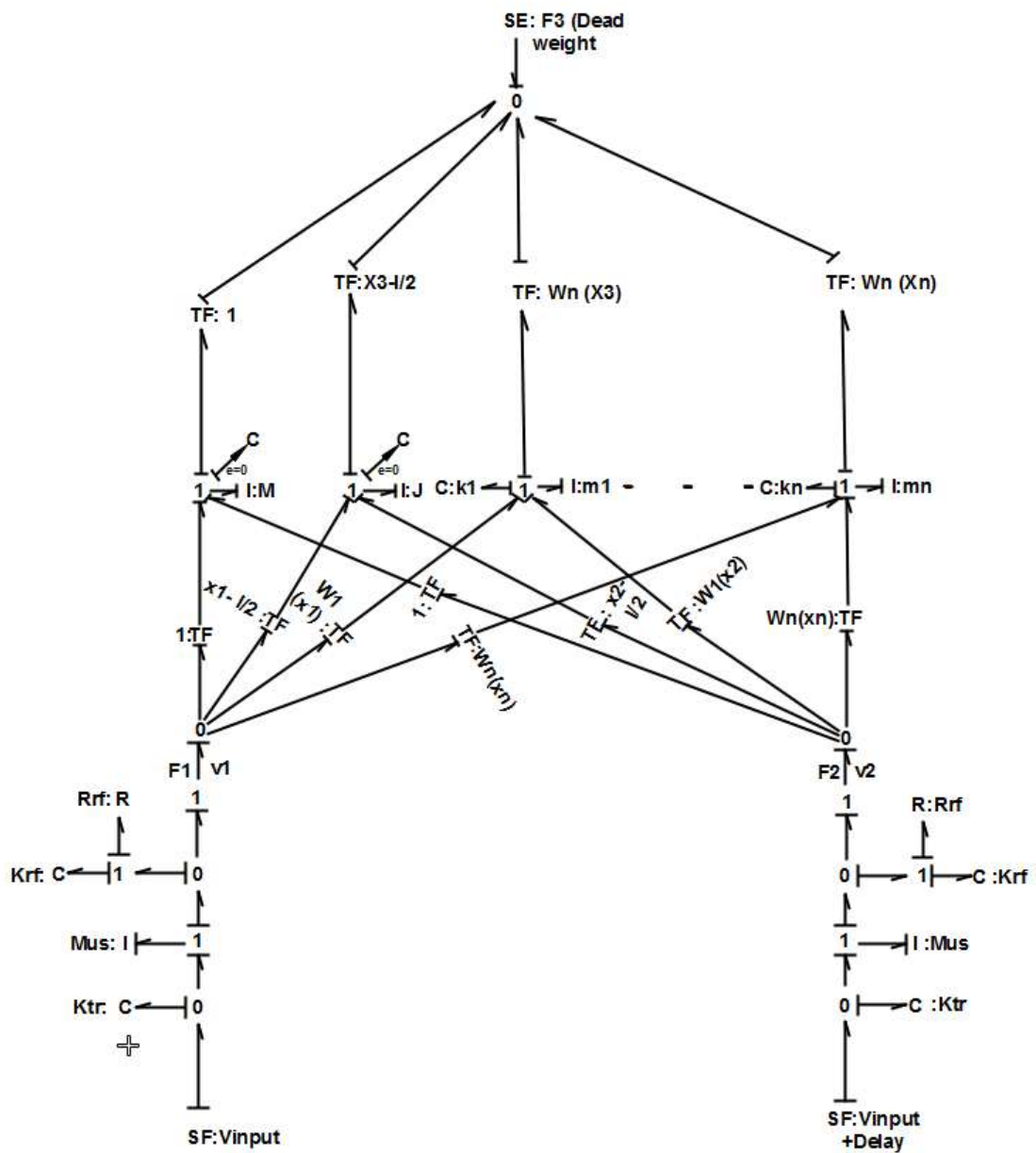
Figure 2.2: Bondgraph model of truck chassis considering internal damping

The system is entirely flexible in transverse and bending but torsionally rigid. Each 0-junction is attached to each 1-junction with modal components through transformer (TF) elements with moduli equal to appropriate mode function.
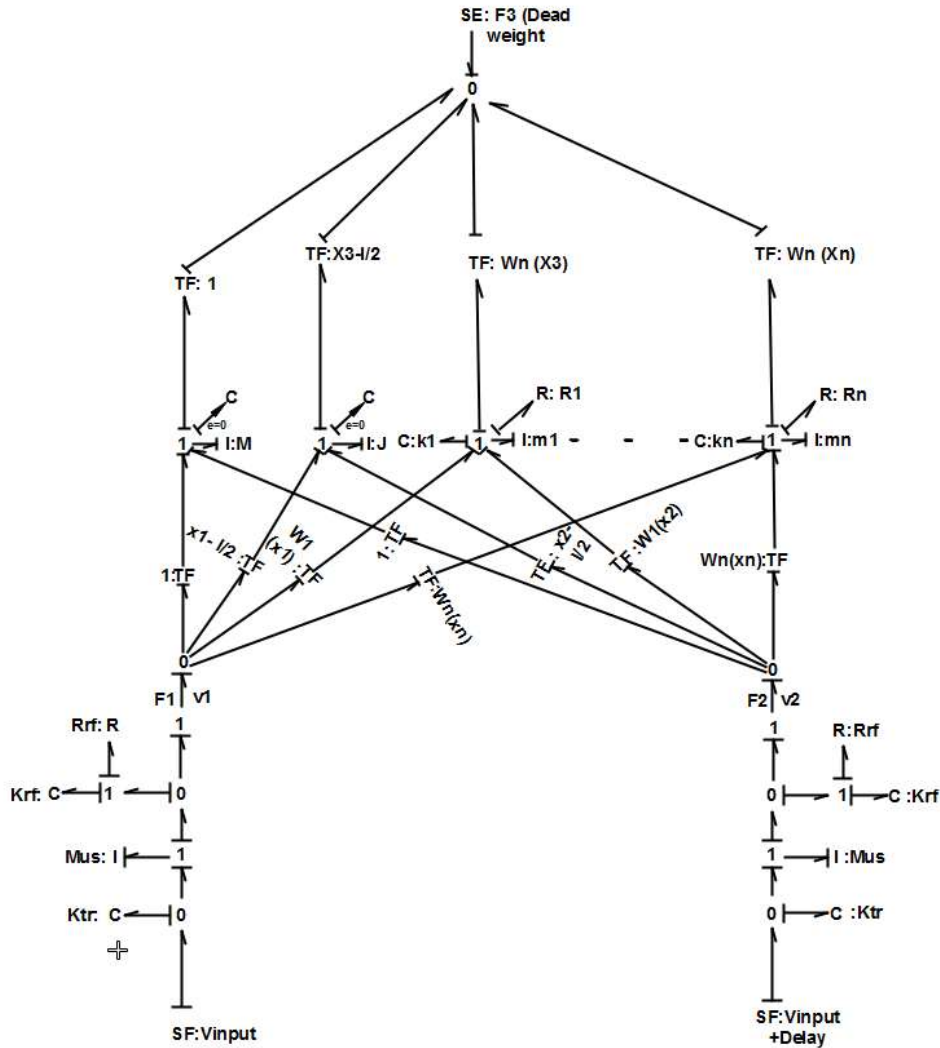
Figure 2.3: Bondgraph model of truck chassis considering internal damping

The transformer function is moduli with shape function (W_n), the values of this function can be determined from Eq. (2.16). The attached systems are then appropriately appended to the external 0-junction bonds to form a complete, low order, very accurate in the model. Figure 2.3 shows a general finite mode representation with two input (front and rear) location, where Eq. (2.26) represents a governing contribution of ith mode.

The TF-element used in the bond graph model (Fig 2.2 and Fig 2.3) is modulus with mode shape functions, which may be achieved through Eq. (2.16). This function will be varied as the value of 'x'. First I-elements (from left side to right side in both Figs 2.2-2.3) represent the Mass of the vehicle and the second denotes the moment of inertia (J). The third and fourth masses are the modal masses, which may be calculated from Eq. 2.36.

In the real world, any distributed elements have some damping property, which resists vibration level up to certain level. Any mechanism cannot quickly identify the value of damping on specific. However, the only quantity of dissipative energy can be determined. It is customary not to attempt to perform detailed modeling of the damping mechanism, but instead to include damping functionally by incorporate its individual modes. This is accomplished by simply appending R-elements to the mode oscillator of the bondgraph. The bondgraph model of the distributed system includes with damping modes are presented in Figure 2.3. The governing equation of this configuration is mentioned in Eq (2.23).

2.4 Numerical simulation

Computer simulation can compress the performance of a system over the years into a few minutes of the computer running time. Simulation models are relatively flexible and can be modified to accommodate the changing environment to the real situation. At present, most of the simulation models are made using differential equations. In this research, a half car flexible model with suspension systems is investigated at different operating speed on different road profile inputs using bondgraph technique and simulator of SYMBOLS-Sonata® and MATLAB/Simulink® software are used. The bondgraph model of the vehicle is simulated for 10 sec to obtain different output

responses. Total 1024 records are used in the simulation and error is kept in the order of

$5.0 \times 10\text{-}4$. Runge-Kutta Gill method of fifth order is used in this present work to solve

the various differential equations generated through bondgraph model.

2.4.1 Road inputs

Two types of road profile inputs are used of the simulation of this system, viz. steady-

state input, and random road input.

(a) Sine wave input

The steady state input has been taken in a sinusoidal form, and the following expression

is used for simulation *(Gupta and Rastogi, 2015)*

$$V_{input} = A_{jump} * \omega * \sin(\omega * t), \text{ for front wheel} \tag{2.39}$$

$$V_{input} = A_{jump} * \omega * \sin(\omega * (t + d/v)), \text{ for rear wheel} \tag{2.40}$$

where, A_{jump} is the amplitude of vibration and ω is the excitation frequency

Table 2.1: Simulation parameters for flexible chassis system (*Rideout,* 2012)

Parameter	Value	Unit
Vehicle length	10	m
Frame mass (Mg)	4350	Kg
Frame Inertia (J)	24000	kg/m^2
Suspension stiffness (K_{sf}, K_{sr})	375, 870	KN/m
Suspension damping (R_{sf}, R_{sr})	31895, 33384	Ns/m
Flexural rigidity (EI)	1.05e+08	N-m^2
Unsprung mass (*Mus*)	50	Kg
x_1, x_2, x_3, x_4	2.95,5.75, 7,3	m

(b) Random road condition

A random road profile is generated according to the International Organization for

Standardization (ISO 8608). It gives a depiction of the road profile through estimation of

the PSD of the vertical displacements G_d, as a function of spatial frequency $n(n = \Omega / 2\pi (cycles)/m)$ and also of angular spatial frequency Ω. ISO 8608 introduces a classification, which is evaluated in accordance with conventional values of spatial frequency $n_0 = 0.1 \; cycles / m$ and angular spatial frequency $\Omega_0 = 1 \; cycles / m$. There are eight classes of roads mainly identified, from class H1 to H8 according to the values of $G_d(n)$ and $G_d(\Omega)$ established in ISO 8608, which are shown in Table 2.2 (*Agostinacchio et al.,* 2014).

Table 2.2: ISO 8608 values of $G_d(n_0)$ and $G_d(\Omega_0)$

Road Class	$G_d(n_0)$ (10^{-6} m^3)		$G_d(\Omega_0)$ (10^{-6} m^3)	
	Lower Limit	**Upper Limit**	**Lower Limit**	**Upper Limit**
H1	-	32	-	2
H2	32	128	2	8
H3	128	512	8	32
H4	512	2048	32	128
H5	2048	8192	128	512
H6	8192	32768	512	2048
H7	32768	131072	2048	8192
H8	131072	-	8192	-
	$n_0 = 0.1 \; cycles / m$		$\Omega_0 = 1 \; cycles / m$	

In the simulation, ISO 8608 provides the roughness of the road surface profile, which may be stated using the following equations:

$$G_d(n) = G_d(n_0)\left(\frac{n}{n_0}\right)^{-w} \tag{2.41}$$

$$G_d(\Omega) = G_d(\Omega_0)\left(\frac{n}{n_0}\right)^{-w} \tag{2.42}$$

where w denotes the waviness, and its value is taken to be 2 in this case. In this research, random road inputs have been developed by taking into consideration the PSD of vertical displacement G_d as a function of spatial frequency n.

Beginning with a distributed road profile to specify the value of spatial frequency n, loped within a frequency band Δn, the PSD function value is represented through the following expression as

$$G_d(n) = \lim_{\Delta n \to 0} \left(\frac{\psi_x^2}{\Delta n} \right) \tag{2.43}$$

where, mean square value is denoted by ψ_x^2 which signifies the component of the signal for the purpose of spatial frequency n, contained by the frequency band Δn. Accordingly, the signal of road profile is discretized and thus it is characterized by a series of elevation points along with evenly spaced. Here, road profile length is denoted by L whereas, sampling interval is denoted by B. Further, the maximum value of sampling spatial frequency c is $1/B$ the maximum effective sampling spatial frequency (n_{eff}) is $n_{max}/2$ and the discretized spatial frequency values n_i are equally spaced under the frequency domain, with an interval of (Δn) as $1/L$. So herein, generic spatial frequency value n_i can be regarded as $i.\Delta n$ and Eq. (2.43) may be written in the discrete form as

$$G_d(n) = \frac{\psi_x^2(n_i, \Delta n)}{\Delta n} = \frac{\psi_x^2(i.\Delta n, \Delta n)}{\Delta n} \tag{2.44}$$

53

where i varying from 0 to N as $\dfrac{n_{max}}{\Delta n}$, one may obtain the road profile by a simple

harmonic function

$$h(x) = A_i \cos(2\pi.n_i.x + \varphi) = A_i \cos(2\pi.i.x.\Delta n + \varphi) \tag{2.45}$$

where, amplitude is denoted by A_i, spatial frequency is denoted by n_i and phase angle

is φ. One may generate harmonic signal through mean square value

$$\psi_x^2 = \frac{A_i^2}{2} \tag{2.46}$$

Therefore,

$$G_d(n_i) = \frac{\psi_x^2(n_i)}{\Delta n} = \frac{A_i^2}{2.\Delta n} \tag{2.47}$$

Table 2.3: k values for ISO road roughness classification

Road Class		k
Lower Limit	**Upper Limit**	
H1	H2	3
H2	H3	4
H3	H4	5
H4	H5	6
H5	H6	7
H6	H7	8
H7	H8	9

It has been shown in several works, where development of an artificial road profile

using the Eq. (2.45) is only possible if the PSD function of vertical displacements is

well-known, presuming a random phase angle φ_i following a uniform probabilistic

distribution within range 0 to 2π. The artificial profile can be given as

$$h(x) = \sum_{i=0}^{N} A_i \cos(2\pi.n_i.x + \varphi_i) = \sum_{i=0}^{N} \sqrt{2.\Delta n.G_d(i.\Delta n)} \cdot A_i \cos(2\pi.i.x.\Delta n + \varphi) \qquad (2.48)$$

Using Eq. (2.47) in Eq. (2.45), a random road profile can be generated according to ISO classification by the following equation,

$$h(x) = \sum_{i=0}^{N} \sqrt{\Delta n.} \cdot 2^k \cdot 10^{-3} \cdot \left(\frac{n_0}{i \cdot \Delta n} \right) \cos(2\pi.i.x.\Delta n + \varphi) \qquad (2.49)$$

where x is the abscissa variable from 0 to L; Δn is $1/L$; n_{max} is taken as $1/B$; N is

$\frac{n_{max}}{\Delta n}$ or L/B; where $L = 250$, $N = 100$; constant is denoted as k, depending from

ISO road profile classification. It has also assumed integers augmenting from 3 to 9, which is corresponding to the profiles from class H1 to H8 (as shown in Table 2.3); here k is assumed to take the value 3 corresponding to the class A road profile and $G_d(n_0)$ is taken to be 32, where n_0 is $0.1 \, cycles/m$; φ_i random phase angle following an uniform probabilistic distribution within range 0 to 2π. In this work, four road conditions (H1-H4) are considered, which is shown in Figures 2.4-2.7.
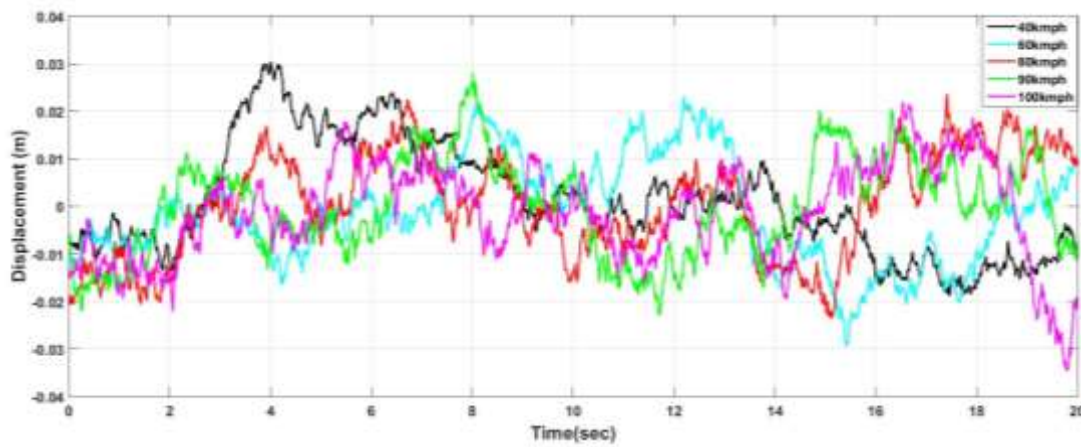
Figure 2.4: Random road profile of H1 road category at 40kmph, 60kmph, 80kmph, 90kmph, and 100kmph
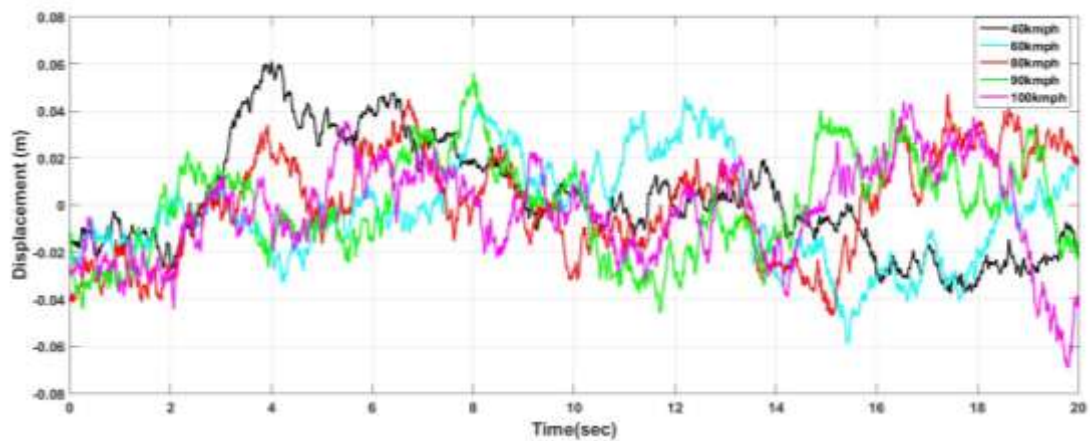
Figure 2.5: Random road profile of H2 road category at 40kmph, 60kmph, 80kmph, 90kmph, and 100kmph
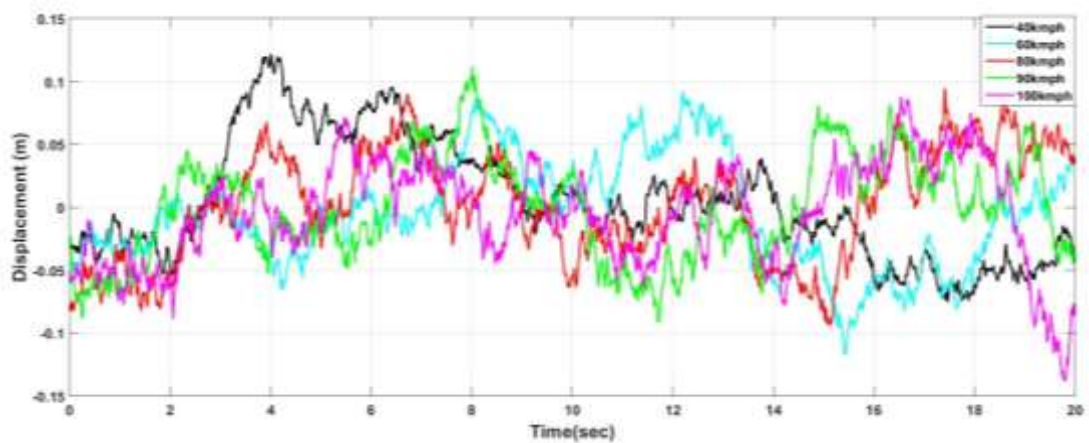
Figure 2.6: Random road profile of H3 road category at 40kmph, 60kmph, 80kmph, 90kmph, and 100kmph
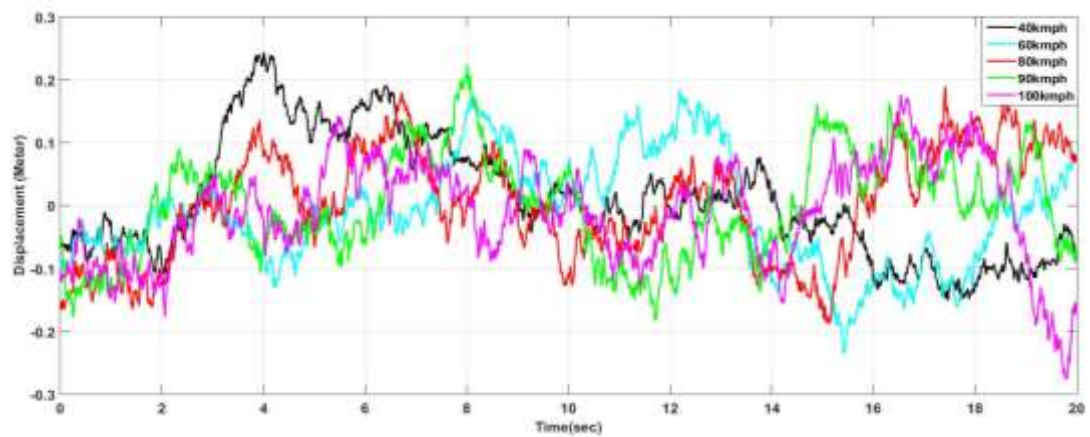
Figure 2.7: Random road profile of H4 road category at 40kmph, 60kmph, 80kmph, 90kmph, and 100kmph

The simulation of different road category is obtained by MATLAB/Simulink of the previously discussed ISO 8608 random input. This road profiles are simulated for five different speeds viz. 40 kmph, 60 kmph, 80 kmph, 90 kmph, and 100 kmph. Figure 4 shows H1 road condition, where unevenness of the random type road with maximum magnitude is 0.03m in an upward direction at 40 km/hr and -.035 m in a downward direction at 100 km/hr. Similarly, H2, H3, and H4 road category having a maximum magnitude 0.06 m, 0.12 m, and 0.24 m respectively in an upward direction at 40 km/hr and -065m, -0.12m, and -0.24 m; in a downward direction at 100 km/hr.

2.4.2 Results and Discussion

The parameters of the vehicle used in the simulation are presented in Table 2. The model is exhibited first on sine wave input from start to end; run for 20 sec with zero initial conditions. The amplitude of sine wave is 0.01m and input frequency is taken 50 Hz.
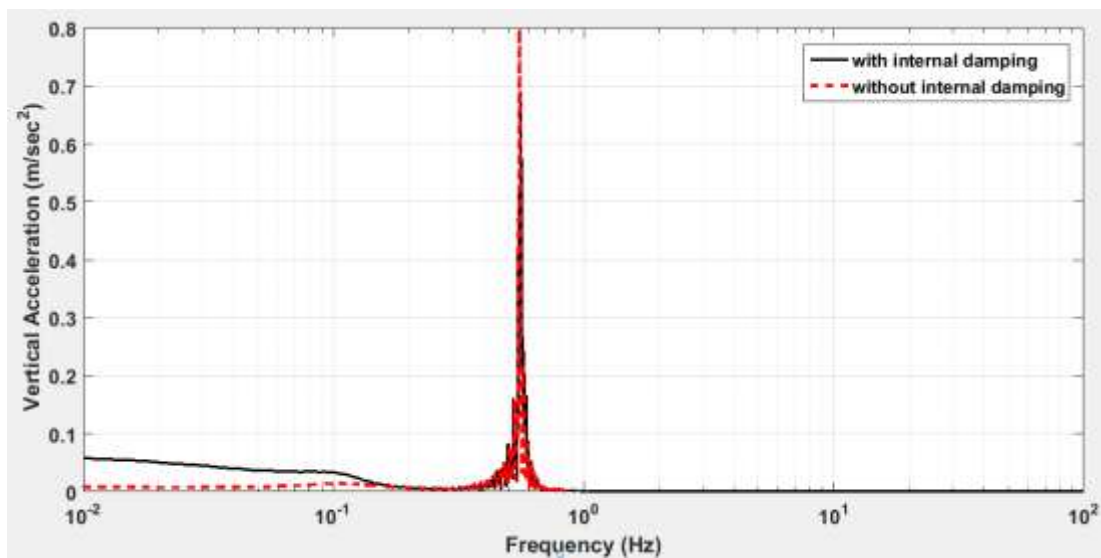
Figure 2.8: Vertical response of vertical acceleration of chassis at steady state input

In Figure 2.8, the magnitude of vertical acceleration is 0.8 m/sec^2 in un-damped condition whereas acceleration amplitude has been reduced to 0.7 m/sec^2 in damped

condition. Thus the magnitude of vibration has been reduced up to 12-15% due to the impact of structural damping of the vehicle chassis. Similarly in Figure 2.9, the amplitude of pitching acceleration has been reduced by 20%, due to the influence of structural damping. However, frequencies in both conditions are having almost similar value. The dead load on the center of chassis has been taken around 500N, which lies in the downward direction.
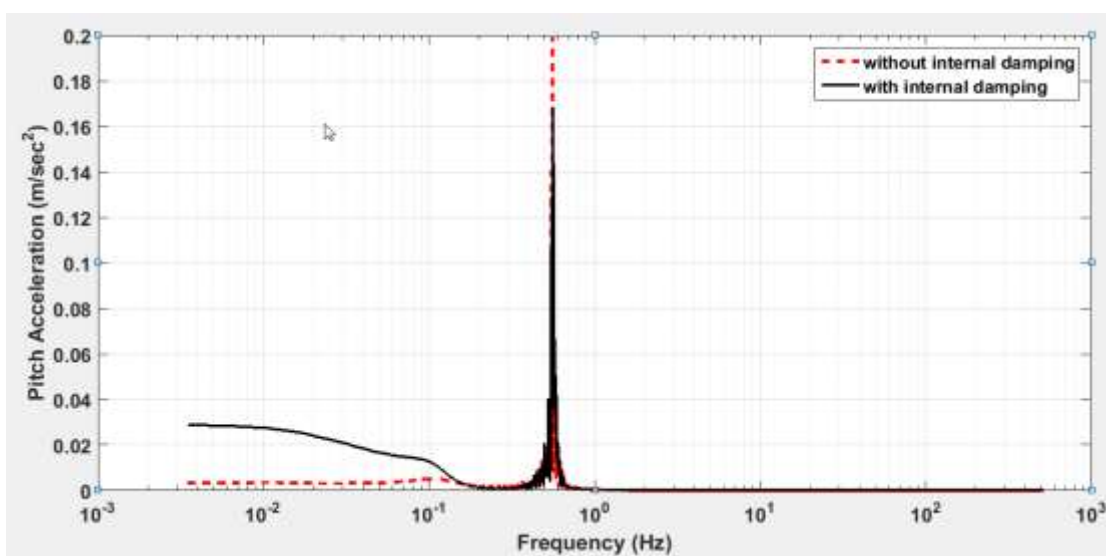
Figure 2.9: Response of pitch acceleration of chassis at steady state input

The PSD responses of different modes at sine wave condition are shown in Figures 2.10-2.11. The un-damped condition of beam is presented in Figure 2.10, where first mode frequency is lower than the third mode frequency, which is higher. However, acceleration magnitude of the second mode is relatively lower than the other two modes. The damped condition of beam is shown in Figure 2.11, where the influence of internal damping is also shown in term of PSD response. The result shows that the magnitude has the reduced due to the effect of internal damping, but the frequency remains same. In both figures, the first mode frequency is comparatively lower than the other two modes.
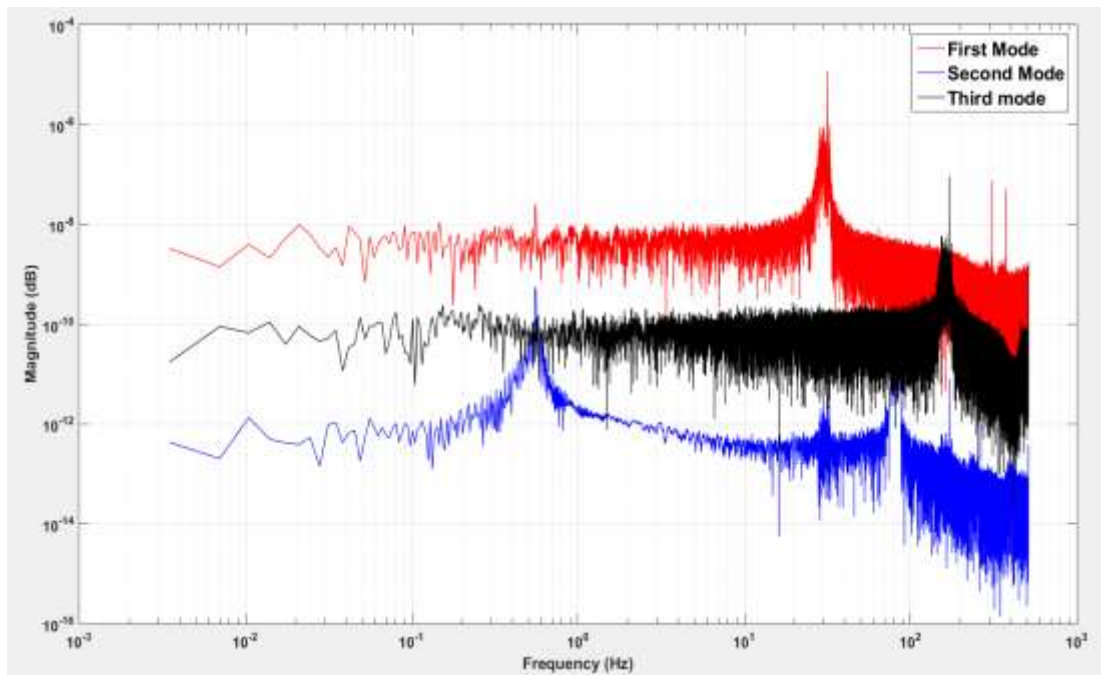
Figure 2.10: PSD Response of different modes under sine wave condition
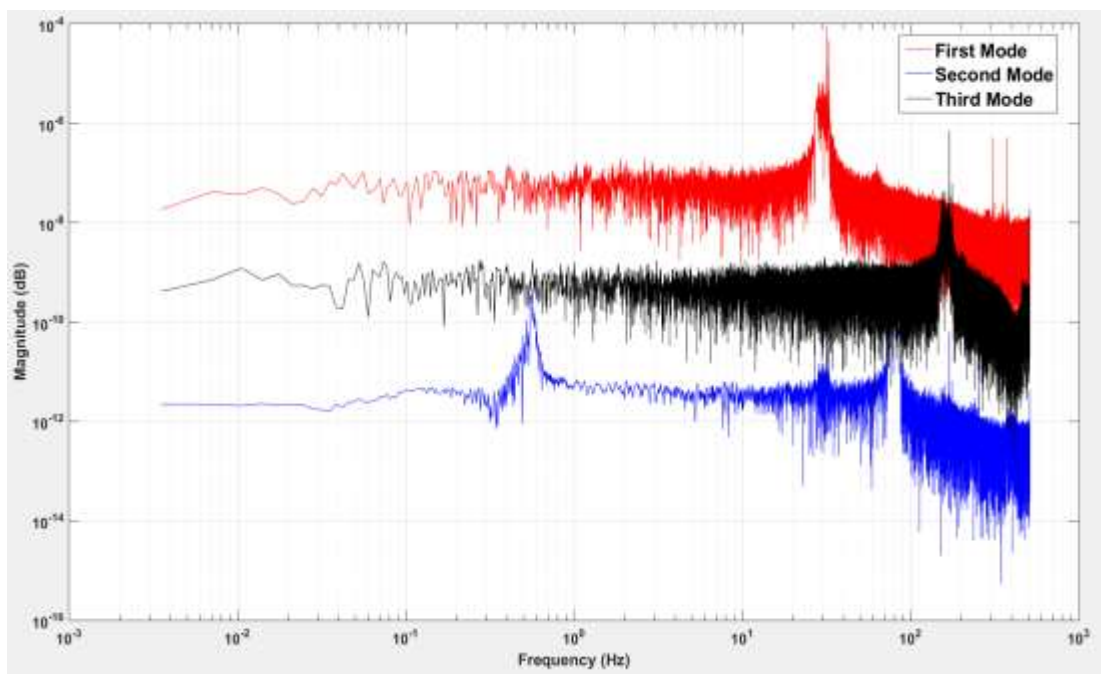
Figure 2.11: PSD Response of different modes of chassis under sine wave condition with internal damping

Figures 2.12-2.15 present the acceleration response of the beam which has been analyzed for four random road conditions (H1- H4) prescribed by ISO 8608, in which H1 and H4 are the best and the worst road conditions respectively. Each road condition is simulated for four different road speeds from 40 kmph to 100kmph.

In the Figure 2.12, the magnitude of acceleration is increased with speed. It is found that magnitude is higher at 100 km/hr and lower at 40 km/hr. Although, the frequency is observed maximum at 40 km/hr and minimum at 100 km/hr. The same pattern has been noticed at H2, H3 and H4 road conditions. Figure 2.12 (a) demonstrates a response of beam in un-damped condition, where maximum magnitude is 0.65 m/sec^2 at 100 km/hr and 0.25 m/sec^2 at 40 km/hr in H1 road condition. This magnitude is reduced up to 0.58 m/sec^2 at 100 km/hr and 0.22 m/sec^2 at 40 km/hr, due to structural damping effect as shown in Figure 2.12 (b).

Similarly in Figure 2.13 (a) the average magnitude of the chassis is 0.45 m/sec^2 in un-damped condition, but it is reduced further up to 0.41 m/sec^2 in damped condition, which can be seen in Figure 2.13 (b).

In Figure 2.14 (a), the average magnitude of the infinitesimal beam is increased up to 1.04 m/sec^2 from H2 road condition in the un-damped situation and 0.97 m/sec^2 in damped condition as depicted in Figure 2.14 (b). In the worst road condition (H4), the average magnitude is maximum (i.e., 2.13 m/sec^2) in un-damped condition, and 2.11 m/sec^2 in damped condition.

In Figure 2.15 (a), the magnitude of acceleration is exceeded from 4.5 m/sec^2 in un-damped condition at 100 km/hr, whereas the maximum magnitude of acceleration is lower from the value of 4.4 m/sec^2 at 100 km/hr (presented in Figure 15(b)).
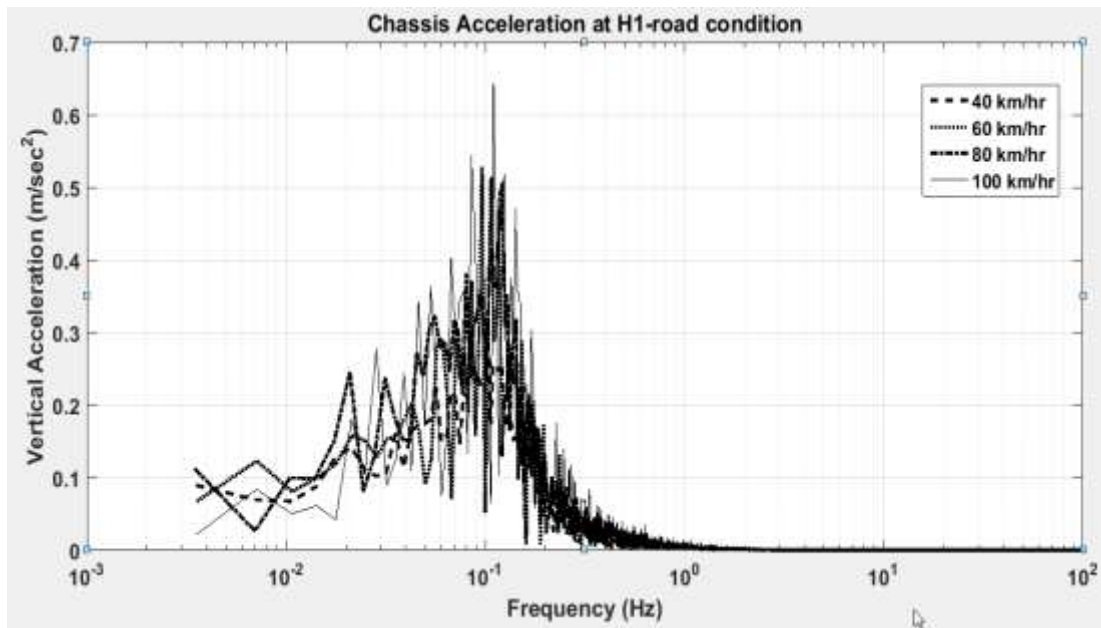
(a)
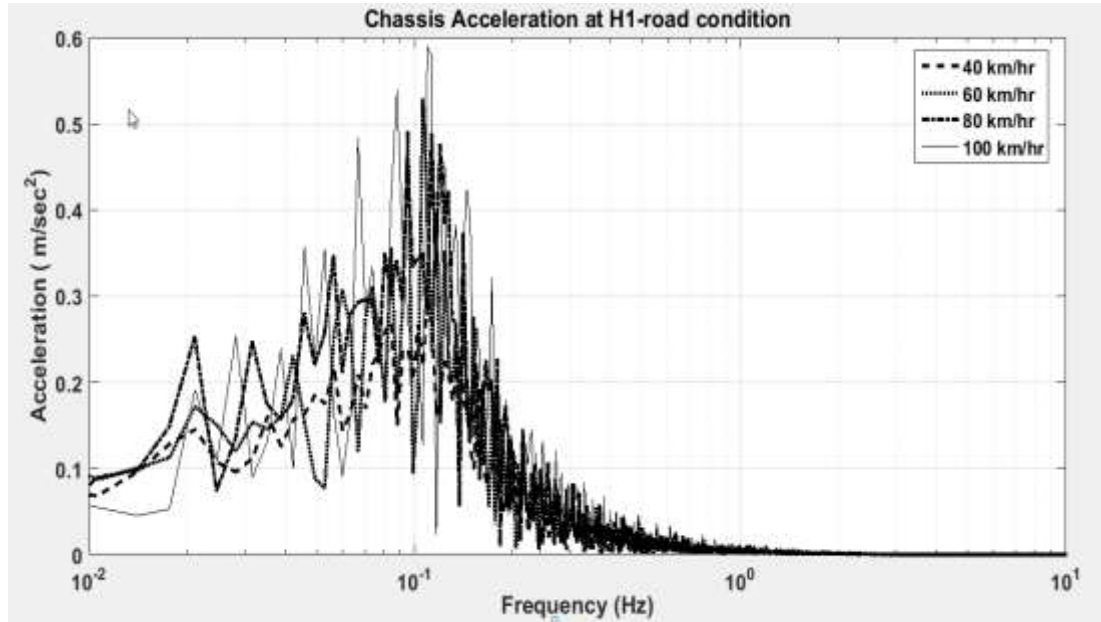
(b)

Figure 2.12: (a) Response of chassis acceleration at various random road input in H1 road as per ISO 8608, (b) Response of chassis acceleration consideration of internal damping at different random input in H1 road condition as per ISO 8608
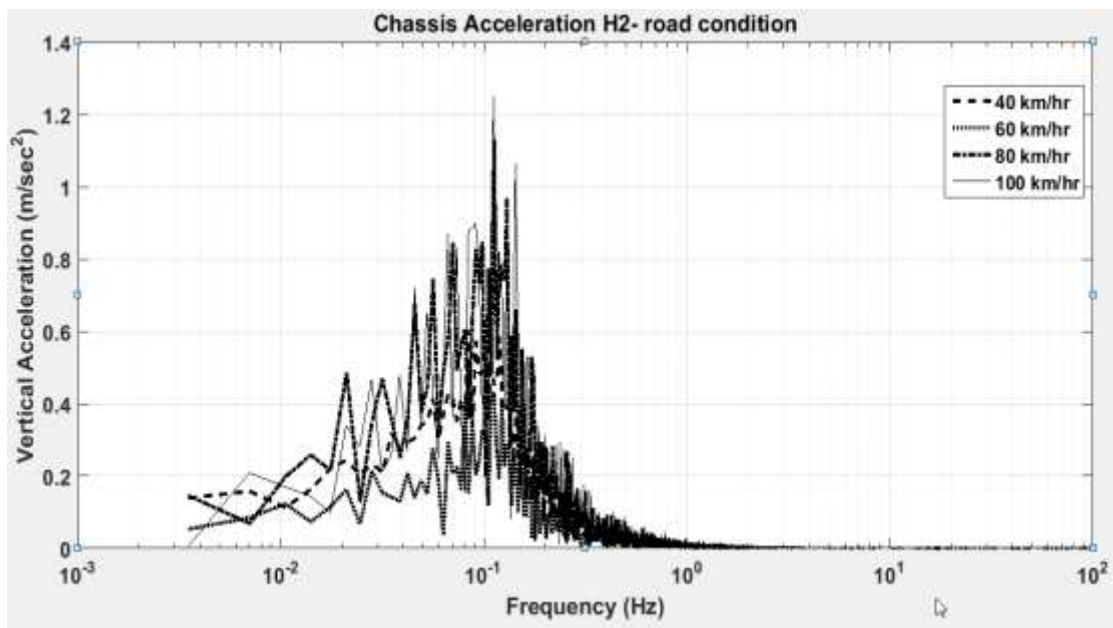
(a)
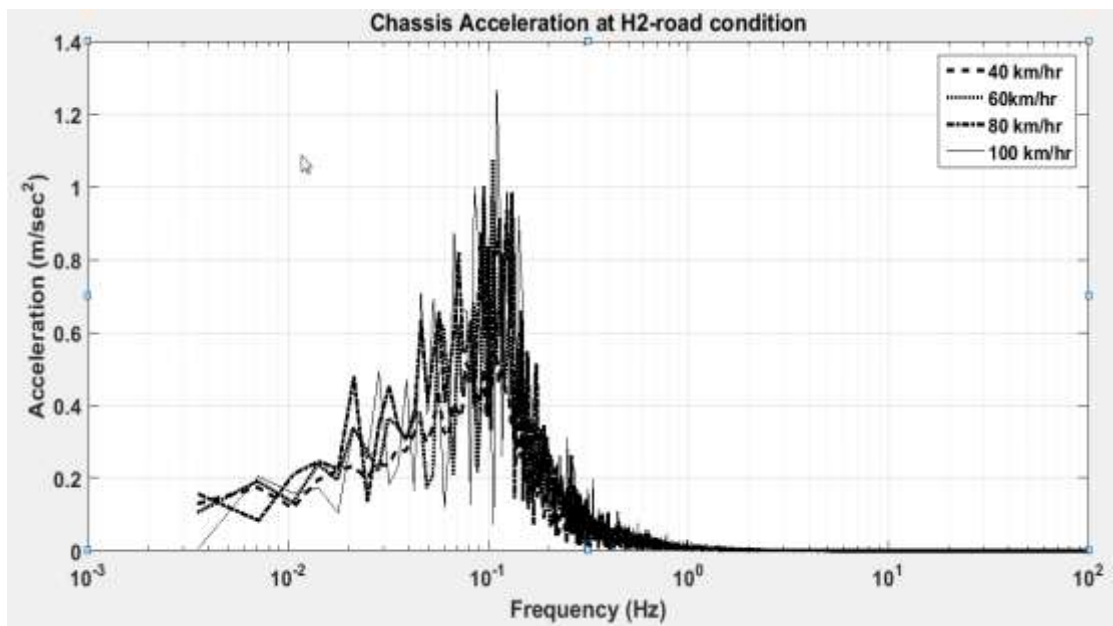
(b)

Figure 2.13: (a) Response of chassis acceleration at various random road input in H2 road as per ISO 8608, (b) Response of chassis acceleration consideration of internal damping at different random input in H2 road condition as per ISO 8608
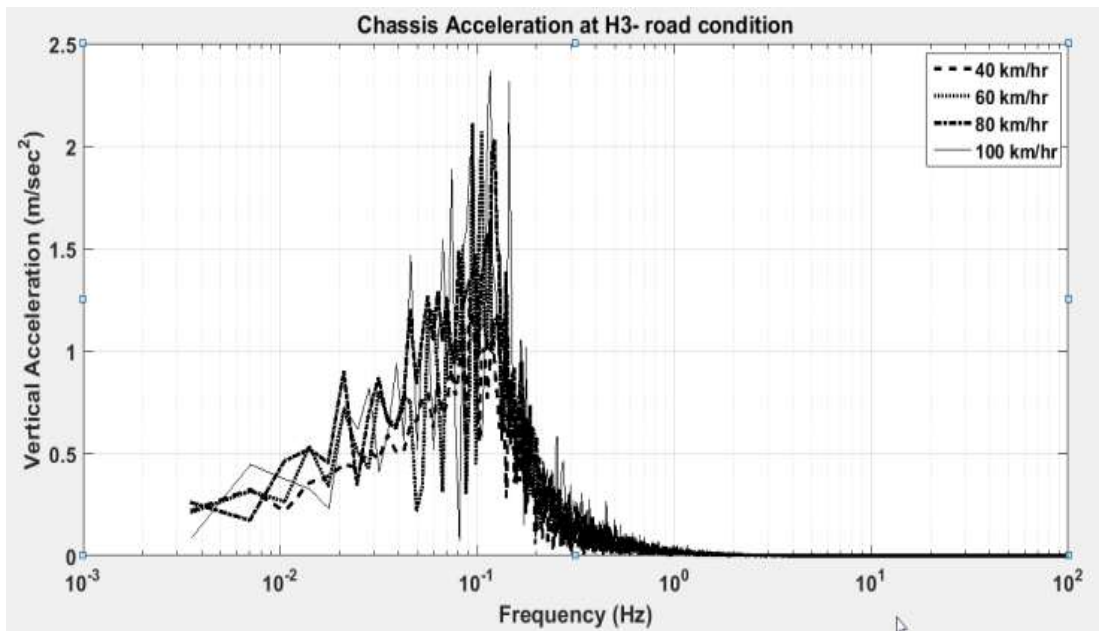
(a)
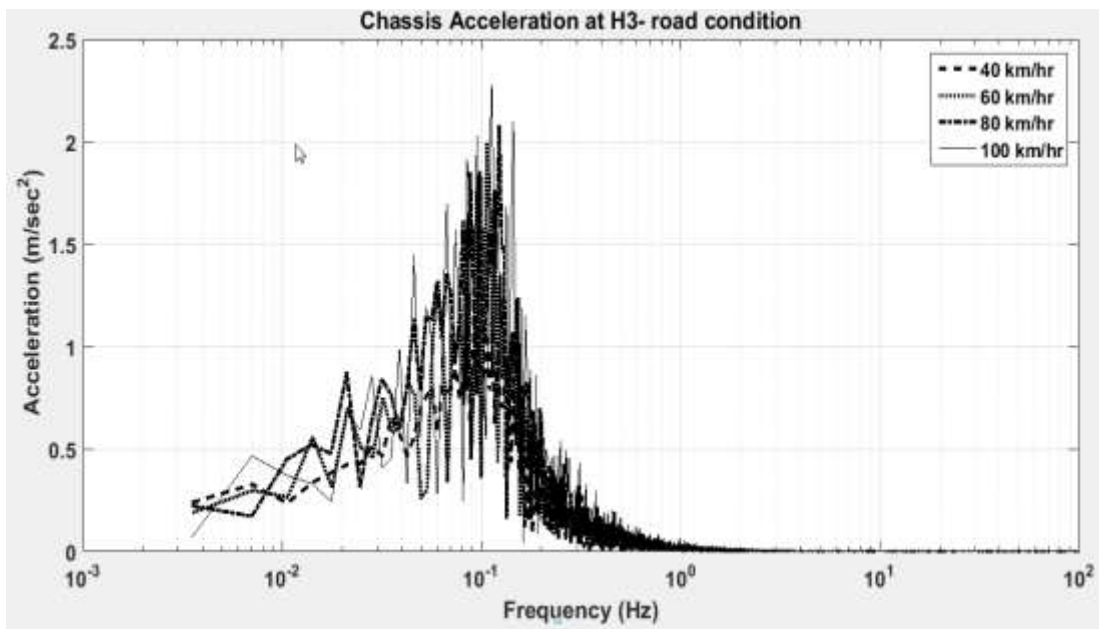
(b)

Figure 2.14: (a) Response of chassis acceleration at various random road input in H3 road as per ISO 8608, (b) Response of chassis acceleration consideration of internal damping at different random input in H3 road condition as per ISO 8608
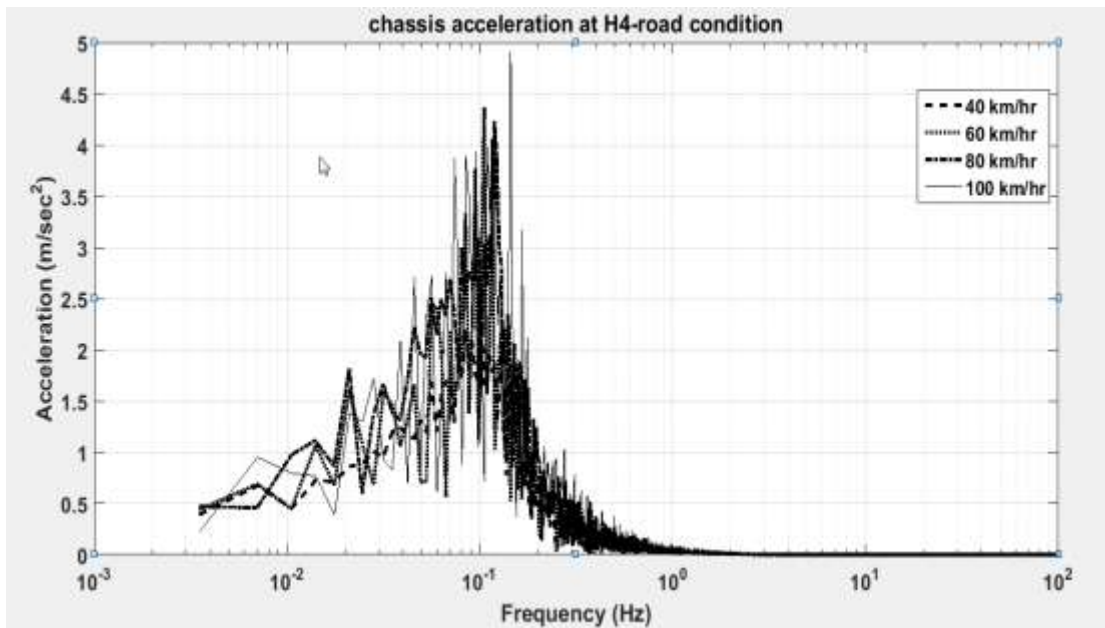
(a)
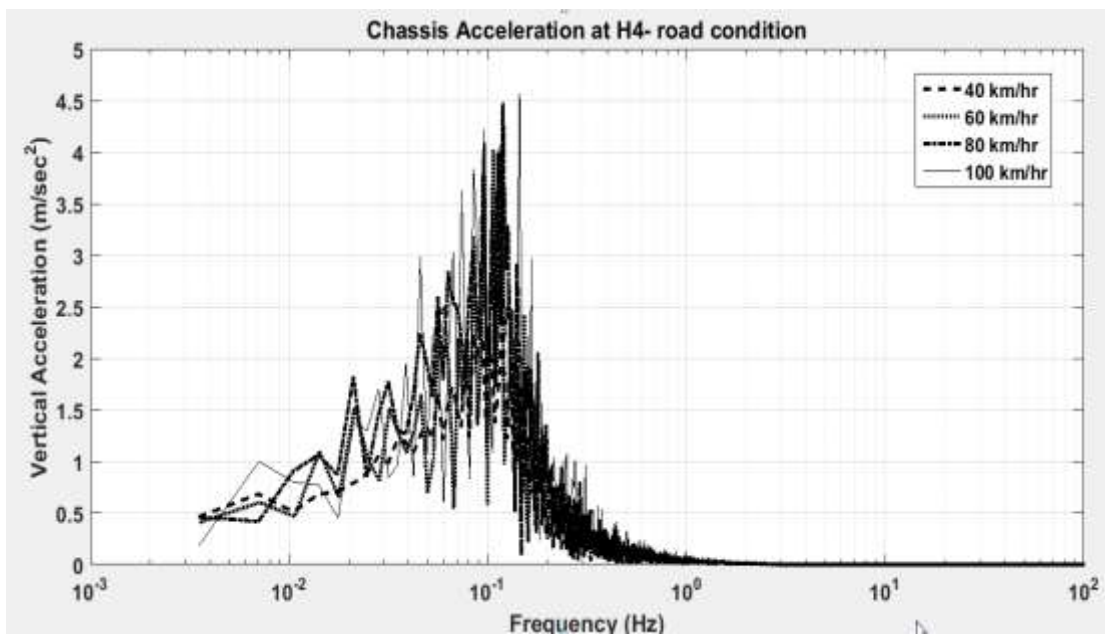
(b)

Figure 2.15: (a) Response of chassis acceleration at various random road input in H4 road as per ISO 8608, (b) Response of chassis acceleration consideration of internal damping at different random input in H4 road condition as per ISO 8608

It is evident from all above figures that the structural damping of the base structure of heavy vehicle plays a significant role in ride vibrations as the magnitude of damping is raised, the magnitude of vibration is reduced drastically. The next section will present an extended formulation for flexural behaviour trauck chassis through extended Lagrangian formalism.

2.5 Alternative formulation of flexural behavior for truck chassis through extended Lagrangian-Hamiltonian approach

The extended formulation is based on extended Lagrangian density function and Hamiltonian density function. Previous studies have been attempted to enhance the scope of Lagrange's equation in their several ways to incorporate all these influences of dissipation, constraints of the non-conservative dynamical system in the Lagrangian formulation, and showed the connection between symmetries and existence of conserved quantities, and thus finding invariants of motion of dynamical systems. Some significant works in this area were reported by *Vujanovic (1989),Vujanovic et al.* (1978) *, Djukic et al.* (1975) *and Djukic* (1973) in their several papers. *Vujanovic* (1989) has formulated a method for finding the conserved quantities of non-conservative holonomic system, which is based on the differential variational principle of d'Alembert. To overcome all these limitations and enlarging the scope of Lagrangian-Hamiltonian mechanics, a new proposal of additional time like variable 'umbra-time' was made by *Mukherjee* (1994) and this new concept of umbra-time leads to a peculiar form of the equation, which is termed as umbra-Lagrange's equation. *Mukherjee and Samantaray* (1997), *Mukherjee and Karmankar* (2000) have extended this formulation for the continuous system over several manifolds where they had presented a case study

of rotor system and finding a cause of asymmetries due to non-potential and non-conservative parameters.

One of the most important insights gained from the umbra-Lagrangian formalism is that its underlying variational principle (*Mukherjee,* 2001*)* is possible, which is based on their cursive minimization of functional. Once such a least action principle is established, many significant results of analytical mechanics may be extended to a general class of system. In this direction, all these notions in an extended manifold comprising of real time, and umbra and real-time displacements and velocities are defined in reference (*Mukherjee et al,* 1999; *Mukherjee and Rastogi,* 2007*; Mukherjee et al.,* 2005*; Mukherjee et al.,* 2006). The umbra Lagrangian theory has been used successfully to study invariants of motion for non-conservative mechanical and thermo-mechanical systems *(Mukherjee et al.,* 2009*; Mukherjee et al.,* 2011*)*.

Thus the main scope of this work is formulate a system with distributed properties, which may be dependent on time and also on the spatial position. Further interior time of the system (which is known as umbra time) will also incorporated with this given positions. In this research work, the continuous system includes rotary inertia or pitch inertia, internal damping and external damping. The vehicle beam experience with various kind of road irregularities. The umbra-Lagrangian density function for vehicle frame may be written as,

$$\mathcal{L} = \int_{x_0}^{x_1} \left[\frac{1}{2}\rho\left(\frac{\partial w(\eta,x)}{\partial \eta} \right)^2 - \frac{1}{2}EI\left(\frac{\partial^2 w(\eta,x)}{\partial x^2} \right)^2 + \frac{1}{2}I_d\left(\frac{\partial^2 w(\eta,x)}{\partial \eta\, \partial x} \right)^2 - \mu_I I \left\{ \left(\frac{\partial^3 w(t,x)}{\partial t\, \partial x^2} \right) \frac{\partial^2 w(\eta,x)}{\partial x^2} \right\} \right] dx$$

(2.50)

where ρ is the mass density, *EI* is the rigidity, μ_I is the internal damping, w (.) is the displacement coordinates of the base frame in real and umbra time. Young's modulus of the

shaft material, I is the cross-section moment of inertia, the third term is contributed by rotary moments with the angular velocity $\partial^2 w(\eta, x) / \partial\eta\, \partial x$, the fourth term is umbra-potential due to external damping. All terms are in per unit length. The expression of homotopic functions and its variation for the umbra-Lagrangian density variation has been adopted from *Rastogi*, 2005. After considering variations in w as $w^* = w + \varepsilon\, \hat{w}$, and homotopic functions as $w(t, x, a)$ and $w(t, x, b)$, this expression has been further extended with notations as a $t, a = t$ and $t, b = \eta$ with $w(t, x, a) = w(t, x)$ and $w(t, x, b) = w(\eta, x)$, thus one may obtain the variations in the action integral and expressed as

$$\delta I = \varepsilon \int_{t_0}^{t_1} \int_{x_0}^{x_1} \left[\left[\left\{ \begin{array}{l} \dfrac{\partial}{\partial t}\left(\rho\, \dot{w}(\eta, x)\right) - \dfrac{\partial^2}{\partial x^2}\left(EI\, \dfrac{\partial^2 w(\eta, x)}{\partial x^2}\right) - \\[2mm] \dfrac{\partial^2}{\partial t\, \partial x}\left(\rho I\, \dfrac{\partial^2 w(\eta, x)}{\partial t\, \partial x}\right) \end{array} \right\} w(\eta, x) - \mu_I I\left\{ \dfrac{\partial^2}{\partial x^2}\left(\dfrac{\partial^3 w(t, x)}{\partial t\, \partial x^2}\right)\right\} \right] \right] dt\, dx$$

$$- \left\{ \begin{array}{l} \dfrac{\partial}{\partial x} E I\, \dfrac{\partial^2 w(\eta, x)}{\partial x^2}\, \hat{w}(\eta, x) + \dfrac{\partial}{\partial x}\, \mu_I I\left\{\left(\dfrac{\partial^3 w(t, x,)}{\partial t\, \partial x^2}\right)\hat{w}(\eta, x)\right\} \\[3mm] - \dfrac{\partial}{\partial t}\displaystyle\sum_{i=1}^{2}\rho\left(I_d\, \dfrac{\partial^2 w(\eta, x)}{\partial t\, \partial x}\right)\hat{w}(\eta, x) \end{array} \right\} \Bigg|_{x_0}^{x_1}$$

$$+ \left\{ EI\, \dfrac{\partial^2 w(\eta, x)}{\partial x^2}\right\}\dfrac{\partial\hat{w}(\eta, x)}{\partial x} + \mu_I I\left\{\left(\dfrac{\partial^3 w(t, x)}{\partial t\, \partial x^2}\right)\dfrac{\partial\hat{w}(\eta, x)}{\partial x}\right\} \Bigg|_{x_0}^{x_1} dt = 0 \qquad (2.51)$$

where, the first part of the Eq. (2.51) gives umbra-field equations by equating the coefficients of W and the second part gives the boundary conditions at two ends. Now re-arranging first part in $\eta - t$ form, umbra field equations may be written after taking the limit $\eta \to t$ as

$$
\left[
\begin{array}{l}
\left[\dfrac{\partial}{\partial t}\left(\underset{\eta \to t}{Lim}\, \rho\, \dot{w}(\eta, x) \right) + \dfrac{\partial}{\partial x^2}\left(\underset{\eta \to t}{Lim}\, EI\, \dfrac{\partial^2 w(\eta, x)}{\partial x^2} \right) \right] \\[4mm]
\left[-\dfrac{\partial^2}{\partial t\, \partial x}\left(\underset{\eta \to t}{Lim}\, \rho I_d\, \dfrac{\partial^2 w(\eta, x)}{\partial \eta\, \partial x} \right) \right] \\[4mm]
\left[-\mu_i\left\{ \dfrac{\partial^2}{\partial x^2}\left(\dfrac{\partial^3 w(t, x)}{\partial t\, \partial x^2} \right) \right\} \right]
\end{array}
\right] = 0
\qquad (2.52a)
$$

whereas the second part of Eq. (2.51) gives a set of boundary condition at each end, which may be expressed after taking the limit $\eta \to t$ as

$$
\text{either } \left\{ -\dfrac{\partial}{\partial x}\left(EI\, \dfrac{\partial^2 w(t, x)}{\partial x^2} + \mu_I I\left(\dfrac{\partial^3 w(t, x)}{\partial t\, \partial x^2} \right) \right) + \dfrac{\partial}{\partial t}\left(\rho I_d\, \dfrac{\partial^2 w(t, x)}{\partial t\, \partial x} \right) \right\} = 0
\qquad (2.52b)
$$

or $w(t, x) = 0$ at each end.

Likewise, other boundary conditions may be written as

$$
\text{either } \left\{ -\dfrac{\partial}{\partial x}\left(EI\, \dfrac{\partial^2 w(t, x)}{\partial x^2} + \mu_i\left(\dfrac{\partial^3 w(t, x)}{\partial t\, \partial x^2} \right) \right) + \dfrac{\partial}{\partial t}\left(\rho I_d\, \dfrac{\partial^2 w(t, x)}{\partial t\, \partial x} \right) \right\} = 0
\qquad (2.52c)
$$

$$
\text{either } \left\{ EI\, \dfrac{\partial^2 w(t, x)}{\partial x^2} + \mu_I I\left(\dfrac{\partial^3 w(t, x)}{\partial t\, \partial x^2} \right) \right\} = 0 \text{ or } \dfrac{\partial w(t, x)}{\partial x} = 0
\qquad (2.52d)
$$

The above boundary conditions reflect different types of physical conditions at two ends. The first one reflects force and moment balance at the boundaries, whereas the second one reflects geometric constraints. There are four pairs of boundary conditions consisting of dynamic and geometric conditions. The first part in each of the above four pairs includes shearing force balance and bending moment balance, and are the dynamic boundary conditions. The second part in each pair depends on displacement or slopes and constitutes the geometric or essential boundary conditions. The next

subsection will present extended Noether's field equation for one dimensional beam for vehicle frame.

2.5.1 Extended Noether's field equation for one-dimensional infinitesimal beam

Extended Noether's field equation for the one-dimensional continuous system is achieved for umbra-Lagrangian density given by Eq. (2.50), and infinitesimal generators of symmetry and its prolongation are expressed in *Appendix D* for ready reference. The function Z_1 and Z_2 for Eq. (2.50) may be written as

$$Z_1 = \rho A \dot{w} + I_d \frac{\partial}{\partial x} \dot{w}' - I_d \dot{w}'' \tag{2.53}$$

$$Z_2 = -I_d \ddot{w}' - EIw'' - EIw'' + \mu_i [-\dot{w}'' + \dot{w}'''] \tag{2.54}$$

Now, one has to compute $\underset{\eta \to t}{Lim} \, p_r^{(3)} \bar{V}_t(\mathcal{L})$, which may be expressed after simplification as

$$\underset{\eta \to t}{Lim} \, p_r^{(3)} V_t(\mathcal{L}) = +\mu_I \dot{w}'' \tag{2.55}$$

The extended Noether's field equation for umbra-Lagrangian density may be obtained through

$$D_t Z_1 + D_x Z_2 + \mu_I \dot{w}'' = 0 \tag{2.56}$$

$$\int_{x_0}^{x_1} D_t Z_1 dx + Z_2 \big|_{x_1} - Z_2 \big|_{x_0} + \int_{x_0}^{x_1} [\mu_I \dot{w}''] dx = 0 \tag{2.57}$$

The umbra Lagrangian density for one-dimensional infinitesimal beam structure may be written considering suspension forces and external forces with including gyroscopic coupling as

$$\mathcal{L} = \mathcal{L}_1 + \mathcal{L}_2$$

where,

$$L_1 = \int_0^l \left[\begin{array}{l} \dfrac{1}{2}\rho\left(\dfrac{\partial w(\eta,x)}{\partial\eta}\right)^2 - \dfrac{1}{2}EI\left(\dfrac{\partial^2 w(\eta,x)}{\partial x^2}\right)^2 + \dfrac{1}{2}I_d\left(\dfrac{\partial^2 w(\eta,x)}{\partial\eta\,\partial x}\right)^2 - \mu_I I\left\{\left(\dfrac{\partial^3 w(t,x)}{\partial t\,\partial x^2}\right)\dfrac{\partial^2 w(\eta,x)}{\partial x^2}\right\} \\ + F_1\delta(x-x_1) + F_2\delta(x-x_2) + F_3\delta(x-x_3) \end{array} \right] dx$$

(2.58)

Recalling the Eq. (2.31) and Eq. (2.32), one may write the following equation expressions as,

$$F_1 = C_s^f(V_f - \dot{w}_1) + K_s^f\left(\int_0^t V_f\,dt - w_1\right)$$

$$F_2 = C_s^r(V_r - \dot{w}_2) + K_s^r\left(\int_0^t V_r\,dt - w_2\right)$$

Simplify these equations, where $\dot{w}_1 = \dot{w} + a\dot{\theta}$ and $\dot{w}_2 = \dot{w} - b\dot{\theta}$, ($\dot{\theta}$ is the pitching velocity, a and b are distances from centroid of the beam to front and rear suspension system respectively), reconstruct the Eq. (2.57)

$$L_2 = \int_0^l \left[\begin{array}{l} \left\{ C_s^f(V_f - \dot{w}_1) + K_s^f\int_0^t(V_f - \dot{w}_1)dt \right\}\delta(x-x_1) + \left\{ C_s^r(V_r - \dot{w}_2) + K_s^r\int_0^t(V_r - \dot{w}_2)dt \right\}\delta(x-x_2) \\ + F_3\delta(x-x_3) \end{array} \right] dx$$

(2.59)

$$\mathop{Lim}_{\eta\to t} p_r^{(3)}\,\overline{V}_t\left(L_2\right) = \int_0^l \left\{ C_s^f\,\frac{\partial w(t,x)}{\partial t}\delta(x-x_1) + C_s^r\,\frac{\partial w(t,x)}{\partial t}\delta(x-x_2) \right\} dx \qquad (2.60)$$

where $x \in (0,L)$

2.5.2 Extended Noether's rate equation for flexural beam

Extended Noether's theorem field equation may be written through Eq. (2.57) as

$$\int_{x_0}^{x_1} D_t \left(\rho A \dot{w} + I_d \frac{\partial}{\partial x} \dot{w}' - I_d \dot{w}'' \right) dx + D_t \left(-I_d \ddot{w}' - EIw'' - EIw'' + \mu_I [-\dot{w}'' + \dot{w}'''] \right) +$$

$$\int_{x_0}^{x_1} [\mu_I \dot{w}''] dx + \int_0^l \left\{ C_s^f \frac{\partial w}{\partial t} \delta(x - x_1) + C_s^r \frac{\partial w}{\partial t} \delta(x - x_2) \right\} dx = 0$$

(2.61)

The end condition of infinitesimal beam has been considered as free-free, the modal function may be expressed as (*Karnopp*,1990)

$$Wn(x) = (\cos k_n L - \cosh k_n L)(\sin k_n x + \sinh k_n x) - (\sin k_n L - \sinh k_n L)(\cos k_n x + \cosh k_n x)$$

(2.62)

and the natural frequency of the beam may be represented as (*Hagedorn*, 2007)

$$\omega_n = \left(\frac{k_n L}{L} \right)^4 \sqrt{\frac{EI}{\rho A}}$$

(2.63)

where L is the length of the beam, E is the young modulus of the beam, I is the cross sectional moment of inertia, ρ is the material density and A is cross sectional area.

$$w(x,t) = A_n \sin \omega_n t W_n(x)$$

(2.64)

where A_n is also slowly varying function of time.

Substituting Eq. (2.56) in Eq. (2.53), one obtains

$$\int_0^l \left(\rho A . \dot{A}_n \omega^2_{\ n} W_n(x) + I_d \ddot{A}_n \omega^2_{\ n} W_n''(x) - I_d \ddot{A}_n \omega^2_{\ n} W_n''(x) \right) dx$$

$$-I_d \ddot{A}_n \omega^3_{\ n} W_n'(x) - EI \ddot{A}_n \omega^2_{\ n} W_n''(x) - EI \ddot{A}_n \omega^2_{\ n} W_n''(x) - \mu_I \ddot{A}_n \omega^2_{\ n} W_n''(x) - \mu_I \ddot{A}_n \omega^2_{\ n} W_n''(x) \quad (2.65)$$

$$\int_0^l \left(\mu_I \ddot{A}_n \omega^2_{\ n} W_n''(x) \right) dx + C_s^f A_n \omega_n W_n(x_1) + C_s^r A_n \omega_n W_n(x_2) = 0$$

The solution of Eq. (2.65) is non-trivial, and it may be clearly depicted from the expression that the symmetry of beam depends on internal or structural damping of the beam. In another on the other hand if it is varying with the motion or time, the system will be chaotic. It is also noticed that the system will be non-linear, if umbra-potential due to internal damping is added to the system. The symmetry of the vehicle frame has direct influence on the random excitation of road, in which chassis or beam dissipate this energy with varying rate. Thus, varying rate of dissipative energy cannot be modeled by any other classical approach. In this way, umbra-Lagrangian approach seems to be best suited for this analysis.

This extended Lagrangian formulation can be need to obtain the amplitudes of vehicle frame analytically.

2.5.3 Umbra-Hamiltonian density of beam of vehicle frame

The extension of Noether's theorem plays a vital role in determining an invariants or so-called first integrals of motion and invariant trajectories, on which some physical entity turns out to be constant. However, the dynamical quantity, which becomes conserved, can be ascertained only by considering the umbra-Hamiltonian of the system. Therefore, the notion of umbra-Hamiltonian is very significant to obtain the conserved dynamical quantity using detailed derivation, which is presented in *Appendix B*. In this way, combined aspects of extended Noether's theorem and umbra-Hamiltonian provide the full details of an insight into the dynamics of systems with symmetries. Umbra-Hamiltonian density for this system may be written as,

$$
\mathcal{H} = \int\limits_{x_0}^{x_1} \left[\sum_{i=1}^{2} \left\{ \begin{array}{l} \dfrac{1}{2\rho} P_i^2(\eta, x) + \dfrac{1}{2} EI\left(\dfrac{\partial^2 w(\eta, x)}{\partial x^2}\right)^2 \\[2mm] + \dfrac{1}{2}\rho I_d \left(\dfrac{\partial^2 w(\eta, x)}{\partial \eta\,\partial x}\right)^2 \\[2mm] + \mu_I \dfrac{\partial^2 w(\eta, x)}{\partial x^2} \dfrac{\partial^3 w(t, x)}{\partial t\,\partial x^2} \end{array} \right\} \right] dx \; + F_1\delta(x - x_1)dx + F_2\delta(x - x_2)dx + \dfrac{1}{2J} p_\theta^2(\eta)
$$

<div align="right">(2.66)</div>

where $P(\eta, x) = \rho\dfrac{\partial w(\eta, x)}{\partial \eta}$ and $P_\theta(\eta) = J_d\dot{\theta}(\eta)$.

From theorems of umbra-Hamiltonian as discussed in *Appendix E*, one has

$$
\underset{\eta \to t}{Lim}\frac{\partial H^*}{\partial \eta} = 0 \Rightarrow \frac{dH_i^*}{dt} = -\underset{\eta \to t}{Lim}\frac{dH_e^*}{\partial \eta}.
$$

Now considering exterior umbra-Hamiltonian density, one may have

$$
\underset{\eta \to t}{Lim}\frac{\partial \mathcal{H}_e}{\partial \eta} = \int\limits_{x_0}^{x_1}\left[\mu_I \frac{\partial^2}{\partial x^2}\frac{\partial w(t, x)}{\partial t\,\partial x^2} + F_1\delta(x - x_1) + F_2\delta(x - x_2) \right]dx
$$

<div align="right">(2.67)</div>

Considering end conditions of continuous beam as free-free, and substituting Eq. (2.23) in Eq. (2.55), one may obtain the forced solution and multiply each term by $W_m(x)$ and integrate with respect to $x = 0$ to $x = l$., then one may use the orthogonal property to the modes and obtain following expressions,

$$
\dot{U}(t)\mu_I I\int\limits_0^L W_n^4\,dx + F_1 W_n(x_1) + F_2 W_n(x_2) = 0
$$

<div align="right">(2.68)</div>

$$
\dot{U}(t) = \frac{F_1 W_n(x_1) + F_2 W_n(x_2)}{\mu_I I\int\limits_0^L W_n^4\,dx} \qquad n \in [1,2,3,...n]
$$

<div align="right">(2.69)</div>

where, $U(t)$ is the magnitude of vibration of beam structure.

2.6 Conclusions

The chapter presented the dynamic response of a Rayleigh beam, which has been supported on two suspension systems subjected to a sine wave input and random road input prescribed by ISO 8608. Analytical framework has been formulated for chassis structure, where Lagrangian variational formulation further develops the equation of motion. Modal analysis was used to convert partial differential equation into a series of the ordinary differential equation. A separation theorem has been used to separate the spatial and the time function. These formulations were categorized with structural damping or without structural damping conditions. The bondgraph model has also been developed, where it has simulated with or without structural damping conditions subjected to a sine wave and random response of the road. Numerical simulation has been performed to analyze the bending and the modal responses of the beam. The result obtained in this simulation revealed that structural or internal damping has significant impact on dynamics of the beam as 12-15% vibration amplitude could be reduced by improving the structural damping of the beam. The next chapter will present the modeling of human BioD model and integrated this model with flexible chassis and suspension system. Further this integrated model will simulate under various random road responses.

Chapter 3

Whole Body Vibration and Assessment of Ride Comfort on Random Road Conditions

In the previous chapter, an analytical formulation of the flexural behavior of infinitesimal beam has been presented. This formulation is further extended to create a dynamic model to investigate its dynamic behavior. This chapter presents a whole-body vibration analysis for a 7-DOF seated driver posture, where driver seat is vertically excited as per standards of ISO 8608. This integrated vehicle-BioD model is followed by comfort evaluation, in which results are superimposed over ISO curves.

3.1 Introduction

Truck vibration problems have increased in recent years due to the high demand of industry, overloading and uncertain road conditions. Since drivers spend most of the time on roads in their cabins, ride comfort is one of the major concerns for heavy road transportation system.

A heavily damped suspension will provide good road holding, but it will transmit much of the road input to the vehicle body. When the vehicle is traversing a rough road at low speed at high speed, this will be regarded as a harsh ride. The diver may find the harsh ride unacceptable, or it may damage freight. A lightly damped system will give a more comfortable ride, but can significantly lessen the vehicle stability in turns or lane change manoeuvers. Good design of a suspension can optimize ride comfort and holding to some extent, but the compromise cannot be completely eliminated.

In general, ride comfort and sedentary activities are affected by many factors such as temperature, noise, vibration, seat parameters, posture, backrest, etc. In most of the

studies concerning with ride comfort, vibration is considered as one of the most significant components of the physical ambiance, which may lead to uneasiness to driver.

3.2 Ride comfort evaluation in road vehicle applications

There are generally psychological and physiological components for ride comfort, though it also direct a manner of comfortability and also eliminate stress condition, discomfort or pain. There are many quantitative descriptors which are used to evaluate the driver ride comfort in road vehicle. The general approach of each of the methods is to obtain acceleration at the rider- vehicle interface, to record the mechanical environment to which the passenger is exposed. The numerical value so obtained is then compared with ride comfort assessment criteria. These acceleration signals are processed further to calculate ride comfort. There are four different methods to determine the comfortability of human ride towards vibrations all over the globe these days. Currently, in Europe, ISO 2631 standard (*ISO 2631-1, 2007*) is profoundly prevailed, and similarly, the BS 6841 (*British standards Institution, 1987*) is used in the United Kingdom. Germany and Austria use VDI 2057 (*Hohl, 1984*) whereas Average Absorbed Power (AAP) (*Pradko, 1966*) is used in United States of America (USA). A brief summary of these four defined protocols i.e., ISO 2631, AAP, BS6841, and VDI are presented in the next subsections.

3.2.1 AAP (Average Absorb Power)

AAP was created by the US army tank Automotive Command (*Pradko, 1966*). This Study was based on elastic beahvior of the human body. This elatic behavior can be produced restoring forces under vibration condition which are connected to displacement. This procedure remains till the energy is removed or dissipated. This term "absorption" associated with the rate of energy is known as absorbed power (*Pradko, 1966*). This

method may be evaluated in both the time domain and the frequency domain as well, which may be presented as

$$AP = \sum_{i=0}^{N} K_i \ (A_{i_{rms}})^2 \tag{3.1}$$

The frequency range between 1 to 80 Hz, the above method is not very successful. The Absorbed Power (AP) weighting curve underlines the primitive resonance around 4-5 Hz.

3.2.2 BS 6841

BS 6841 standard considers a frequency range of 0.5–80 Hz. This new concept is based on Vibration Dose Value (VDV), where time dependency curves are not used. Primarily, the accelerations responses are weighted, along with the different weighted functions for different directions. In order to evaluate ride comfort, the weighted signal is being used for the RMS value, which may be expressed as:

$$RMS = \sqrt{\frac{1}{N} \cdot \sum_{n=1}^{N} a_n^2} \tag{3.2}$$

To estimate the most probable human reaction related to vibration, these RMS values are compared with the subjective values. To compensate motion sleekness according to measurements, the frequency range is sometimes extended up to half hertz. The overall value of the ride achieved, which may be equated with another value directly, and obtained by additional vehicle moves on the same speed on the same road.

3.2.3 VDI-2057

The Society of German Engineers (VDI) reported the first VDI-2057 standard in the year 1963, which was the first standard to calculate the ride comfort. A huge number of individual were exposed to sine-wave vibrations with a definite intensity and frequency. Principally, the VDI describes a evaluated ride comfort index (K-factor), which is significantly compared with a subjective table to demonstrate the ride according to the

subject perceived by human beings (*Hohl, 1984*). The VDI standard in 1979, acquired the ISO-2631 (1978) tolerance curves, however considering the K-factor for the subjective compared to the response by experienced human beings. The acceleration response is further transformed into the frequency domain by virtue of a Fast Fourier Transform (FFT). Furthermore, the RMS values at the third-octave center frequency are determined from the FFT. These results are obtained in single values, which is found at the center frequency of third octave. The weighted values of RMS acceleration data and K-values for z-direction are identified as follows:

$1 \leq f \leq 4$ Hz $\qquad K_Z = 10.\, a_Z.\, \sqrt{f}$ $\qquad\qquad$ (3.3)

$4 \leq f \leq 8$ Hz $\qquad K_Z = 20.\, a_Z,$ $\qquad\qquad$ (3.4)

$8 \leq f \leq 80$ Hz $\qquad K_Z = 160 a_Z.\, \sqrt{f}$ $\qquad\qquad$ (3.5)

The weighted signal is later plotted with limit plots. These weighted signals are found in the similar fashion of limit plots approved by ISO-2631. Whereas, the bandwidth frequency range lies in between 1 and 80 Hz.

3.2.4 Comfort guidelines -ISO 2631 (*ISO*-2631, 1997)
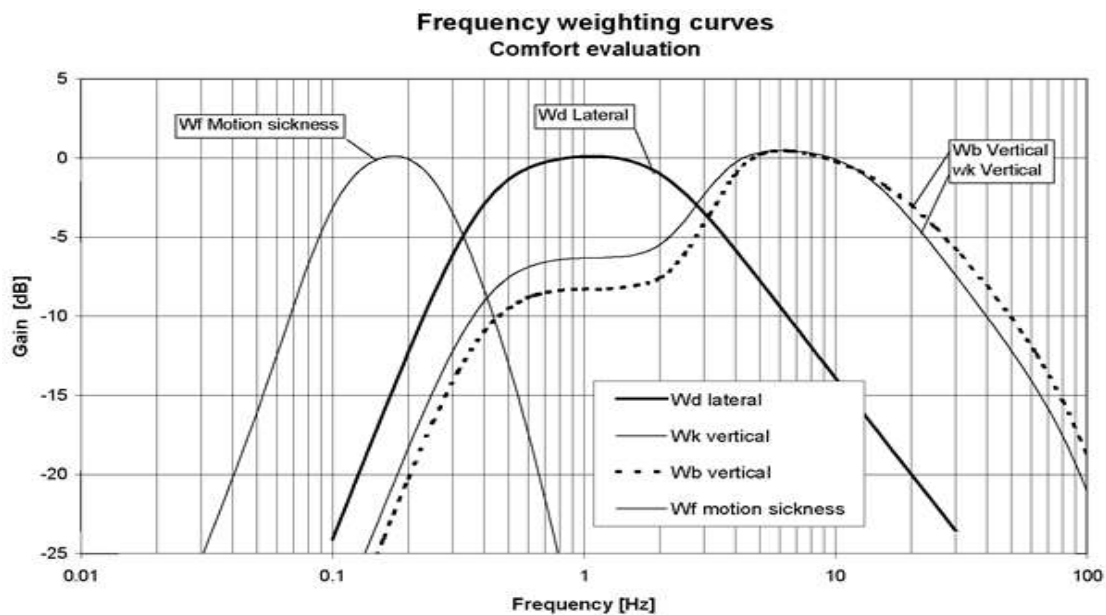
Figure 3.1: Weighing curves of W_k, W_d, and W_f (ISO 2631-1)

78

ISO 2631 standard outlines methodology for the measuring periodic, random and transient whole-body vibrations. It specifies few primary factors that determine the extent of tolerable vibration exposure. It provides guidelines to speculate the likely effects of vibration on health, comfort and motion sickness.

Table 3.1: Principal frequency weighting in one third octave

Frequency f, Hz	W_k		W_d		W_f	
	Factor ×1000	dB	Factor ×1000	dB	Factor ×1000	dB
0.1	31.2	-30.11	62.4	-24.09	695	-3.16
0.125	48.6	-26.26	97.3	-20.24	895	-0.96
0.16	79	-22.05	158	-16.01	1006	0.05
0.2	121	-18.33	243	-12.28	992	-0.07
0.25	182	-14.81	365	-8.75	854	-1.37
0.315	263	-11.60	530	-5.52	619	-4.17
0.4	352	-9.07	713	-2.94	384	-8.31
0.5	418	-7.57	853	-1.38	224	-13.00
0.63	459	-6.77	944	-0.50	116	-18.69
0.8	477	-6.43	992	-0.70	53	-25.51
1	482	-6.33	1011	0.10	23.5	-32.57
1.25	484	-6.29	1008	0.07		
1.6	494	-6.12	968	-0.28		
2	531	-5.49	890	-1.01		
2.5	631	-4.01	776	-2.20		
3.15	804	-1.90	642	3.85		
4	967	-0.29	512	-5.82		
5	1039	0.33	409	-7.76		
6.3	1054	0.46	323	-9.81		
8	1036	0.31	253	-11.3		
10	988	-0.10	21	-13.91		
12.5	902	-0.89	161	-15.87		
16	768	-2.28	125	-18.03		
20	636	-3.93	100	-19.90		
25	513	-5.80	80.0	-21.94		
30.1	405	-7.86	63.2	-23.98		
40	314	-10.05	49.4	-26.13		
50	246	-12.19	38.8	-28.22		
63	186	-14.61	29.5	-30.60		
80	132	-17.56	21.1	-33.53		

In the above table, the frequency range considered is - 0.5 Hz to 80 Hz for health, comfort and perception and - 0.l Hz to 0.5 Hz for motion sickness. This part of ISO 2631 is relevant to vibration transmitted to the human body through the supporting surfaces, and this kind of vibration is normally seen in vehicles, machinery, and buildings. The standard uses RMS values of frequency-weighted accelerations. The weighted RMS. acceleration is expressed in m/s^2 for translational vibration and rad/s^2 for rotational vibration. The weighting curves used are W_d for horizontal (lateral and longitudinal) accelerations and W_k or W_b for vertical accelerations. For railway applications, the weighting curve W_b is considered appropriate for vertical acceleration. The weighting curves are presented in Figure 3.1.

The weighted RMS acceleration shall be calculated in accordance with the following equation or its equivalents in the frequency domain.

$$a_w = \left[\frac{1}{T} \int_0^T \left(a_{wi}(t)\right)^2 dt \right]^{0.5} \tag{3.6}$$

where a_{wi} the frequency-weighted acceleration in m/sec^2, T is the integration time for running average and t is the time.

The acceleration signal may be analyzed either as a constant bandwidth or as a proportional bandwidth spectrum of un-weighted acceleration. In the proportional bandwidth case, usually, the frequency range is divided into one-third octave bands. The weighted RMS acceleration is calculated by weighting and the proper addition of one-third octave band data. For converting one third octave band data frequency

weighing is given in Table 3.1. The overall weighted acceleration shall be determined in accordance with the following equation in frequency domain as

$$a_w = \left[\sum_i (a_i w_i)^2 \right]^{\frac{1}{2}} \qquad (3.7)$$

where, a_w is the frequency-weighted *RMS.* acceleration, a_i is the RMS. acceleration of ith one-third octave band and w_i is the weighting factor for the ith one-third octave band. The main acceptable values of acceleration magnitude for comfort depend on many factors that differ with applications. Therefore, a particular limit is not defined in this part of ISO 2631. The values given in Table 3.2 provides an approximate indication of likely reactions towards vibration in accordance with the frequency weighted RMS acceleration in public transport.

Table 3.2: ISO comfort level characterization

Subjective Comment	Accelerations value (m/s^2)
Not Uncomfortable	<0.0315 m/sec^2
A Little uncomfortable	0.0315 to 0.63 m/sec^2
Fairly uncomfortable	0.5 to 1.0 m/sec^2
Uncomfortable	0.8 to1.6 m/sec^2
Very uncomfortable	1.25 to 2.5 m/sec^2
Extremely uncomfortable	>2.0 m/sec^2

3.2.4 Model for ride comfort

Road irregularities, vehicle characteristics, and vehicle speed generate motion quantities that are perceived by passengers. The combinations of these quantities affect the passengers' perception of ride comfort as shown in Figure 3.2.
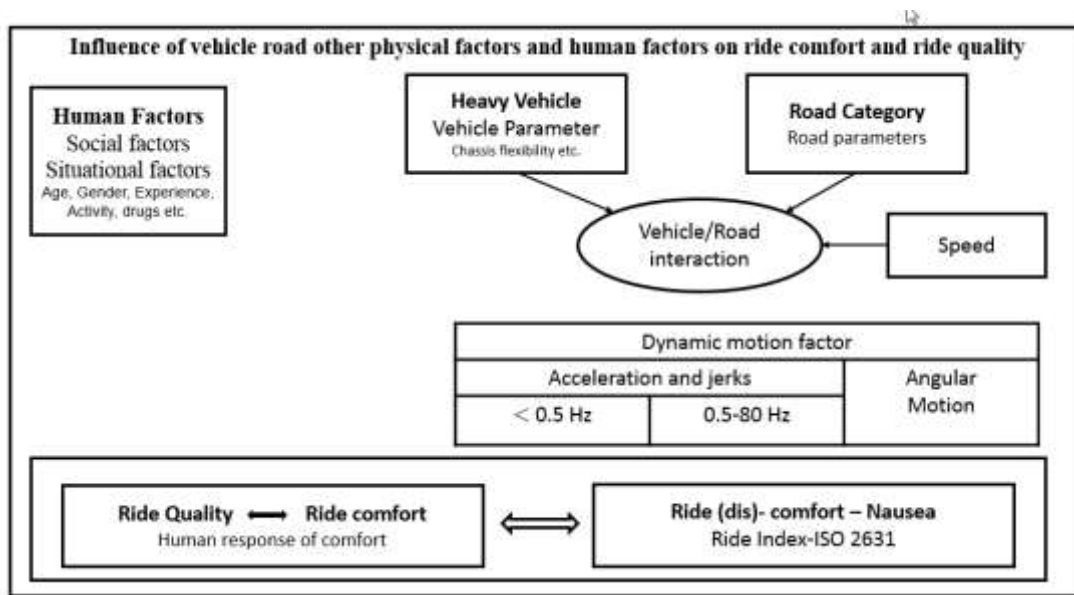
Figure 3.2: Significant road and vehicle parameters for ride comfort

3.3 Vibration analysis of human body for assessment of ride comfort in ride vehicle assessment

Figure 3.3 illustrates the pitch plane model of heavy vehicle with human biodynamic model, which consists of a vehicle frame, suspension system and dead load frame. The length of the vehicle body is *L,* which has been modeled according to the flexible beam with uniform cross-section and having homogeneously distributed mass, along with the mass M_c with bending module *EI.* The displacement magnitude of a beam section is $w(x,t)$, in which *t* and *x* are the time and distance respectively. The dead load frame/structure is assumed to be a rigid body, represented as a mass M_d. and displacement for dead load frame/structure is assumed as a $w_1(x,t)$. The spring and the damper for the front suspension system are characterized by damping coefficient C_{sf} and spring stiffness K_{sf} and for the rear suspension system are characterized by damping coefficient C_{sr} and spring stiffness K_{sr}. Coordinate is definined with certain dimensions

82

which is depicted in Figure 3.3. Whilst, the a typical heavy vehicle parameters are addressed in Table 2.4

In the previous chapter, the analysis of frame flexibility was evaluated through Rayleigh beam approach. In this chapter, since one may interest only deflection in transverse direction and the integrated system is very complex. So that the chassis structure is modeled to be a Euler-Bernoulli beam of uniform cross-section, which is having homogenously distributed mass with the bending modulus *EI (Gupta and Rastogi, 2018)*. First three flexible modes with its rigid body modes are being used for the purpose of simulation. The deflection in transverse direction of the chassis body being represented as $w(x,t)$, in which x differs from *0* to *L* of chassis body length. The beam partial differential equation may be developed and presented as follows

$$EI\frac{\partial^4 w(x,t)}{\partial x^4} + \rho A\frac{\partial^2 w(x,t)}{\partial x^2} = F_1\delta(x-x_1) + F_2\delta(x-x_2) + F_3\delta(x-x_3) + F_4\delta(x-x_4) \qquad (3.8)$$

where, F_1, F_2, F_3 and F_4 *are* the force form front tire, rear tire, biodynamic model and the dead load frame respectively and x_1, x_2 x_3 and x_4 denotes coordinates position of the point of application of different forces F_1, F_2, F_3 and F_4 correspondingly whereas, $\delta(.)$ is dirac's delta function.

The partial differential equation of beam is transformed into ordinary differential equation with the separation of variable approach. This approach will yield a well-designed lumped-parameter bondgraph depiction of flexible frame and driver model through suspension elements. Separation of the variable method may be applied by temporarily putting zero value to the force terms on the right-hand side of Eq. (3.8).
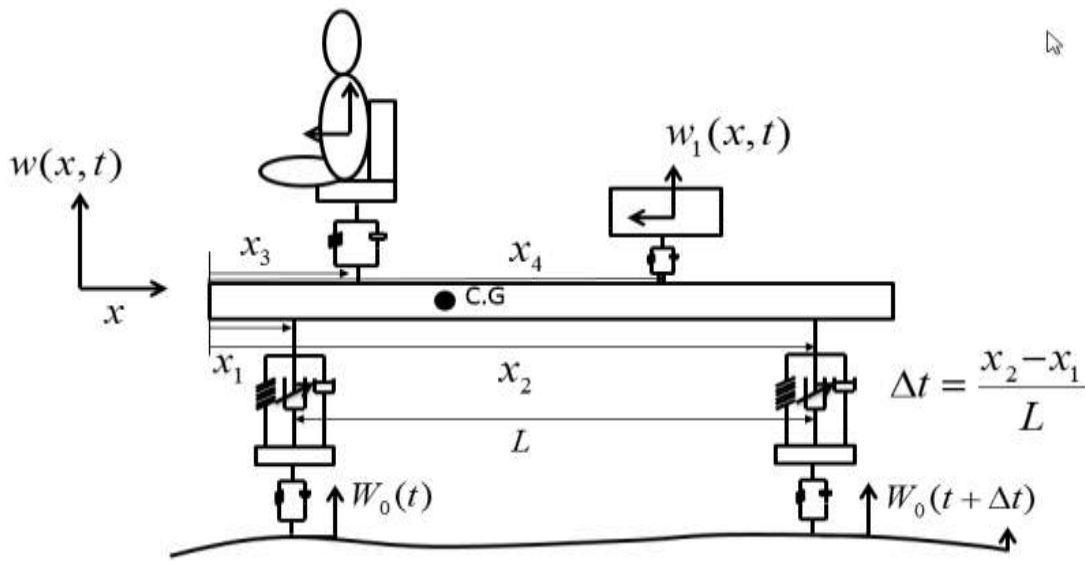
Figure 3.3: Integrated model human-vehicle system for analyzing vertical dynamics

The displacement at x and time t is assumed to be separated into a product of a function of position x as $W(x)$ and a function of time t as $q(t)$ i.e. $w(x,t) = W(x)q(t)$ (*Karnopp, 1990*). On substituting the value of $w(x,t)$ into the homogeneous form of Eq. (3.8) and applying the boundary condition, one gets the solution of these equation as an infinite sum of the product of the modal amplitude $q_i(x,t)$ and the shape function $W_i(x,t)$.

For a chassis body, there are two modes to be calculated, in which First mode bounce of the rigid mode is and later is pitching mode. Further, there shape functions are considered as $W_{00}(x) = 1$ and $W_0(x) = x - L_2$ respectively. This current analysis involved five modes in total, which are mainly supposed along with the rigid modes. Herein, the chassis body displacement has been taken at time t and position x is given by Eq. (3.9)

$$w(x,t) = W_c + (x - L_2)\theta_c + \sum W_i(x)q_i(t) \tag{3.9}$$

where, θc denotes pitching angle and W_c is the vertical displacement of frame C.G. of the chassis body about its C.G.

The shape functions may be expressed as

$$W_i(x) = (\cos k_i L - \cosh k_i L)(\sin k_i x + \sinh k_i x) - (\sin k_i L - \sinh k_i L)(\cos k_i x + \cosh k_i x)$$ (3.10)

Considering free-free beam condition with its zero bending moment and the shear force for chassis body as boundary condition, which may attains

$$\cos k_i L \cosh k_i L = 1$$ (3.11)

The solution of Eq. (3.11) gives

$$k_i L = 4.73004,\ 7.8532,\ 10.9956,\ 14.1372,\ 17.2788,...$$

where w, is the vertical displacement of chassis body and the pitching angle of the chassis body, denoted by θ_c is about its C.G.

Substituting Eq. (3.9) into Eq. (3.8) and integrating with respect to x with length of a chassis body, supposing the orthogonality property of shape functions, which obtains Eq. (3.10) and Eq. (3.11) for flexible body modes and Eq. (3.12) for rigid body modes.

$$M\dot{q}_{00} = F_1 + F_2 + F_3 + F_4$$ (3.12)

Eq. (3.12) simply demonstrates that external forces uplift the C.G. of the chassis body with vertical acceleration,

$$\ddot{q}_{00} = \ddot{z}_c$$ (3.13)

$$J\dot{q}_0 = F_1\left(x_1 - \frac{L}{2}\right) + F_2\left(x_2 - \frac{L}{2}\right) + F_3\left(x_3 - \frac{L}{2}\right) + F_4\left(x_4 - \frac{L}{2}\right)$$ (3.14)

Eq. (3.14) simply demonstrates that moment of external forces for the chassis body C.G. generates pitching acceleration, $\dot{q}_0 = \dot{\theta}$

$$m_i \ddot{q}_i + m_i \omega_i^2 q_i = F_1 W_i(x_1) + F_2 W_i(x_2) + F_3 W_i(x_3) + F_4 W_i(x_4) \tag{3.15}$$

where, m_i denotes modal mass and ω_i denotes i^{th} frequency mode, which may be attained through placing the k_i value from Eq. (3.11) into Eq. (3.16b)

$$m_i = \int \rho A W_i^2 dx, \, i=1,2,3\ldots \tag{3.16a}$$

$$\omega_i = \sqrt{\frac{EI(k_i L)^4}{\rho A L^4}}, \, i=1,2,3\ldots \tag{3.16b}$$

Herein, Eqs. (3.12-3.14) suggest that acceleration generated by the external forces $\ddot{q}_{00}=aG$ at the centre of mass of the chassis body whereas, the external moment forces generates pitching acceleration $\ddot{q}_0=\theta c$ with respect to the centre of the mass of chassis body.

Let us explain the modal displacement as q_i and momentum as

$$P_i = m_i q_i \tag{3.17}$$

Now, Eq. (3.15) may be represented as

$$p_i = m_i \omega_i^2 q_i + F_1 W_i(x_1) + F_2 W_i(x_2) + F_2 W_i(x3) + F_3 W_i(x_4) \tag{3.18}$$

$$\dot{q}_i = \frac{p_i}{m_i} \tag{3.19}$$

Further, now i^{th} modal equation is diminished into two first-order state equations in the form of variables associated with bondgraph. Eq. (3.19), for $x = x_i$ may be represented in the form of p_i and q_i as

$$\frac{\partial w}{\partial t}(x_i, t) = W_{00}(x_i)\frac{p_{00}}{m_{00}} + W_0(x_i)\frac{p_0}{m_0} + W_1(x_i)\frac{p_1}{m_1} \ldots\ldots + W_3(x_i)\frac{p_3}{m_3} \tag{3.20}$$

In this equations, W_{00} and W_0 denote rigid mode shape functions whereas, flexible mode

shape functions is presented by $W_1 - W_2$
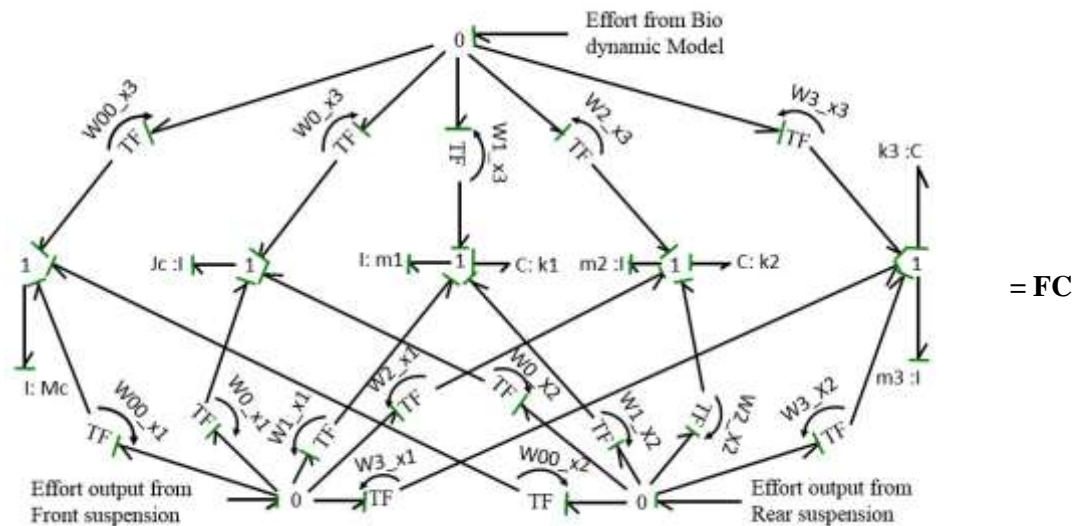
Figure 3.4: Modal bondgraph model for flexible chassis of heavy vehicle

The bondgraph submodel of the flexible chassis body is presented in Figure 3.4, which

includes almost all the equations of both flexible and rigid modes. Further, this

submodel is represented by FC sub-model. The rigid body modes are commonly

noticed, when force-free boundaries are presented and also found as an inertia element

without modal stiffness. Further, the first and second inertia element are the masses of

the base body and moment of inertia of base body respectively. The TF-element used in

the bondgraph model is simply modulus with mode shape functions, which may be

achieved through Eq. (3.10).

3.3.1 Bondgraph modeling of seated driver bio-dynamic model

In literature, there are several discrete models, which are used for addressing the

biodynamic features of a human body (*Chung, 2006*). The human body of these

physical models is supposed as lumped masses, representing the different body segments and are interlinked by dampers and springs. In this work, the whole-body vibration in heavy road vehicle will be analysed by incorporating the driver BioD model as the 7-DOF lumped/discrete human biodynamic model (Figure 3.5(a)) as proposed by *Patil et al., 1977*.
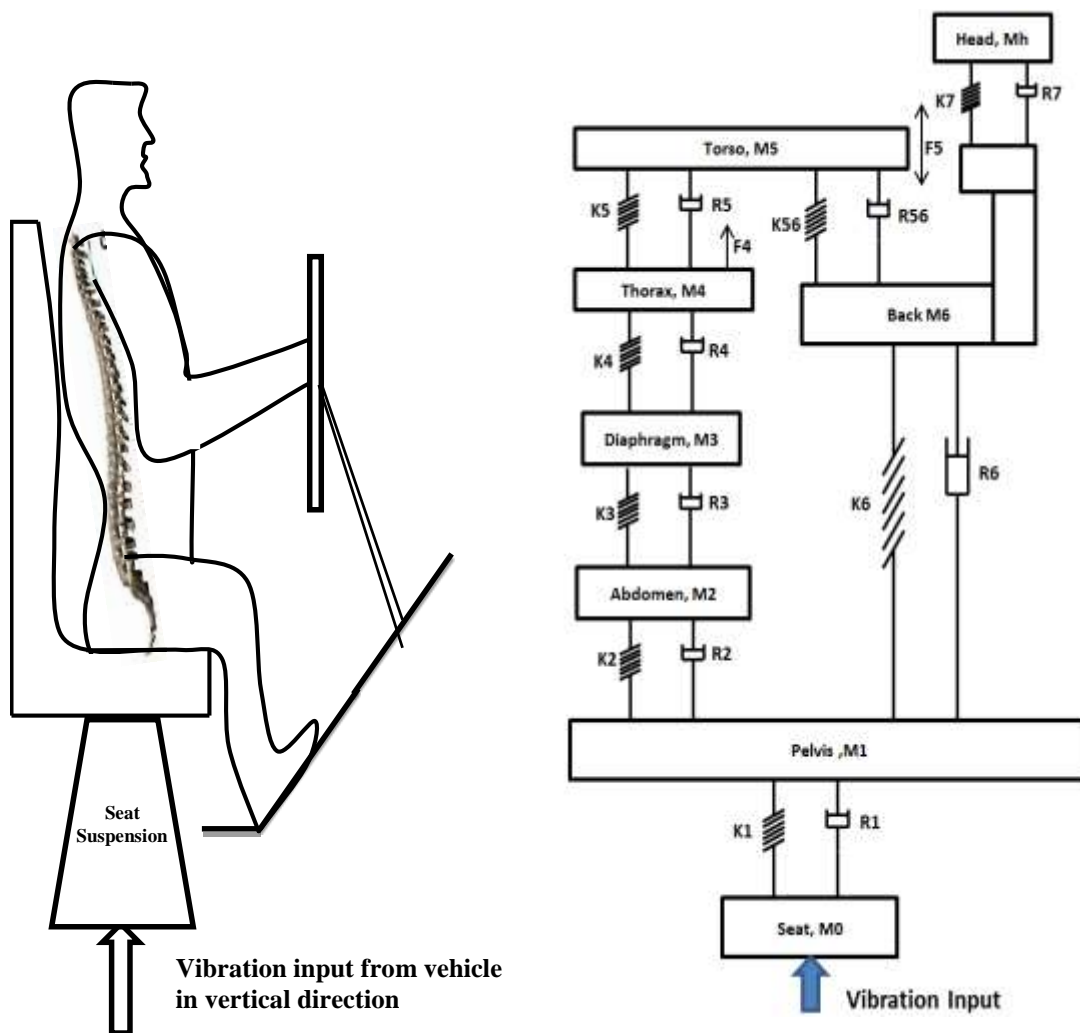
Figure 3.5: (a) Human seated biodynamic model (b) Human Patil (7 DOF) discrete model

The lumped/discrete parameter models are commonly restricted to one-dimensional analysis. Hence, the human body in the present study is supposed to be sitting erect with no backrest support regardless of hands' position. Herein, the driver body is made with seven

distinct mass segments representing appropriate anatomical parts of the human and are body interlinked by eight sets of dampers and springs as shown in Figure 3.5(b) with a total mass of 79.97 kg. This model can accommodate the vertical motion. The biomechanical parameters of the 7 DOF human biodynamic model are listed in Table 3.3.

Table 3.3: Simulation parameters for driver-biodynamic model

Biomechanical properties					
Mass	**(kg)**	**Damping**	**(N-s/m)**	**Stiffness**	**(N/m)**
Mh	5.450	Rh	3580	Kh	52600
M0	50	R0	151	K0	67000
M1	27.230	R1	292	K1	877
M2	5.921	R2	292	K2	877
M3	.455	R3	292	K3	877
M4	1.362	R4	292	K4	877
M5	32.762	R5	292	K5	877
		R56	3580	K56	52600
M6	6.820	R6	3580	K6	52600

Following assumptions are to be made for modeling of seated driver BioD model.

- The vehicle is travel with the constant velocity in the longitudinal direction as the objective is to study the effect of vertical vibration on passengers.

- The car body is flexible whereas, other components of the heavy vehicle are rigid.

- The wheel-road interaction force is realized in the vehicle-occupant through linear model Hertzian theory.

- In present study, the human body is considered in sitting posture with no backrest support.

A bondgraph fragment shown in Figure 3.6 represents the bondgraph human biodynamic model, which is also denoted as BioD sub model. The force from the vehicle model becomes input to this model. The body parts are characterized by the center of mass velocity.
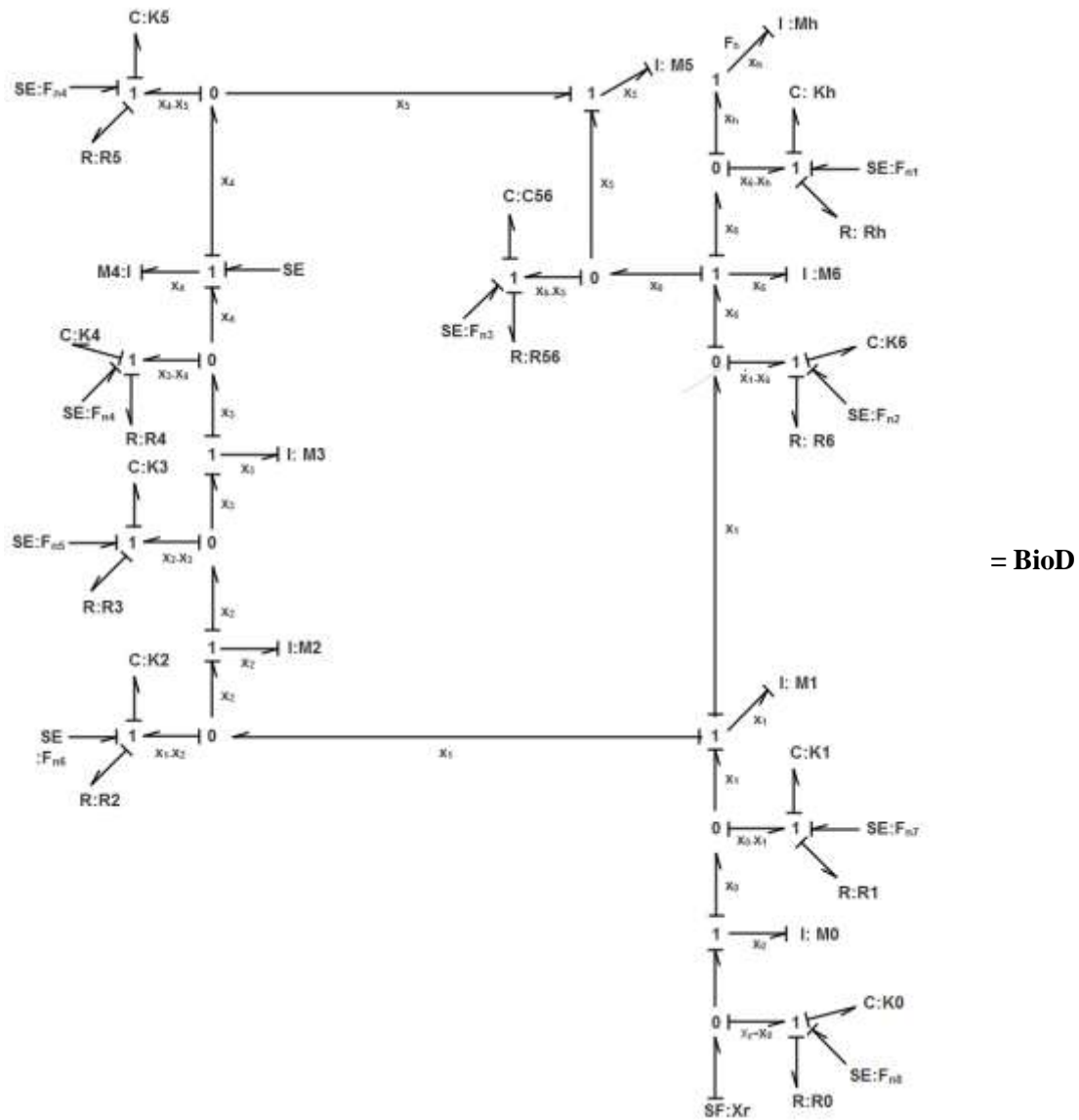
Figure 3.6: Bondgraph model of 7-DOF human BioD physical system

So, I-elements for the masses of respective parts is attached to the appropriate 1-junctions. The weight is an external force, which can be realized through the source

of effort (SE) element attached to respective 1-junction. In this model, C-element represents the stiffness and R-element represent the damping characteristics of the respective spring-damper system, which makes the connection between lumped masses.

3.3.2 Integrated road vehicle BioD model

The integrated bondgraph model associated with driver-road heavy vehicle system is created through joining sub-models of flexible chassis, driver BioD and suspension system as presented in previous sub-section, which is shown in Figure 3.7. In addition, the pad element, known as a spring-damper combination is used, whereas the differential causality of the system can be avoided by putting the higher values of C and R elements to make a difference of flows at 0-junction, where SSf and SSr are the front suspension and rear suspension of heavy road vehicle respectively.

The velocity inputs transmit to driver-vehicle model for evaluating a response of the proposed model at time *t* has already been discussed in previous *chapter* in *section 2.4.1*. The next subsection will present the simulation results of the integrated vehicle driver model.
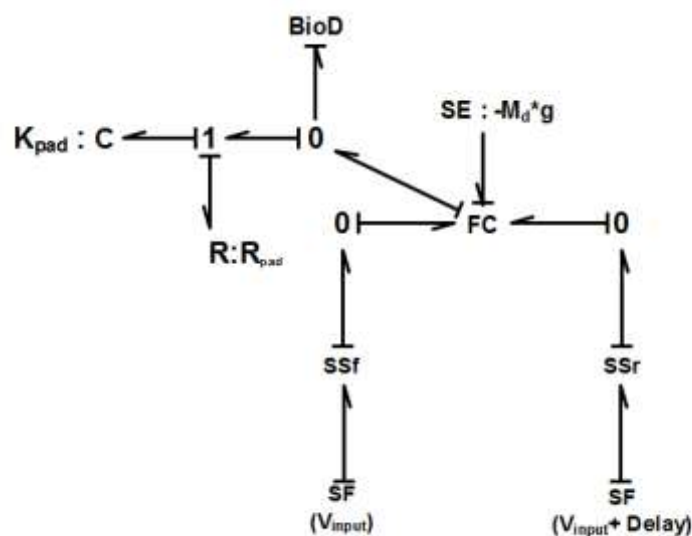
Figure 3.7: Integrated vehicle –driver bondgraph model

3.4 Numerical results

The integrated driver-BioD model is simulated with vehicle and driver parameters, which is presented in Table 3.3. and Table 3.4 respectively, to investigate the comfort characteristics of the proposed model. The simulation results of the proposed model have been categorized in three parts; First part presents the modal acceleration response of vehicle at different speeds in different road condition, second part presents the acceleration variation of human body segments at various vehicle speeds over the random road conditions. Third and final part presents the comfort evaluation for each body parts as per ISO 2631-1 criteria.

Table 3.4: Simulation parameters for flexible chassis system (*Rideout,* 2012)

Parameter	Value	Unit
Vehicle length	10	m
Frame mass (Mg)	4350	kg/m
Frame Inertia	24000	kg/m^2
Suspension stiffness (K_{sf}, K_{sr})	375, 870	KN/m
Suspension damping (R_{sf}, R_{sr})	31895, 33384	Ns/m
Unsprung mass (*Mus*)	50	Kg
x_1, x_2, x_3, x_4	2.95, 5.75, 7, 3	m

It has been observed from simulation results that the acceleration response of multi segments of human body is found in the similar fashion for flexible and rigid body modes. The value of rigid mode is almost similar to the first mode, whereas the value of other two modes relatively negligible in all type road conditions at all vehicle speeds. Figures 3.8-3.15 show the modal response of vehicle body, when the model is simulated for two vehicle speeds (40 km/h and 100 km/h) for each road condition.
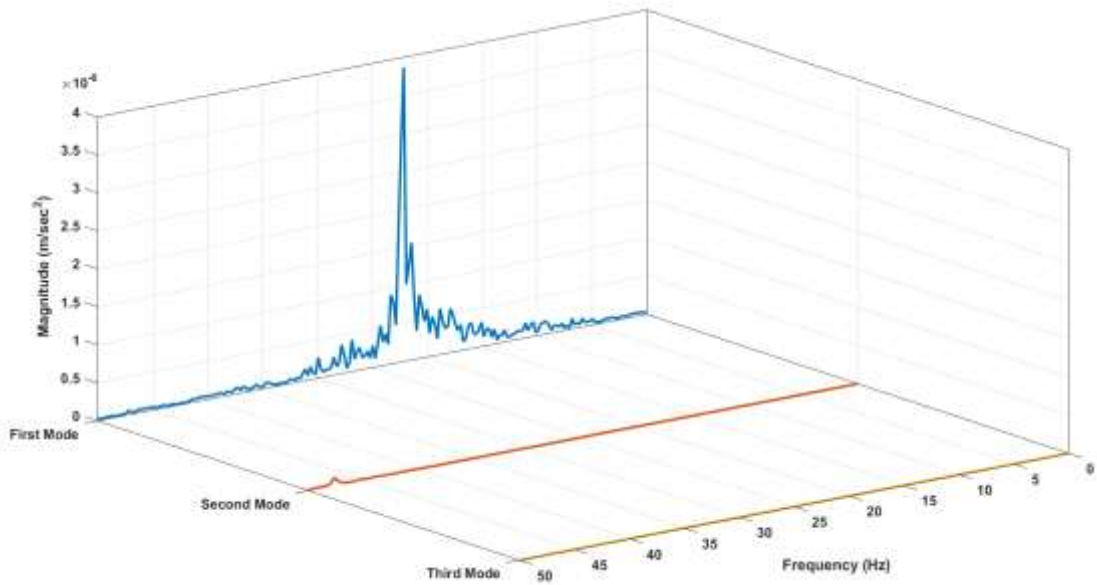
Figure 3.8: Modal response of beam at 40 Kmph in H1 road condition
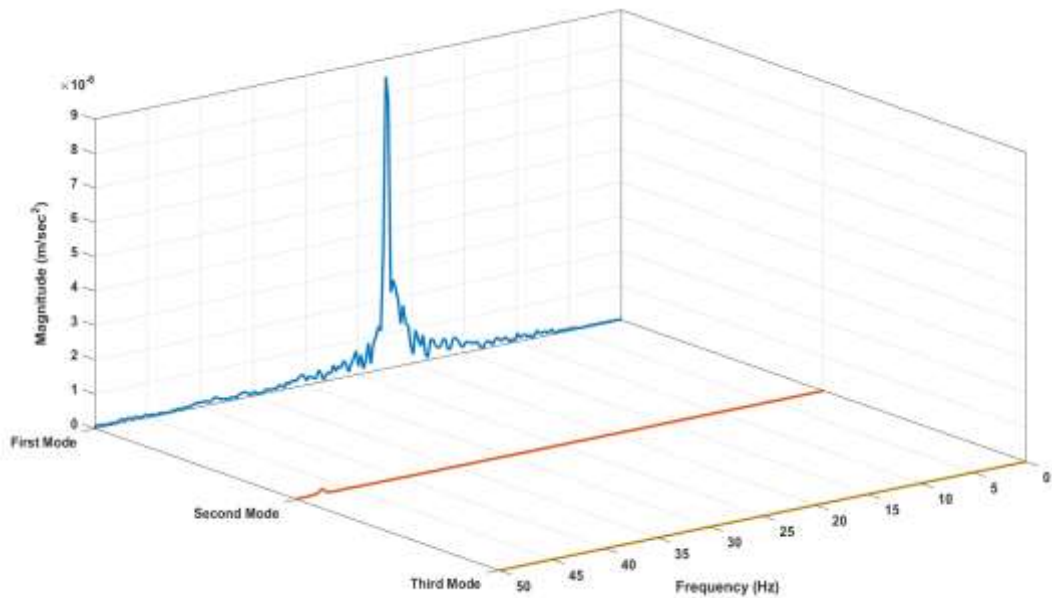
Figure 3.9: Modal response of beam at 100 Kmph in H1 road condition
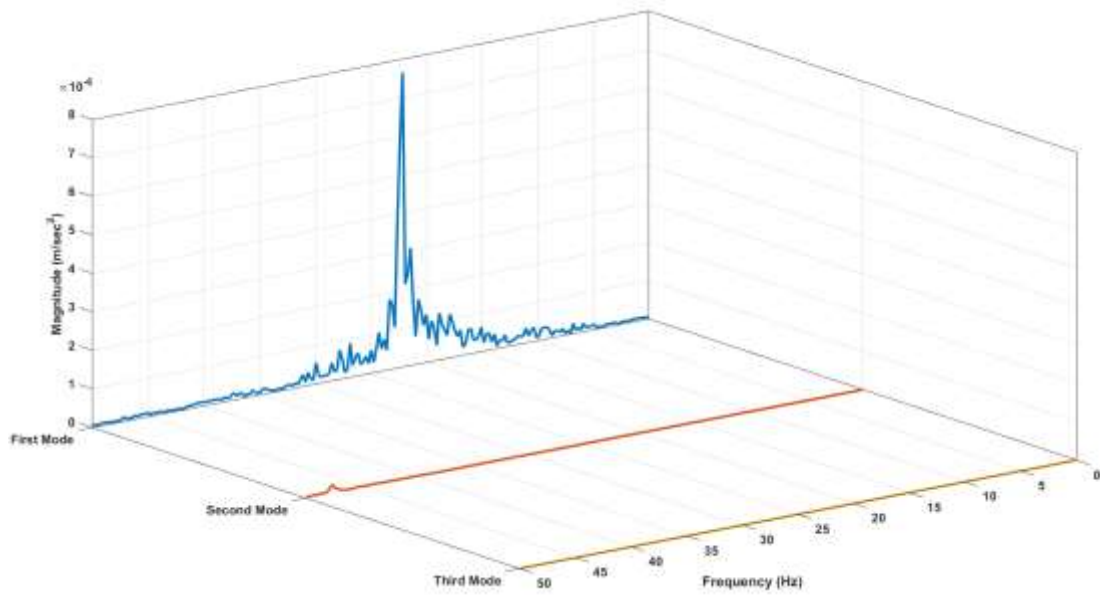
Figure 3.10: Modal response of beam at 40 Kmph in H2 road condition
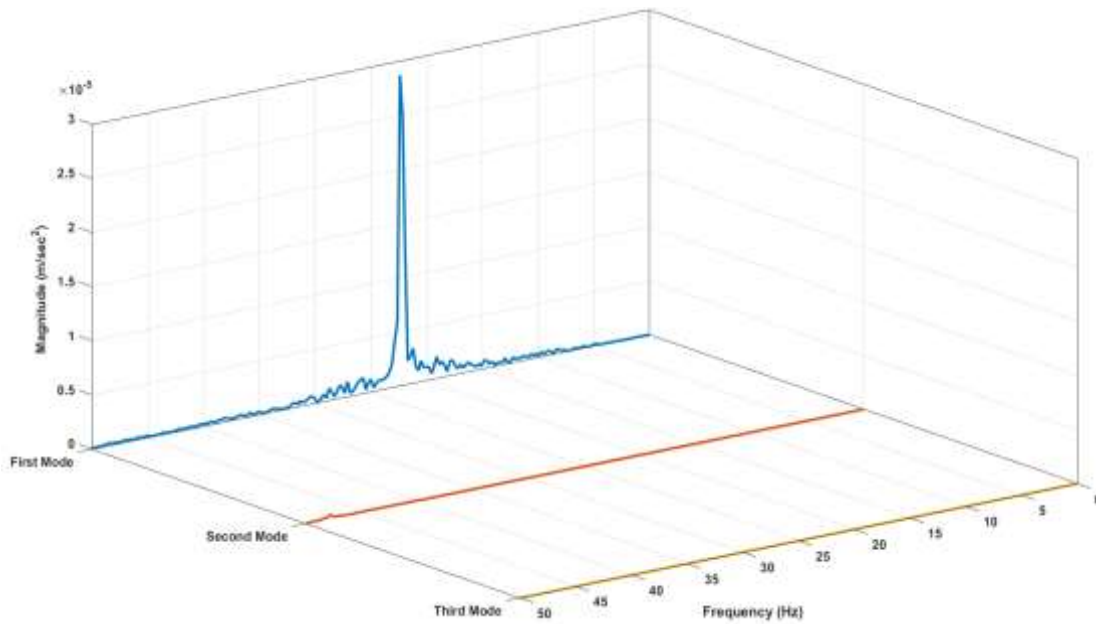
Figure 3.11: Modal response of beam at 100 Kmph in H2 road condition
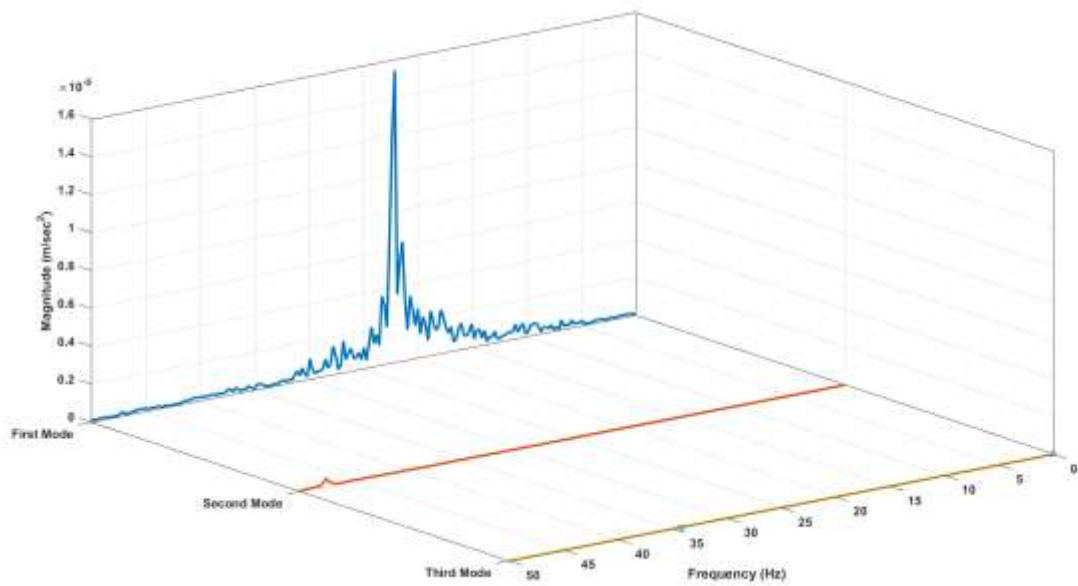
Figure 3.12: Modal response of beam at 40 Kmph in H3 road condition
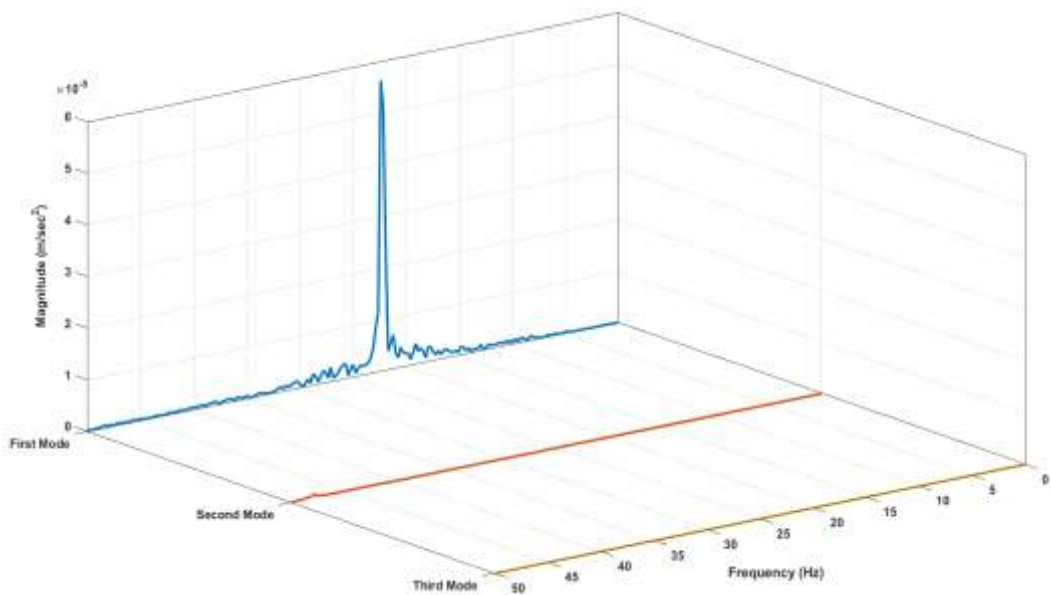
Figure 3.13: Modal response of beam at 100 Kmph in H3 road condition
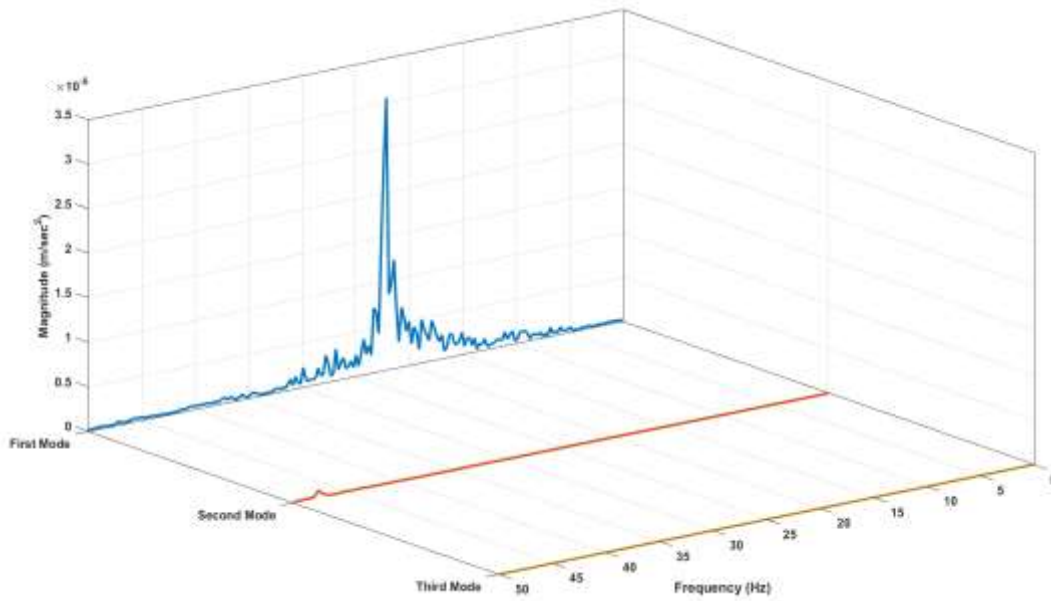
Figure 3.14: Modal response of beam at 40 Kmph in H4 road condition
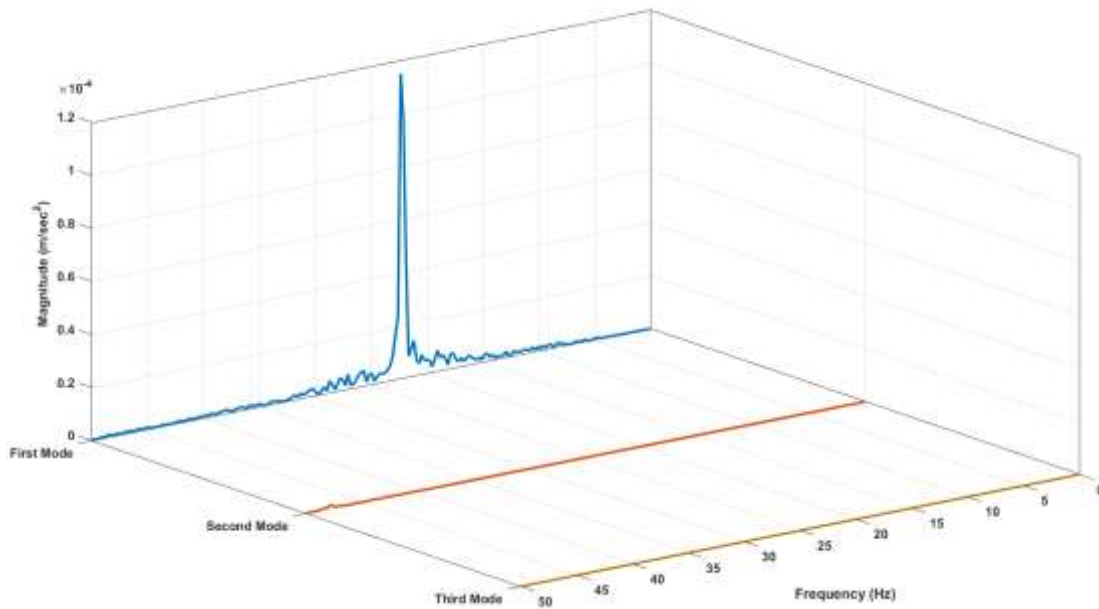
Figure 3.15: Modal response of beam at 100 Kmph in H4 road condition

These figures reveal that the magnitude of acceleration increases with changing the road condition. Besides this, the vehicle speed also have some influence on the acceleration response of the vehicle. The modal response of the first mode is 9e-6 m/sec^2 in H1 condition at 100 km/hr, but it is found slightly lower (around 8e-6 m/sec^2) in H2 condition at 40 km/hr. A similar pattern has been noticed in Figures 3.12- 3.13 and Figures 3.14-3.15. The maximum response (1.2e-4 m/sec^2) has been achieved in H4 road condition at 100 km/hr.

The acceleration response of all body parts with a seat at various vehicle speeds in different road conditions are shown in Figures 3.16-3.31. It is evident from figures that the human head experiences lesser vibration as compared to the other body parts. However pelvis part of the body experieneces the maximum vibration in all mentioned road condition at all speeds (40 km/h, 60 km/h, 80 km/h, and 100 km/h). The value of acceleration is increasing with vehicle speed and also with the road condition, whereas the maximum magnitude is achieved in H4 road condition with speed 80 km/h.
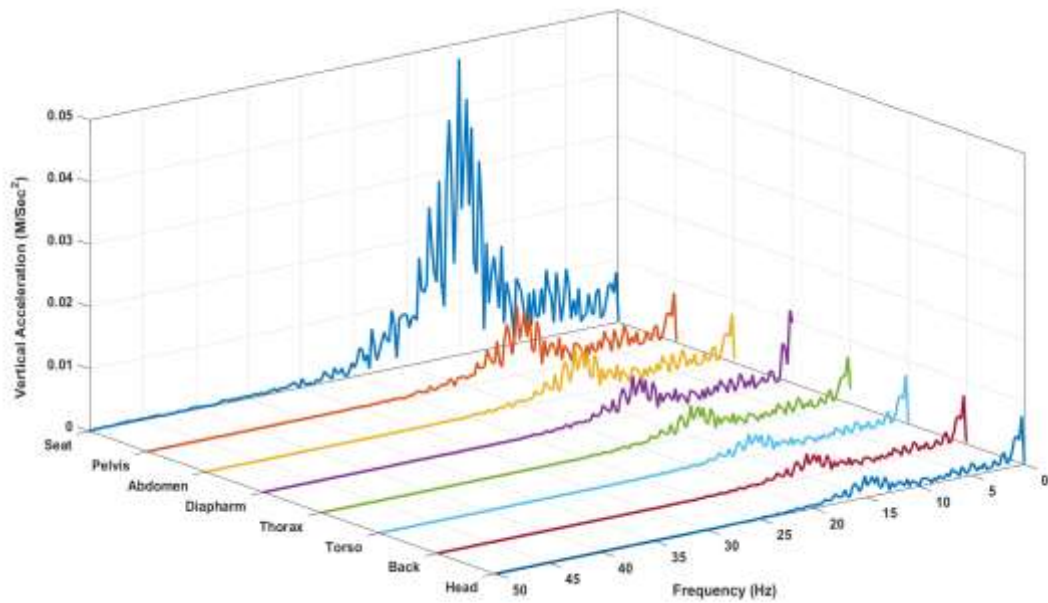
Figure 3.16: Vibration response measures at different parts of BioD at 40 Kmph in H1 road condition
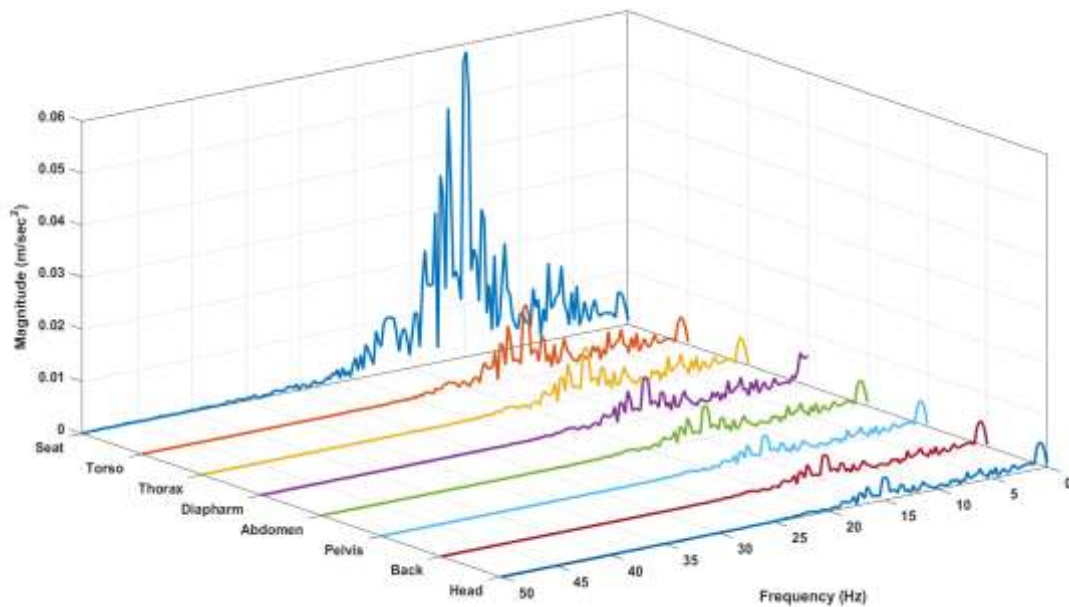
Figure 3.17: Vibration response measures at different parts of BioD at 60 Kmph in H1 road condition
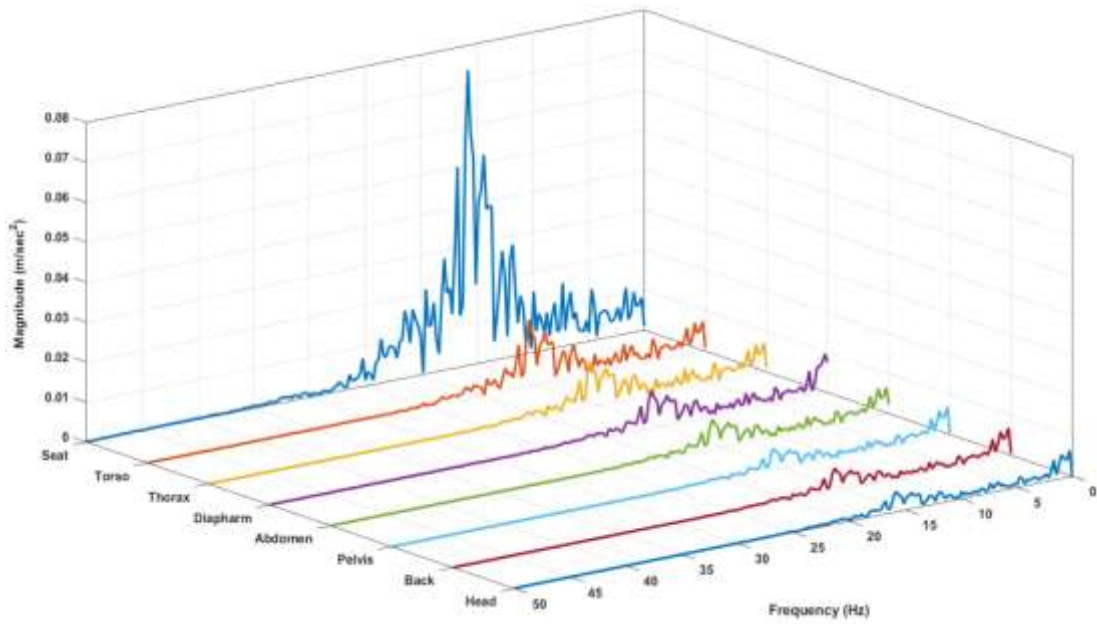
Figure 3.18: Vibration response measures at different parts of BioD at 80 Kmph in H1 road condition
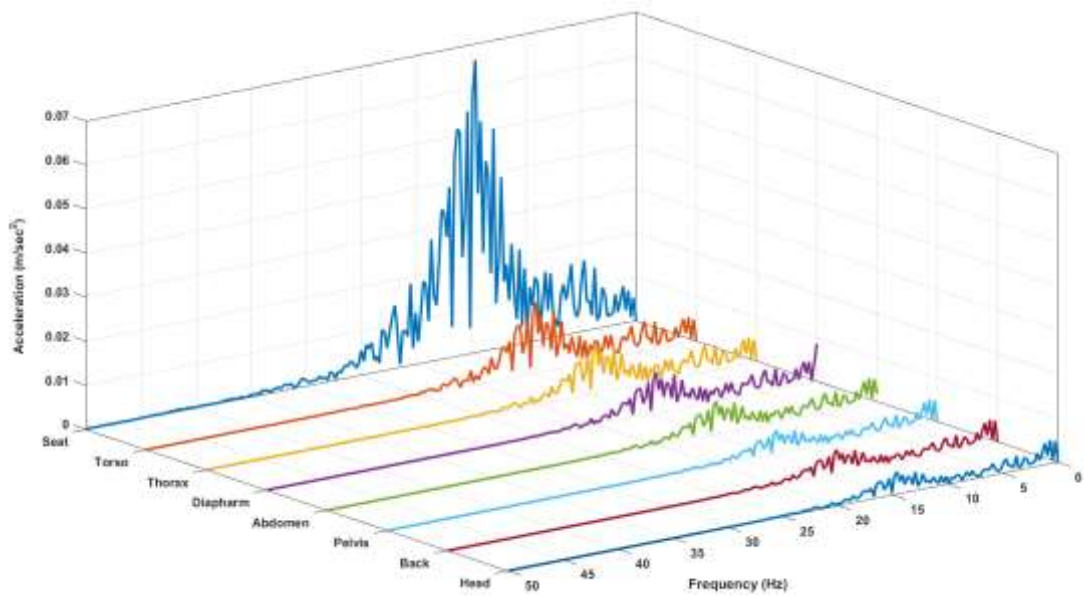
Figure 3.19: Vibration response measures at different parts of BioD at 100 Kmph in H1 road condition
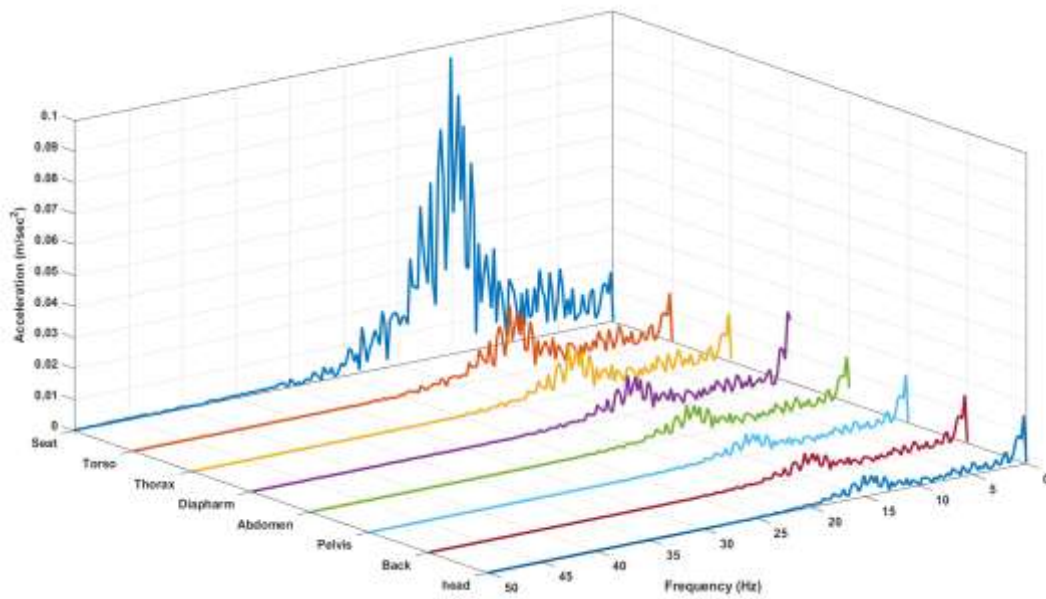
Figure 3.20: Vibration response measures at different parts of BioD at 40 Kmph in H2 road condition
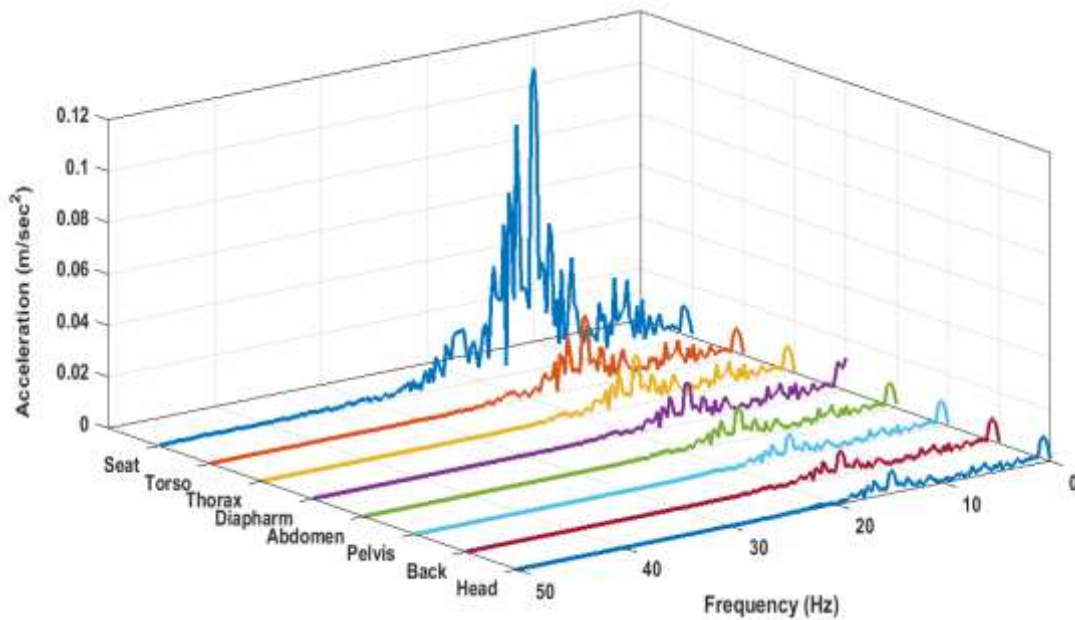
Figure 3.21: Vibration response measures at different parts of BioD at 60 Kmph in H2 road condition
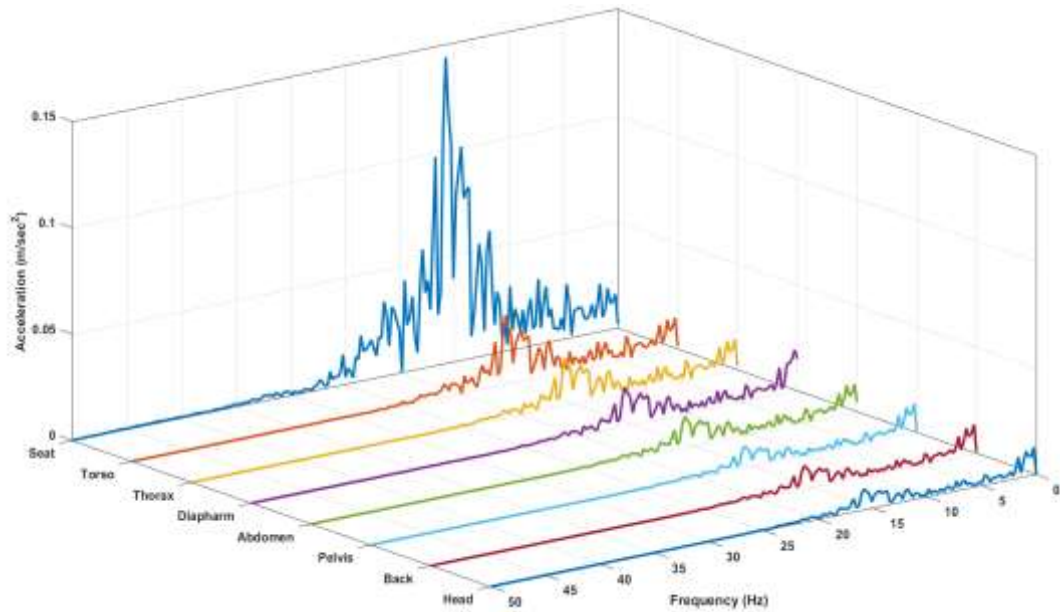
Figure 3.22: Vibration response measures at different parts of BioD at 80 Kmph in H2 road condition
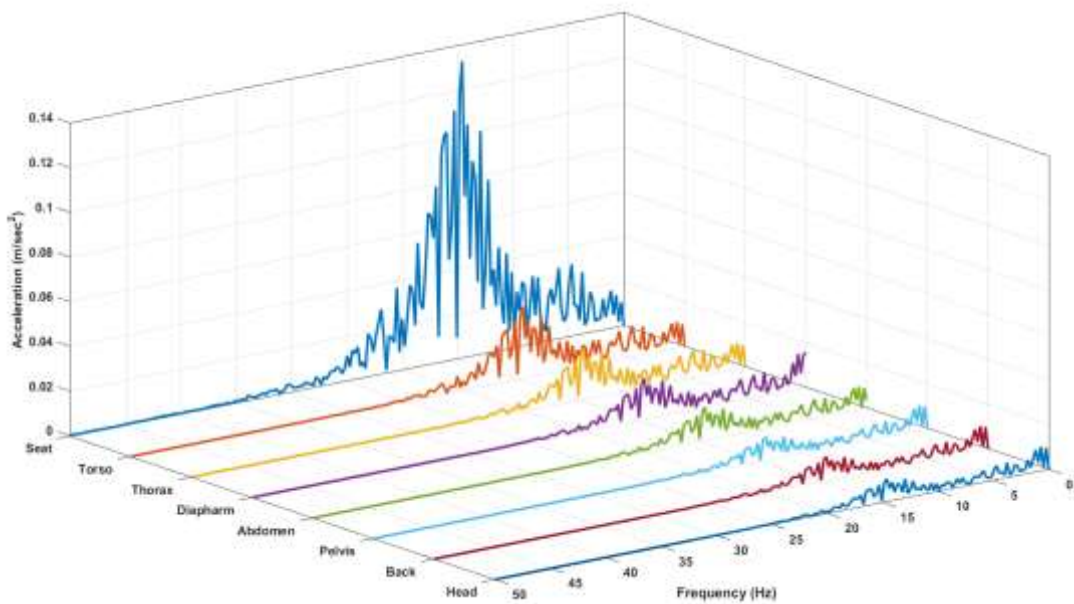
Figure 3.23: Vibration response measures at different parts of BioD at 100 Kmph in H2 road condition
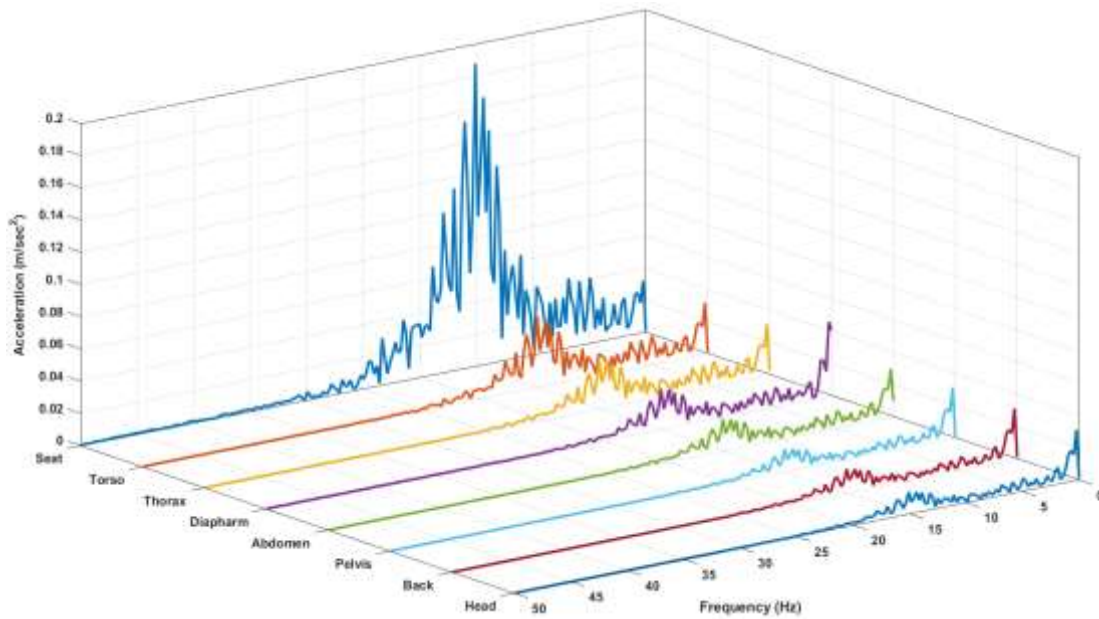
Figure 3.24: Vibration response measures at different parts of BioD at 40 Kmph in H3 road condition
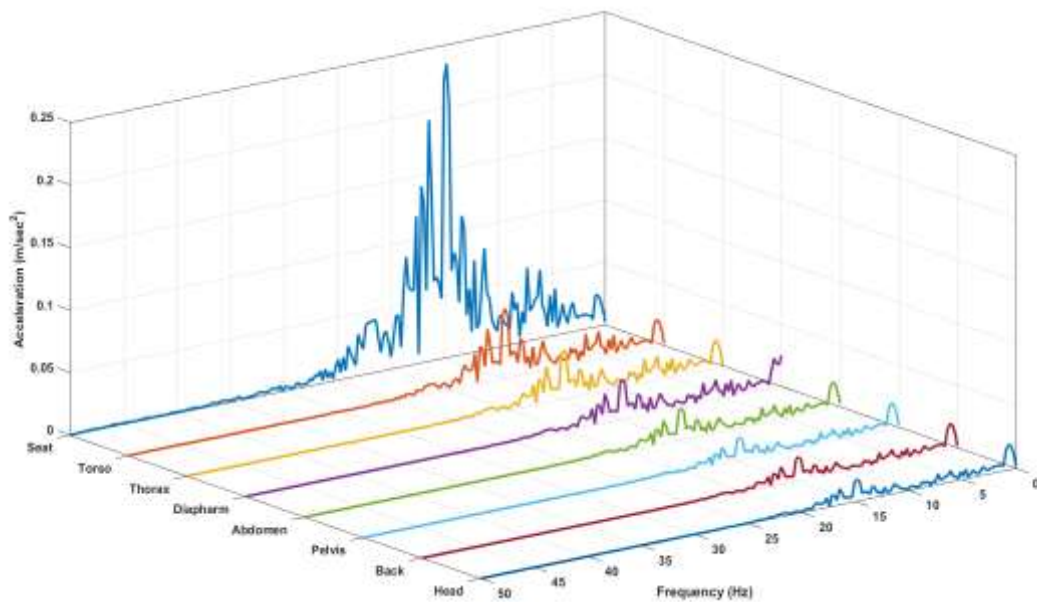
Figure 3.25: Vibration response measures at different parts of BioD at 60 Kmph in H3 road condition
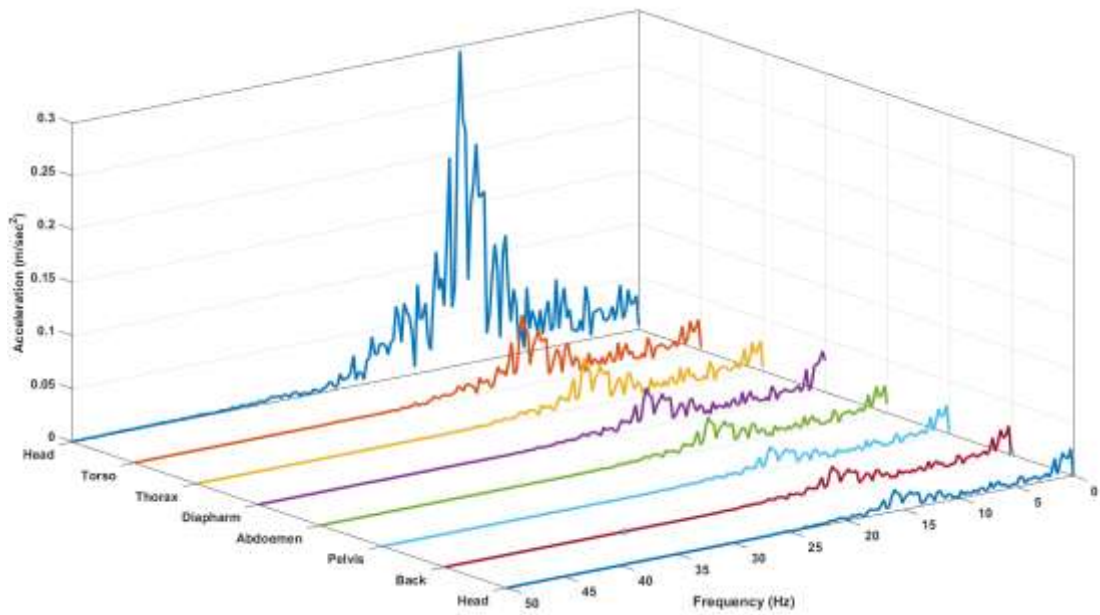
Figure 3.26: Vibration response measures at different parts of BioD at 80 Kmph in H3 road condition
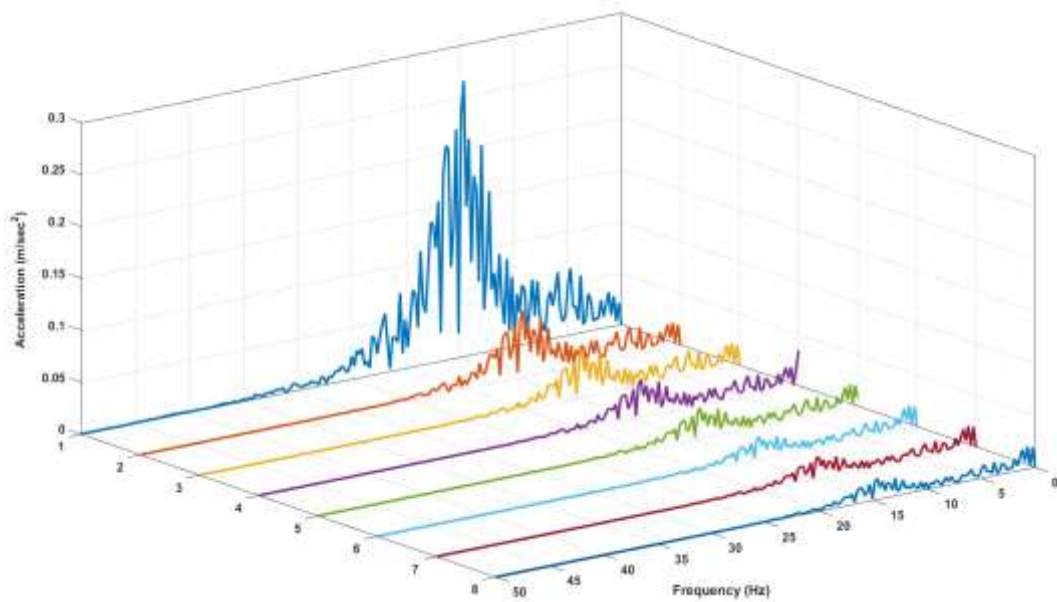
Figure 3.27: Vibration response measures at different parts of BioD at 100 Kmph in H3 road condition
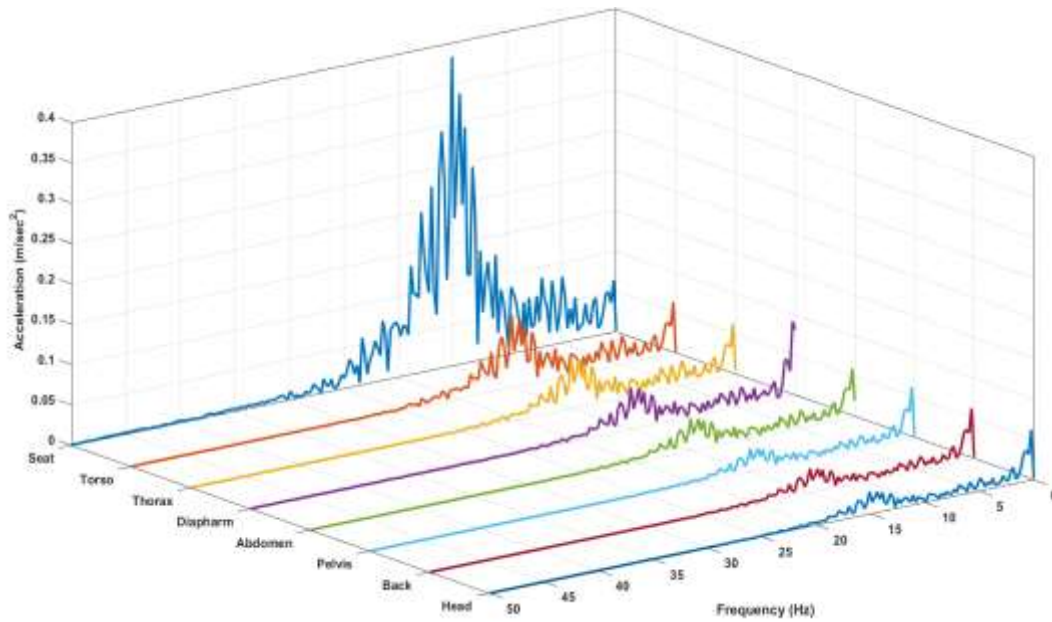
Figure 3.28: Vibration response measures at different parts of BioD at 40 Kmph in H4 road condition
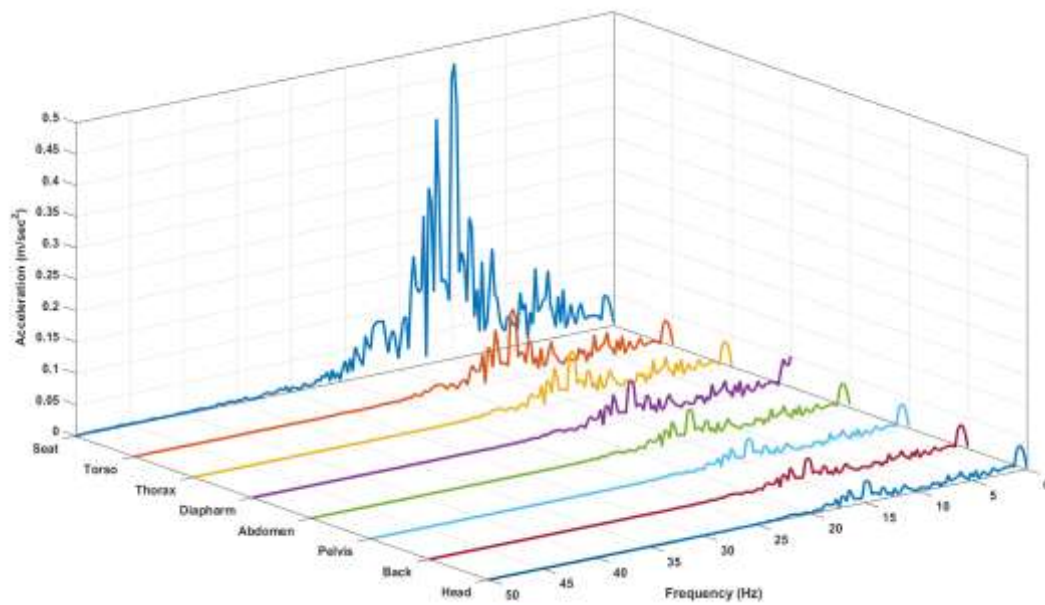
Figure 3.29: Vibration response measures at different parts of BioD at 60 Kmph in H4 road condition
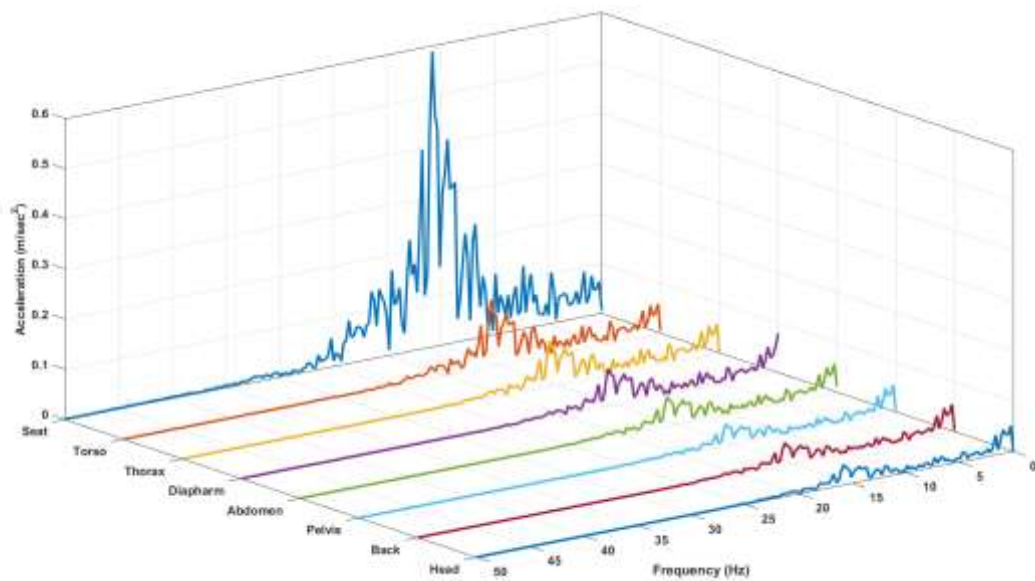
Figure 3.30: Vibration response measures at different parts of BioD at 80 Kmph in H4 road condition
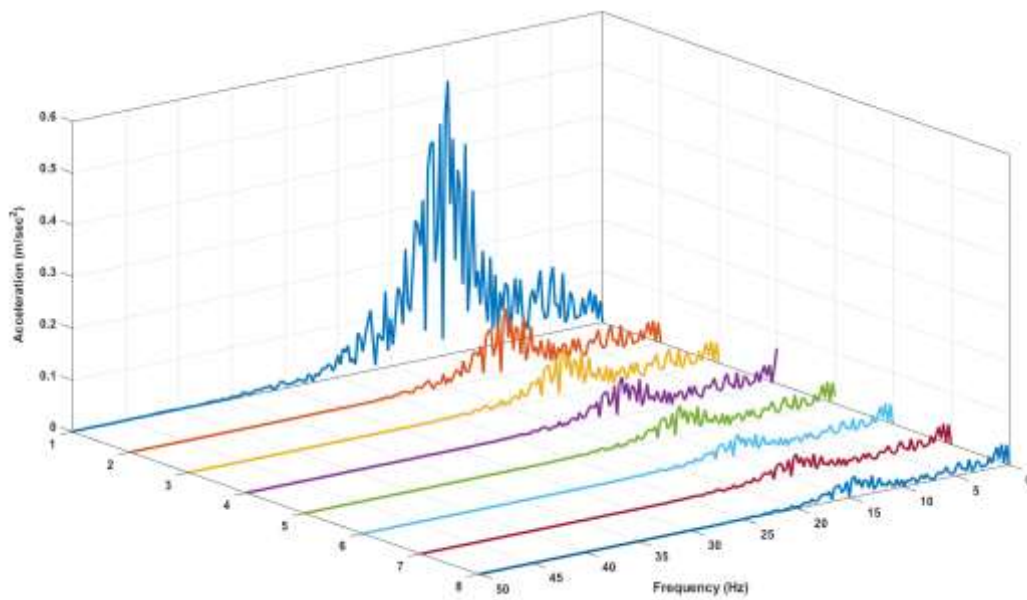
Figure 3.31: Vibration response measures at different parts of BioD at 100 Kmph in H4 road condition

3.4.1 Guidelines for ride comfort (ISO-2631 approved)

The ride comfort assasment consists the response of human body towards vibration. This indeed does not completely depend on the biomechanical and physiological factors, but also on several others factors like physiological ambiances including, heat, pressure, ventilation and many more. However, the International Standards Organization (*ISO*-2631, 1997) has already enumerated the limitations of acquaintance to vibrations transformed from a contact surface to the human body, which is of the frequency range from 1−80 Hz. Further, it is also suggested by ISO that acquaintance to the vibrations associated with frequency range lie between 0.5 Hz to 80 Hz, which later on may cause numerous fatal complications to the human health such as, fatigue, discomfort, obesity and other severe health consequences (*Griffin*, 2012). However, frequent exposure to vibration from a road vehicle transmitting through the seat into the human body via pelvis may cause fatal damage to back, and the other health consequences. Likewise, the spreading of vibration within the human body during whole-body vibration also generates complex sensations. The exact location and specific character of these complex sensations differ significantly and remarkably with the frequency of vibration, axis, and other factors.

Furthermore, the term "discomfort" is contributed to the sensations, generating due to vibration. Most importantly, the comfort is sometimes being used in transportation systems that involve reactions to other environmental parameters as well. The degree of "discomfort" under the prescribed limit may also depend on many factors. A limiting value should be identified for specific applications by the user as per value specificity. Interestingly, different limiting value for "discomfort" may apply in different situations.
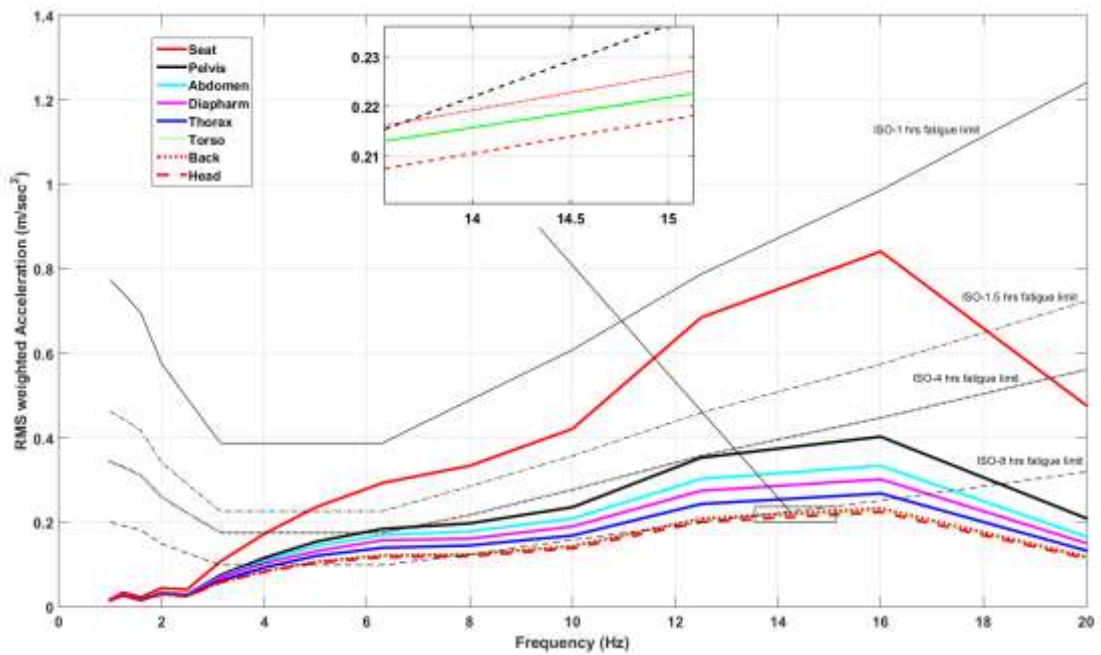
Figure 3.32: RMS weighted acceleration response of human body parts with ISO curves for diminished comfort boundary at 100 km/h in H2 road condition
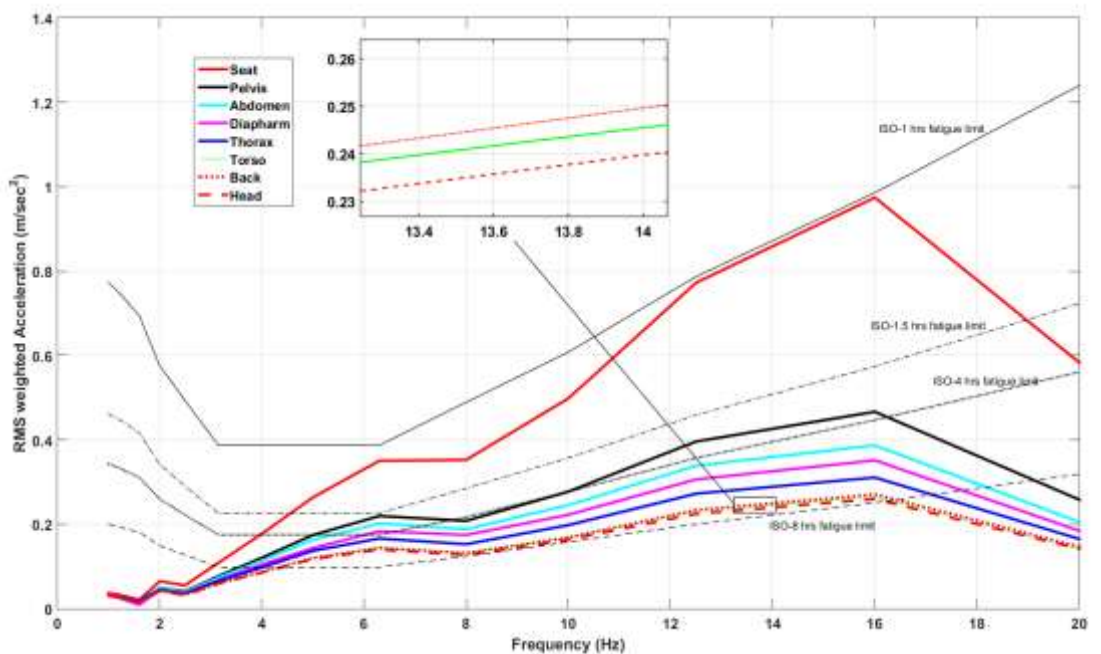
Figure 3.33: RMS weighted acceleration response of human body parts with ISO curves for diminished comfort boundary at 40 km/h in H3 road condition
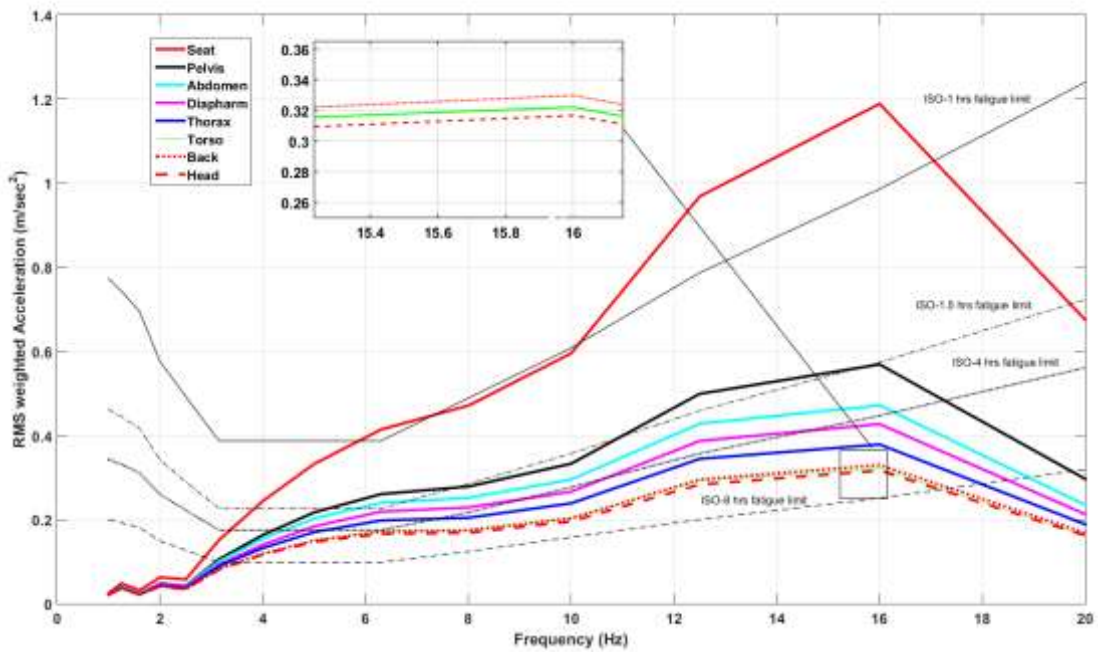
Figure 3.34: RMS weighted acceleration response of human body parts with ISO curves for diminished comfort boundary at 100 km/h in H3 road condition
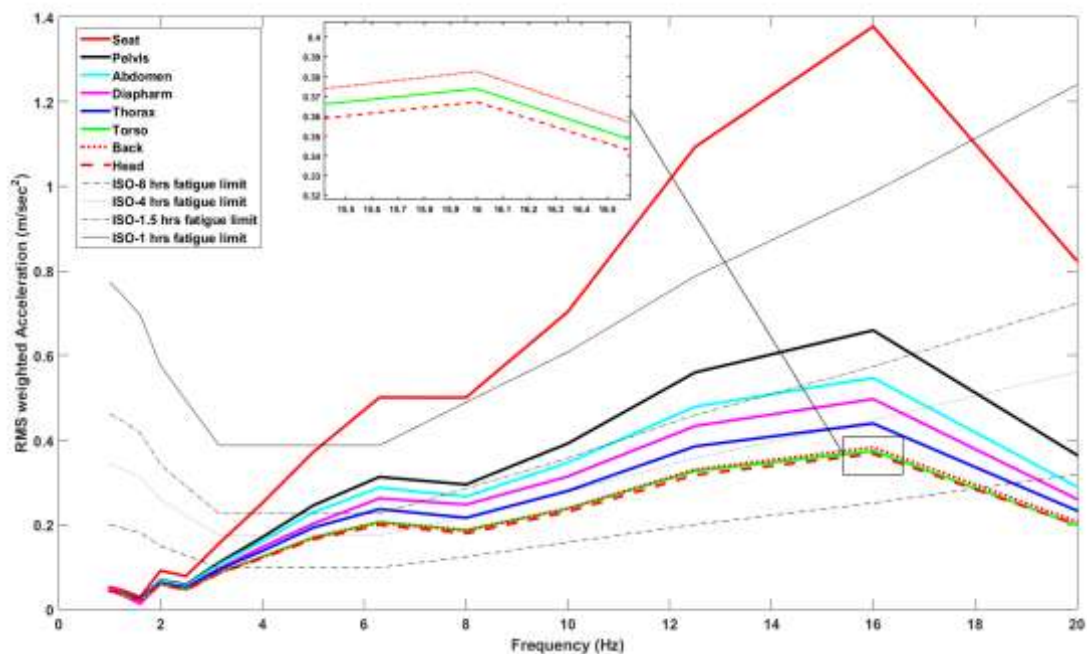
Figure 3.35: RMS weighted acceleration response of human body parts with ISO curves for diminished comfort boundary at 40 km/h in H4 road condition

Figures 3.32-3.36 shows the vertical RMS acceleration in one-third octave bands at various speeds for different body segments of BioD model and seat. The accelerations are superimposed over ISO curves for 1 hr, 2.5 hr, 4 hr and 8 hr 'reduced comfort boundaries'. In Figure 3.32, the acceleration responses of all body parts are below 4 hr curve, up to 100 km/hr in H1 road condition, whereas this fatigue limit is increased for seat vibration up to 8 hr. Therefore, it is likely that driver may feel a normal or common sense of discomfort if exposed to ride vibrations in course of traveling for more than 4 hours at speed greater than 100 km/h in H3 road conditions. For speed below 90km/h, the driver may comfortably ride in the heavy vehicle up to 1.5 hrs (Figures 3.33-3.34). Figures 3.32-3.36 also reveal that head part of human body model slightly estimate higher fatigue limit compare to other body parts. However, the RMS value of seat acceleration is the highest in all road conditions at all vehicle speeds.
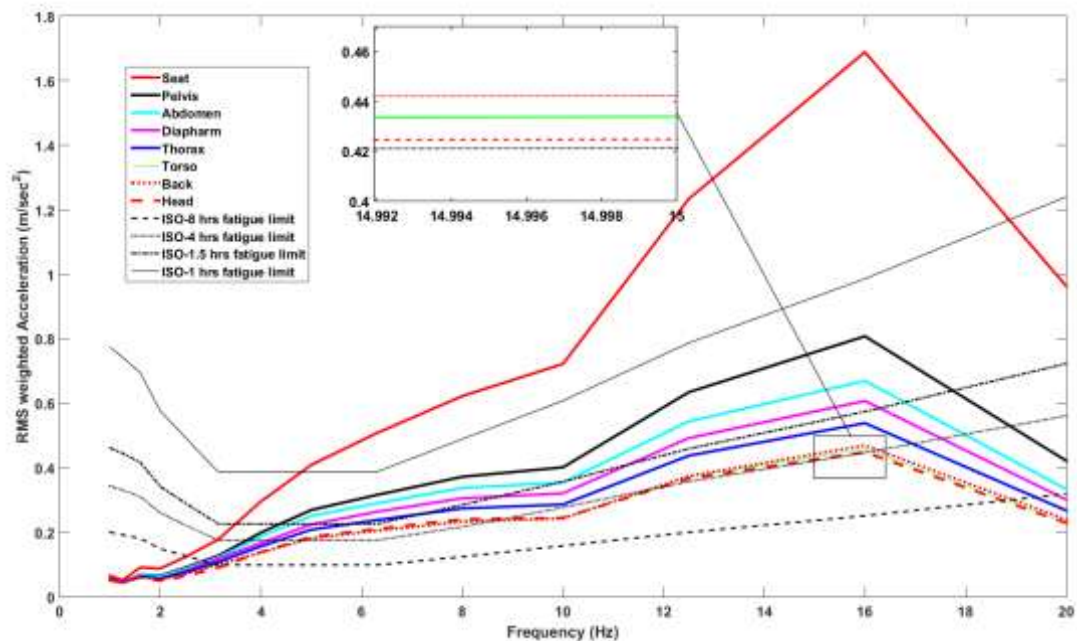
Figure 3.36: RMS weighted Acceleration response of human body parts with ISO curves for diminished comfort boundary at 80 km/h in H4 road condition

Since the RMS weighted curves show that the H1 road condition is perfect for riding the vehicle for long time while it is harmful, if driver ride more than 1.5 hr in H4 road condition. However, Indian roads lies between H2 and H3 conditions, so driver cannot ride more than 4hrs for the given vehicle configuration. Thus, vehicle can be ride comfortably 4hrs in one ride in Indian road condition at the speed range of 60-80 km/hr.

3.4 Conclusions

The issue of comfort in heavy road vehicle has been presented in this chapter. An integrated human BioD-vehicle bondgraph model has been created to investigate the physiological effects of vibrations on the human health. To evaluate the efficacy of the proposed model, root mean square weighted values are calculated for different body parts according to ISO-2631 standards. All results have shown that driver can comfortably travelled if it runs at a speed below 80 kmph in H1 road condition.

The next chapter will describe the detailed control evaluation for the suspension system of a heavy road vehicle. The chapter will focus on various control strategies, which will be modeled through bondgraphs. These controllers will be incorporated with a simplified road truck model and results will then be compared with conventional road truck system with passive system.

Chapter 4

Semi-Active Control Framework for Suspension System of Heavy Road Vehicle

In the previous chapter, whole body vibration has been analyzed for a 7 DOF seated driver along with vehicle model, which was excited vertically as per ISO 8608. The amplitude of different body parts due to given excitement was superimposed over ISO 2631 curves. In this chapter semi-control strategies will be implemented through bondgraph modeling and a proposal of new hybrid control strategies is being presented proposed to extend the scope of vibration reduction and hence fourth improving the comfort level in the heavy vehicle.

4.1 Introduction

Vehicle suspension performs a vital role in vehicle dynamics, contributing to enhance the ride comfort and the vehicle stability. The vehicle suspension system design is having a great potential for research, where one of the goals is to enhance the passenger's comfort through the vibration reduction of the internal vehicle system as well as external road disturbances. Suspension systems can be broadly classified into three basic classes, passive suspensions, semi-active suspensions and active suspensions.

A passive suspension system is one in which the spring stiffness and the damping coefficient are constant. These characteristics are decided by the designer of the suspension, according to the design objectives and the intended application. In an active suspension, force actuator is used instead of passive spring and damper. The

force actuator is capable of adding and dissipating energy from the system, whereas a passive damper can only dissipate energy. The force applied by the force actuator does not dependent on the relative velocity or displacement across the suspension. Though active suspension systems are capable of improving ride comfort as well as stability, they have some added disadvantages. The force actuators required for an active suspension system generally have large power requirements (typically 4-5 hp). The power requirements reduce the overall efficiency of the vehicle, and therefore are usually unacceptable. Moreover, if the actuator fails, the vehicle would be left un-damped, and probably un-sprung. This is a potentially hazardous situation for both the vehicle and the driver.

Besides the above two suspension, semi-active suspensions came into picture in early 1970's. In semi-active suspension system, the conventional spring element is kept but the damper is substituted with a controllable damper as shown in Figure 4.1.
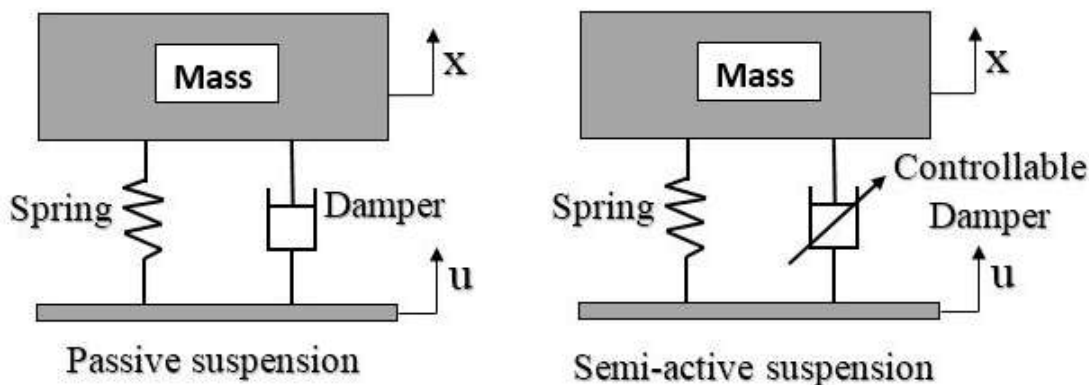
Figure 4.1: Passive and Semi-active suspensions

A semi-active system uses external power only to regulate the damping levels, and operate an embedded controller and a group of sensors. The controller decides the

damping level on the basis of a control strategy, and accordingly adjusts the damper to attain that damping. If the controllable damper required in a semi-active suspension fails, it will simply revert back to a conventional damper. Semi-active systems not only have a less or critical failure mode, but are also less complex, less chances to fail mechanically, and have much lower power requirements as compared to active systems.

Semi-active damper may be of two types: on-off and continuously variable. An on-off damper is varied between "on" and "off" states of damping according to a appropriate control algorithm. The value of damping coefficient in 'on' state is relatively high, whereas value of damping is low in 'off' state. Ideally, the off state damping value should be zero, but this is not feasible practically. It has also been reported that the continuously variable damper is also switched between both "on" and "off" states, conversely, the "on" state damping coefficient is varied, thus varying the corresponding damping force. The next subsection will present the mathematical model of 2-DOF quarter car model with semi-active suspension.

4.2 Mathematical model of a 2-DOF quarter car with semi-active suspension

The model for 2-DOF quarter vehicle with a semi-active suspension is shown in Figure 4.2. The mass M_s represents the vehicle body; the mass M_u represents the wheel. The parallel spring and damper combination is placed in between the vehicle body and the wheel (k_s and c_d), which also represents the stiffness and damping of the suspension system. The damper used in this case is a controllable damper, which is essentially required for a semi-active suspension.
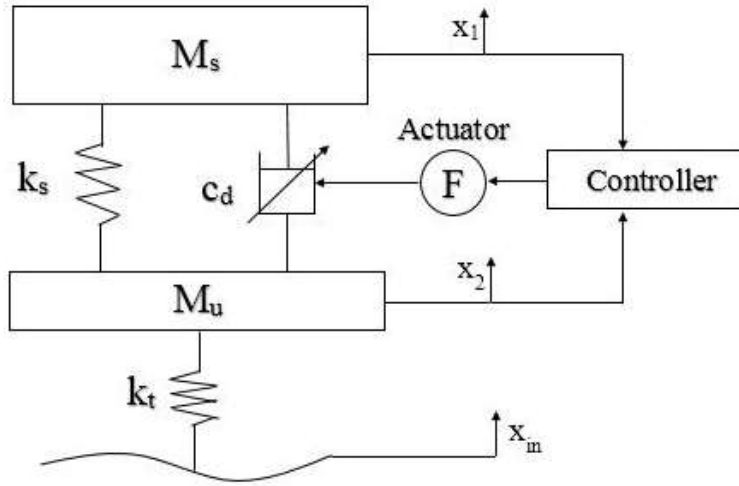
Figure 4.2: 2-DOF quarter car model with controllable damper

A controller is incorporated, which regulates an actuator, and in turn, controls the damping level of the controllable damper. The tire stiffness is shown by the spring k_t. x_1, x_2 and x_{in} are the vehicle displacement, wheel displacement and the road input to the quarter car model.

Now, for the semi-active suspension system, the governing equations may be presented as,

$$M_s \ddot{x}_1 + k_s(x_1 - x_2) + F_d = 0 \tag{4.1}$$

$$M_u \ddot{x}_2 - k_s(x_1 - x_2) - F_d + k_t(x_2 - x_{in}) = 0 \tag{4.2}$$

where, F_d represents the damping force of the controllable damper, which can be regulated by controlling the value of the damping coefficient and given as;

$$F_d = c_d(\dot{x}_1 - \dot{x}_2) \tag{4.3}$$

The state-space representation for the above equation may be given as

$$\begin{bmatrix} M_s & 0 \\ 0 & M_u \end{bmatrix} \begin{Bmatrix} \ddot{x}_1 \\ \ddot{x}_2 \end{Bmatrix} + \begin{bmatrix} 1 \\ -1 \end{bmatrix} \{F_d\} \begin{bmatrix} k_s & -k_s & 0 \\ -k_s & k_s + k_t & -k_t \end{bmatrix} \begin{Bmatrix} x_1 \\ x_2 \\ x_{in} \end{Bmatrix} = 0 \tag{4.4}$$

4.3 Bondgraph models of various semi-control strategies

This section presents various control algorithms for semi-active damping control viz., skyhook, balance control and ground hook control with two variances of all control algorithms, with on-off and continuous. A proposal of hybrid control strategies are also presented which combines two or more of the said control algorithms. Further, this section is extended to describe two new robust control strategies i.e., PID based $H\infty$ controller and PID based double $H\infty$ controller.

4.3.1 Skyhook control

The skyhook configuration shown in Figure 4.3 consists of a damper connected to some inertial reference in the sky. With this configuration, the compromise between resonance control and high-frequency isolation, which is common in passive suspensions, is removed (*Goncalves, 2014*). The skyhook control concentrates on the sprung mass; with the increase in C_{sky}, the sprung mass motion decreases. The isolation of the sprung mass from base excitations by skyhook control comes at the expense of heightened un-sprung mass motion. The basic algorithm may be represented as

$$F_d = F_{skyhook} = \begin{cases} c_{sky}\dot{x}_1, & \dot{x}_1(\dot{x}_1 - \dot{x}_2) \geq 0 \\ 0, & \dot{x}_1(\dot{x}_1 - \dot{x}_2) < 0 \end{cases} \tag{4.5}$$

where, damping force is denoted by F_d, the required damping force of the skyhook damper is denoted by $F_{skyhook}$, and damping coefficient of the hypothetical skyhook damper is c_{sky}. Whereas, sprung mass velocity is $\dot{x}_1$ and the un-sprung mass velocity is $\dot{x}_2$.

4.3.1.1 Continuous skyhook control for quarter vehicle

Considering a 2-DOF system with a skyhook damper as shown in Figure 4.3, the damping force (*Liu*, 2005) can be written as

$$F_{skyhook} = c_{sky}\dot{x}_1 \tag{4.2}$$

where skyhook damping force is denoted by $F_{skyhook}$, the velocity of the vehicle body is denoted by $\dot{x}_1$ is and the damping coefficient of the skyhook damper is c_{sky}. Herein, the main focus of this study is to imitate the skyhook damping force along with a controllable damper mounted between the vehicle body and the wheel/un-sprung mass as shown in Figure 4.3. But, a passive damper can merely absorb vibration energy. So the product of the damping force denoted by F_{sa}, and $\dot{x}_1 - \dot{x}_2$ is the relative velocity, must satisfy the inequality

$$F_{sa}(\dot{x}_1 - \dot{x}_2) \geq 0 \tag{4.3}$$

where, $c_{sky}\dot{x}_1$ denotes the desired damping force, but the semi-active damper can produce this force only whenever $\dot{x}_1$ and $\dot{x}_1 - \dot{x}_2$ should be having the same sign. On the other hand, the damper can generate a force opposite to the desired control force, when $\dot{x}_1$ and $\dot{x}_1 - \dot{x}_2$ are having a opposite sign. It is better not to supply any force in this situation. Thus, the continuous skyhook control algorithm may be represented as
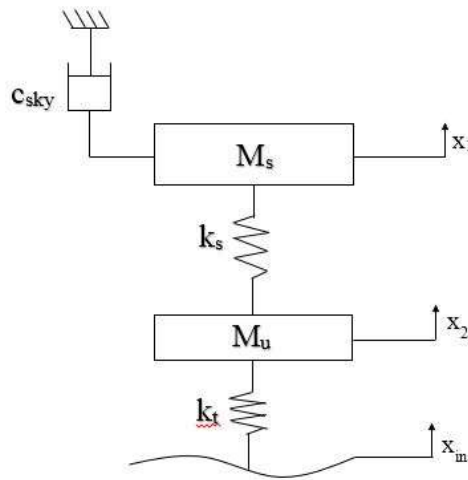
Figure 4.3: Skyhook damper configuration

$$F_{sa} = \begin{cases} c_{sky}\dot{x}_1, & \dot{x}_1(\dot{x}_1 - \dot{x}_2) \geq 0, \\ 0, & \dot{x}_1(\dot{x}_1 - \dot{x}_2) < 0. \end{cases} \tag{4.4}$$

The switching of the damper is regulated by the term $\dot{x}_1(\dot{x}_1 - \dot{x}_2)$, which is the condition function. On state damping force can be expressed as

$$F_{sa} = c_d(\dot{x}_1 - \dot{x}_2) \tag{4.5}$$

Where semi-active damping coefficient is denoted by c_d. Here, the value that c_d have to take to imitate a skyhook damper can be found by equating Eq. (4.4) to Eq. (4.5), which obtains

$$c_d = \begin{cases} \dfrac{c_{sky}\dot{x}_1}{(\dot{x}_1 - \dot{x}_2)}, & \dot{x}_1(\dot{x}_1 - \dot{x}_2) \geq 0, \\ 0, & \dot{x}_1(\dot{x}_1 - \dot{x}_2) < 0. \end{cases} \tag{4.6}$$
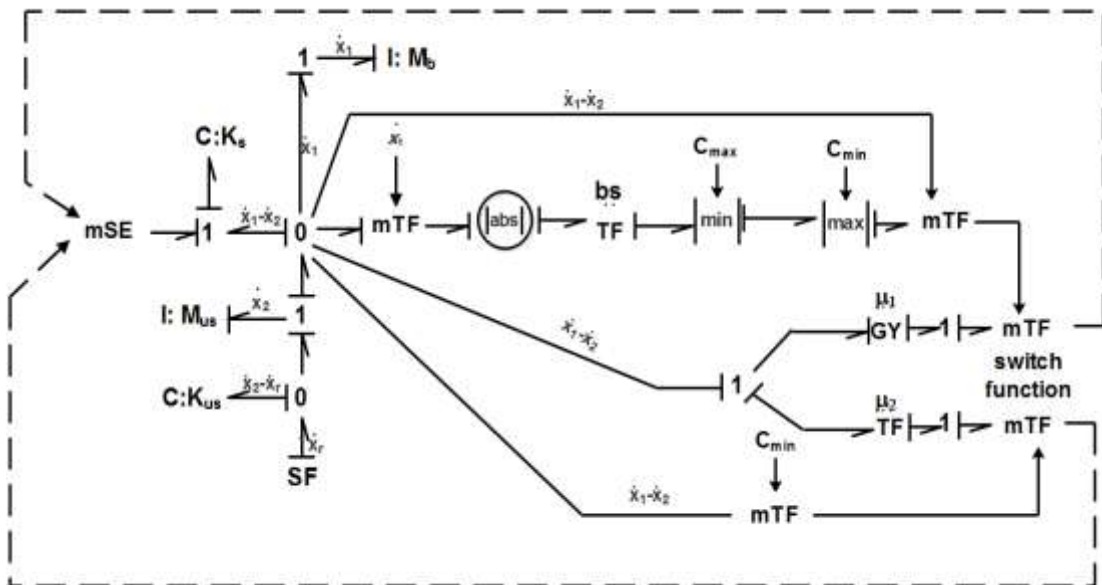
Figure 4.4: Bondgraph model of 2-DOF quarter car suspension system with continuous skyhook controller

It can be seen from Eq. (4.6) whenever, the value of relative velocity $(\dot{x}_1 - \dot{x}_2)$ is very less, the needed damping coefficient augments abruptly and approach to infinity.

Practically, the damping coefficient of a conventional damper is limited by its physical parameter, i.e., there is an upper bound c_{max} and a lower bound c_{min}. Thus, the damping coefficient in Eq. (4.6) can be rewritten as

$$c_d = \begin{cases} max\left[c_{min}, min\left[\dfrac{c_{sky}\dot{x}_1}{(\dot{x}_1 - \dot{x}_2)}, c_{max}\right]\right], & \dot{x}_1(\dot{x}_1 - \dot{x}_2) \geq 0, \\ c_{min}, & \dot{x}_1(\dot{x}_1 - \dot{x}_2) < 0. \end{cases} \tag{4.7}$$

The bondgraph model of continuous skyhook controller is presented in Figure 4.4. In this model, mSE element is used to incorporate a varying damping force in quarter car model while spring stiffness is connected through C-element. The 0-junction describes the difference of sprung and unsprung mass displacement, which is being used as a control logics for controller, TF-element is modulated through damping coefficient 'bs', C_{max} and C_{min} are the maximum and minimum values of damping coefficient, whereas $\mu_1 = 1$ and $\mu_2 = 1$ are the modulus of TF-element and GY-element respectively The switch function is also used to enable the control logic as per aforementioned equation decides the suitable damping force, and input to the mSE element. The detail descriptions of $|min|$, $|max|$, and $|abs|$ subsystems (capsules) are presented in *Appendix A*.

4.3.1.2 On-off skyhook control for quarter vehicle

In case of continuous skyhook, the damping coefficient requires to be varied uninterruptedly. To make the situation simple, an on-off strategy (*Liu, 2005*) has been implemented. The on-off damper generally behaves as a conventional passive damper in the course of vibration depletion portion of the cycle. However, the damping coefficient is presumed to be zero when, the damping force produced in the opposite direction to that of an ideal skyhook damper. Further, the damping force in case of on-off control is given by

$$F_{sa} = \begin{cases} c_{on}(\dot{x}_1 - \dot{x}_2), & \dot{x}_1(\dot{x}_1 - \dot{x}_2) \geq 0, \\ 0, & \dot{x}_1(\dot{x}_1 - \dot{x}_2) < 0, \end{cases} \tag{4.8}$$

where, c_{on} is the on-state damping coefficient of the on-off damper. In a real world situation, a zero damping coefficient is not possible in the off-state. So, the damping coefficient is switched between a maximum value c_{max} and a minimum value c_{min}. The control algorithm is changed accordingly as

$$c_d = \begin{cases} c_{max}, & \dot{x}_1(\dot{x}_1 - \dot{x}_2) \geq 0, \\ c_{min}, & \dot{x}_1(\dot{x}_1 - \dot{x}_2) < 0. \end{cases} \tag{4.9}$$
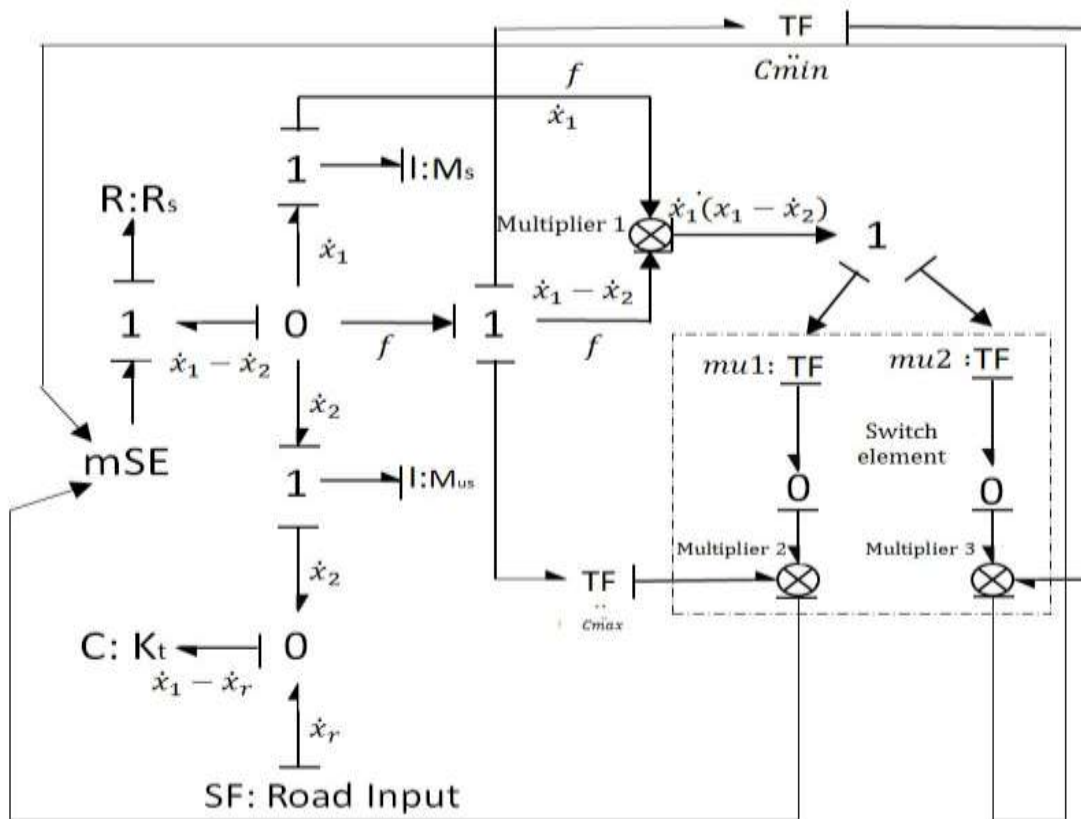
Figure 4.5: Bondgraph model of 2-DOF quarter car suspension system with On-Off skyhook controller

It is again required that on-state damping coefficient, c_{max} must be higher than the off-state damping coefficient c_{min}. Moreover, off-state damping coefficient should be as

small as possible. The bondgraph model of on-off skyhook for quarter car model is shown in Figure 4.5. The bondgraph model of suspension part is almost similar to Figure 4.4. However switch function is designed as per on-off skyhook logic.

4.3.2 Balance control

The fundamental concept of this semi-active control strategy is to balance the spring force by means of damping force. For instances, when both the forces act in opposite directions and to set the damping force to a low value (possibly zero) otherwise. Therefore, the force transmitted through the system is significantly reduced or even cancelled out during the instances, when the damper is acting and is slightly more than the spring force otherwise (*Guglielmino, 2008*). It is also referred to as "relative control" since the control variables are the relative displacement and velocity between the vehicle body and the wheel.

4.3.2.1 On-off balance control for a quarter vehicle

Considering a 2-DOF system shown in Figure 4.2, the acceleration response of the vehicle mass can be expressed as

$$\ddot{x}_1 = -\frac{1}{m}(F_k + F_d) \tag{4.10}$$

Where the spring and damping force is denoted by F_k and F_d respectively. They are represented by the following equations

$$F_k = k_s(x_1 - x_2) \tag{4.11}$$

and

$$F_d = c_d(\dot{x}_1 - \dot{x}_2) \tag{4.12}$$

where, the spring stiffness and the damping coefficient are denoted by k_s and c_d correspondingly. The acceleration magnitude of the vehicle body due to harmonic excitation can be represented as

$$|\ddot{x}_1| = \frac{|F_k|+|F_d|}{m} \begin{cases} t_0 < t < t_0 + \frac{\tau}{4}, \\ t_0 + \frac{\tau}{2} < t < t_0 + \frac{3\tau}{4}, \end{cases} \tag{4.13}$$

$$|\ddot{x}_1| = \frac{|F_k|-|F_d|}{m} \begin{cases} t_0 + \frac{\tau}{4} < t < t_0 + \frac{\tau}{2}, \\ t_0 + \frac{3\tau}{4} < t < t_0 + \tau, \end{cases} \tag{4.14}$$

where, time point is denoted by t_0 at which $\ddot{x}_1 = 0$ and also increases, whereas, period of vibration is denoted by τ. Further, it is noticed from Eq. (4.13), where the damping force leads to increased acceleration for two quarters of the cycle. However, for the remaining part of the cycle, it leads to deceleration of the mass (Eq. (4.14)).

The acceleration will be increased, whenever the damper and spring forces are having the same sign, i.e. the relative velocity and displacement have the similar sign. A control algorithm is being used, which ensure that this condition does not arise, can be represented as

$$F_{sa} = \begin{cases} c_{on}(\dot{x}_1 - \dot{x}_2), & (x_1 - x_2)(\dot{x}_1 - \dot{x}_2) \leq 0, \\ 0, & (x_1 - x_2)(\dot{x}_1 - \dot{x}_2) > 0, \end{cases} \tag{4.15}$$

Where, on-state damping coefficient of the on-off damper is denoted by c_{on}. Further, damping coefficient of corresponding algorithm for the semi-active on-off damper is

$$c_d = \begin{cases} c_{max}, & (x_1 - x_2)(\dot{x}_1 - \dot{x}_2) \leq 0, \\ c_{min}, & (x_1 - x_2)(\dot{x}_1 - \dot{x}_2) > 0, \end{cases} \tag{4.16}$$

where, c_{max} is the maximum and c_{min} is the minimum damping coefficients of the on-off damper. The bondgraph model of on-off balance controller for quarter car model is presented in Figure 4.6. The displacement of sprung mass is connected to the 0-junction with displacement of un-sprung sprung mass, and this difference value (also called suspension displacement) is provided to multiplier 1. The switch function of this controller is modelled through multiplier 2 and multiplier 3. The detail of such multiplier is described in *Appendix A*.
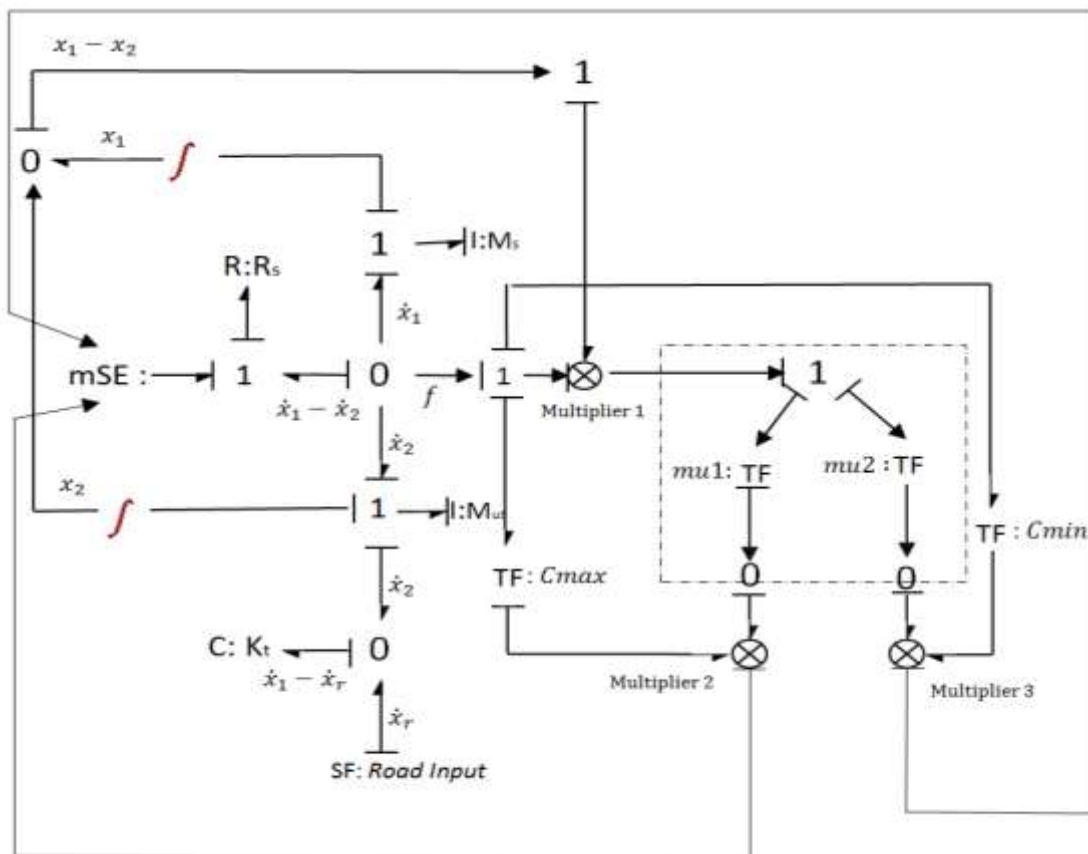
Figure 4.6: Bondgraph model of a 2-DOF quarter car suspension system with on-off balance controller

4.3.2.2 Continuous balance control for quarter vehicle

During on-state condition, the immediate damping force is hardly equal to the immediate spring force in magnitude. The excess force will add to the acceleration of

the vehicle body. *Liu et al. (2005)* have recommended a continuously variable control logic. In this logic, the damping coefficient is continuously varied on the basis of relative displacement and velocity, likewise, the spring and damper force balance out completely during on-state. The needed force is given by

$$F_{sa} = \begin{cases} -k_s(x_1 - x_2), & (x_1 - x_2)(\dot{x}_1 - \dot{x}_2) \leq 0, \\ 0, & (x_1 - x_2)(\dot{x}_1 - \dot{x}_2) > 0. \end{cases}$$
(4.17)

The damper in this case will act like a spring with a negative stiffness during on-state. The damping force is controlled to balance the magnitude of the spring force such that the zero acceleration is produced. The damping coefficient according to this control algorithm can be given by

$$c_d = \begin{cases} \dfrac{-k_s(x_1 - x_2)}{(\dot{x}_1 - \dot{x}_2)}, & (x_1 - x_2)(\dot{x}_1 - \dot{x}_2) \leq 0, \\ 0, & (x_1 - x_2)(\dot{x}_1 - \dot{x}_2) > 0. \end{cases}$$
(4.18)

In the Eq. (4.30), the damping coefficient will approach infinity when $(\dot{x}_1 - \dot{x}_2) \rightarrow 0$, which is practically not possible. The damping coefficient is having an upper and a lower bound on the basis of the physical parameter of the damper. Taking into consideration the physical constraints, the damping coefficient is expressed as

$$c_d = \begin{cases} \max\left[c_{min}, \min\left[\dfrac{-k_s(x_1 - x_2)}{(\dot{x}_1 - \dot{x}_2)}, c_{max}\right]\right], & (x_1 - x_2)(\dot{x}_1 - \dot{x}_2) \leq 0, \\ c_{min}, & (x_1 - x_2)(\dot{x}_1 - \dot{x}_2) > 0. \end{cases}$$
(4.19)

In this case, both the on-off and continuous balance algorithm balance out the damping force and spring force to the some limit, if both the forces have opposite signs. In on-state, the on-off logic can generate a damping force which is proportional to the relative velocity across the damper. Hence, it cannot assure that the damping force cancels out the spring force totally. Further, the spring force can be somewhat balanced or may

even be cancelled depending upon c_{min}, c_{max} and the frequency. Moreover, the spring force in case of continuous balance control can be balanced by the damping force partially or fully. The bondgraph model of continuous balance controller for quarter car model is presented in Figure 4.7.

4.3.3 Groundhook control

The groundhook control logic aims at reducing the dynamic tire force, and hence, leads to better handling as well as less road damage. Similar to skyhook damper, the groundhook damper is assumed to be hooked to a fixed point, i.e. ground in this case. The schematic diagram of a groundhook damper is shown in Figure 4.8. The damping force (*Blanchard,* 2003) may be expressed as

$$F_d = F_{groundhook} = \begin{cases} c_{gnd}\dot{x}_2, & -\dot{x}_2(\dot{x}_1 - \dot{x}_2) \geq 0 \\ 0, & -\dot{x}_2(\dot{x}_1 - \dot{x}_2) < 0 \end{cases} \tag{4.20}$$

where, F_d is the damping force, $F_{groundhook}$ is the required damping force of the groundhook damper and c_{gnd} is the damping coefficient of the groundhook damper.
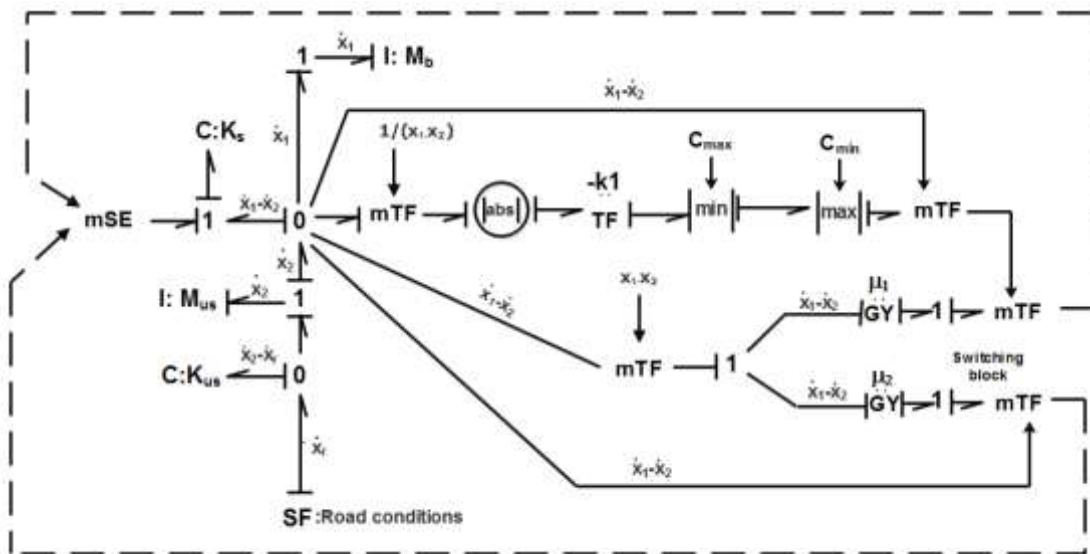
Figure 4.7: Bondgraph model of 2-DOF quarter car suspension system with continuous balance controller

124

4.3.3.1 Continuous groundhook control for quarter vehicle

Considering a 2-DOF system with a groundhook damper as shown in Figure 4.8, the damping force may be written as

$$F_{groundhook} = c_{gnd}\dot{x}_2 \tag{4.21}$$

where groundhook damping force is denoted by $F_{groundhook}$, the velocity of the unsprung mass is denoted by $\dot{x}_2$ and the damping coefficient of the groundhook damper is c_{gnd}. Here, the main purpose is to reproduce the groundhook damping force with a controllable damper mounted between the vehicle body and the wheel/unsprung mass as depicted in Figure 4.2. Moreover, a passive damper may only absorb vibration energy. In this cases, F_{sa} denotes the product of the damping force and the relative velocity, $\dot{x}_1 - \dot{x}_2$, must satisfy the inequality

$$F_{sa}(\dot{x}_1 - \dot{x}_2) \geq 0 \tag{4.22}$$

Where, $c_{gnd}\dot{x}_2$ denotes the desired force, and semi-active damper can produce this force, when $\dot{x}_2$ and $\dot{x}_1 - \dot{x}_2$ are having the opposite sign. It is also reported that when $\dot{x}_2$ and $\dot{x}_1 - \dot{x}_2$ are having the same sign, the damper can give a force opposite to the desired control force.
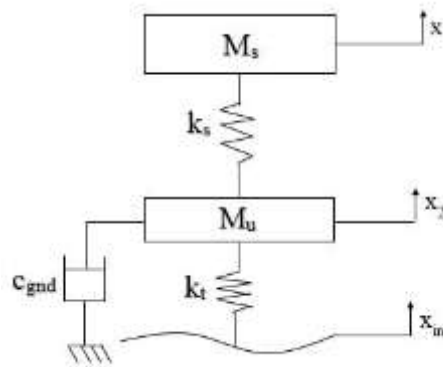
Figure 4.8: Groundhook damper configuration

It is better not to release any force in this situation. Thus, the continuous skyhook control algorithm may be expressed as

$$F_{sa} = \begin{cases} c_{gnd}\dot{x}_2, & -\dot{x}_2(\dot{x}_1 - \dot{x}_2) \geq 0, \\ 0, & -\dot{x}_2(\dot{x}_1 - \dot{x}_2) < 0. \end{cases} \tag{4.23}$$

The switching of the damper is regulated by the term $-\dot{x}_2(\dot{x}_1 - \dot{x}_2)$, which is the condition function. On-state damping force may be written as

$$F_{sa} = c_d(\dot{x}_1 - \dot{x}_2) \tag{4.24}$$

where c_d is the semi-active damping coefficient. Further, the value c_d have to take to imitate a groundhook damper which can be presented by equating Eq. (4.23) to Eq. (4.24), which gives

$$c_d = \begin{cases} \dfrac{c_{gnd}\dot{x}_2}{(\dot{x}_1 - \dot{x}_2)}, & -\dot{x}_2(\dot{x}_1 - \dot{x}_2) \geq 0, \\ 0, & -\dot{x}_2(\dot{x}_1 - \dot{x}_2) < 0. \end{cases} \tag{4.25}$$
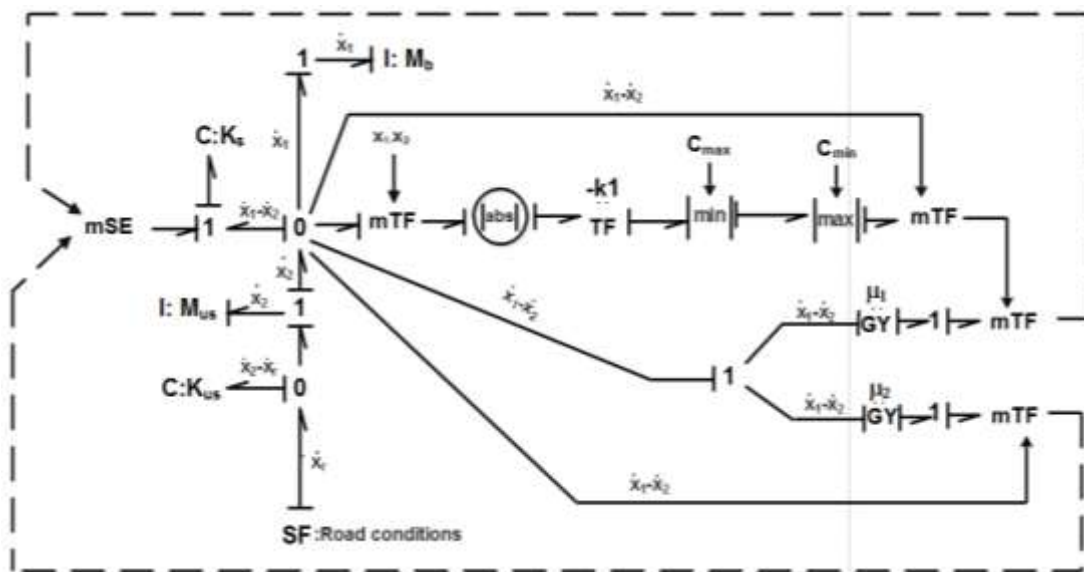
Figure 4.9: Bondgraph model of 2-DOF quarter car suspension system with continuous groundhook controller

It can be seen from Eq. (4.25) that, when even the relative velocity $(\dot{x}_1 - \dot{x}_2)$ is very small, the needed damping coefficient augments abruptly and approaches infinity. Practically, the damping coefficient of a conventional damper is limited by its physical parameter, including, an upper bound denoted by c_{max} and a lower bound denoted by c_{min}. Thus, the damping coefficient in Eq. (4.25) can be rewritten as

$$c_d = \begin{cases} max\left[c_{min}, min\left[\dfrac{c_{gnd}\dot{x}_2}{(\dot{x}_1 - \dot{x}_2)}, c_{max}\right]\right], & -\dot{x}_2(\dot{x}_1 - \dot{x}_2) \geq 0, \\ c_{min}, & -\dot{x}_2(\dot{x}_1 - \dot{x}_2) < 0. \end{cases} \tag{4.26}$$

The bondgraph model of continous ground hook logic controller for quarter car system may be presented in Figure 4.9.

4.3.3.2 On-off groundhook control for quarter vehicle

The on-off damper acts as a conventional passive damper during the vibration depletion portion of the cycle, but the damping coefficient is assumed to be zero, when the damping force generated is in opposite direction to that of an ideal groundhook damper. The damping force in case of on-off control is presented as

$$F_{sa} = \begin{cases} c_{on}(\dot{x}_1 - \dot{x}_2), & -\dot{x}_2(\dot{x}_1 - \dot{x}_2) \geq 0, \\ 0, & -\dot{x}_2(\dot{x}_1 - \dot{x}_2) < 0, \end{cases} \tag{4.27}$$

where, c_{on} is the on-state damping coefficient of the on-off damper. In a real world situation, a zero damping coefficient is not possible in the off-state. So, the damping coefficient is switched between a maximum value c_{max} and a minimum value c_{min}. The control algorithm is changed accordingly as

$$c_d = \begin{cases} c_{max}, & -\dot{x}_2(\dot{x}_1 - \dot{x}_2) \geq 0, \\ c_{min}, & -\dot{x}_2(\dot{x}_1 - \dot{x}_2) < 0. \end{cases} \tag{4.28}$$

The on-state damping coefficient c_{max} should be much greater than the off-state damping coefficient c_{min}. The off-state damping constant should be as small as possible.

4.4 Hybrid control strategy

Further, hybrid control strategies can be developed by integrating two or more control strategies, which have discussed above in previous section. They can provide the benefit of both the control strategies and hence may provide better performance in terms of vibration isolation as well as vehicle handling.

4.4.1 Hybrid skyhook-groundhook control

This control logic is intended at reducing both the body acceleration and the dynamic tire force. The sprung mass considered here, to be linked to a hypothetical damper, which is connected to an inertial reference in sky, whereas the unsprung mass has a damper, which is connected to a reference point in ground as shown in Figure 4.10.
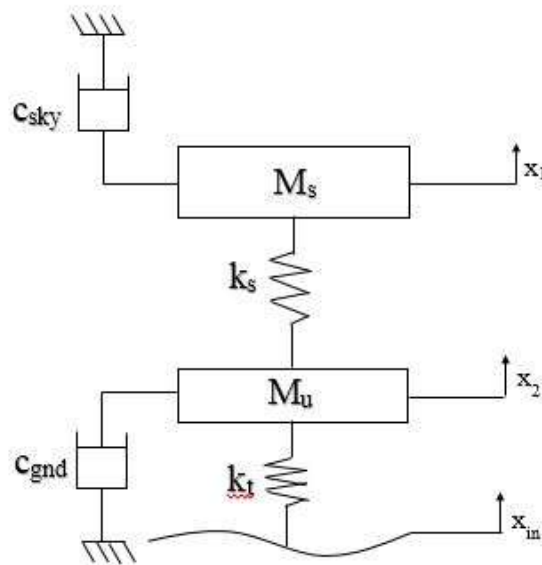
Figure 4.10: Hybrid skyhook-groundhook damper configuration

Table 4.1: Detailed summary of various hybrid control strategies

Hybrid damper type		Damping force	Damping coefficient		Condition function
HS-1	Hybrid Skyhook-Groundhook control	$F_{hybrid-SH-GH} = \alpha F_{skyhook} + (1-\alpha)F_{groundhook}$	On-state	$C_{d,sky}=C_{max}$	$\dot{X}_1(\dot{X}_1 - \dot{X}_2) \geq 0$
				$C_{d,ground}=C_{max}$	$-\dot{X}_2(\dot{X}_1 - \dot{X}_2) \geq 0$
			Off-state	$C_{d,sky}=C_{min}$	$\dot{X}_1(\dot{X}_1 - \dot{X}_2) < 0$
				$C_{d,ground}=C_{min}$	$-\dot{X}_2(\dot{X}_1 - \dot{X}_2) < 0$
HS-2	Hybrid Groundhook-Balance control	$F_{hybrid-GH-B} = \gamma F_{groundhook} + (1-\gamma)F_{balance}$	On- state	$C_{d,ground}=C_{max}$	$-\dot{X}_2(\dot{X}_1 - \dot{X}_2) \geq 0$
				$C_{d,balance}=C_{max}$	$(X_1 - X_1)(\dot{X}_1 - \dot{X}_2) \leq 0$
			Off-state	$C_{d,ground}=C_{min}$	$-\dot{X}_2(\dot{X}_1 - \dot{X}_2) < 0$
				$C_{d,balance}=C_{min}$	$(X_1 - X_1)(\dot{X}_1 - \dot{X}_2) > 0$
HS-3	Hybrid Skyhook-Balance control	$F_{hybrid-SH-B} = \beta F_{skyhook} + (1-\beta)F_{balance}$	On-state	$C_{d,sky}=C_{max}$	$\dot{X}_1(\dot{X}_1 - \dot{X}_2) \geq 0$
				$C_{d,balance}=C_{max}$	$(X_1 - X_1)(\dot{X}_1 - \dot{X}_2) \leq 0$
			Off-state	$C_{d,sky}=C_{min}$	$\dot{X}_1(\dot{X}_1 - \dot{X}_2) < 0$
				$C_{d,balance}=C_{min}$	$(X_1 - X_1)(\dot{X}_1 - \dot{X}_2) > 0$
HS-4	Hybrid Skyhook-Groundhook-Balance control	$F_{hybrid-SH-GH-B} = \delta F_{skyhook} - \mu F_{groundhook} + (1-\delta-\mu)F_{balance}$	On-state	$C_{d,sky}=C_{max}$	$\dot{X}_1(\dot{X}_1 - \dot{X}_2) \geq 0$
				$C_{d,ground}=C_{max}$	$-\dot{X}_2(\dot{X}_1 - \dot{X}_2) \geq 0$
				$C_{d,balance}=C_{max}$	$(X_1 - X_1)(\dot{X}_1 - \dot{X}_2) \leq 0$
			Off-state	$C_{d,sky}=C_{min}$	$\dot{X}_1(\dot{X}_1 - \dot{X}_2) < 0$
				$C_{d,ground}=C_{min}$	$-\dot{X}_2(\dot{X}_1 - \dot{X}_2) < 0$
				$C_{d,balance}=C_{min}$	$(X_1 - X_1)(\dot{X}_1 - \dot{X}_2) > 0$

The control algorithm is obtained by combining both skyhook and groundhook control algorithms (*Strydom, 2014; Goncalves, 2001*).

$$F_{hybrid-SH-GH} = \alpha F_{skyhook} + (1 - \alpha)F_{groundhook} \tag{4.29}$$

where, $F_{hybrid-SH-GH}$ is the damping force of the hybrid controller, $F_{skyhook}$ is the skyhook damping force, $F_{groundhook}$ is the groundhook damping force and α is the weighing factor to adjust comfort or handling as considered, $\alpha \in (0,1)$ (*Kashem*, 2015). The skyhook damping force is controlled with the on-off skyhook strategy as discussed in previous sub-sections before and the groundhook force is controlled by the on-off groundhook logic respectively.

4.4.2 Hybrid skyhook-balance control

Similar to the hybrid logic discussed above, other hybrid strategies can be developed by combining two or more control strategies. One can combine skyhook and balance logic to provide the hybrid control logic, which may be expressed as

$$F_{hybrid-SH-B} = \beta F_{skyhook} + (1 - \beta)F_{balance} \tag{4.30}$$

where, $F_{hybrid-SH-B}$ is the damping force of hybrid controller, $F_{balance}$ is the balance control force and β is the weighing factor to adjust the level of skyhook control or balance control. If β is set to 1, the control will be purely skyhook control, whereas, if β is set to 0, it will be a pure balance control. Similar as before, the skyhook and balance damping forces are controlled by the on-off skyhook and on-off balance control algorithms.

4.4.3 Hybrid groundhook-balance control

Groundhook and balance control logics are considered together to achieve a hybrid control strategy as shown below,

$$F_{hybrid-GH-B} = \gamma F_{groundhook} + (1 - \gamma)F_{balance} \qquad (4.31)$$

where, $F_{hybrid-GH-B}$ is the damping force of hybrid controller and γ is the weighing factor to adjust the level of groundhook control or balance control. If γ is set to 1, the control will be purely groundhook control, whereas, if γ is set to 0, it will be a pure balance control. Here, the groundhook damping force is regulated by the on-off groundhook logic whereas, balance damping force is controlled with on-off balance logic.

4.4.4 Hybrid skyhook-ground hook-balance control

All the three control strategies are integrated to get a hybrid control strategy which will have the advantages of all the three strategies. The contribution of different control strategies have been decided by the weighing factors δ and μ as shown in the following expression.

$$F_{hybrid-SH-GH-B} = \delta F_{skyhook} - \mu F_{groundhook} + (1 - \delta - \mu)F_{balance} \qquad (4.32)$$

The next subsection will present the PID based H∞ controller logic.

4.5 PID based *H∞* controller methodology

The H∞ controller is used as a robust technique to provide stability and performance to the vehicle system. This optimization approach is considered to be effective and efficient design methods for linear and time variant control systems. The main objective is to obtain a design methodology, which minimizes a given performance under random road disturbances or unpredictable conditions. Therefore, this method is incorporated in present work, where it is combined with PID controllers. Detailed description about the mathematical properties of this methodology is referred in the paper (*Doyle, 1989*). However, the basic structure of *H∞* controller is shown in Figure 4.11.

131
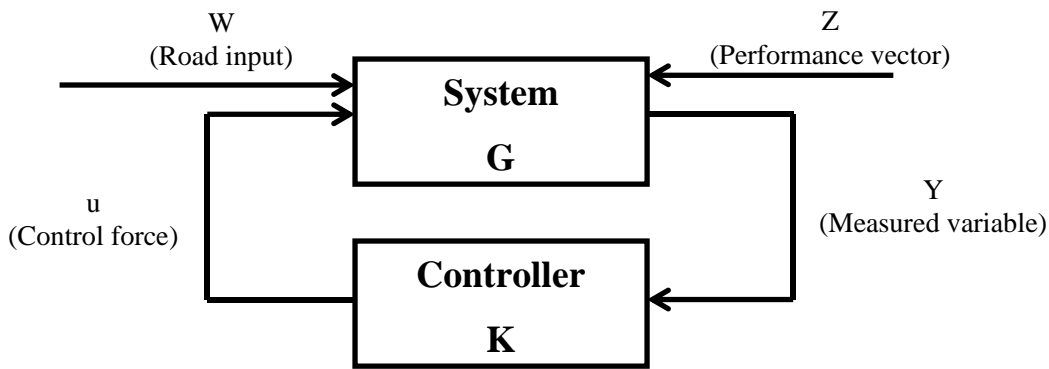
Figure 4.11: Basic configuration of $H\infty$ controller

The Figure 4.11 represents the system G, and LTI model defined by a finite dimensional state space model.

$$\dot{x} = Ax + B_1 w + B_2 u \tag{4.33}$$

$$z = C_1 x + D_{11} w + D_{12} u \tag{4.34}$$

$$y = C_2 x + D_{21} w + D_{22} u \tag{4.35}$$

where x stands for state variables, $\dot{x}$ stands for derivative of state variables, w represents road input, u is control force, y consists of measured variables, z is performance vector (which is to be minimized to meet the control objectives) and the coefficient matrices A_i, B_i, C_i, D_i are known. Now, for designing the coefficients of controller K, one may consider a closed loop transfer functions, which is presented in *Appendix F*. The transfer functions w to z may be given by the Linear Fractional Transformation (LFT), and expressed as,

$$z = F_l(G, K)w \tag{4.36}$$

The standard $H\infty$ optimal control problem is to find all stabilizing K controllers, which can be minimized (*Doyle, 1989*),

$$\left\| F_l(G, K) \right\|_\infty = \sup_w \bar{\sigma}(F_l(G, K)(jw)) \tag{4.37}$$

In practice, it is usually not necessary to obtain an optimal controller for the H∞ problem, and it is often computationally (and theoretically) simpler to design a suboptimal one (i.e. one close to the optimal ones in the sense of the H∞ norm). Let min be the minimum value of $\left\| F_l(G, K) \right\|_\infty$ for overall stabilizing controllers K. Then, the H∞ sub-optimal control problem is given by $\gamma > \gamma_{\min}$ find all stabilizing controllers K such that

$$\left\| F_l(G, K) \right\|_\infty < \gamma \tag{4.38}$$

This inequality can be solved efficiently using the algorithm of *Doyle et al.* (1989), and by reducing γ iteratively, one may achieve an optimal solution. The algorithm is customized with various simplify assumptions, which are presented in details in *Appendix F*.

Proportional integrated derivative (PID) controller is the closed loop feedback mechanism that can be used in wide variety of industrial control applications. The repose of the PID controller depends on how close linear model represents the actual behavior of the real system. This controller continuously calculates an error value *e(t)* as the difference between a desired set point and a measured process variable. The controller attempts to minimize the error over time by adjustment of a control variable, such as the position of a control valve, or damping characteristics of damper. The configuration of this controller is presented in Figure 4.12. One may obtain an expression for PID controller as

$$F_{PID} = K_P e(t) + K_I \int_0^t e(\tau)d\tau + K_D \frac{de(t)}{dx} \qquad (4.39)$$
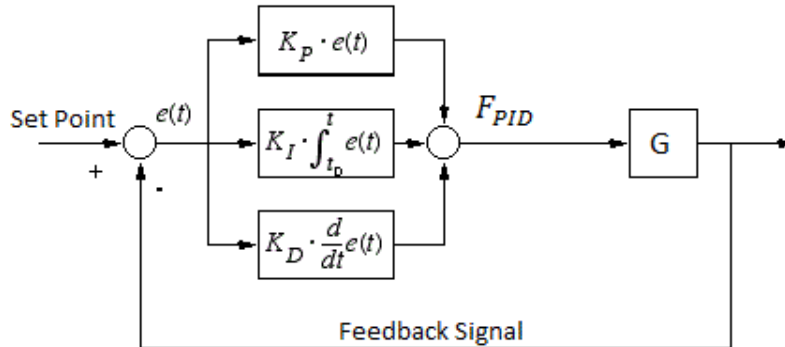
Figure 4.12: PID Controller configuration

where, K_p, K_D, and K_I all non-negative denote the coefficients for the proportional, integral, and derivative terms, respectively. $e(t)$ is error (difference between set point and process variable) and G is a LTI model with state space configuration. From the output, the acceleration is send back as feedback and error signal is generated, which finally results in obtaining the control force. The PID based $H\infty$ controller involves PID controller with $H\infty$ configuration in order to diminish the sprung mass displacement up to a certain limit. The $H\infty$ controlled system is provided by an extra PID control loop (Figure 4.13) which further enhances the required output.
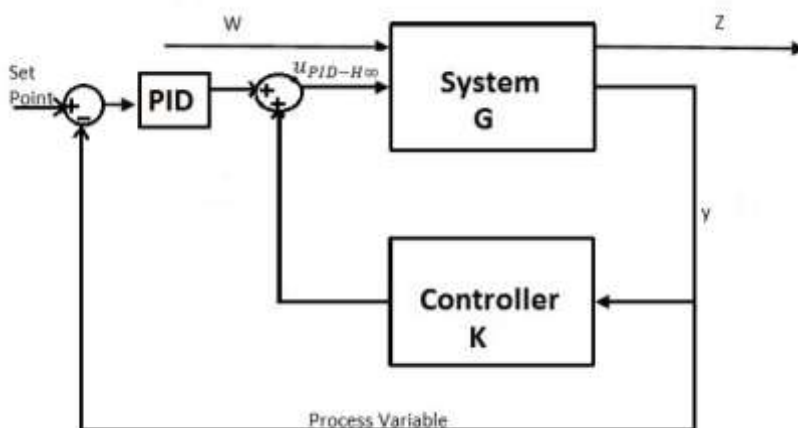
Figure 4.13: PID based $H\infty$ controller

134

The contribution of PID and H∞ has been decided by the α weighing factor as shown in the following expression.

$$u_{PID} = \alpha u_{H_\infty} + (1-\alpha)u_{PID} \tag{4.40}$$

where, u_{H_∞} is the damping force of H∞ controller (*i.e K*) and u_{PID} is damping force due to PID controller. The H∞ controller design is based upon the above algorithm. But addition of PID feedback loop helps to minimize the sprung mass displacement. In Eq.(4.68), if α is 1, then the controller act as pure H∞ and if it α is 0, it represents a pure PID controller. Finally, the outputs are simulated and robust data is achieved.

4.6 PID based double *H*∞ controller methodology
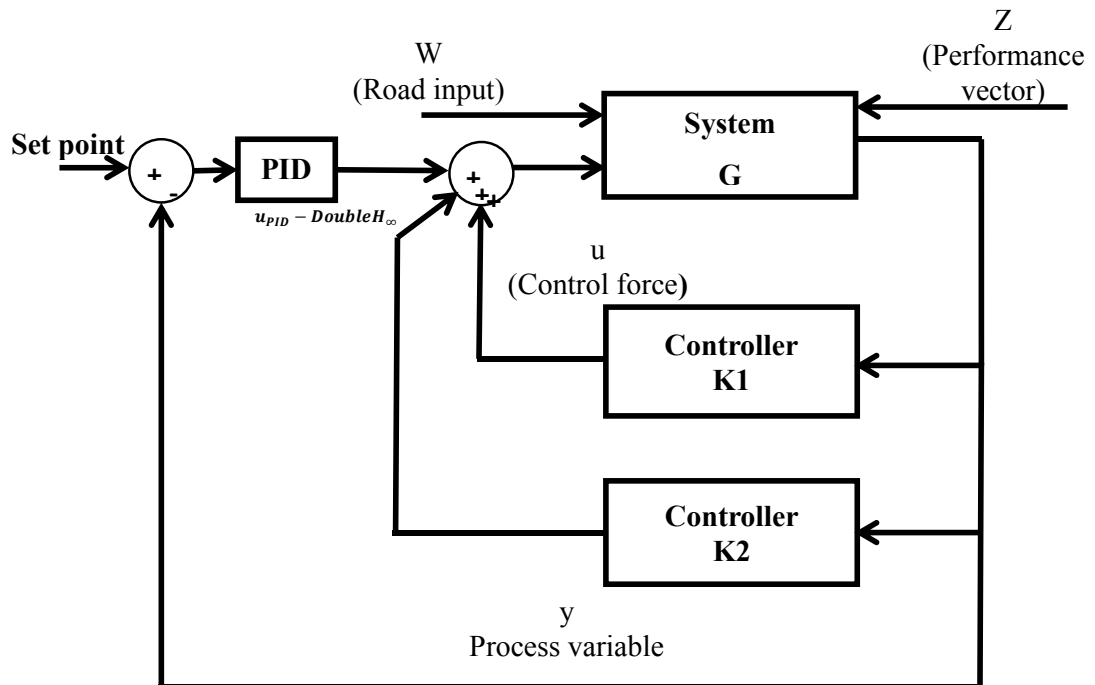
Figure 4.14: PID based Double-*H*∞ controller

To enhance both ride comfort and road holding capability, a new approach of considering two H∞ Controller along with PID is modeled and then performance is

evaluated. In this case, two different H∞ controllers are designed namely *K1* and *K2*, where *K1* is designed for ride purpose and *K2* is designed to increase road holding capability of vehicle. Further PID feedback loop is added to minimize sprung mass displacement. The configuration of this controller is shown in Figure 2.8.

The contribution of PID and double H∞ controller with gains K_1 and K_2 have been decided by the weighing factors α and β as shown in the following expression

$$u_{PID-double\ H\infty} = \alpha u_{K_1} + \beta u_{K_2} + (1 - \alpha - \beta)u_{PID} \tag{4.41}$$

In this Eq. (4.41), u_{K1}, u_{K2} and u_{PID} are the damping force due to controllers K_1, K_2 (based on H∞) and *PID*. α and β are the weighing factors to adjust the level of controllers K_1, K_2 and *PID*. Values of both α and β ranges from (0,1).

4.7 **Numerical simulation**

The bondgraph model of the vehicle is simulated for 10 sec to obtain different output responses. Total 1024 records are used in the simulation and error is kept in the order of 5.0×10^{-4}. Runge-Kutta Gill method of fifth order is used in this work to solve the differential equations generated through bondgraph model. A quarter car model is being subjected to a random road input as discussed in the previous chapter. Simulations is being carried out for the Simulink model of the quarter car model in the software environment of MATLab/Simulink®. The results are being presented in three sections as- i) On-off strategies, ii) Continuous strategies and iii) Hybrid strategies.

4.7.1 Runge-Kutta method

Runge-Kutta methods propagate a solution over an interval by combining the information from several Euler-style steps (each involving one evaluation of the state

equations), and then using the information obtained to match a Taylor series expansion up to some higher order. This method treats every step in a sequence of steps in an identical manner. This is mathematically correct, since any point along the trajectory of an ordinary differential equation can serve as an initial point. Fifth-order Runge-Kutta method is used in the simulation study.

4.7.2 Simulation parameters

Bondgraph models for a two-DOF quarter vehicle is created. In the expression window, the control algorithms are incorporated in the expression in terms of damping coefficient. The model is now subjected to the base excitation of a single half sine bump or random road disturbance for performance evaluation. The disturbance in the form of velocity is also fed into the expression of the source of flow (SF) of the bondgraph model. Parameters for the simulation of a two-DOF quarter car model are presented in Table 4.2. Parameters used by *Blanchard* (2003) for a complete car model are considered in this simulation. The sprung mass or the mass of the full car is being scaled down to one forth for considering a quarter car model, whereas other parameters for the front suspension are taken straightway.

Table 4.2: Model Parameter for 2-DOF quarter car model *(Blanchard,* 2003)

Parameter	Value	Unit	Parameter	Value	Unit
M_s	365	kg	c_{min}	258	Ns/m
M_u	40	kg	c_{max}	2838	Ns/m
k_s	19960	N/m	c_{sky}	1290	Ns/m
k_t	175500	N/m	c_{gnd}	1290	Ns/m
$c_{min,f}$	258	Ns/m	d_b	1.803	m

4.7.3 Road input

In this case, mainly two types of road profile inputs are used for the simulation of a quarter vehicle model viz. half sine bump and random road inputs.

The transient input chosen is a half sine bump (*Gupta, 2016*), may be represented as

$$y = \begin{cases} h * \sin\left(PI * \dfrac{V}{L} * t\right), & for\ 0 \leq t \leq \dfrac{L}{V} \\ 0, & otherwise \end{cases} \qquad (4.42)$$

where, h is the height of the bump, which is 0.1m; L is the length of the bump, which is 0.3m; t is the time and V is the velocity of the vehicle. One may consider the three conditions for velocity, i.e., 60kmph, 80kmph and 100kmph. The bump profile is shown in Figure 4.15.
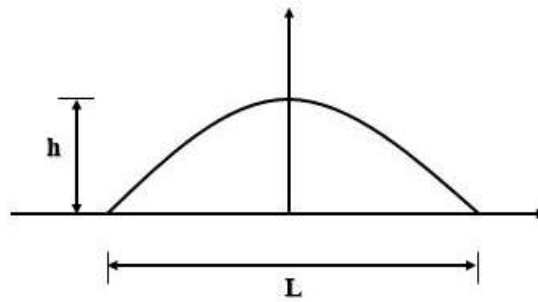
Figure 4.15: Bump type surface irregularity

The expressions for $\dfrac{dy}{dt}$ with a switch function is used as an input in the expression of SF, which may be expressed as

$$SF = PI * h * \dfrac{V}{L} * \cos\left(PI * \dfrac{V}{L} * t\right) * swi(t, 0) * swi\left(\dfrac{L}{V}, t\right) \qquad (4.43)$$

The random road profile category is adopted as a second type road input, which presented in chapter 2.

138

4.7.4 Performance of a Quarter Car Model for Bump Type Profile Input

A quarter car model has been subjected to a road input of half sine bump as discussed in the previous sections. Simulations have been carried out for the bondgraph model of a quarter car model in the software environment of SYMBOLS Sonata®. The results are presented in the following sub-sections

i)   Performance of on-off control strategy

ii)   Performance of continuous strategies

iii)   Performance of hybrid strategies.

4.7.4.1 Performance of on-off control strategies

The performance of the various on-off control strategies are presented in this section. A two-DOF quarter car model has been subjected to a half sine bump road input and different on-off logic controller such as skyhook, balance and groundhook strategies have been applied to control the damping force of the suspension system. The results were obtained in terms of body acceleration, unsprung mass acceleration, vehicle body displacement and transmissibility, both in time and frequency domain.

(a)   Body acceleration

Figure 4.16 shows the body acceleration vs time plot for the passive suspension system and semi-active suspension system controlled with various on-off strategies. Figure 4.16 (a) shows the acceleration for the passive system. The maximum amplitude of body acceleration reached with various on-off control strategies is slightly more than that of a passive suspension system, which is clearly depicted from Figures 4.16 (b-d). However, the settling time for the passive suspension system is approximately 2.5 seconds whereas, that of an on-off skyhook logic is found to be approximately 1 second. The settling time has been reduced by 60% approximately. The one added

disadvantage of the on-off skyhook control, whenever the condition function i.e., the product of the absolute velocity of the sprung mass and the relative velocity across the suspension changes its sign, the damper is switched between the on and off states. Hence, there is a sudden rise in the amplitude of body acceleration and the passenger or the driver may feel a sudden jerk, which can be considered uncomfortable.
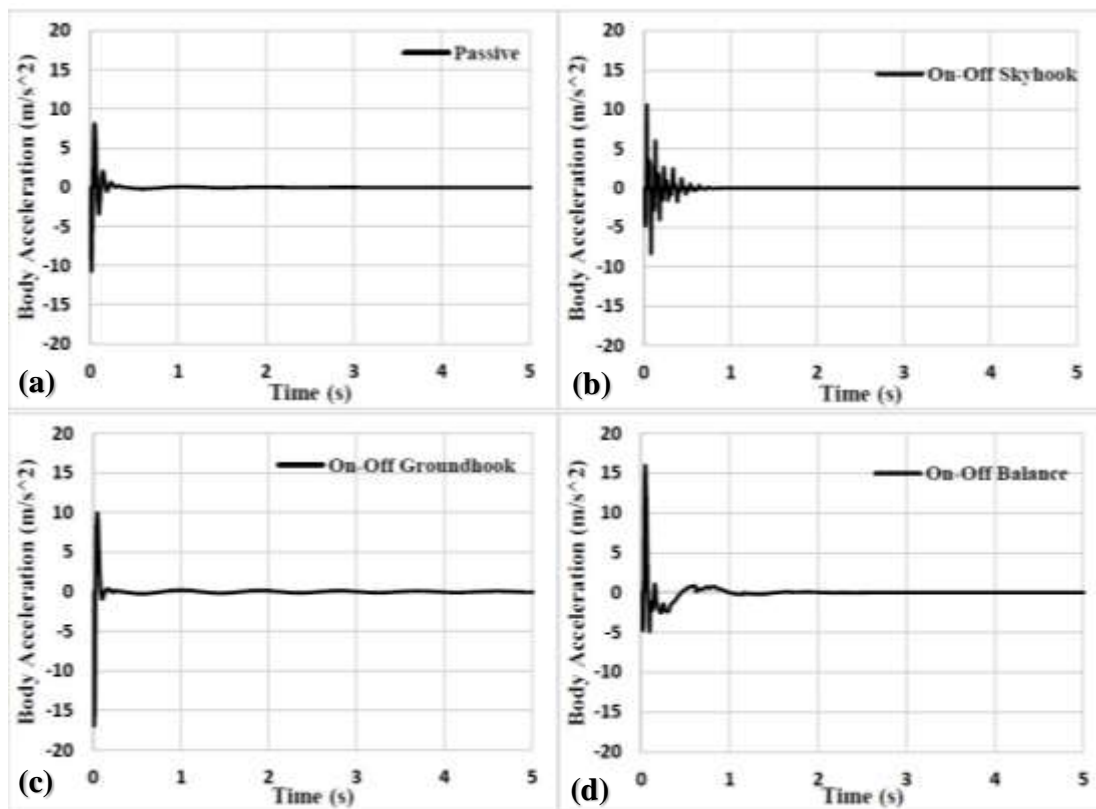
Figure 4.16: Body acceleration vs time plot of a quarter car at 60 kmph for (a) passive suspension system (b) on-off skyhook control (c) on-off groundhook control and (d) on-off balance control

The on-off groundhook logic controller does not show such sudden jerks as shown in Figure 4.16 (c). However the settling time for this logic is relatively large and hence, the vibration can be felt for a longer duration. In case of on-off balance logic, there is a significant reduction in the sudden jerks, but the settling time is almost same as that for a passive system as shown in Figure 4.16 (d).

(b) Unsprung mass acceleration

Figure 4.17 demonstrates the response of the system's un-sprung mass acceleration in time domain. Un-sprung acceleration of passive system is shown in Figure 4.17 (a). It can be noticed from Figure 4.17 (b) that on-off skyhook logic controller increases the magnitude of the unsprung mass acceleration, which requires more settling time.
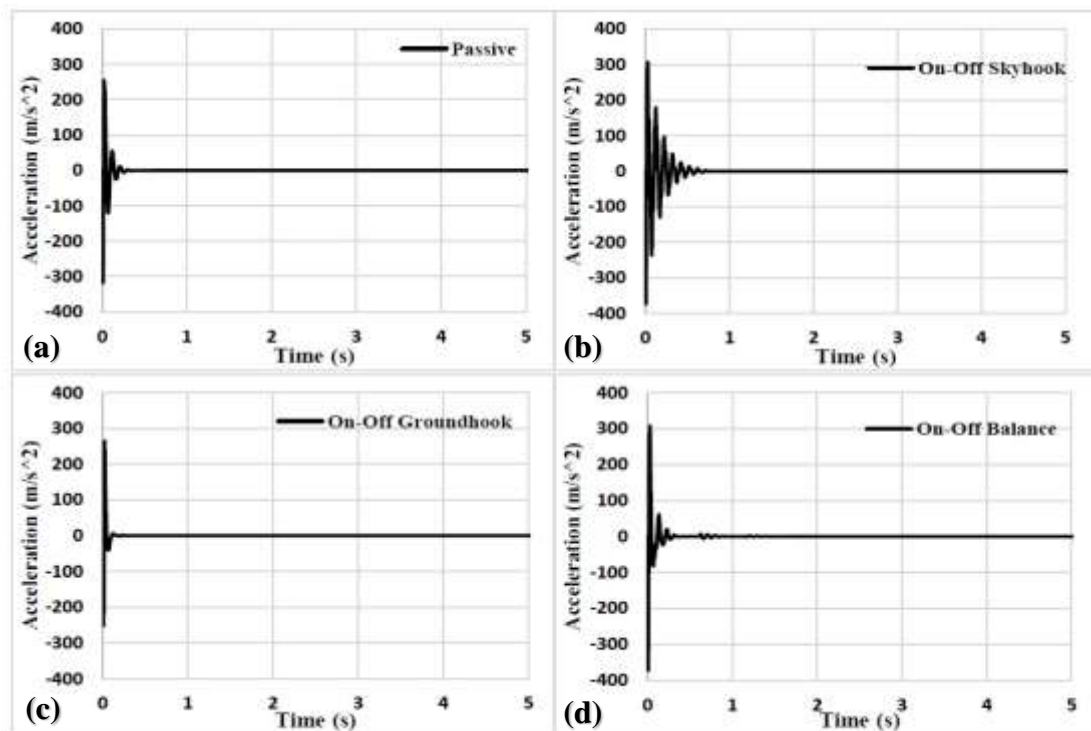
Figure 4.17: Unsprung mass acceleration vs time plot of quarter car at 60 kmph for (a) passive suspension system (b) on-off skyhook control (c) on-off groundhook control and (d) on-off balance control

The groundhook logic provides better performance in this regard. The magnitude is relatively less than that of a passive system or the other two control strategies as evident in Figure 4.17 (c). The settling time is also less in the case of on-off groundhook control, which is approximately 0.25 seconds whereas the settling time for passive system is near about 0.5 seconds. This is due to an inherent nature of groundhook logic, which gives better road holding as compared to the other logics. In Figure 4.17 (d), on-

off balance logic again increases magnitude at the beginning but immediately dampens out to smaller values. However, the settling time is more in this case.

(c) Vehicle body displacement
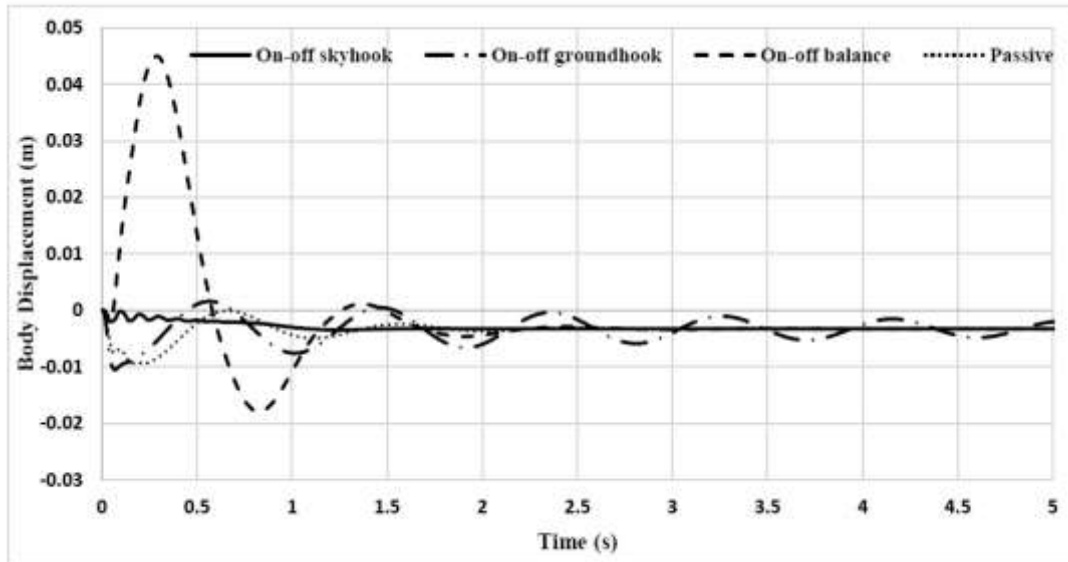
Figure 4.18: Vehicle body displacement vs time of quarter car at 60kmph for on-off logics

Figure 4.18 exhibits the vehicle body displacement vs time plot for the passive as well as semi-active suspension systems controlled with various on-off strategies. It is evident in the Figure 4.18 that the magnitude of displacement is relatively lesser for on-off skyhook control as compared to other two system. The balance logic exhibits a drastic increase in magnitude of displacement as shown in Figure 4.18. Groundhook logic has the maximum settling time as it continues to vibrate in a periodic manner as shown in figure. The maximum value of displacement achieved by passive system is approximaltely 0.009m whereas, the same has been reduced drastically to 0.0035m in case of on-off skyhook control which is approximately 60% reduction. The settling time for passive system is approximaltely 4.5 seconds. The same has been reduced to 2.5 seconds in case of on-off skyhook logic which is almost 45% lesser than that of passive

system. The displacement response in case of on-off skyhook control strategy seems better in both aspects discussed above.

(d) Transmissibility
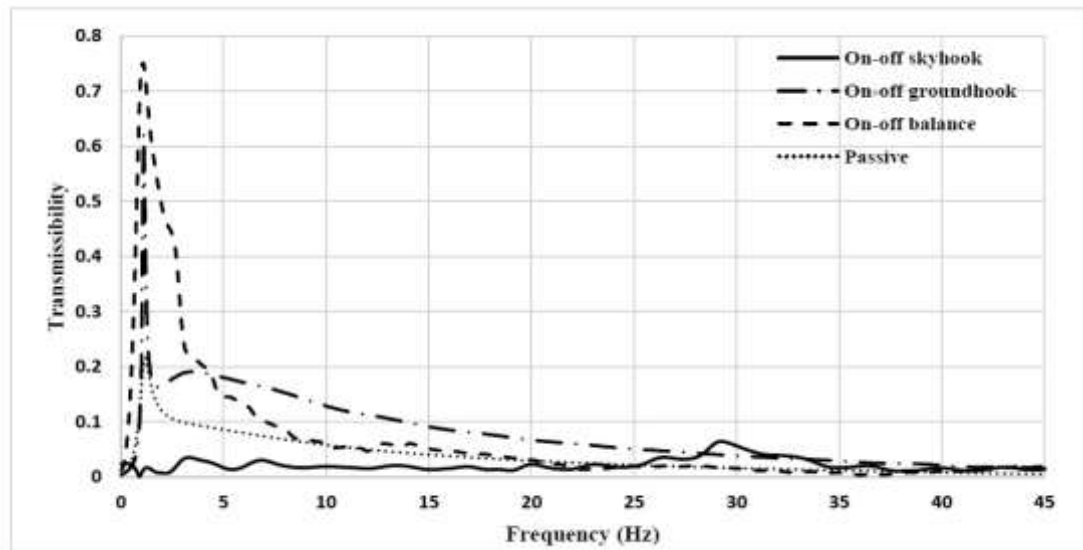
Figure 4.19: Transmissibility of acceleration of quarter car at 60 kmph for on-off logics

Figure 4.19 represents the transmissibility of acceleration between sprung mass and un-sprung mass in the frequency domain. It is evident from the figure that on-off skyhook logic has shown extreme performance regarding reducing transmissibility of vibration from the un-sprung to sprung mass. However, the transmissibility is found to be more in case of groundhook and balance logic. Maximum value of transmissibility is achieved by a passive system is approximately 0.22, whereas, it is less than 0.1 in case of skyhook. On the contrary, groundhook and balance logics have the maximum value of transmissibility at 0.6 and 0.75 respectively.

4.7.4.2 Performance of continuous control strategies

This section presents the performance evaluation of continuous control algorithms. The various performance indicates are discussed in subsequent subsection.

(a) Body acceleration
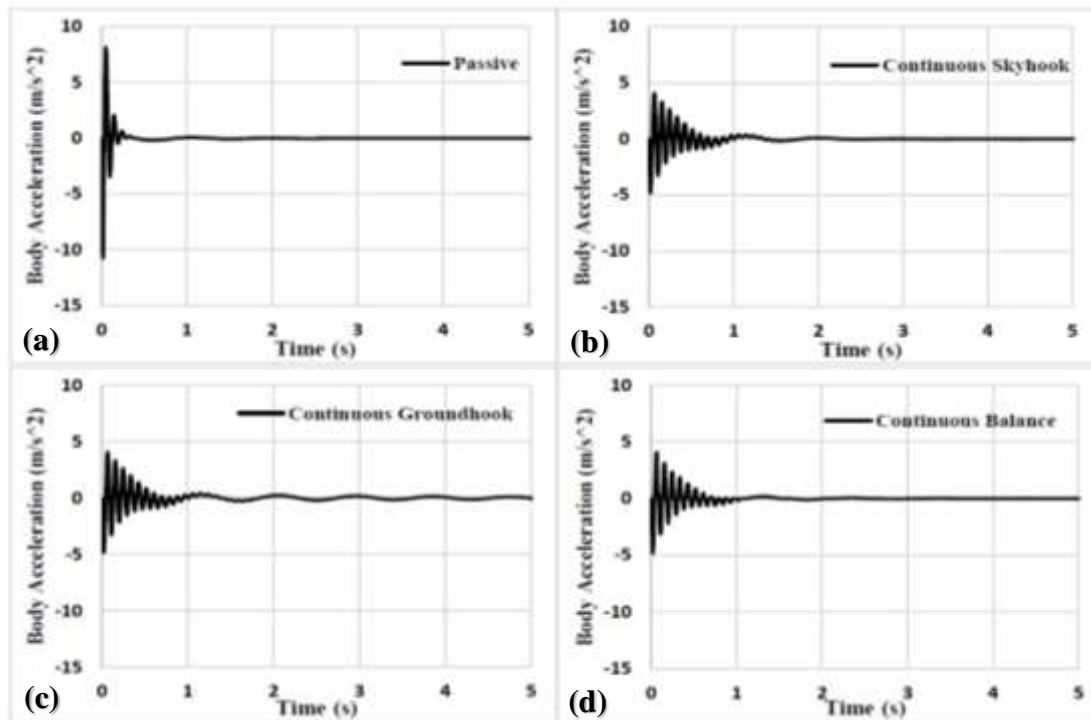
Figure 4.20: Body acceleration vs time plot of quarter car at 60 kmph for (a) passive suspension system (b) continuous skyhook control (c) continuous groundhook control and (d) continuous balance control

The body acceleration responses of various continuous control strategies in time domain are presented in Figure 4.20. It is observed from Figure 4.20 that for all the three continuous strategies, the maximum magnitude of acceleration is reduced to almost half of that of a passive suspension system. However, the settling time is compromised in the case of continuous strategies; as there is continuous vibration reduction over time. The settling time for continuous skyhook and continuous balance logics is found to be around 3-3.5 seconds as evident in Figure 4.20 (b) and (d) respectively, whereas that for passive system is 2.5 seconds (Figure 4.20 (a)). Groundhook logic has poor settling time, a periodic disturbance is present for a prolonged duration in case of continuous groundhook logic as shown in Figure 4.20 (c).

(b) Unsprung mass acceleration
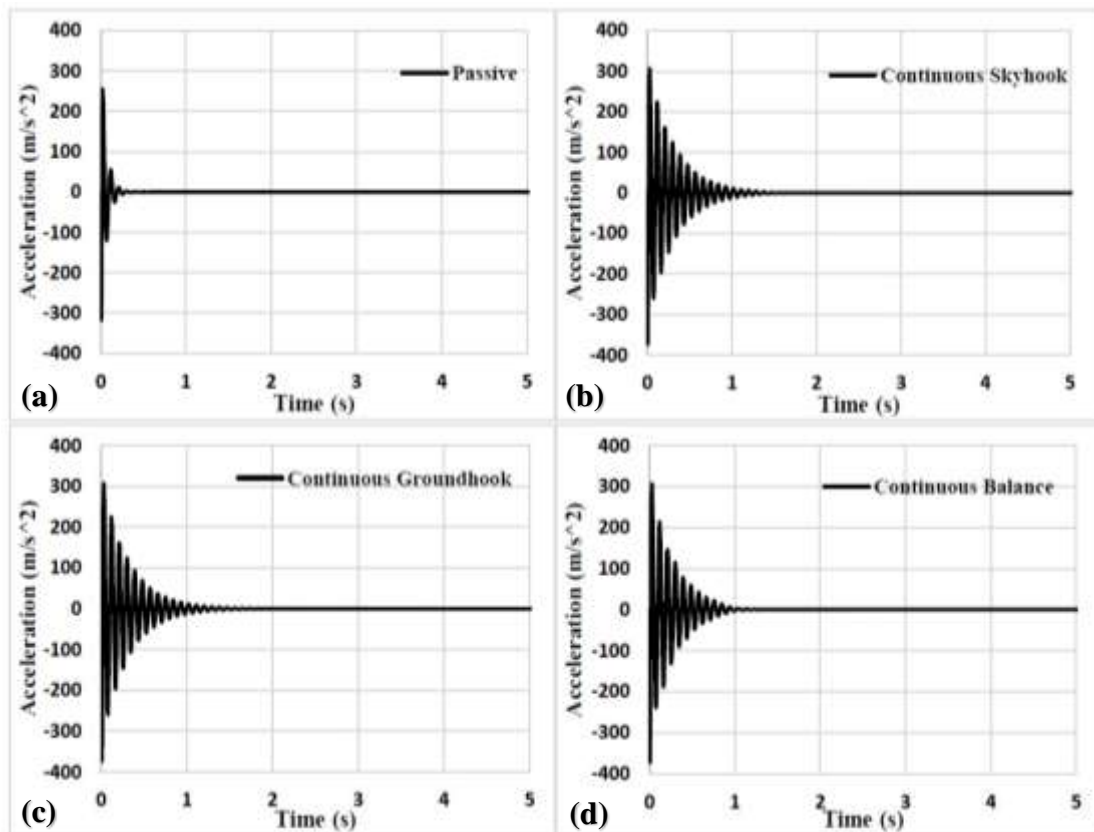
Figure 4.21: Unsprung mass acceleration vs time plot of quarter car at 60 kmph for (a) passive suspension system (b) continuous skyhook control (c) continuous groundhook control and (d) continuous balance control

Figure 4.21 displays the acceleration responses of the un-sprung mass of the vehicle model in time domain. It is shown that for all three continuous control strategies, the magnitude as well as the settling time has been compromised for the unsprung mass acceleration compared to passive logic. However, the amplitude is slightly higher in each case, the settling time is more. The wheel of the vehicle has to undergo a prolonged vibration before coming to a steady state.

(c) Vehicle body displacement

Figure 4.22 demonstrates the vehicle body displacement vs time plot for all three strategies. The maximum magnitude of displacement is more for all three strategies as

compared to passive system. Settling time for continuous skyhook logic is at par with the passive system. Continuous balance and continuous groundhook logics have more settling time. A prolonged periodic oscillation of the displacement response can be noticed for the continuous groundhook.
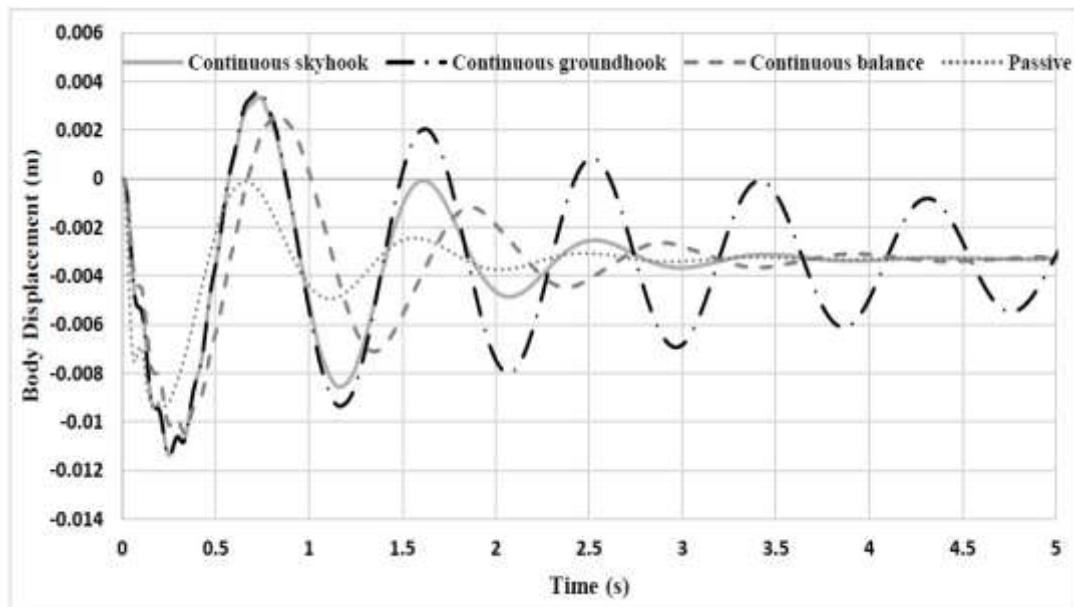
Figure 4.22: Vehicle body displacement vs. time of quarter car at 60kmph for continuous logics

(d) Transmissibility

The transmissibility of acceleration at average speed of 60 kmph is shown in Figure 4.23. It is observed that the transmissibility of acceleration is more in all the three continuous strategies. Maximum transmissibility for continuous balance is found to be comparatively less than the skyhook and groundhook logics, which is approximately 0.25. For continuous skyhook logic, the value of maximum transmissibility is found to be approximately 0.4 whereas, and for the case of the continuous groundhook, it's even more.
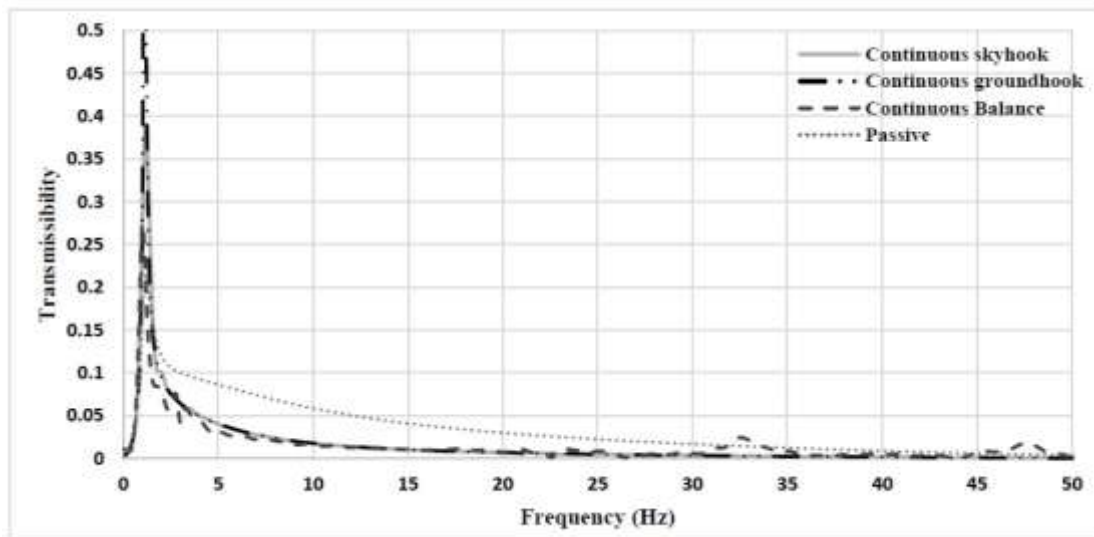
Figure 4.23: Transmissibility of acceleration of quarter car at 60 kmph for continuous logics

Table 4.3: Optimized value of weighing factors for hybrid logic

Hybrid logic	α	β	γ	δ	μ
HY-SH-GH	0.85	---	---	---	---
HY-SH-B	---	0.4	---	---	---
HY-GH-B	---	---	0.45	---	---
HY-SH-GH-B	---	---	---	0.65	0.15

4.7.4.3 Performance of hybrid control strategies

The performance a quarter car model has been carried out for four different hybrid combinations, which are as follows; - i) Hybrid skyhook-groundhook (HY-SH-GH), ii) Hybrid skyhook-balance (HY-SH-B), iii) Hybrid groundhook-balance (HY-GH-B) and iv) Hybrid skyhook-groundhook-balance (HY-SH-GH-B). The responses of semi active suspension with various hybrid control strategies is also presented in this work.

(a) Body acceleration

Figure 4.24 demonstrates the acceleration response of a sprung mass of a quarter vehicle controlled by different hybrid strategies. The weighing factors for all the four

147

hybrid logics are being optimized by hit and trial method and final values are presented

in Table 4.3.
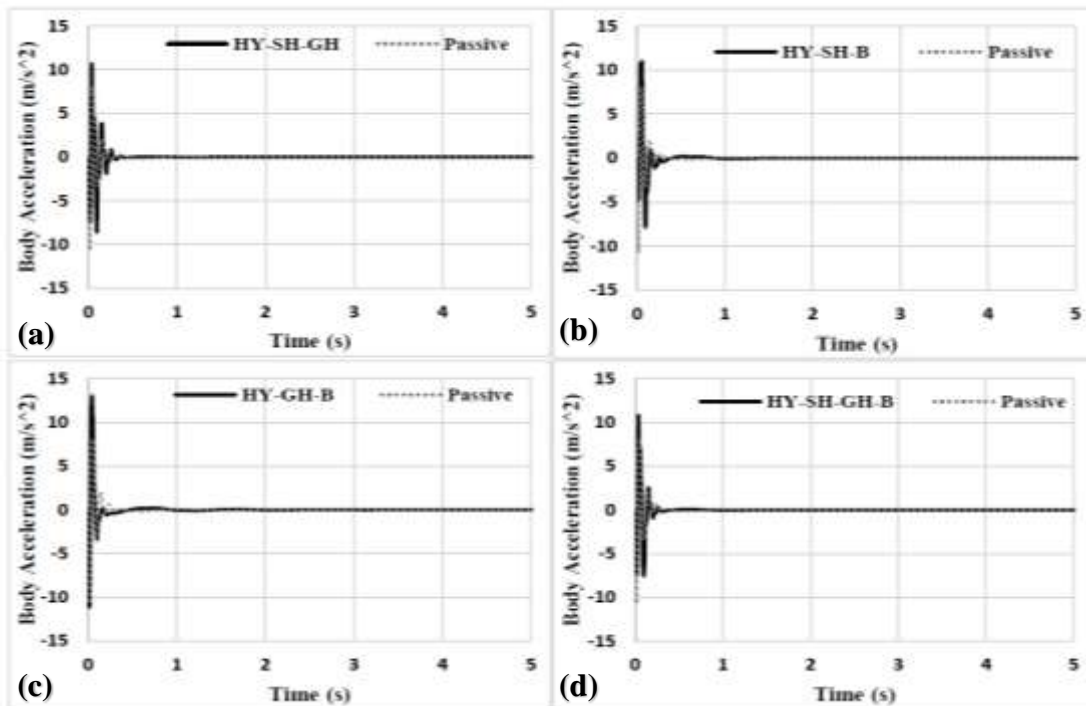
Figure 4.24: Body acceleration vs time plot of quarter car at 60 kmph for (a) HY-SH-GH (b) HY-SH-B (c) HY-GH-B and (d) HY-SH-GH-B control

It is observed from Figures 4.24 (a) and (d) that the responses of HY-SH-GH and HY-SH-GH-B logics are better in terms of both magnitude and settling time respectively. However, the magnitude of acceleration is maximum for the HY-GH-B combination. The settling time is almost better for HY-SH-GH and HY-SH-GH-B logics than HY-SH-B and HY-GH-B logics, which may be noticed in Figures 4.24 (b) and (c). The comparison study of HY-SH-GH and HY-SH-GH-B logics shows that HY-SH-GH-B logic have a slightly lower value of peak acceleration. The sudden jerks due to uneven road in on-off skyhook logic has been significantly reduced in case of hybrid strategies. HY-SH-GH-B logic has somewhat lesser severe sudden jerks, when the condition functions changed their sign as compared to HY-SH-GH logic, which is shown in

Figure 4.25. The settling time for both the logic controller have been found to be approximately 0.5 seconds, which is 80% less than the passive suspension system and 50% less than the simple on-off skyhook logic implemented controller.
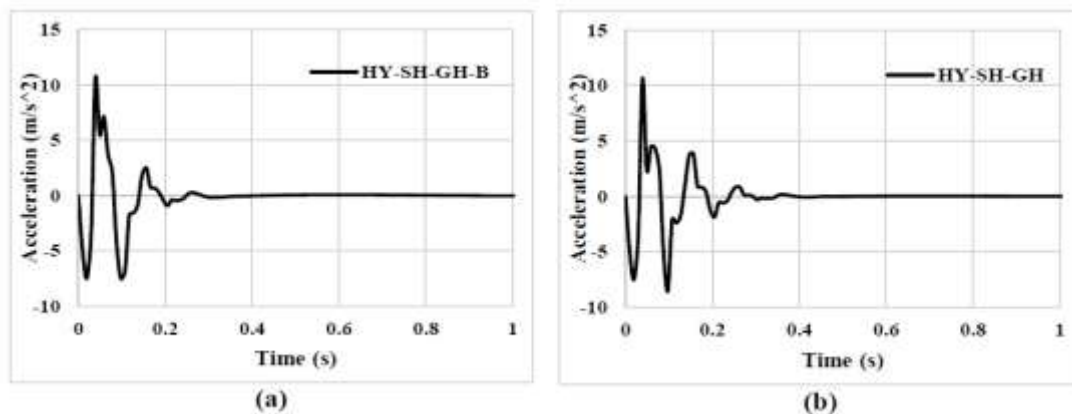
Figure 4.25: Acceleration response of sprung mass of quarter car for (a) HY-SH-GH-B and (b) HY-SH-GH

In Figure 4.25, it is observed that the magnitude of acceleration for sprung mass is less for the HY-SH-GH-B logic (Figure 4.25 (a)) as compared to HY-SH-GH logic (Figure 4.25 (b)). Moreover, the sudden jerks caused by the switching of the damper between on and off state as the condition functions change their direction is less severe in the case of HY-SH-GH-B control strategy. It is a well-known fact that the severity of the jerks is directly related to passenger's comfort. In this way, HY-SH-GH-B logic implement vehicle can provide a better comfort as compared to HY-SH-GH logic controller. Both the logics have better performance as compared to conventional on-off strategies, especially on-off skyhook logic, which provides numerous jerks before coming to a steady state condition.

(b) Un-sprung mass acceleration

Acceleration responses of un-sprung mass in time domain are displayed in Figure 4.26. It is shown that the acceleration response of the un-sprung mass is best for the hybrid

combination of groundhook and balance logic (Figure 4.26 (c)). The magnitude as well as the settling time is minimum for this strategy. Other remaining strategies have a slightly higher settling time and also the magnitude of acceleration is comparatively more than HY-GH-B and passive system. The settling time is approximately 0.5 seconds for the passive systems and also for all hybrid strategies except for HY-GH-B, for which the settling time is 0.25 seconds, which is 50% less. The magnitude of peak acceleration is maximum for the HY-SH-B logic as can be seen in Figure 4.26 (b).
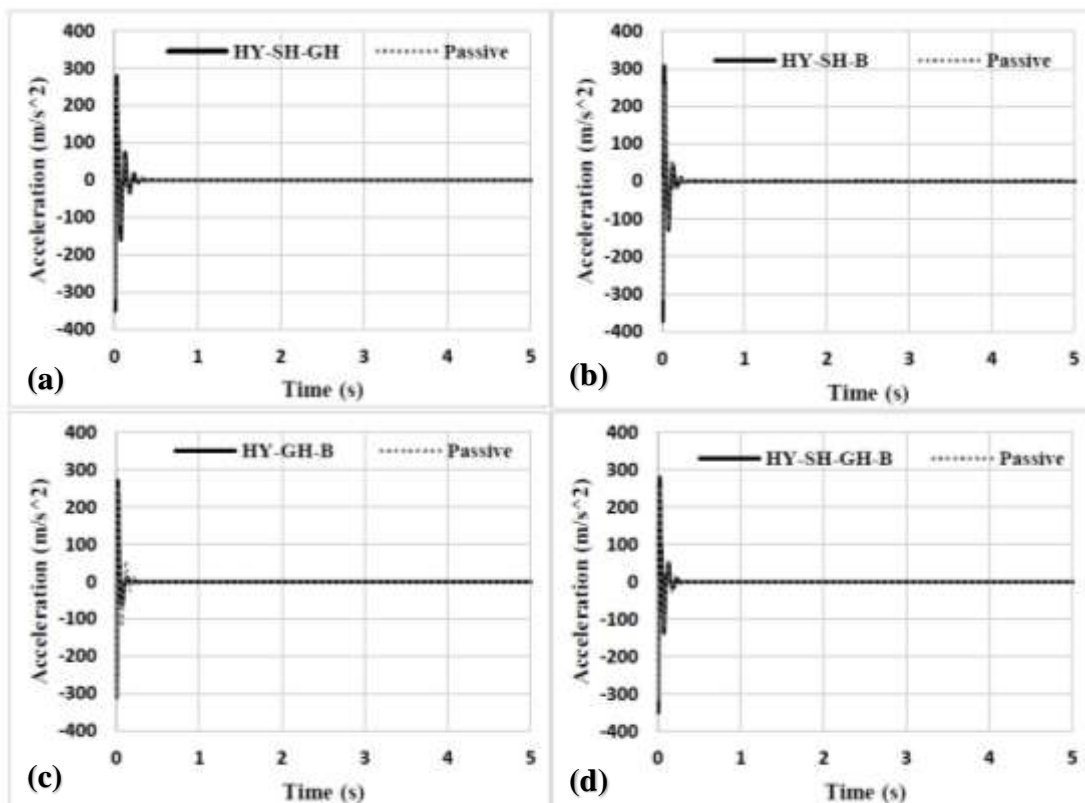
Figure 4.26: Unsprung acceleration vs time plot of quarter car at 60 kmph for (a) HY-SH-GH (b) HY-SH-B (c) HY-GH-B and (d) HY-SH-GH-B control

(c) Vehicle body displacement

Vehicle body displacement vs time at speed of 60kmph is being plotted and shown in Figure 4.27. It is observed from Figure 4.27 (a) that the HY-SH-GH logic has the best

performance regarding displacement response as the maximum amplitude achieved is less for this logic. HY-SH-GH-B logic provides a comparable result with slightly higher amplitude of displacement (Figure 4.27(d)). Other two remaining logics have more magnitude of vehicle body displacement as well as the settling time. The combination of skyhook-groundhook and skyhook-groundhook-balance has less settling time as well.
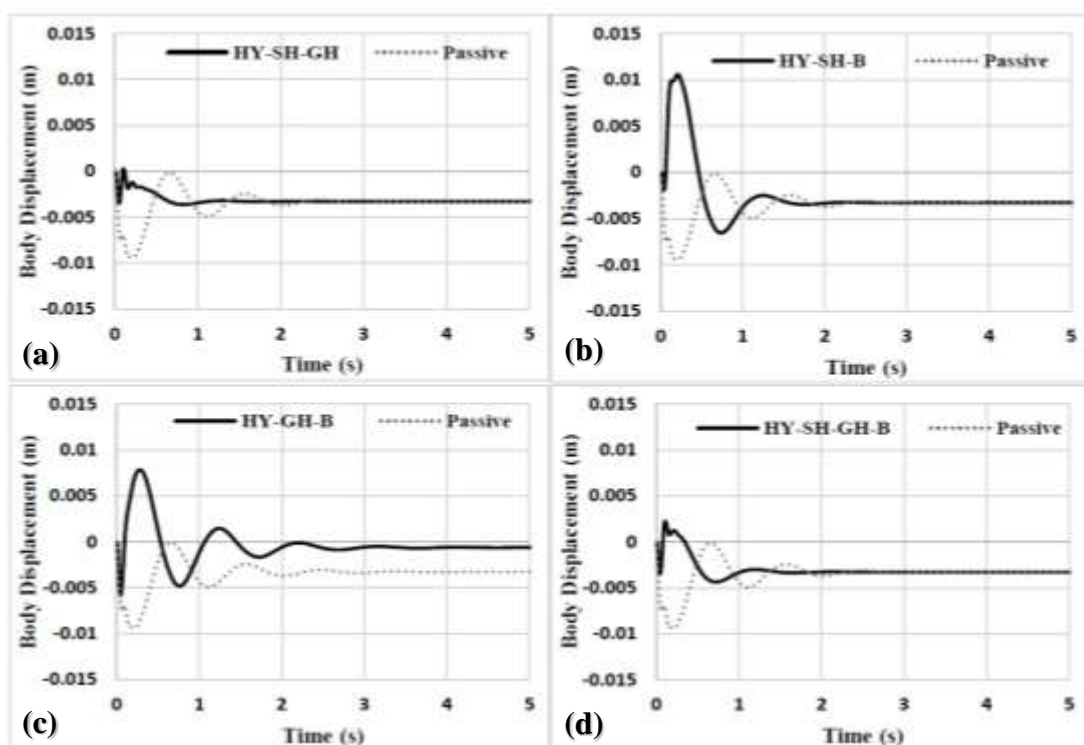
Figure 4.27: Vehicle body displacement vs time plot of quarter car at 60 kmph for (a) HY-SH-GH (b) HY-SH-B (c) HY-GH-B and (d) HY-SH-GH-B control

(d) Transmissibility

The transmissibility of acceleration between sprung and un-sprung masses for all hybrid control logics is presented in Figure 4.27. It is found that the HY-SH-GH and HY-SH-GH-B logics have better performance in terms of transmissibility of acceleration. The maximum transmissibility achieved is much less than that of a passive system. For both

the logics, the maximum transmissibility is found to be approximately about 0.07 whereas for a passive system, the maximum transmissibility is found to be around 0.22. For HY-SH-B and HY-GH-B logics, the maximum transmissibility is found to be approximately 0.25, which is even more than the passive system.
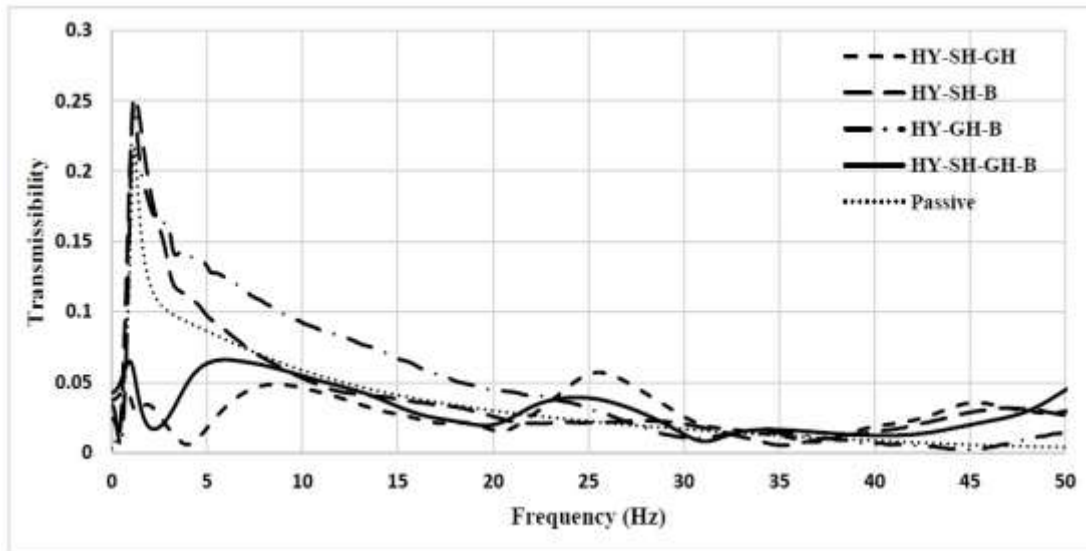
Figure 4.27: Transmissibility of acceleration of quarter car at 60 kmph for hybrid logics

4.7.5 Performance of hybrid control strategies in random road condition

Four hybrid control strategies have been considered for performance evaluation of semi-active suspension system for a quarter car model as discussed in the previous sections. These strategies are i) HY-SH-GH, ii) HY-SH-B, iii) HY-GH-B and iv) HY-SH-GH-B. The results are given in this section.

Figure 4.28 presents the sprung mass acceleration response of the HY-SH-GH control strategy. It is observed that the maximum value of acceleration achieved by passive system is about to ± 3 m/s^2, whereas, in case of Hybrid skyhook-ground hook, the value of acceleration is found to be about ± 1.5 m/s^2. The pattern also shows reduction in the value of acceleration.
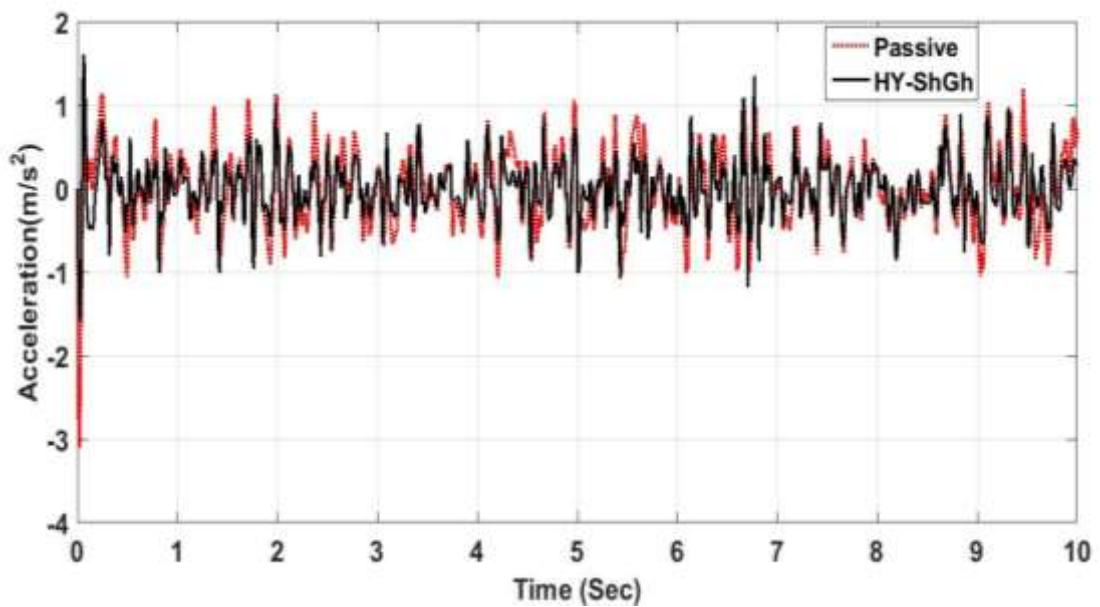
Figure 4.28: Body acceleration response of quarter car HY-SH-GH control for random input
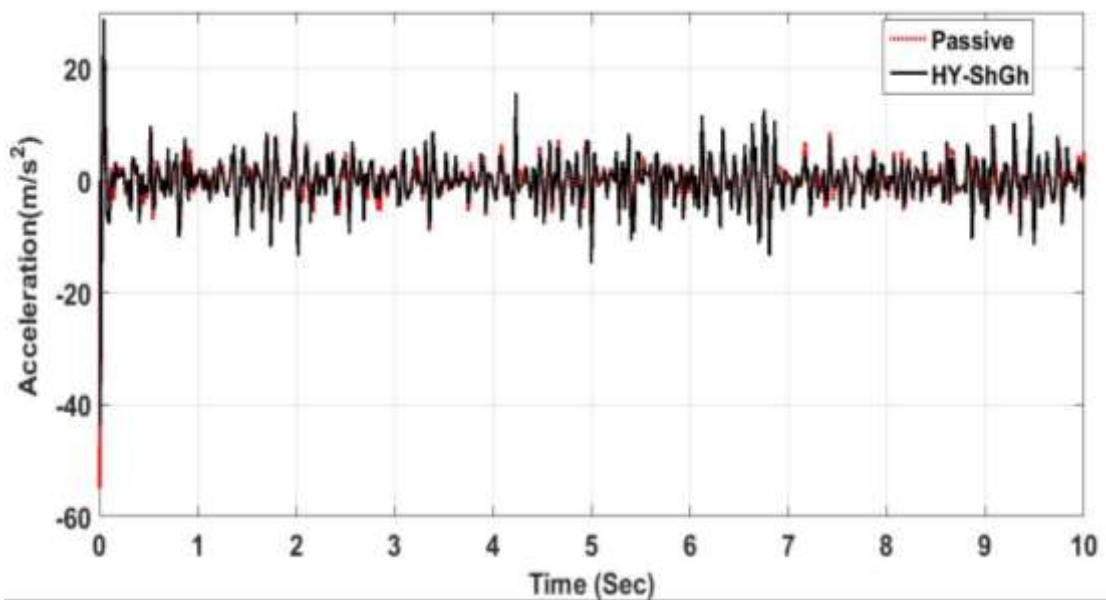
Figure 4.29: Tire- acceleration response of quarter car HY-SH-GH control for random input

Further, Figure 4.29 presents the unsprung mass acceleration response of HY-SH-GH control strategy. It is noticed that initial magnitude has been reduced by almost $\pm$ 10 m/sec^2 from passive system.

153
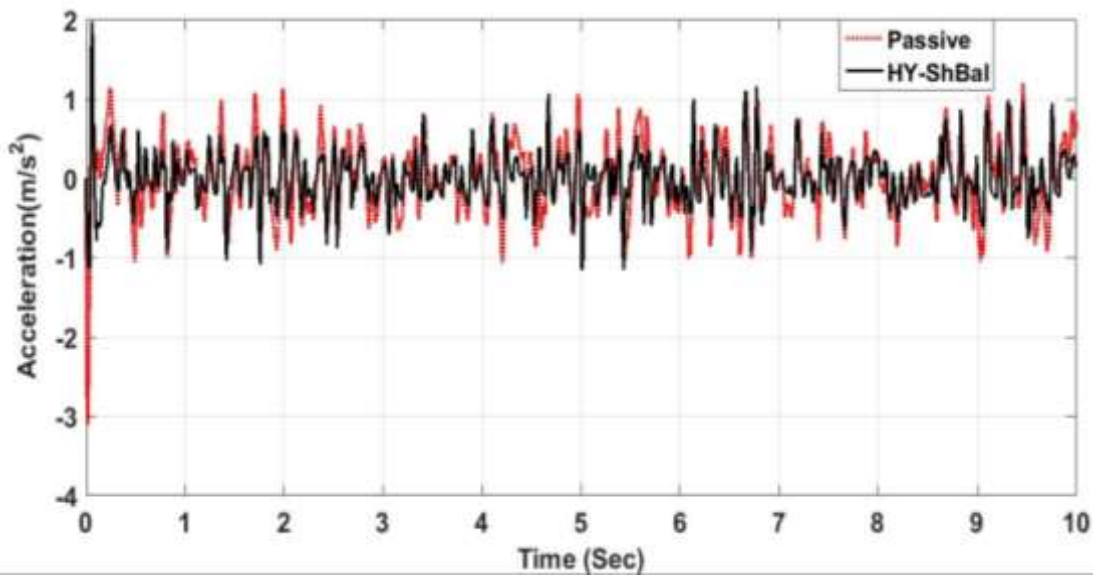
Figure 4.30: Body acceleration response of a quarter car HY-SH-B control for random input
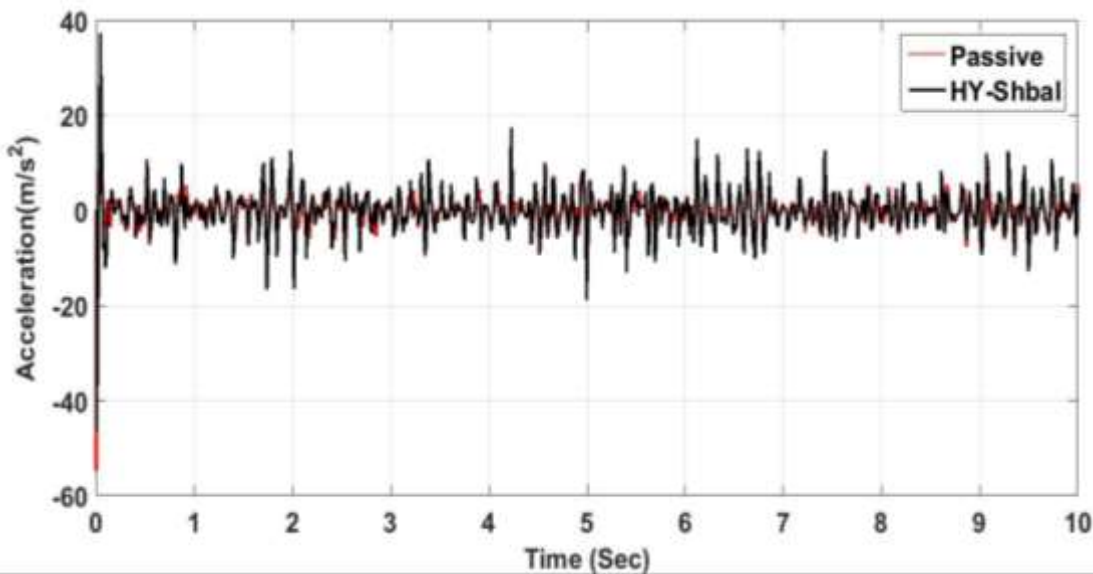
Figure 4.31: Unsprung mass acceleration response of quarter car HY-SH-Balance logic control for random input

In case of HY-SH-B control, the results are also shown to be comparable with that of HY-SH-GH. The initial amplitude is lowered to even less than $3m/s^2$ as shown in Figure 4.30. Severity and number of uncomfortable jerks are significantly reduced in this case as well. In case of unsprung mass acceleration the amplitude is found almost

equal to passive system; but initially the value is slightly down up to ± 20 m/sec^2, which can be clearly seen in Figure 4.31.
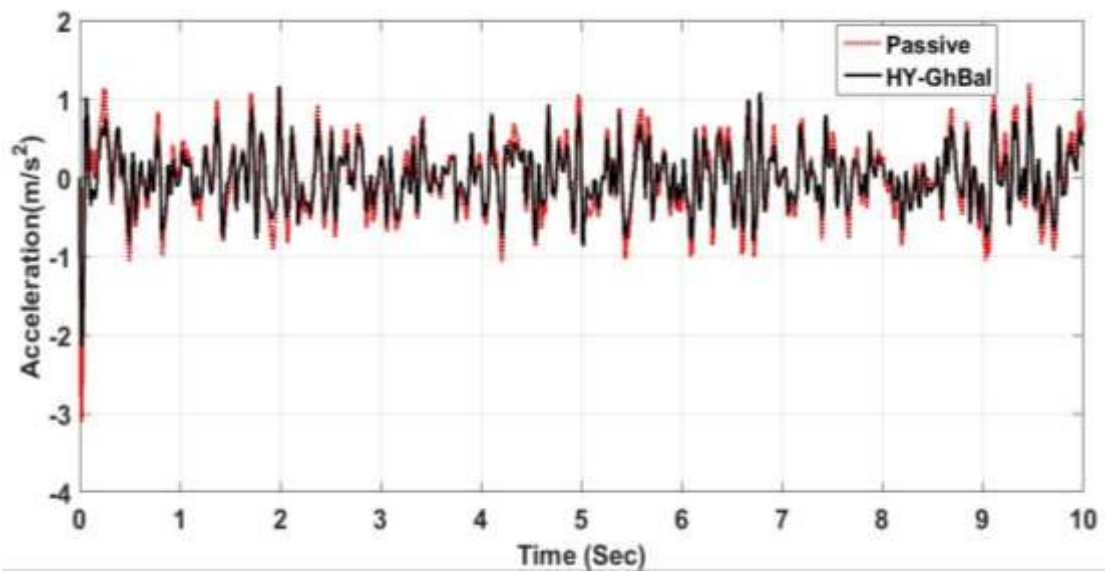
Figure 4.32: Body acceleration response of quarter car HY-GH-B control for random input
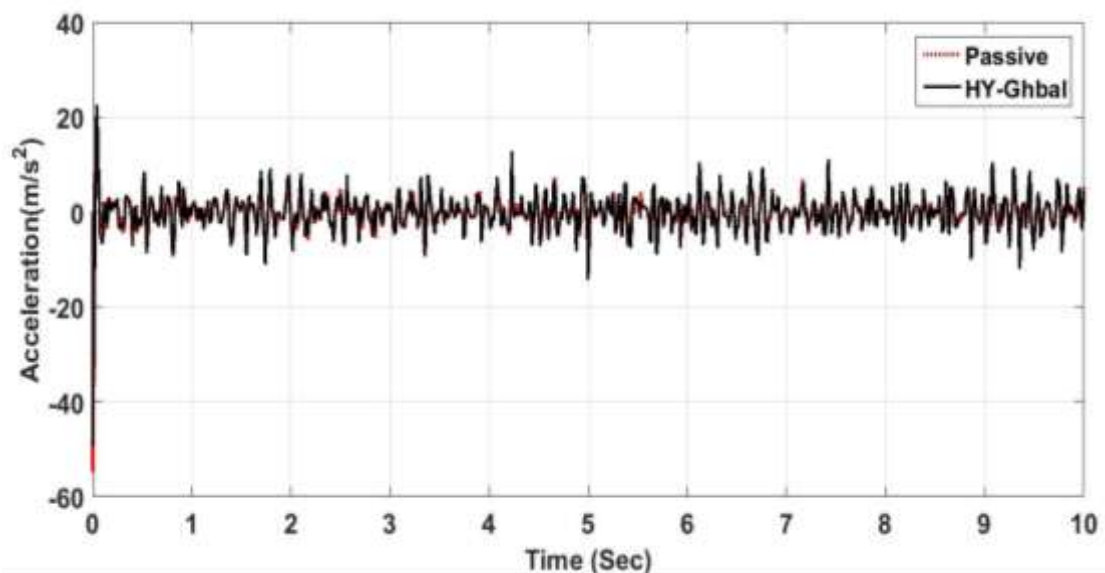
Figure 4.33: Unsprung mass- acceleration response of quarter car HY-GH-Balance logic control for random input

Figure 4.32 represents the acceleration response of HY-GH-B logic for a random road input. In this case, the initial magnitude is also lowered around $\pm$ 1 m/sec^2 than a passive

system. The trend can also be observed throughout the span of 10 seconds. The logic almost follows the passive response with somewhat less values at few places. The trend of un-sprung mass response is observed in Figure 4.33, whereas the magnitude is slightly higher than the passive system. However, it is depicting reduced than a passive system.
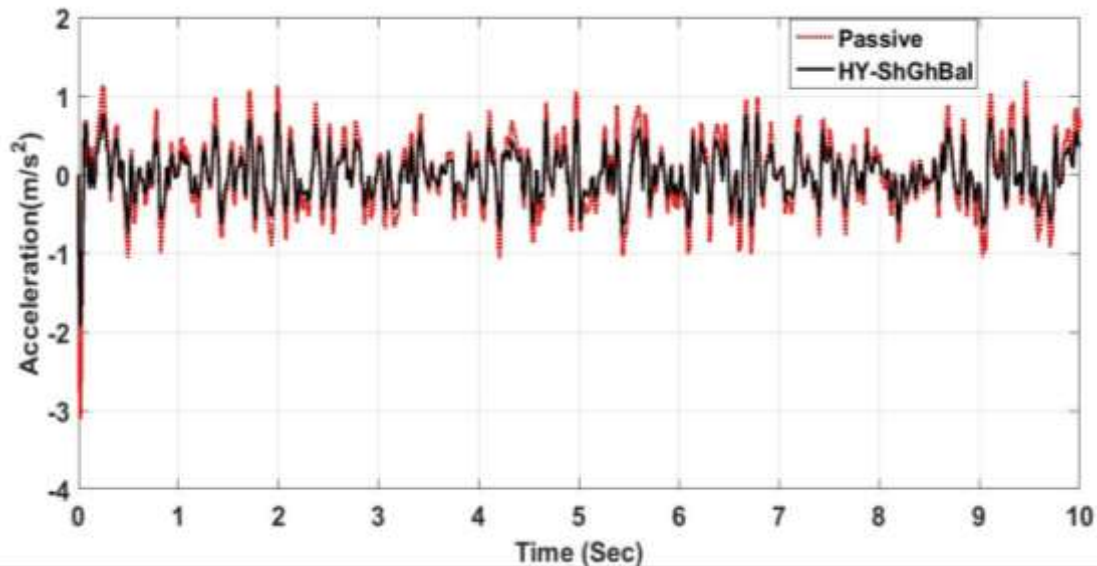
Figure 4.34: Body acceleration response of quarter car HY-SH-GH-B control for a random input
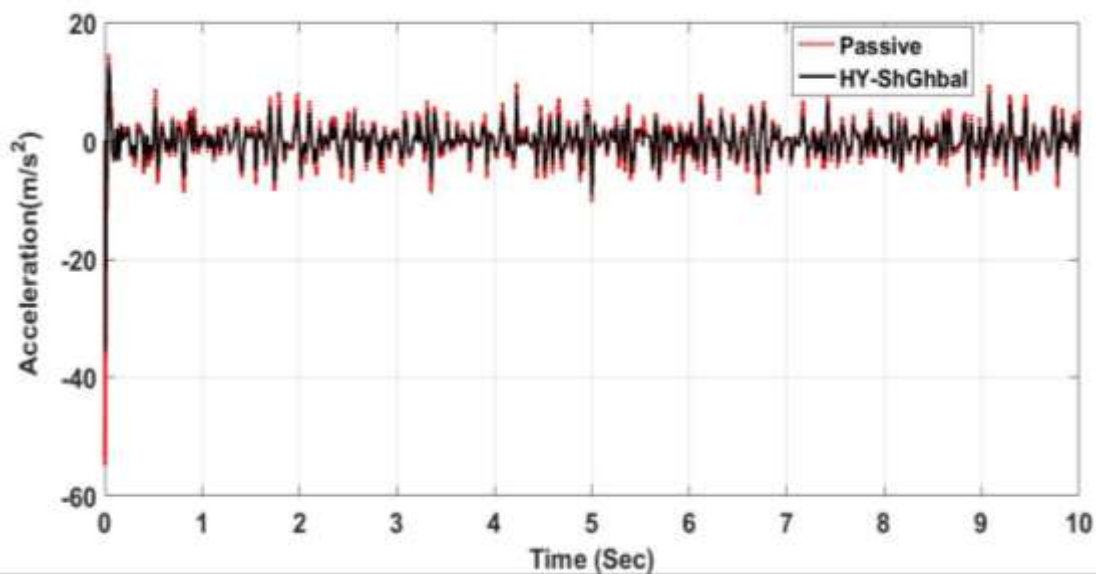
Figure 4.35: Unsprung- acceleration response of quarter car HY-SH-GH-B control for a random input

For HY-SH-GH-B control, the initial value of acceleration is about $\pm$ 1m/s^2 (approximately) as shown in Figure 4.34, which is lesser than passive system. Also, the system shows same type of trend in terms of severity of jerks. The amplitude in the opposite direction is immediately reduced to -1 m/s^2 whereas, for other remaining logics, it is somewhat more than -1 m/s^2 (except for HY-GH-B). The severity of the jerks is achieved to be reduced in case of HY-SH-GH-B control than depicted in HY-SH-GH control.

Similarly, the un-sprung acceleration response (presented in Figure 4.35) is greatly reduced than the other hybrid logics. The initial response of the system is lesser around 25 m/sec^2 in the opposite direction. Furthermore, similar pattern is being followed in terms of jerks, even better in comparison of other remaining hybrid logics.

4.7.6 Performance of PID based $H\infty$ controller (robust controller)

Vehicle quarter car model with a PID based optimal control algorithm is also simulated for the random type of road input at 60 kmph in H1 condition. The results obtained are discussed in this section. The constants of PID and values of weighting factors for PID based $H\infty$ and double $H\infty$ are presented in the Table 4.4.

Table 4.4: Tuned values of PID constants and value of weighting factors for Robust Controllers

Algorithms	K_P	K_I	K_D	α	β
PID – H∞	100	16000	1	0.5	---
PID – Double H∞	500	206854.87	10	0.45	0.45
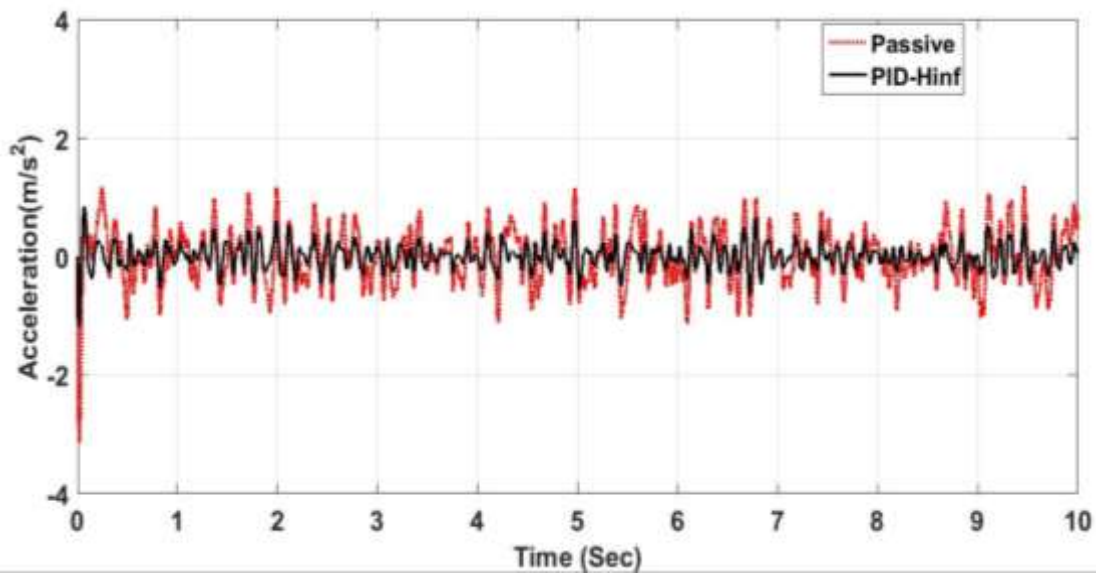
Figure 4.36: Sprung mass acceleration response of PID based $H\infty$ controller for quarter car with H1 random road condition at 60 kmph
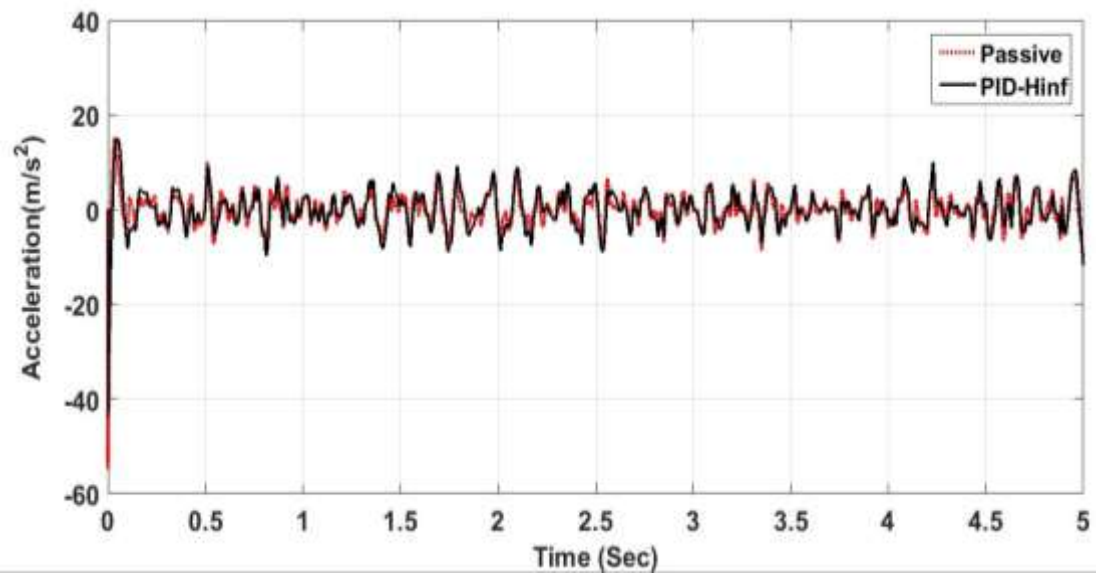
Figure 4.37: Un sprung- mass acceleration response of PID based $H\infty$ controller for quarter car with H1 random road condition at 60 kmph

Figures (4.36 - 4.39) shows the body acceleration vs time plot for the passive and robust

controlled semi-active suspension system.

It is observed from Figure 4.36 that the maximum value of acceleration

achieved by the passive system is about -2.3 m/s^2, whereas, in case of H∞ is found to be

about ±0.987 m/s^2, which is almost 57% less than the passive system The pattern also shows significant reduction in the values of acceleration. However, whenever tire deflection is observed to be more disturbed in comparison to passive system, it is observed in Figure 4.37. This problem may be solved by PID based double-H∞ controller, which is taken into account in next subsection.

4.7.7 Performance of PID based double $H\infty$ controller (robust controller)

Figure 4.38 presents the response of a PID - double H∞ controller, where it is found that the initial acceleration is decreased to almost 3m/s^2. However, the maximum acceleration of un-sprung mass/tire acceleration is in passive system and this value is significantly reduced due to PID-double Hinf controller, which is clearly depicted in Figure 4.39. Thus, the overall response of this controller is found to be significantly decreased in terms of acceleration and a trade-off is done between fun ride and road holding.
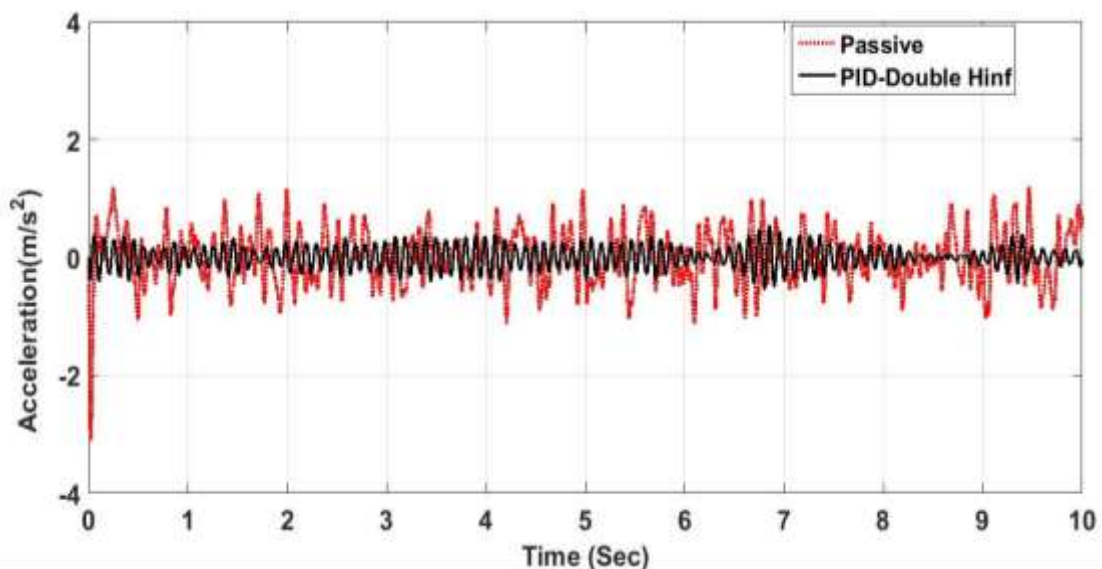
Figure 4.38: Sprung mass acceleration response of PID based double $H\infty$ controller for quarter car with H1 random road condition at 60 kmph
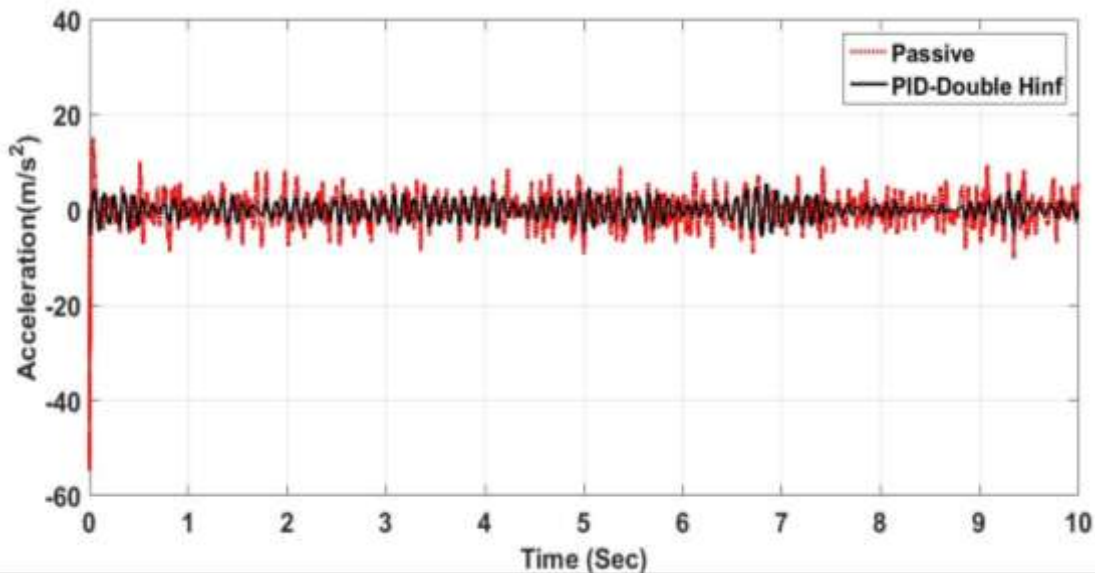
Figure 4.39: Tire acceleration response of PID based double $H\infty$ controller for quarter car with H1 random road condition at 60 kmph

Optimization of weighting factors may further create a balance between performance and stability. However tire deflection is also significantly reduced and thus a trade-off is created between fun ride and road holding force.

4.8 Conclusions

The dynamic model of road vehicle has been constructed through bondgraph technique and simulated in a MATLAB/Simulink® environment. Whereas, vertical dynamics has been carried out for the road vehicle model. A 2-DOF quarter car model is used for this analysis. Road input at the tire is given by considering random road type irregularity as presented in previous chapter two. The results are obtained for a vertical acceleration of sprung and un-sprung masses, displacement of body and transmissibility of acceleration from wheel to vehicle body. Among all on-off logics have provided on-off skyhook logic gives better performance in diminishing vertical acceleration of the body for bump type input. However, sudden jerks caused by this logic may lead to an uncomfortable

160

ride. On-off groundhook logic on the other hand has given a better performance regarding acceleration of un-sprung mass. Hence, the vibration of the wheel will be diminished quickly providing a better road holding force. The continuous logic controllers have shown a decline in the value of body acceleration. However, the settling time has been found to be more.

Further, performance of quarter car model has been evaluated for four different control logics, whereas HY-SH-GH are given better performance in terms of sprung mass acceleration. However this value is slightly higher for HY-SH-B combination. But the settling is reduced almost half for all hybrid control strategies. The HY-SH-GH-B gives better performance in all cases. Two more combination of robust controller are suggested, in which PID logic was incorporated with H∞ controller in one combination and double H∞ in other combination. It has been observed that robust control strategies have significantly improved the performance of vehicle in terms of both ride comfort and road holding both.

The next chapter will present the experimental framework for quarter car test rig for a heavy vehicle system. This chapter will show the fabrication of quarter car test rig with MR damper system. Further, a computational model of test rig will also be created through bondgraphs and results will be verified with experimental study.

Chapter 5

Experimental Framework for a Quarter Car Test Rig of a Heavy Vehicle System

In the previous chapter, various control strategies have been integrated with a quarter car model and some new hybrid control strategies have been suggested. This chapter presents the fabrication and experimental study of a quarter car suspension test rig for a heavy road vehicle. The primary purpose of this chapter is to describe an each step of design and provide a detail analysis of components, and finally measure the various responses of a test rig. Through the experimentation, the effect of sinusoidal vertical vibration on the test rig integrated with MR damper is investigated, which incorporates a semi-active suspension model for heavy vehicle. The computational model of integrated quarter car test rig is also created through bondgraphs in the later section of the chapter and simulation results are further verified with experimental results. In the last section, the response surface methodology for optimization parameters is obtained through experiments of heavy vehicle test rig to improve the ride comfort level of a driver.

5.1 Introduction

In order to determine the performance of a heavy vehicle in the real environment, distinct experimental models have been presented in many previous studies. Some of researchers have evaluated the performance of a suspension of heavy vehicle in real dynamic condition, whereas several researchers have developed a dedicate test rig for this purpose. Earlier, most of the experimental test rigs were developed for small

vehicles, and specifically design for passive suspension system. Very few test rigs were dedicatedly designed for a heavy vehicle system, however none of the test rig was integrated with damper with varying damping properties as per archival literature.

For designing an experiment, the main focus is to tune the suspension setting in such a way that the load occurred on leaf spring and the least load acted on MR damper system, which also shows the effect of electric current setting on the dynamics of the suspension system. The other significant focus is to validate the computational model with the experimental results. So, this computational model can be extended to reproduce the contributory dynamic effects on truck considering real or random road conditions.

5.2 Development and fabrication of a quarter car test rig

The work has been extended to develop a quarter car test rig for the heavy vehicle, which are configured for a semi-active control damper. There are various components such as accelerometers, tachometer, which are mounted on the test rig for sensing the response of the sprung mass, and a DAQ (Data Acquisition) system is used for recording the signal.

A wide dimension of a test rig 109cm×254cm×231cm was used for fabricating the base frame due to its flexural rigidity. The CAD model was examined and analyzed on ANSYS software and found to be safe. The vibration analysis of a suspension system was performed through vibration analyzer tool OROS® . The responses of the sprung mass have been measured at different values of electric current. The magnitude of sprung mass is varied through screw arrangement mounted on the head of columns. Suspension system is mounted between the sprung mass and the tire axle and configured with a leaf spring and MR (Magneto-rheological) Damper. Leaf spring is

having 9 leaves (1 full length and 8 gradual) and RD 8040-1 type MR damper are used in this study. A cam is also designed to provide a half sine bump input to the tire, and the rotation has been made through 5 HP/3.7 KW motor.
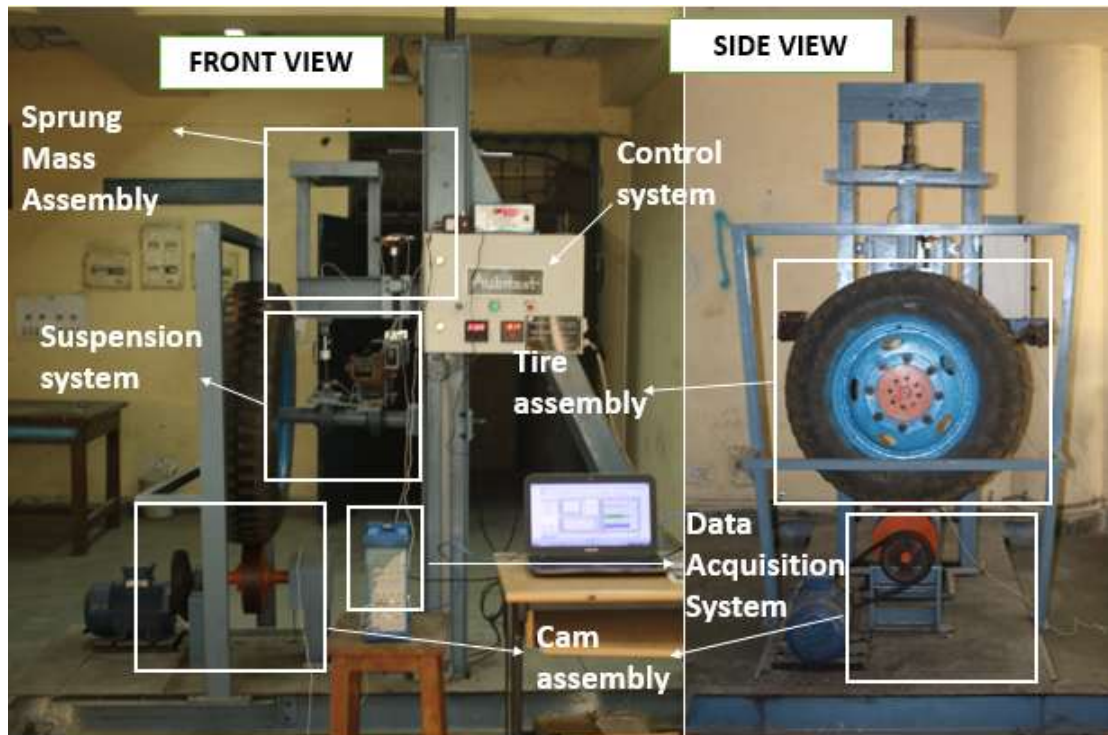
Figure 5.1: Pictorial view of fabricated quarter car test rig of heavy road vehicle

Schematic diagram of a quarter car test rig is presented in Figure 5.1 and the detailed description of each of the component of test rig is presented in next sub-sections.

5.2.1 Base frame structure

The base frame-structure is capable to withstand the enormous amount of shocks and moments generated during the testing different heavy vehicle suspension setups. The frame structure is required to be strong enough to resist fatigue and creep failures but flexible enough to handle twists and sways. An 'I-section' of base dimension 109cm×254cm was used for fabricating the base due to its flexural rigidity. The CAD

model of the test rig is presented in Figure 5.2 (a) and (b), which was created for different components. After assembling into a single structure and it was analyzed in ANSYS and which is found to be safe.
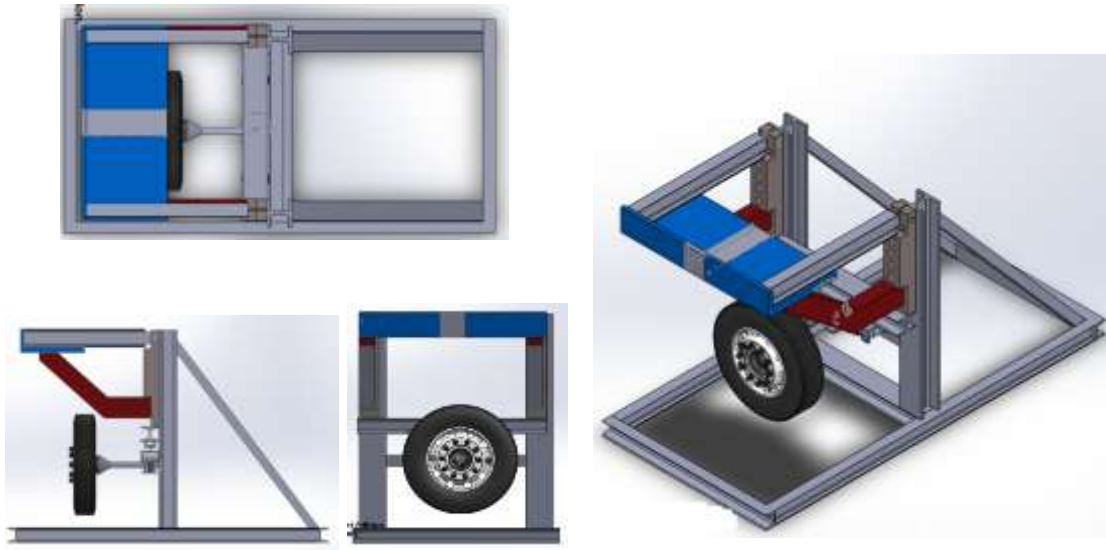
Figure 5.2 (a): Orthographic view of CAD model of frame structure

Figure 5.2 (b): Isometric view of a CAD model of the frame structure

5.2.2 Vertical column

The vertical column must be able to support the sprung mass assembly through roller bearings. Both columns were exactly parallel to each other in order to maintain a center to center distance of 231 cm throughout the entire height. The columns were drilled with M8 for mounting the guide support for a linear bearing. Vertical column were mounted by using a plate and bolting arrangement for maintaining the perpendicularity.

5.2.3 Linear bearing

The maximum dynamic load is required to be sustained during experimentation, which must be supported by frictionless guide. To develop the frictionless sliding of the sprung mass assembly, a linear bearing with bearing number 6202-2RS1 with stainless

steel guide were selected. The sprung mass is supported through four bearings, which may be shown in Figure 5.3.
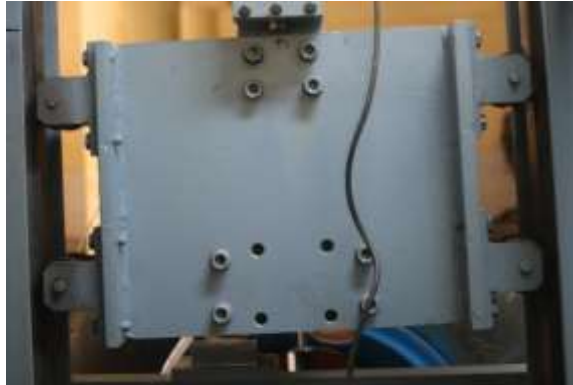
Figure 5.3: linear bearings used for support

5.2.4 Road input arrangement

For generating the replica of a half sine wave profile of a general profile road bump, a cam has been designed and being rotated is with the help of an induction motor, to provide a relative motion between the wheel and the road analogous to real dynamic interactions. The cam is made of mild steel solid disc mounted on a shaft with keyways and flanges. The shaft is connected to a pulley, where pulley rotation was made through a belt and the entire assembly is mounted on the base frame structure through bolts. The road input arrangement to facilitate free rotation is shown in Figure 5.4.

Figure 5.4: Road input arrangement

The rotation of the cam is provided to simulate the vertical dynamic characteristics of a vehicle in real dynamic scenario made through an induction motor. The basic requirement of a motor is evaluated through following calculations:

Excitation frequency range: 5 Hz to 7 Hz

Excitation magnitude: 0.008m

The basic specification of an induction motor is 5 HP power rating, 3 phase, with permanent magnet induction motor.

5.2.5 Sprung mass assembly

The vehicle body with its occupants and all its components, which are supported by the suspension system or oriented above the control armed, is termed as the sprung mass. In case of a quarter car model, the sprung mass is taken as one fourth of the total mass of the vehicle.

Figure 5.5: Sprung mass assembly

Figure 5.6: Screw lever arrangement for dead weight

The sprung mass was designed as a detachable unit with mounting points for three linear bearing, damper assembly and a leaf spring assembly. Arrangements are also extended to facilitate the attachment of dampers of different heights. The upper part of sprung mass assembly is attached with the dead weight assembly. This dead weight assembly can be able to encounter weight on the sprung mass through screw lever as per the requirement of an experiment.

5.2.6 Suspension mounting

A leaf spring and a MR damper system was integrated as a suspension system in the test rig. This spring- damper arrangement are mounted on an axle of the wheel through bearings support, whereas one end of the damper is hinged to the sprung mass, whereas, both ends of the leaf spring are hinged with the cross beam (which is bolted with parallel vertical columns). The wheel axle is configured with a special bearing arrangement, which is presented in Figure 5.8. This special bearing arrangement may be able to enable translation as well as rotation movement to an axle.
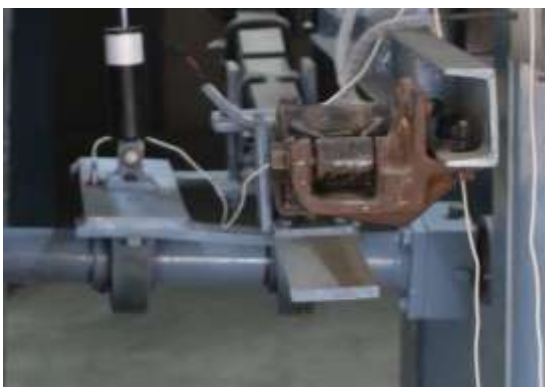
Figure 5.7: Non parallel axle with suspension mountings

Figure 5.8: Special bearing arrangement for making hinge at one end of axle

5.2.7 Selection of multi stage leaf spring

A leaf spring is as an elastic body, whose function is to distort, when loaded and to recover its original shape, when the load is removed. Leaf spring consists of number of leaves that are varying in different lengths. Initially, these leaves are usually given some curvature so that it will tend to strengthen, when loaded. In this rig, spring is placed between sprung mass assembly and wheel axle. The longest leave has an eye on its ends, which is termed as master leaf and the remaining leaves are called gradual leaves. All the leaves are bound together through the steel strap. The spring is mounted between the sprung mass and the wheel axle. Thus entire vehicle load rests on the leaf spring. The specification of leaf spring is presented in Table 5.1. The installation of leaf spring in test rig is presented in Figure 5.9.

Figure 5.9: Leaf spring installation

Table 5.1: Specification of the leaf spring

Material	50Cr1V23
Total length of the spring (Eye to Eye) (mm)	1100
No. of full length of leaves	01
No. of first stage of leaves	01
Total no of leaves	08
Thickness of each leaf (mm)	8.2
Width of each leaf spring	51

5.3 Magneto rheological damper (MR damper) and wonder box controller

Magneto Rheological (MR) damper is basically used for various industrial applications, whereas damping force can be varied with time. Varying property of damping can be achieved by applied electric current that can generate internal particles of the bond, which causes resistance to the flow. The MR damper is divided into two chambers by the piston, and it is completely filled with MR fluid. The MR fluid is a controllable fluid, which flow through orifices at both ends from one end to another during the motion of a piston. This controllable fluid is comprised of micron sized, para-magnetic polarized iron particles suspended in a liquid, which can be water, glycol, synthetic water. When electric current is applied into the system, a magnet field is created along the length of a piston. This para-magnetic particles line up with the magnetic field and form chains, changing the rheological behavior of the controllable fluid. In other words, it can change the viscosity of the fluid. The intensity of viscosity in the fluid depends on the change of the magnetic field.

Figure 5.10: RD-8040-1 MR damper

Figure 5.11: Wonder box controller kit

The experimentation was conducted on RD-8040-1 type MR damper supplied by Lords Corporation. The test configuration is shown in Figure 5.1, where one end of the damper is connected with the sprung mass, while other end is mounted on the wheel axle, and configured parallel to a leaf spring. The current of the MR damper is controlled by a wonder ball controller kit (details provided in next sub section), whereas voltage may be kept constant during the experiment trial. The details provided in physical and electrical parameters are presented in Table 5.2.

Table 5.2: Technical description of RD 8040-1 supplied by Lords Corporation

Technical description	
Stroke	55 mm
Extended length	208 mm
Body diameter	42.1 mm
Shaft diameter	10 mm
Tensile strength	8896 N
Damper force	> 2447 @ 1A
	<667 @ 0A
Operating temperature	71 ^{0}C
Electrical description	
Input current	
Continuous for 30 second	1 max
Intermittent	2 max
Input voltage	12 DC Volt
Resistance	
@ ambient temperature	5 ohm
@ 71^{0}C	7 ohm

5.3.1 Wonder box controller

Lord wonder box$^®$ controller test kit is used to varying the current (0-1 Amp) during the experimental trials, which includes the device controller, 12 volt DC power supply, and

two plugs. This controller kit provides an open loop controller to compensate for changing the electrical loads up to a certain limits of the power supply. This controller rig is used as an interface device for PLC or computerized control of MR fluid device. The wonder box device controller is shown in a Figure 5.11, where output can be measured from 'B' power supply, connected to 'A', and current can be adjusted through potentiometer device, which can be switched on-off by pressing the switch 'E'.

5.4 Implementation of data analyzer system and its transducer

This work using a vibration analyzer OROS36® vibration system for capturing and analyzing a vibration signal, which was operated through NV gate software, and records the signal in form of acceleration and displacement.

Figure 5.12: Experimental equipment for vibration analysis

OROS36: OROS36 is made for high channel count capacity without comprising the analyzer geographies. All the channels are handled in real time: FFT, 1/3rd Octave. OR36 and OR38 keep these real-time capabilities up to 20 kHz. There are LCD screen controls on the OR36 and OR38 hardware that allow running and stopping the analyzer and also changing the fan speed etc.

NV Gate® *software*: NV Gate platform offers a comprehensive set of tools for noise and vibration acquisition, recording and analysis. The graphical user interface of NV Gate® software is presented in Figure 5.13.
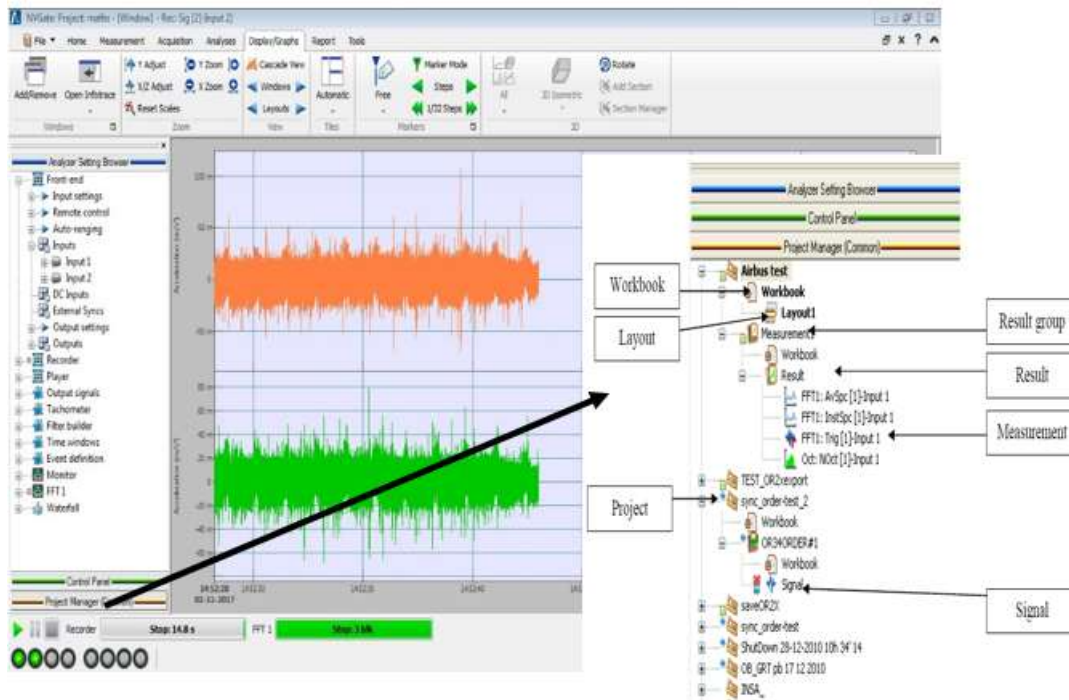
Figure 5.13: Graphical user interface of NV gate software

Accelerometers: An accelerometer is an instrument that produces an electric charge directly proportional to an applied acceleration. A schematic model of an accelerometer is shown in Figure 5.14. Mass is supported on a piece of piezoelectric crystal, which is attached to the frame of the transducer body. Piezoelectric material has a property that if it is compressed, it is proportional to an amount of compression. As the frame experiences an upward acceleration, it experiences a displacement also. As the mass is attached to the frame through the piezoelectric element, the resultant displacement it experiences is of different amplitude and phase than that of the displacement of the frame. This relative magnitude of displacement between the frame and mass leads

173

piezoelectric crystal to be compressed, that provides a voltage proportional to the acceleration of the frame. The detailed specification of uniaxial and tri-axial accelerometer is presented in Table 5.3 and Table 5.5 respectively.
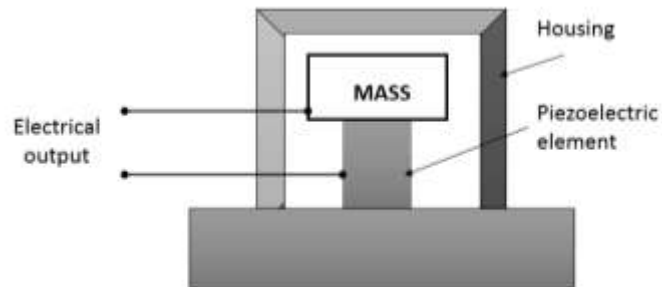
Figure 5.14: Basic model of accelerometer

Table 5.3: Specification(s) of tri-axial accelerometer

Identifier	Tri-axial ISOTRON accelerometer - 13925
Model	65-100-X
Coupling	ICP
Sensitivity	X: 104.0 mV/g Y: 101.3 mV/g Z: 98.64mV/g

Table 5.4: Specification(s) of uniaxial accelerometer

Identifier	ISOTRON accelerometer -13976
Model	256-100-X
Coupling	ICP
Sensitivity	95.77mV/g

Tachometer: PCB[®] type tachometer is used for measuring a speed of eccentric disc, whereas display digital dial is mounted on control box and displays speed in revolution per minute (RPM). The specification of tachometer is presented in Table 5.5.

Table 5.5: Specification of PCB® tachometer

Operating distance	61cm and 45^0 offset from target
Speed range	1-50,000 rpm
Operating temperature	-13^0 to 257^0F
Power input	6-24 Vdc
Output signal	TTL same as source
Standard cable	25 feet
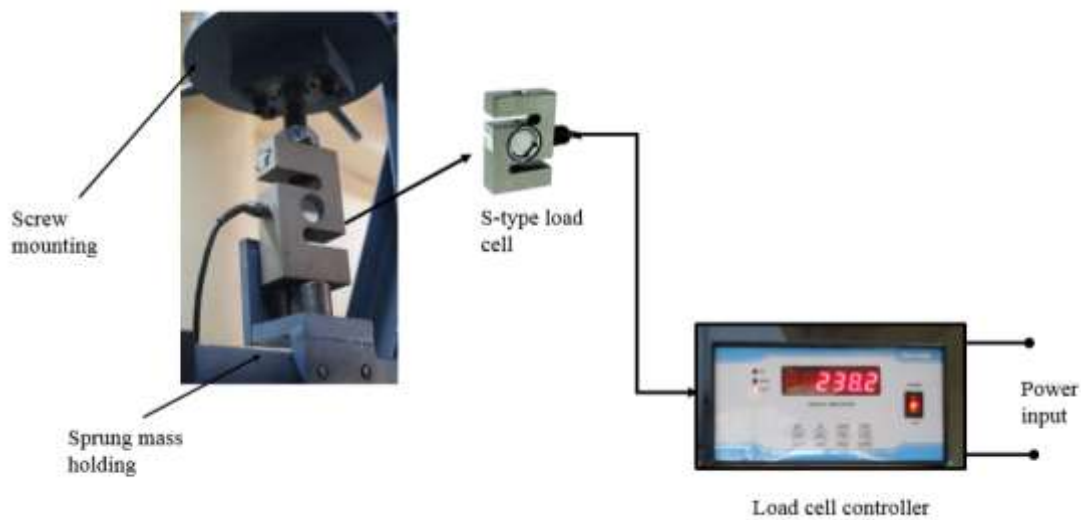
Figure 5.15: S-type load cell with mounting

Table 5.6: Specification(s) of S-type load cell

Standard Capacities	20,30,50,75,100,150,200,250, 300,500,750 Kgf
Excitation Voltage	10 VDC-Maximum 15 VDC
Nominal Output	3.0 mv/v
Input Resistance	392±15 Ohms
Output Resistance	350±3 Ohms
Insulation Resistance (50VDC)	> 1000 Mega Ohms
Safe Overload of Rated Capacity	150%
Ultimate Overload of Rated Capacity	250%
Allowable Side Load	50%

Load cell: This type of transducer is used to create an electrical signal, which is directly proportional to force being measured. This s-type load cell is configured in wheat stone bridge with four strain gauges. The force being measured deforms the strain gauge, and the deformation is measured as change in electrical signal. The S-type load cell system is mounted between screw lever arrangements and sprung mass, whereas load can be applied through screw-jack, and the value can be seen on display of load cell controller. The arrangement of S-type load cell with load cell controller is presented in Figure 5.15, whereas detailed specification of load cell is given in Table 5.6.

5.5 Analytical frame work for MR damper

Several approaches have been suggested to develop a mathematical model of MR damper. The physical model of the damper is presented in Figure 5.16, where MR damper attached with one dimensional vertical vehicle system.
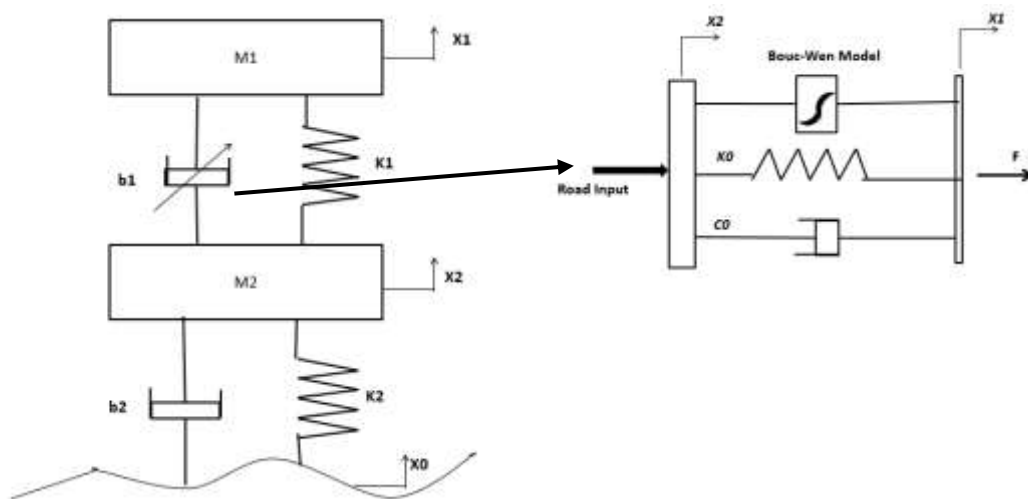
Figure 5.16: Physical Model of Quarter Car with MR damper

The Bouc-ben model is a very popular approach to damper modeling because it includes hysteresis and phenomenological approach to the yield characteristics of the

damper fluid (*Ma et al., 2003).* However, in order to determine the force of damper, the analytical model of MR damper proposed by spencer (*Spencer et al.,1996)* was used.

In this research work, a mathematical model of MR damper and incorporated with Bouc-wen hysteresis model, whereas arrangement of spring and dampers was suggested by *Spenser et al* (1996). The schematic model of test rig integrated with MR Spencer model is shown in Figure 5.16, and the dynamics is governed by the equation.

$$F_d = C_0(\dot{x}_1 - \dot{x}_2) + k_0(x_1 - x_2) + \alpha w \tag{5.1}$$

$$\dot{w} = -\gamma|\dot{x}_1 - \dot{x}_2|w|w|^{n-1} - \beta(\dot{x}_1 - \dot{x}_2)|w|^n + B_1(\dot{x}_1 - \dot{x}_2) \tag{5.2}$$

With the parameter defined as,

$$\alpha(i) = \alpha_a + \alpha_b i$$

$$C_0(i) = C_{0a} + C_{0b}i$$

where, x_1 is the sprung mass displacement and x_2 is the un-sprung mass displacement, w is the internal displacement of MR damper, additional variables are constants and values are; γ, β, and B_1 which governed the loop of the hysteresis curve.

Table 5.7: MR damper parameters (*Ho et al., 2013*)

Parameter	Value	Unit	Parameter	Value	Unit
γ	45570.4	m^{-2}	α_b	3152	N(Am)$^{-1}$
β	212114	m^{-2}	C_{0a}	6949	Nsm^{-1}
$B1$	121	---	C_{0b}	60789	Ns(Am)$^{-1}$
α_a	672	N-m^{-1}	k_0	732	Nsm^{-1}

The values of other parameters such as α_a, α_b, C_{0a}, C_{0b}, k_0 (all values are listed in Table 5.7) suggested by *Ho et al.* (2013) by experimental data obtained from an MR damper RD-10053 manufactured by lord corporation.

5.6 Bondgraph model for quarter car test rig

The bondgraphs is used to create a computational model of quarter car test rig, where it is attached with MR damper. This integrated bondgraph model of test rig is presented in Figure 5.17.
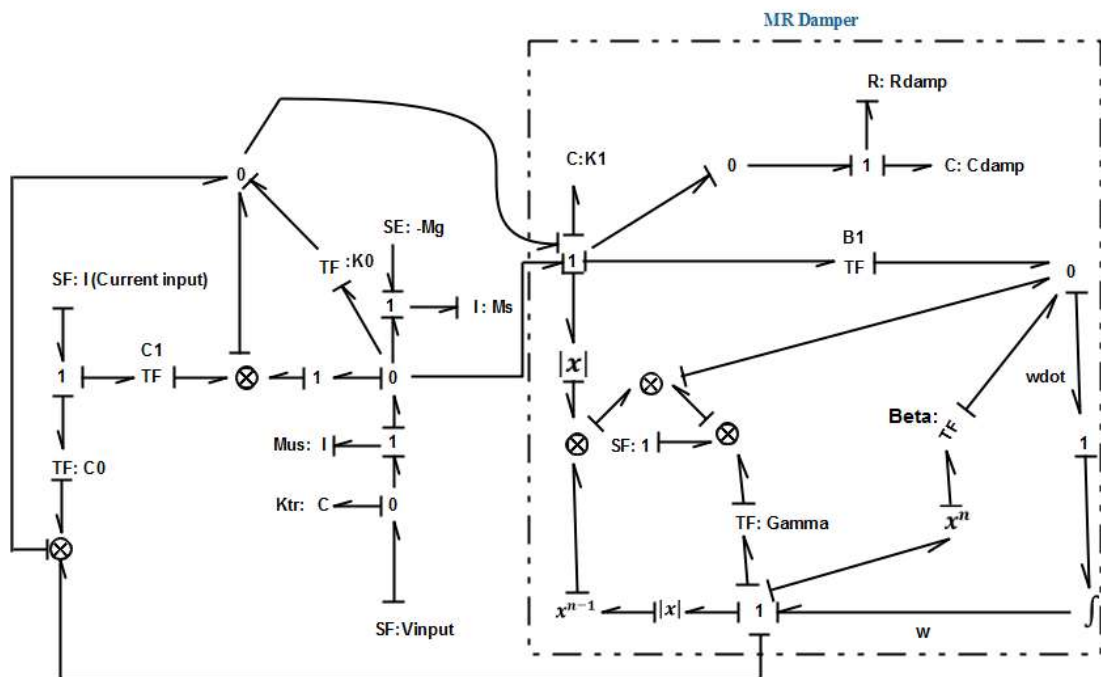
Figure 5.17: Bondgraph model of quarter car test rig

In this model, multiplier-$\otimes$, $|x|$-absolute, x^n – power and x^{n-1}- power elements are used as a capsule element, whereas description of these elements are available in library of Symbols sonata® software as briefly presented in *Appendix A*. However, the dead weight on sprung mass is applied through SE- element, I-element (*Ms, Mus*) represent

the sprung mass and un-sprung mass of the rig, and the SF- element is used for input an electric current to the MR damper, C-element (K_{tr}) describes the tire stiffness, C_0, C_1, K_0, gamma, and beta are the modulus of -TF- elements.

The simulation of computational model of test rig is carried on Matlab/Simulink software. The responses of MR damper are measured under sinusoidal input and strictly validated with results obtained from experimental data by ref (*Ho et al.* 2013).

The characteristics of MR damper are highly non-linear, which depends on applied electric current. It has been observed that the damper has provided highly a force when the value of current increased. This computational model is used to produce the force velocity relationship presented in Figure 5.18, which was implemented in Matlab/Simulink software. It is observed that inherent hysteresis effect of MR damper dominates the force profile, when the velocity is lower, but it is the less significant at the high velocities.
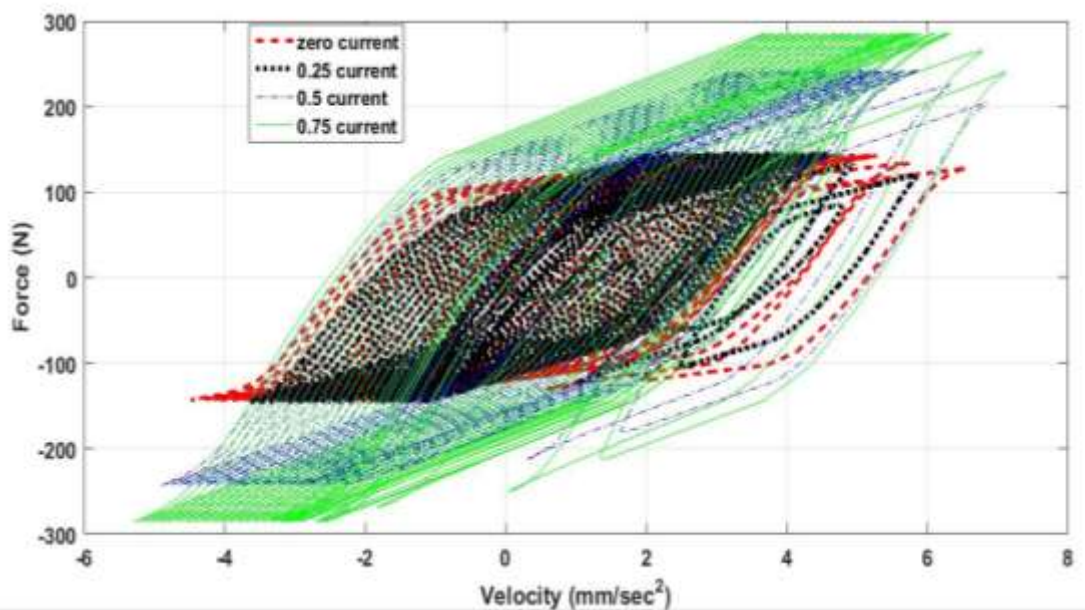
Figure 5.18: Damping force at 1 hz excitation frequency with 0.01m jump as per ref [49]
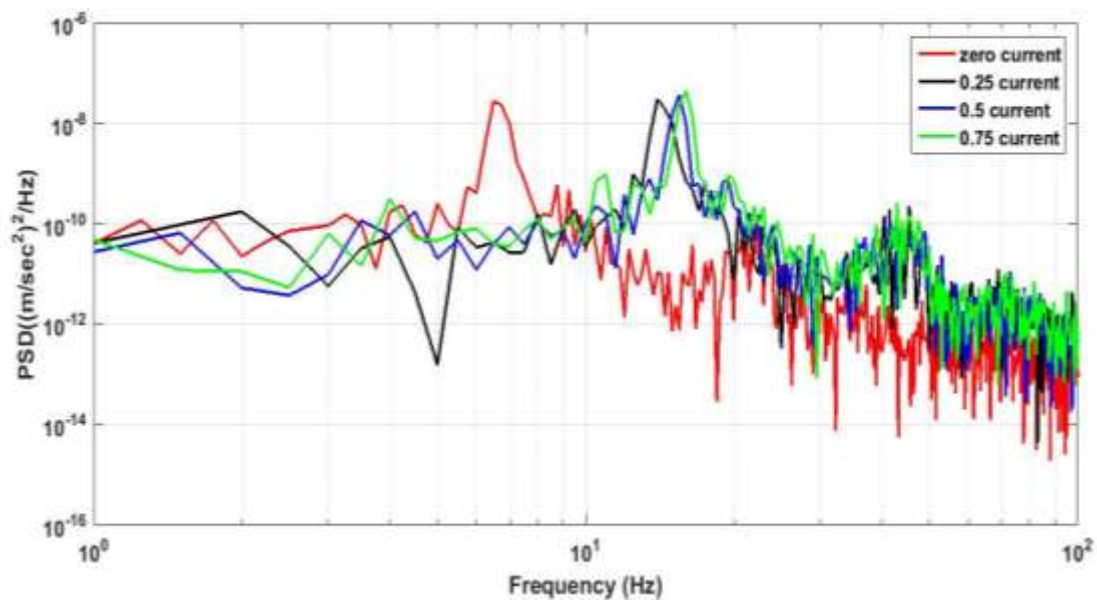
Figure 5.19: PSD acceleration of sprung mass at 1 Hz excitation frequency with 0.01m jump as per ref (*Ho et al. 2013*)

The curve has been plotted at four values of current i.e., 0,0.25, 0.5 0.75, whereas road input is constant for each simulation by a 1 Hz , ±0.01m displacement. It is also seen that the hysteresis loop size is increased with increasing the level of electric current. Figure 5.19 presents the PSD response of MR damper at four different value of current, whereas the zero current value provides relatively higher value. It is depicted from figure that when the current of MR damper increases the damping force will also increase, which can be further reduced the low frequency vibration. The lowest current level of damper is appropriate to resist the high frequency level of vibrations.

5.7 Experimentation and its validation

In order to validate the performance of test rig bondgraph model is being created along with MR (Magneto-Rheological) damper, and the response of this computational model was verified with archival literature (*Ho et al, 2013*) After this verification, an experiment has been performed, where it is categorized as per excitation frequencies,

180

i.e. 5 Hz, 5.85 Hz and 6.68 Hz. However, ground excitation amplitude and dead weight are kept constant during the test, i.e 0.008m and 1000N respectively. In each test, three input currents (0.002, 0.15, 0.38 A) are applied to the MR damper through LORD Wonder box® device controller. Experimental analysis has been carried out for three different condition; In the first condition, sprung mass= 1000N; excitation frequency =5 Hz; excitation amplitude= 0.008m, second condition, sprung mass= 1000N; excitation frequency =5.84 Hz; excitation amplitude= 0.008m, third condition sprung mass= 1000N; excitation frequency =6.68 Hz; excitation amplitude= 0.008m. However, each condition is run for three different current values, i.e 0.025A, 0.15 A, and 0.38A. Figures 5.20-5.22, demonstrates in PSD form for all the three above mentioned conditions, where (a) presents the response of sprung mass obtained through experimentation, and (b) represents the response of sprung mass evaluated through simulation. In the first condition, the value obtained through simulation is 5-7% marginally differ from the value obtained from experimentation. It has also been observed that the PSD value is maximum at higher value of electric current. The other two condition has also been followed on the same pattern as the first condition.
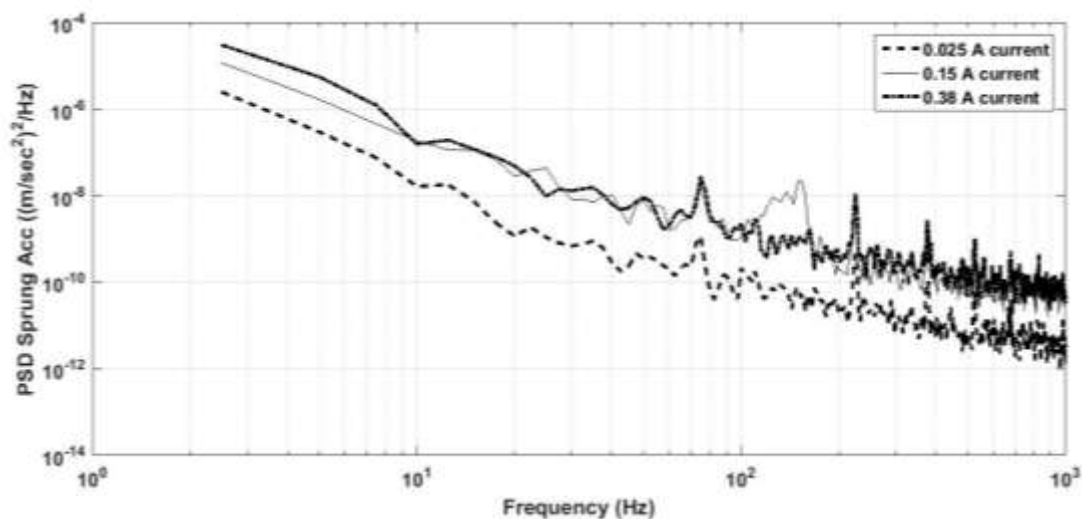
Figure 5.20 (a): PSD sprung acceleration of the sprung mass at condition I
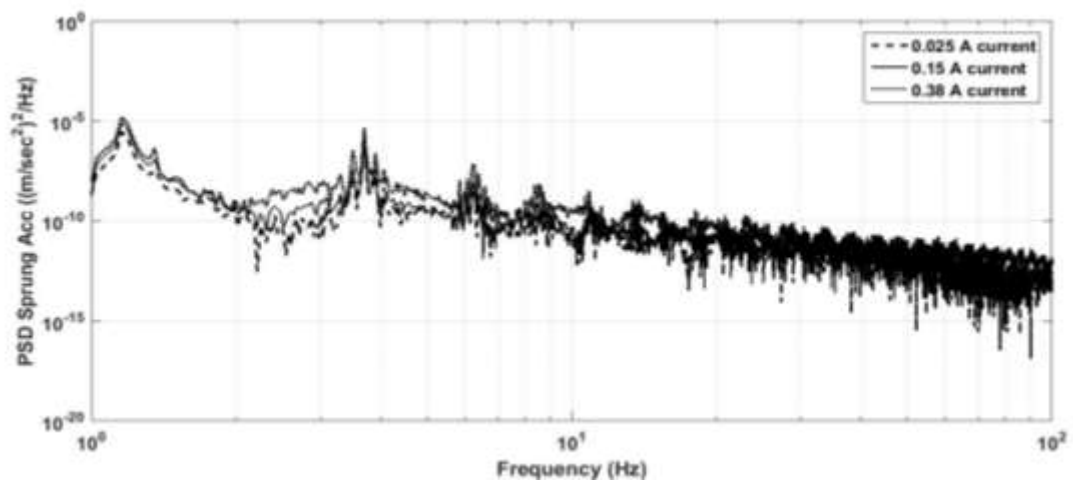
Figure 5.20 (b): PSD acceleration of sprung mass obtained through the simulation for condition I
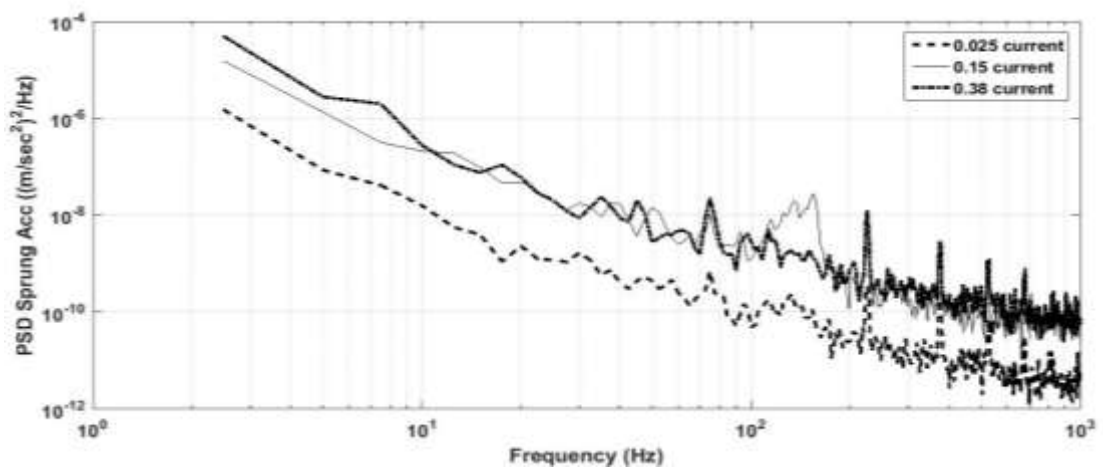
Figure 5.21(a): PSD acceleration of sprung mass obtained through experimentation for condition II
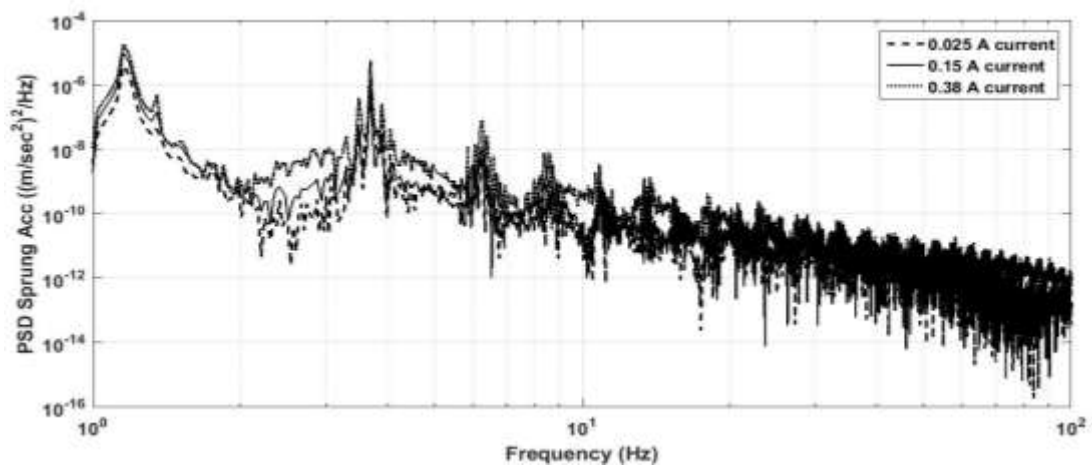
Figure 5.21 (b): PSD acceleration of sprung mass obtained through simulation for condition II
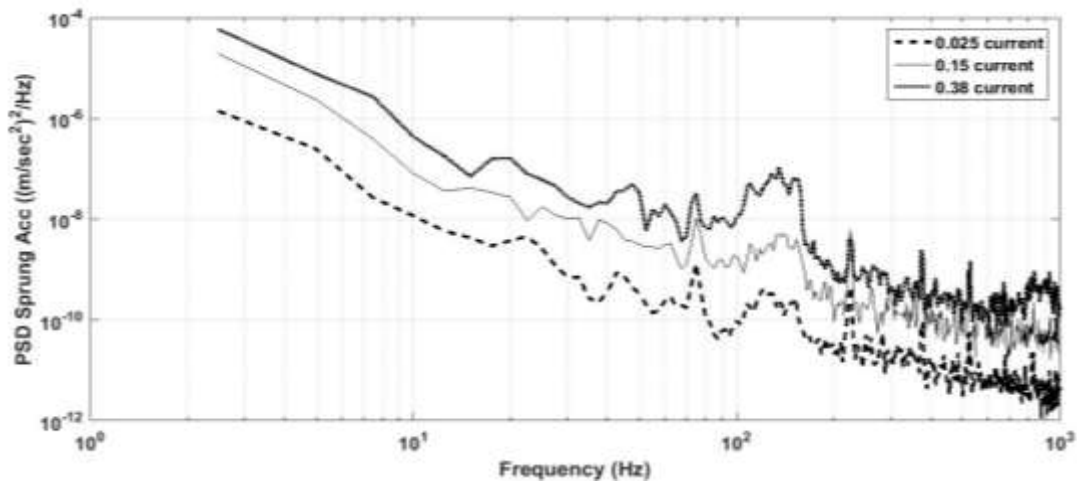
Figure 5.22 (a): PSD acceleration of sprung mass obtained through experimentation for condition III
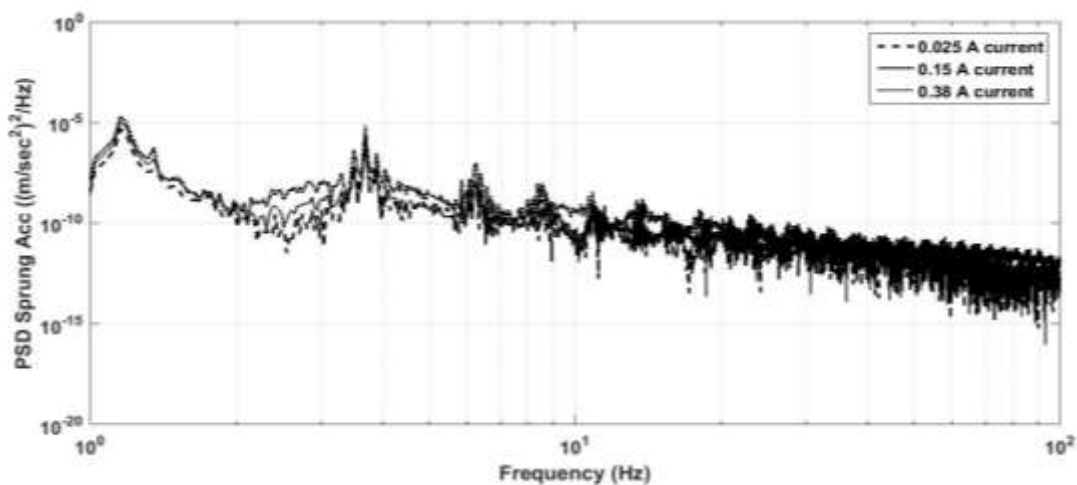
Figure 5.22 (b): PSD acceleration of sprung obtained through simulation for condition III

5.8 Optimization

This section presents the application of response surface methodology (RSM) technique for a optimization of a quarter car test rig and MR damper parameters in order to improve the ride comfort level of a heavy vehicle system. The suspension of the vehicle should be modified to compensate the deteriorated performance in terms of reduced comfort and safety. It is very tedious to conduct an experiment for MR damper with

183

heavy vehicle passive suspension system with real load conditions. Therefore, the experiment work was conducted with least loading conditions and minimum vehicle speed. There were three combinations of parameter used to conduct an experiment, which resulted 30 responses of sprung mass. The experimentation was conducted to verify the veracity of computational model for a quarter car test rig. This section of the thesis dedicate to figure out the optimum parameter to attain a minimum magnitude of acceleration at sprung mass so that the ride comfort level of the driver can be maintain in the real environment. It is very challenging task for a designer to select the best combination of parameter for suspension system of a heavy vehicle in such a way that it will minimize the vibration level at sprung mass and enhance the comfort level. Typically to tackle such problems different design solutions can be tested by comparing the results through numerical simulations. However, sometimes it becomes too costly and time consuming to even do simulations due to complexity of the system. So, it becomes unrealistic to empirically assess all or even a significant fraction of possible design solutions.

At present, there are numbers of global approximation techniques, which can undoubtedly generate optimizable analytical models. Response surface methodology (RSM) is one such technique, which can be used efficiently and effectively for optimizing the road vehicle parameters (*Mitra et al*., 2014). In general, RSM includes the creation of a polynomial approximation function that is fit via regression analysis to a set of data points collected from the design space.

The next section will provide the details of the methodology employed to develop predictive and optimization model for the ride comfort.

5.8.1 Design of experiments

The design of experiments is a powerful technique to improve product design or process performance. It is used to systematically inspect the process variables affecting the process performance. It is possible to find the process parameters affecting the product quality and costs. With the help of DOE, the resources needed to carry out the experiment can be optimized. The parameters affecting the response characteristics of the product or process can be studied. Based on planning, the design of experiments includes several techniques like factorial design, Taguchi method, response surface methodology etc. In this research, the response surface methodology based on the centre composite face centred cubic design has been used for optimization of quarter car suspension parameters for the ride comfort.

5.8.1.1 Response surface methodology

Response surface methodology (RSM) is a combination of mathematical and statistical tools useful for the modelling and analysis of problems in which an output is influenced by number of variables, and the target is to optimize the output. It is a systematic procedure for empirical model building and optimization. By conducting experiments and applying regression analysis, a mathematical relation between response *'y'* and independent input variables $x_1, x_2, \ldots x_k$ can be found by Eq. (5.3).

$$y = \int (x_1, x_2 \ldots \ldots x_k) + \varepsilon \tag{5.3}$$

where, ε represents the error observed in the response. If the response is well modelled by a linear function of the independent variables, the approximating function is the first order model as presented in Eq. (5.4).

$$y = \beta_0 + \beta_1 x_1 + \beta_2 x_2 + \ldots\ldots + B_k x_k + \varepsilon \tag{5.4}$$

In case there is curvature in the relationship, a higher degree polynomial must be employed to model the relationship between response and input variables, such as the second order model as expressed by Eq. (5.5).

$$y = \beta_0 + \sum_{i=1}^{k} \beta_i x_i + \sum_{i=1}^{k} \beta_{ii} x_i^2 + \ldots\ldots + \sum_{i\langle j}^{k} \beta_{i1} x_i x_j + \varepsilon \tag{5.5}$$

where, β's are the second order regression coefficients and ϵ is the error observed in the response. The second term contributes to linear effect, the third term contributes to the higher-order effects, and the fourth and onward terms contributes to the interactive effects of the input parameters. Almost all RSM problems uses one or both of these models. A polynomial model can be a reasonable approximation for the true functional relationship over the entire space of the independent variables, but for a relatively small region they usually work quite well (*Montgomery,* 2007).

In the present research, RSM has been applied to develop the mathematical model in the form of multiple regression equation for the ride comfort. Second order models have been developed which contain linear, squared and cross product terms of independent variables. The objective of employing RSM is not only to examine the response over the full factor space, but also to identify the area of interest, where the response approaches the optimal value.

The application of RSM to design optimization is intended to cut the cost of expensive investigation methods. Application of the RSM for modelling and optimization requires approximation of the regression coefficients. Many experimental

design are available for fitting quadratic models ex. Central Composite Design (CCD) and Box-Behnken Design. In the present work central composite design (CCD) is used to develop second order prediction model for ride comfort. The procedure of Optimization by RSM design is as follows:

i. To establish a relationship between the response and the input parameters by properly designing the experimentation.

ii. To determine, through hypothesis testing, significance of the input parameters.

iii. Finding the optimal set of simulation parameters that produce a maximum or minimum value of response over a certain region of interest.

5.8.1.2 Central composite design (CCD)

The central composite design (CCD) is a design widely used for estimating second order response surfaces. It is perhaps the most popular class of second order designs. A central composite design is a 2^k full factorial to which the central point and the star points (axial points) are added.

A CCD has three groups of design points (*Montgomery,* 2007)

a. Two-level factorial or fractional factorial design points (2^k), consisting of possible combinations of $+1$ and -1 levels of factor.

b. $2k$ axial points (sometimes called star points) fixed axially at a distance say α (distance of axial point from centre) from the centre to generate quadratic terms.

c. Centre points which represent replicated terms. Centre points provide a good and independent estimate of the experimental error.

Considering these points, the total number of experiments as designed by CCD will be given by Eq. (5.4)

$$N_{exp} = 2^k + 2^k + n_{cp} \qquad (5.6)$$

where, N_{exp} is the total number of experiments, k is the number of factors studied, and n_{cp} is the number of replicates.

The fact of having more samples than those strictly essential for a bilinear interpolation (2^k), permits the curvature of the design space to be approximated.
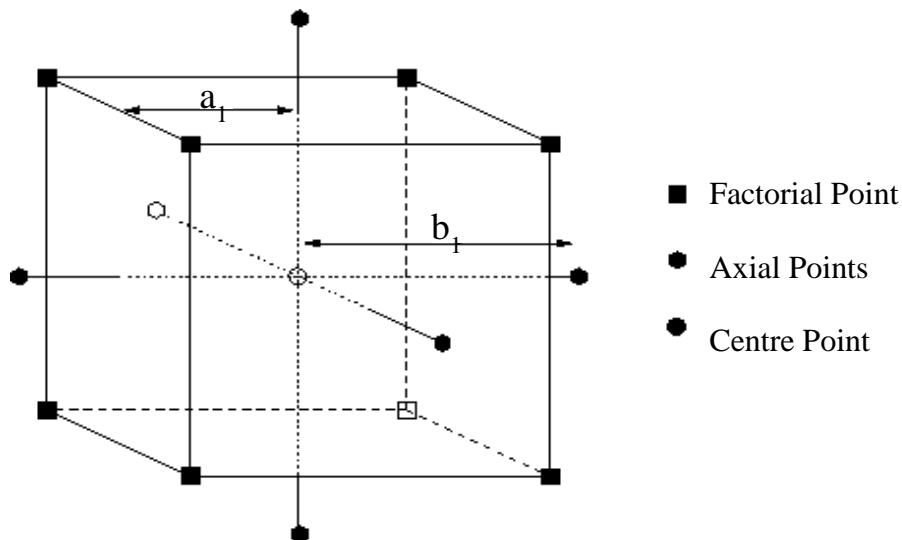
Figure 5.23: Central composite design for 3 factor experiment

The value of α is important to calculate as it could determine the location of axial points in experimental domain. Depending on α value, design is spherical, orthogonal, rotatable, or face centred. Practically, it is in between face centred and spherical. The value of α must be taken as 1 to make the design face centred cubic It is called face centred design and offers three levels for the factors to be put in the experimental design matrix. The design points for 3 factor experiment are shown in Figure 5.23.

In this thesis, the RSM based on central composite face centred cubic design has been used to develop the ride comfort prediction models in the form of regression equations.

5.8.1.3 Selection of parameters

The range of parameters of quarter car semi active suspension model for heavy road vehicle has been selected for keeping in view the stability of vehicle. The semi active suspension elements that have vital impact on the ride comfort and stability of test rig. Table 5.8 represents 3 levels of four independent suspension parameters and their level for each.

Table.5.8: Semi active suspension parameters and their level

Factor	Symbol	Level 1	Level 2	Level 3
Spring stiffness (N/m)	Ks	4.7×10^5	5.7×10^5	6.7×10^5
Current (Amp)	I	0.02	0.21	0.4
Tire stiffness (N/m)	Kt	2×10^5	3×10^5	4×10^5
Tire Pressure (psi)	P	60	65	70

5.8.1.4 Ride comfort measurement

Maximum value of acceleration of a sprung mass for each configuration of quarter car model has been used to measure a ride comfort. The experimentally validated computational model of quarter car test rig was used. However PSD acceleration of sprung mass has been evaluated through simulation with real parameters of vehicle (*Rideout*, 2010). The vehicle is assumed to harmonically displaced of 0.08m in vertical direction with 1 Hz frequency.

5.8.2 Design layout

The number of experiments required in an experimental investigation depend primarily on design of experiment. The success of an investigation depends on how well an experiment scheme has been designed. A good experiment scheme minimizes the number of required experiments. In this research, the design suggested by RSM based on central composite face centred cubic has been used to study the effect of four independent suspension parameters on ride comfort application of CCD reduces the number of runs to 30 (2^4+2x3+6) runs with 6 replications.

Table 5.9: Design layout and simulation results

S.No.	Spring Stiffness (N/m)	Damper Current (Amp)	Tire Stiffness (N/m)	Tire Air Pressure (PSI)	Max Acc (m/sec^2)
1	670000	0.02	4000000	60	0.855251
2	570000	0.21	3000000	65	1.12604
3	570000	0.21	3000000	65	0.346532
4	670000	0.02	2000000	60	0.269494
5	570000	0.21	3000000	65	1.129253
6	670000	0.4	2000000	60	0.165057
7	470000	0.02	2000000	60	0.494607
8	670000	0.4	4000000	60	0.392729
9	670000	0.02	4000000	70	1.471058
10	570000	0.21	3000000	65	0.345785
11	570000	0.21	4000000	65	0.182936
12	570000	0.21	3000000	65	0.319763
13	570000	0.21	3000000	60	0.317433
14	670000	0.21	3000000	65	1.223341
15	470000	0.02	4000000	60	1.458446
16	570000	0.4	3000000	65	0.319763
17	670000	0.4	4000000	70	1.508636
18	470000	0.02	4000000	70	1.459916
19	470000	0.4	2000000	70	1.385496
20	470000	0.4	4000000	60	1.458446
21	570000	0.21	2000000	65	0.655091
22	470000	0.21	3000000	65	1.741496
23	470000	0.4	2000000	60	1.371545
24	670000	0.02	2000000	70	0.174567
25	470000	0.4	4000000	70	1.461152
26	570000	0.21	3000000	70	0.32111
27	670000	0.4	2000000	70	0.174567
28	570000	0.02	3000000	65	0.346532
29	570000	0.21	3000000	65	0.319763
30	470000	0.02	2000000	70	1.385496

In case of computer experimentation, one gets the same value of response in each replicated run. Therefore, the total number of effective runs reduces to 25. The data set collected as per the design layout based on central composite face centred cubic design is presented in Table 5.9. Based on design layout, simulation is carried out to obtain the ride comfort in terms of minimum acceleration at sprung mass. These response values are used to develop ride comfort model in the form of second order polynomial function.

5.8.2.1 Ride comfort prediction model

(i) Prediction model without transformation

The prediction model has been developed using RSM based on central composite face centred design. Responses of sprung mass obtained through experimentation are fed to the Design Expert® software for further analysis. ANOVA is normally employed to examine the significance of the regression model, significance of individual model term and lack-of-fit of the model. The analysis is based on two assumptions as given below

(a)　　The variables are normally distributed, and

(b)　　Homogeneity of variance.

Any violation of these assumption can increase the probability of committing either a Type I or II error, depending on the kind of the analysis and violation of the assumption (*Osborne*, 2010). To examine the viability of assumptions of ANOVA for residuals, the normal probability plot of the residuals is presented in Figure 5.24. The normal probability plot specifies whether the residuals follow a normal distribution or not. If maximum number of points on a normal probability plot fall on a straight line, then the model is said to adequate and follows a normal distribution. One can observe

from normal probability plot of Figure 5.24, that few of the points are lying away from the straight line, indicating that residuals doesn't follow the normal distribution completely.
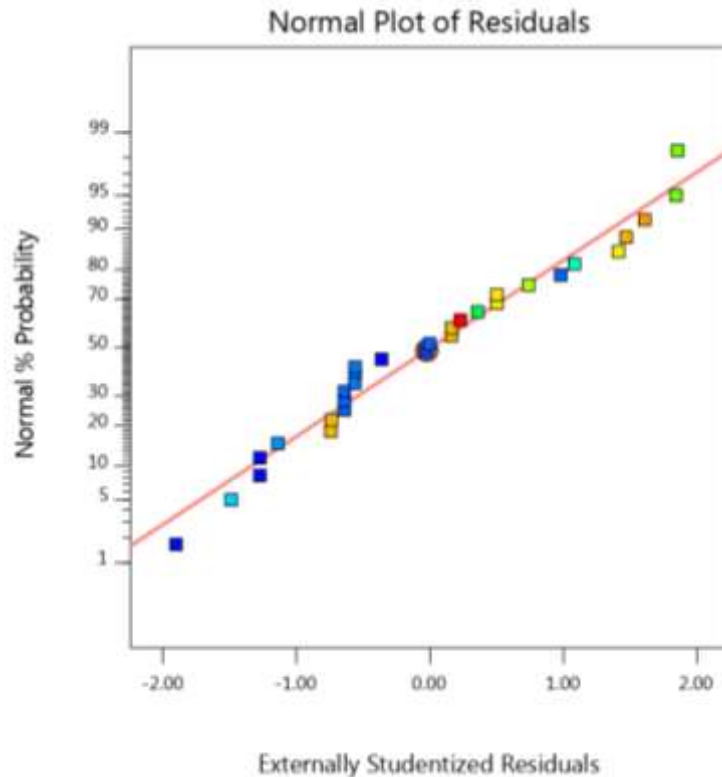
Figure 5.24: Normal probability plot of residuals

Table 5.10 shows the ANOVA table for reduced quadratic model for ride comfort by selecting the forward elimination procedure to reduce the non-significant terms. The F-value of 8 .21indicates that the model is significant. The analysis has been performed for a significance level of $\alpha = 0.05$, i.e. for a confidence level of 95 %. The value of "*Prob. > F*" for the model is 0.0001 which is very small as compared to 0.05, indicates that the model is significant. Similarly, the value of "*Prob. > F*" for main effect of K_y, *I*, K_t, *P* and two-level interaction of K_sI, K_sK_t, K_tP,, K_sP , indicating these to be the significant model terms. Other terms are not significant and can be removed by using

forward elimination method. The final empirical model for ride comfort (RC) in terms of coded and actual factors are represented by Eq. (5.7) and Eq. (5.8) respectively.

Table 5.10: ANOVA results for ride comfort response surface quadratic model

Source	Sum of Squares	df	Mean Square	F-value	p-value	
Model	5.92	5	1.18	9.57	< 0.0001	Significant
A-Tire Stiffness	1.99	1	1.99	16.07	0.0005	
C-tire stiffness	0.9673	1	0.9673	7.82	0.0100	
D-tire damping	0.3638	1	0.3638	2.94	0.0992	
A²	2.24	1	2.24	18.08	0.0003	
D²	0.4401	1	0.4401	3.56	0.0714	
Residual	2.97	24	0.1237			
Lack of Fit	2.13	19	0.1119	0.6638	0.7654	
Pure Error	0.8427	5	0.1685			
Cor Total	8.89	29				

$$RC = 0.5371 - 0.3323A + 0.2318C + 0.1422D + 0.8057A^2 - 0.3574D^2 \qquad (5.7)$$

$$RC = -34.34029 - 0.000095.K_s + 2.31814 \times 10^{-7}.K_s + 1.88707.P + \\ 8.05717 \times 10^{-11}.K_s{}^2 - 0.014297.P^2 \qquad (5.8)$$

(ii) Development of prediction model with transformation

To improve the results obtained from the quadratic model, the Box-Cox transformation (*Box and Cox,* 1964) has been employed. The Box-Cox provides a group of transformations that will normalize the data which are not normally distributed by using an appropriate exponent (Lambda =λ). The Lambda value indicates the power to which all data should be raised. Box and Cox originally intended this transformation as a solution for simultaneous correction of normality, linearity and homogeneity (*Osborne,* 2010).
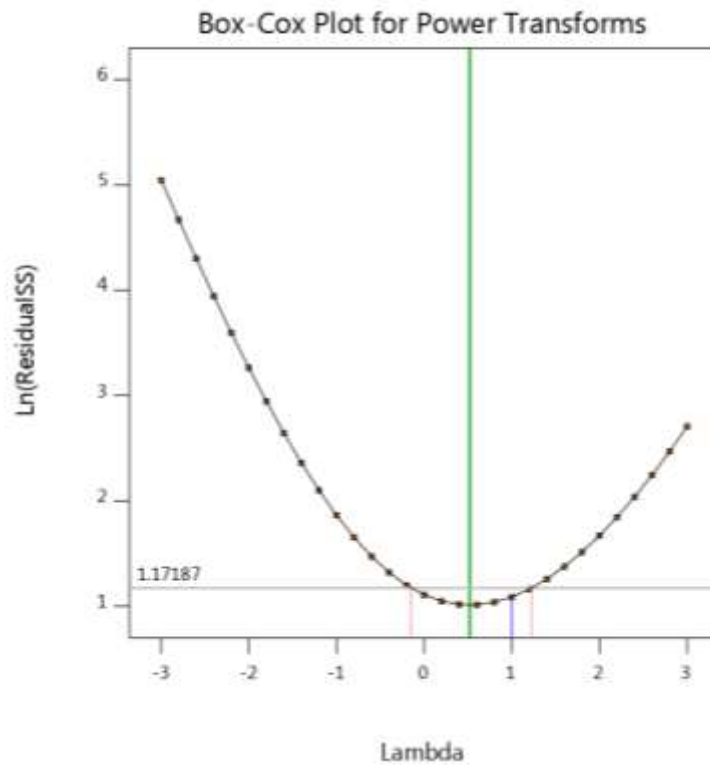
Figure 5.25: Box Cox plot for power transformation

Figure 5.25 shows the Box Cox plot for power transformation of residuals. The dotted line indicates current value of λ for residuals, which is lying outside 95 % confidence limits. But plot also shows the best recommended value of λ which is 1.59 as indicated by long dashed line. The normal probability plot after applying the Box-Cox transformation is presented in Figure The plot shows that after applying Box Cox power transformation the points fall on a straight-line indicating normal distribution of the residuals.

Table 5.11 shows the ANOVA result for the improved quadratic model for ride comfort by selecting the forward elimination procedure to automatically remove the insignificant terms. The F-value of 315.15 and *Prob. > F* value of 0.0001 implies that

the model is still significant. Also, the value of "*Prob. > F*" for main effect of K_s, *I*, K_t, R_t and two-level interaction of K_sI, K_sKt, K_tP,, K_sP, indicating these to be the significant model terms. The adjusted R^2 value is equal to 0.660, it is particularly useful when comparing models with different number of terms.
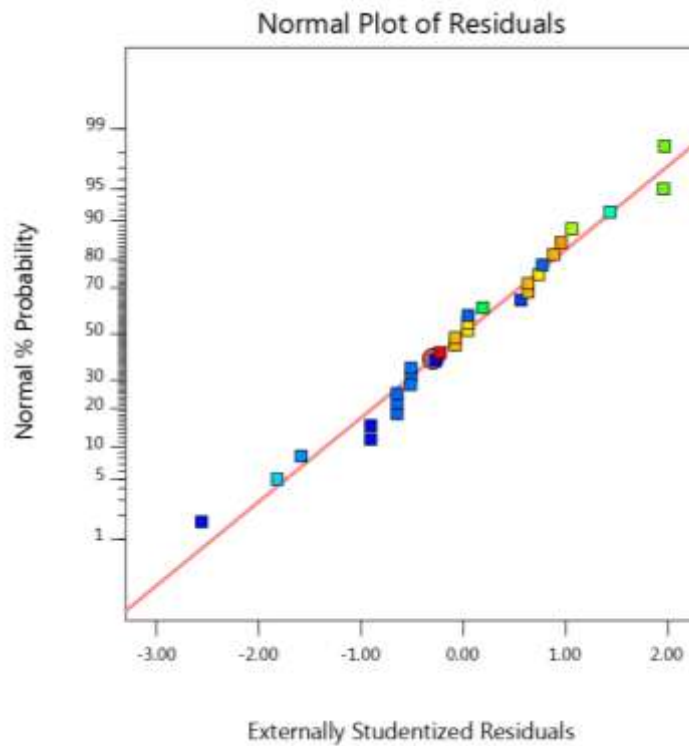
Figure 5.26: Normal probability plot of residuals after Box-Cox transformation

The result shows that the difference between adjusted and predicted R^2 value (0.5789) and R^2 value (0.4290) is less, thus there is no problem in the model. Adequate precision value for this model is equal to 8.99, a ratio greater than 4 is desirable, which indicates an adequate signal. The final regression model after transformation for ride comfort in terms of coded and actual factors is represented in Eq. (5.9) and Eq. (5.10) respectively. The equation in terms of actual factors can be used to predict the response for given levels of each factor.

$$RC^{0.25} = 0.825 - 0.1095A + 0.0762C + 0.035D - 0.629AC + 0.2361A^2 - 0.1124D^2 \tag{5.9}$$

$$RC^{0.25} = -9.49853 - 0.000030 \cdot Ks - 2.822 \cdot 10^{-07} \cdot Kt + 0.591790 \cdot P + 6.2896 \cdot 10^{-13} \cdot Ks \cdot Kt$$
$$+ 2.36104 \cdot 10^{-11} \cdot K_{s^2} - 0.004497 \cdot P^2 \tag{5.10}$$

Table 5.11: ANOVA results for ride comfort response surface quadratic model

Source	Sum of Squares	DOF	Mean Square	F-value	p-value	
Model	0.6230	6	0.1038	7.64	0.0001	Significant
A-Tire Stiffness	0.2158	1	0.2158	15.89	0.0006	
C-tire stiffness	0.1046	1	0.1046	7.70	0.0108	
D-tire damping	0.0230	1	0.0230	1.69	0.2062	
AC	0.0633	1	0.0633	4.66	0.0415	
A²	0.1920	1	0.1920	14.14	0.0010	
D²	0.0435	1	0.0435	3.21	0.0866	
Residual	0.3124	23	0.0136			
Lack of Fit	0.2143	18	0.0119	0.6065	0.8019	
Pure Error	0.0981	5	0.0196			
Cor Total	0.9354	29				
Std dev	0.1165			R^2		0.6660
Mean	0.8992			Adjusted R^2		0.5789
C.V %	12.96			Predicted R^2		0.4290
PRESS				Adeq R^2		8.9929

The residual versus predicted response plot presented in Figure 5.27 shows that the data is randomly scattered and there is no obvious pattern and unusual structure truing the assumption of constant variance. A plot of the actual versus predicted response values is shown in Figure 5.28. It generally helps to find out a value or group of values that are not easy to predict through the model. The figure reveals that all the data points split evenly around the 45° line showing a strong correlation between the model's predictions and the actual results obtained through simulation.
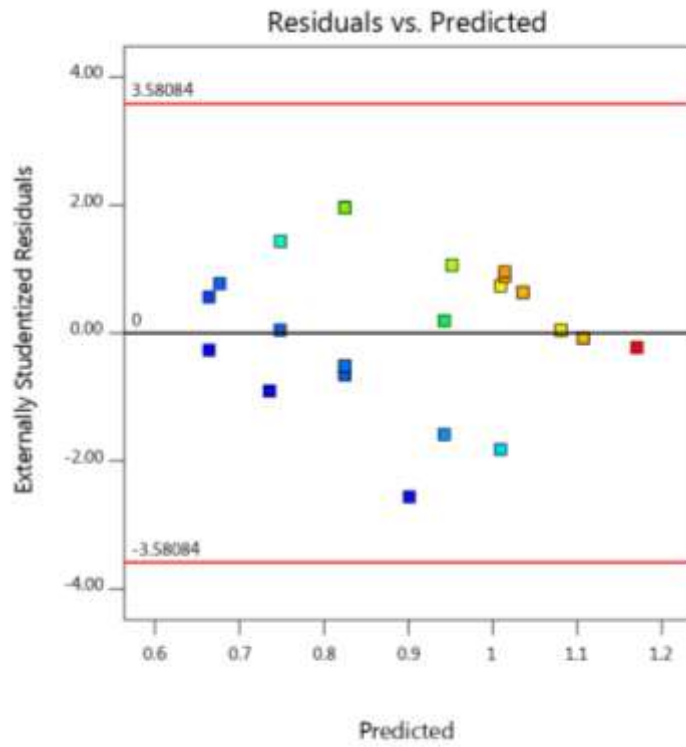
Figure 5.27: Plot of residual versus predicted response
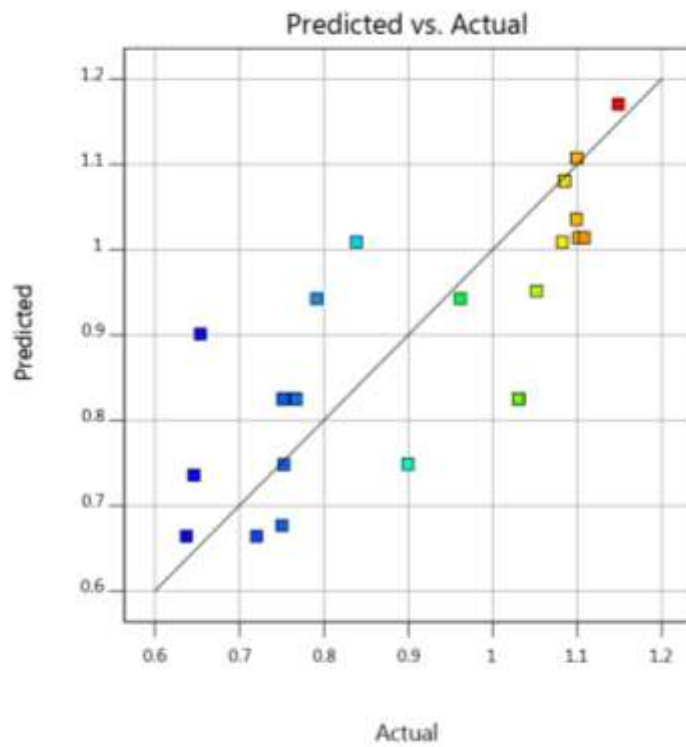
Figure 5.28: Plot of predicted vs. actual response

5.8.2.2 Optimization of suspension parameters for ride comfort

Once the mathematical model is developed to predict the ride comfort and checked for adequacy, the next logical step is to obtain optimal suspension parameter for maximum comfort. Selection of optimum suspension setting has always been a challenge for vehicle designer. The optimal setting of suspension parameter is obtained through response surface optimization.

(i) Optimization problem formulation

The performance characteristics, which are of prime concern while designing the suspension system of a heavy vehicle for ride comfort, suspension travel, wear and stability of the vehicle. Among these the most important characteristic is ride comfort and the stability condition. In the present thesis, ride comfort is chosen as the main criterion to obtain the optimal suspension setting, while meeting the stability condition at the same time. Thus, the parameters range is selected in such a way that for all the values within the range the vehicle remains stable. Based on the requirement, the optimization problem may be expressed as:

$$\min RC$$

subjected to

$$4.7 \times 10^5 \text{ N/m} \leq K_s \leq 6.7 \times 10^5 \text{ N/m}$$

$$0.02 \text{ Amp} \leq I \leq 0.4 \text{ Amp}$$

$$2 \times 10^5 \text{ N/m} \leq K_t \leq 4 \times 10^5 \text{ N/m}$$

$$60 \text{ psi} \leq P \leq 70 \text{ psi}$$
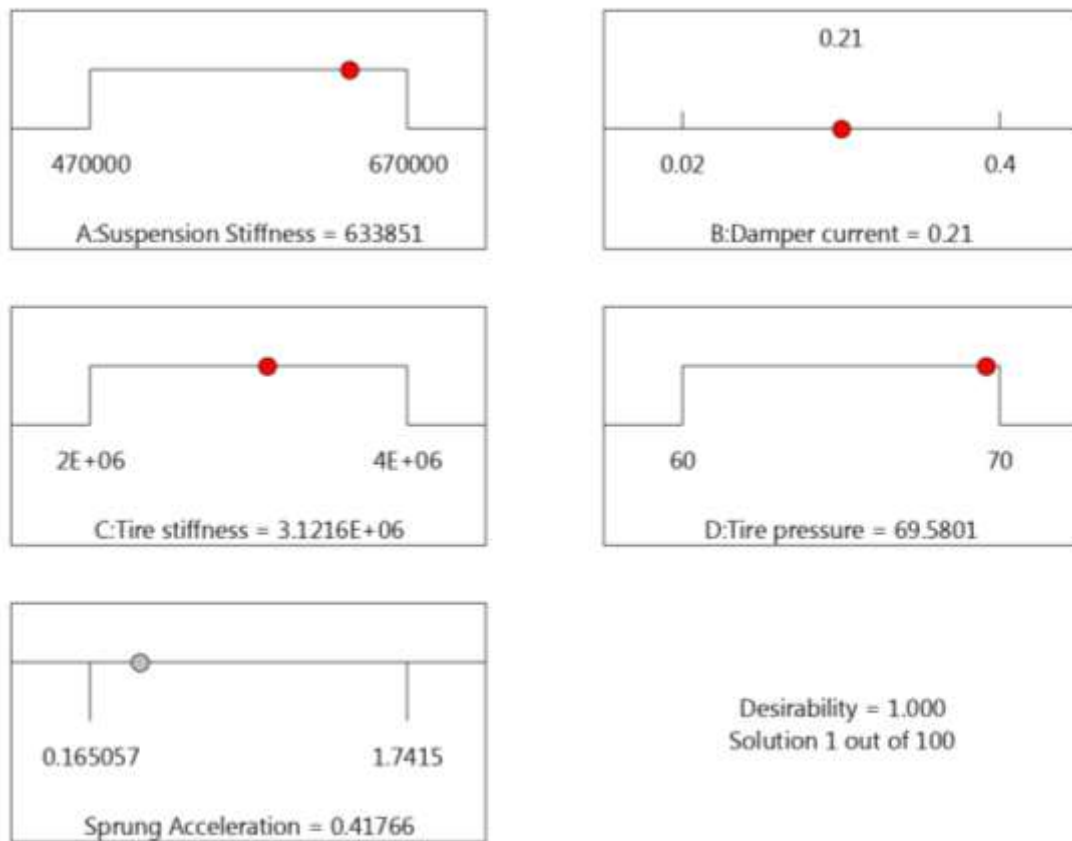
Figure 5.29: Ramp function graph of desirability for ride comfort

The method of desirability function was proposed by *Derringer and Suich (1980)* in 1980. Desirability is an objective function that has zero value outside the limits and becomes one at the goal. The numerical optimization gives a point that maximizes the desirability function. The characteristics of a goal may be adjusted by suitably setting the weight. It is based on reduced gradient algorithm. The algorithm starts with multiple solutions and finally provides the optimal parameters setting with maximum value of the desirability. The desirability function is built on the idea, that if a product or process have number of quality attributes and if any of the feature falls outside the "desirable" limit, the product or the process is unacceptable (*Candioti et al.,* 2014).

Several researchers have used desirability function for the solution of optimization problem. In this thesis also, it is used to find the optimum suspension setting of road vehicle. The first step in desirability function analysis is the calculation of the desirability index (d) by using Eq. (5.11). The scale of the desirability function ranges between 0 and 1. If d is 1, then the response is at its goal or target and if d is 0, then the response lies outside the acceptable region. then the response is perfectly on the target value. The desirability function for the single objective minimization problem is given by Eq. (5.10)

$$d = \begin{cases} 1 & if & y \le y_{min} \\ \left(\dfrac{y - y_{max}}{y_{max} - y_{min}} \right)^r & ,if & y_{min} \le y \le y_{max} \\ 0 & if & y \ge y_{max} \end{cases} \tag{5.11}$$

where, y is the output during optimization, y_{min} and y_{max} are the lower and the upper limit of response and r is weight.

The response optimization analysis has been done to get minimum ride comfort value i.e. maximum comfort, based on mathematical model given in Eq. (5.11). The goal of optimization is to obtain a good parameter setting that will meet all the goals. The ramp function graph drawn using Design Expert presented in Figure 5.29 show the desirability for each factor and the response. The dot on each ramp reflects the parameter setting or response prediction. The height of the dot shows factor importance. A linear ramp function is developed between the low value and the goal or the high value and the goal because the weight for each parameter was set equal to one.
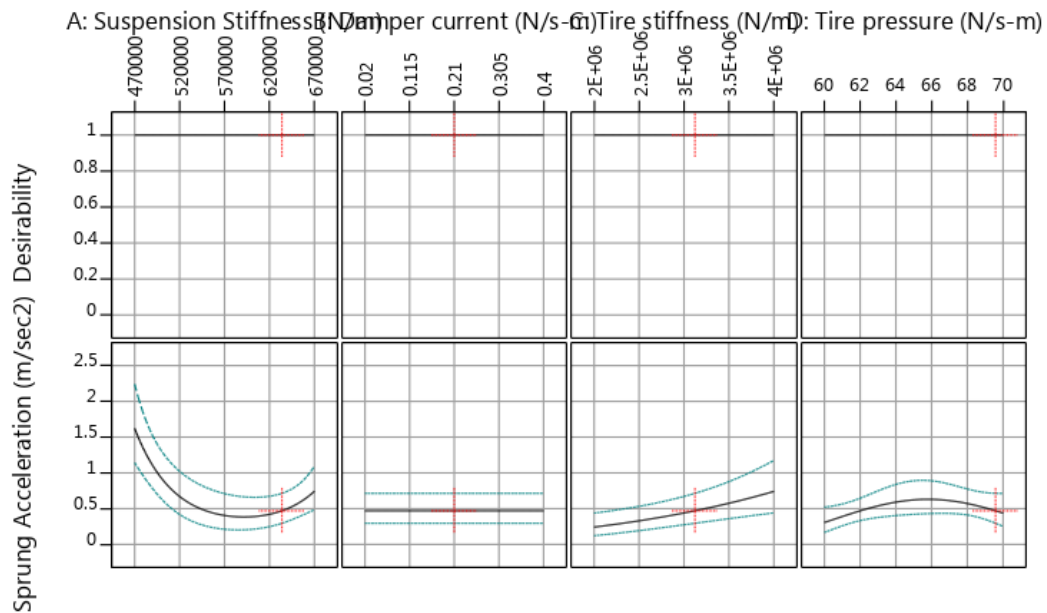
Figure 5.30: Response optimization plot for ride comfort

An interactive optimizer plot showing the optimum suspension setting and the response value along with the respective desirability value are presented in Figure 5.30. Optimal suspension parameters obtained are suspension stiffness 633851 N/m, damper current value of 0.21 Amp, tire stiffness 3.126 e+06 N/m and tire pressure value 69.58 psi. The optimized acceleration value for ride comfort is 0.4703 m/sec^2 at desirability function value of 1.

5.9 Conclusions

In order to verify the computational model of quarter car model for heavy vehicle system with MR damper, a quarter car test rig is designed and fabricated. In this rig, MR damper (8040-1), which was mounted parallel to leaf spring on axle of wheel. Damping value of MR damper can be varied by the change of input current through wonder box controller. The experimental study was conducted for three different configurations whereas it is considered three values of current, three values of road

excitations at different frequency, and three values of dead weight. Thus total 27 sprung mass responses was captured through accelerometers and recorded in OROS analyzer. Similarly, further these results was used for validate the computational model.

In the next section, validated computational was run for real parameters of truck and obtained the 30 responses for different configuration of parameters. So that this study can be extended to implement a RSM methodology for obtaining an optimal setting parameters for quarter car test rig.

The conclusions and recommendations for future work will be presented in next chapter, which will finally conclude the thesis.

Chapter 6
Conclusions and Future Directions

In the previous chapter, the simulation for a quarter car suspension system has been carried out and obtained responses was validated with the experimental study. Further, the computational model was run for real parameters of heavy vehicle system and various responses of sprung mass were recorded with different configurations of truck parameters. Also, developed a ride comfort predictive model, which was used to optimize the suspension parameters for heavy vehicle system. This chapter presents an overview of the conclusions drawn from the study and gives direction for future research.

6.1 Conclusions

In this thesis, the behavior of heavy road commercial vehicle has been shown under different road conditions and computational model of vehicle has also been proposed for evaluating the vertical dynamics of the vehicle. It has also contained involved the effect of chassis flexibility during riding and results has been presented in terms of PSD form. In addition, this work also suggested the mechanism to reduce the vibration level by incorporating various control strategies to the suspension model. The current results have shown the impact of flexural rigidity on vehicle and human body, which were presented in different sections of the thesis. The other outcome is to compared the previously presented various semi-active control strategies and suggest the suitable controller for the heavy road vehicle. Moreover, a new hybrid control strategy has been proposed which gives the better performance with respect to the

previously suggested control strategies. The overall conclusions drawn from the thesis chapters are listed below:

Numerous models have been constructed for the heavy vehicle system but most of the models are developed with lumping process. In this work, an analytical framework for truck chassis has been developed through classical mechanics and through extended Lagrangian approach. In the classical mechanics approach, the idea of lumped-distributed modelling has been explored within the framework of bondgraphs. The Lagrange variation of truck chassis including flexural behavior has been constructed, where it was integrated with lumped suspension system. However, the structural damping effects were also involved in terms of fifth order partial differential term in generalized equation of motion. The detailed derivation for fifth-order differential term has been presented in Appendix A. The integrated bondgraph model of flexural beam was the extended form of the analytical model. Results have been presented under the two type of road conditions i.e., sine wave input and random road input. In sine wave road conditions, the vertical response of flexural beam is reduced up to 12-15 % and pitch response of beam is reduced up to 20% due to the structural damping effect. In random road conditions, four type road category (H1, H2, H3, H4) have been used at four different speeds (40 kmph, 60 kmph, 80 kmph and 100 kmph). It is depicted from the result that maximum acceleration at maximum speed (100 kmph) of chassis has been increased up to 0.5 m/sec^2 in H1 to H2 condition, 1 m/sec^2 in H2 to H3 condition, 2.25 m/sec^2 in H3 to H4 condition. Similarly, the solution has been extended for structural or internal damping, whereas maximum acceleration at maximum speed has been reduced up to 10 %, 5%, 7% and 5% (approx.) in H1, H2, H3 and H4 road condition respectively.

Further, this analytical expression was generated with extended Lagrangian approach. This methodology has overcome the limitation of classical Lagrangian approach and it can accommodate non-potential, non-conservative and gyroscopic elements in the system. The distributed model of beam has also considered structural damping effect, which was considered as a non-potential field of the system.

In the chapter *three*, the issues of ride comfort in heavy vehicle system has been addressed. In this section, the whole-body vibration analysis has been carried out for assessment of driver ride comfort in four types of random road condition as per ISO 8608 considering the flexibility of vehicle, whereas the two road conditions are similar to Indian road condition. The detailed explanation of random road condition has been presented in chapter *two*. A combined human bio-dynamic vehicle bondgraph model has been developed to perform the comfort analysis of the human body as exposed to vibrations from a vehicle. The model was used to evaluate the vehicle performance in terms of weighted root mean square acceleration as per ISO 2631 standards.

A physiological effects of the human body due to vibration has been analyzed as per specified criteria ISO 2631. The modal analysis of the truck chassis and the issue of comfort for different body parts in the vehicle has been addressed under the four different random road conditions (H1, H2, H3 & H4) prescribed by ISO 8608, in which H1 and H4 are the best and the worst road conditions respectively. The RMS weighted value of different body parts was superimposed over ISO curves. It has been found that at a vehicle speed of 100 km/h for H1 and H2 road conditions, weighted RMS acceleration levels are almost below the 1 hr. curve for all body parts including

driver seat. However, the RMS weighted accelerations are totally changed for H3 and H4 road conditions. It has been evident that the body parts were below 1.5 hr line for speed below 60 km/hr. It has been raised from 1hr for H3 road condition at 60 km/hr. It is evident that the driver may experience comfortable travel in the vehicle under the following conditions:

i.   If the vehicle runs between 60 to 80 km/h speed for not more than 4 hrs. in case of the H1 condition.

ii.   If the vehicle runs below 60 km/h speed for not more than 1.5 hrs. in case of H2 road condition.

iii.   If the vehicle runs below 40 km/h speed for not more than 1 hr. for H3 road condition.

iv.   If the vehicle runs below 30 km/h speed for not more than 1 hr. for H4 road condition.

Chapter *four* has analyzed the enhancement of comfort level of driver through the integration of semi-active controller to the suspension system. For reducing the complexity of the simulation, the complete model was assumed as a 2-DOF quarter car model. Various semi-active control strategies have been integrated with quarter car system. Firstly, results were obtained for previously available semi-active controllers for comparative study under the steady state input and random road conditions. It is observed that on-off skyhook controller has reached a maximum magnitude of body acceleration than passive system whereas settling time of the controller was reduced up to 60%. Since, the sudden rise in amplitude created a sudden jerk problem to the driver, which can be considered as an uncomfortable.

However settling time of this controller is lower, so that the driver will not feel jerks for a long time as compared to the passive system. In on-off ground hook logic, the sudden jerks has been reduced but the settling time was very high. Thus, this controller has reduced the sudden jerk problem but it generated vibration for a long duration, which may also create an uncomfortable environment to the driver. Similarly, for on-off balance logic controller, the sudden jerk problem was significantly reduced, but settling was very large compared to the passive system. For un-sprung mass, the on-off skyhook controller has provided sudden jerks as well as more settling time, and on-off balance has given comparatively fewer jerks but settling time was little higher. However, on-off ground logic has given better performance in both regard. The maximum magnitude of sprung mass acceleration is almost half as that of a passive suspension system for all the three continuous control logics. But the settling time for all continuous logics has been increased up to 40% compared with the passive system. Similarly, the magnitude, as well as the settling time has been compromised for the un-sprung mass acceleration.

Further, the thesis has proposed several new hybrid control logics, which has enhanced the exceptional performance in terms of acceleration of sprung mass and un-sprung mass from the conventional control strategies. In case of hybrid logics i.e. HY-SH-GH strategy and HY-SH-GH-B strategy have provided better results in terms of vertical acceleration of the vehicle body. However, HY-SH-GH-B strategy was better in comparison to other remaining hybrid logics. The magnitude and the severity of both were found to be less in these cases. The robust controllers were found to be the best among all control algorithms. H∞ control has enhanced the fun ride and addition of PID loop further enhanced the road holding capability. Finally, the

proposed PID- double H∞ controller has created a trade-off between fun ride and the road holding capability.

Chapter *five* has detailed about the fabrication of a quarter car suspension test rig for conducting experimental works. This test rig involved a controlled MR damper (RD 8040-1), which was mounted parallel to leaf spring on the axle of the wheel. The experimental results were presented in form of PSD acceleration. The response of sprung mass has been captured for three values of current with three different road excitations. It has been observed whenever the value of current reached up to 60 %, the PSD acceleration of sprung mass increased up to 70% at the same excitation frequency and amplitude. A bondgraph model has also been created along with MR damper of this test rig, in which results were validated with archival literature and experimental results. Further, this work was extended to implement a RSM (Response Surface Methodology), to find an optimal setting parameters for a quarter car test rig. Design of experiment often needs a precise representation of the independent variables which are usually difficult to measure. The optimal suspension parameters obtained are suspension stiffness 633851 N/m, damper current value of 0.21 Amp, tire stiffness 3.126 e+06 N/m and tire pressure value 69.58 psi.

In the present scenario, automobile industries are more concern about enhancing the ride comfort level of driver during the long rides of the heavy vehicle. In this way, work related problems of truck driver can be eliminated and there will be lesser chances of road accidents of the heavy vehicles. This research work will also useful to mathematical and computational framework for vehicle structure, which also involves flexural vibrations of truck chassis with structural damping effect. The

suggested model is capable to evaluate a performance of heavy vehicle system with different parameters over the various real/random road conditions. Moreover, proposed hybrid suspension control strategies would be able to reduce the sprung mass vibration up to a certain level and will increase durability of a heavy vehicle structure for a longer period of ride in Indian road conditions. The fabricated test rig may be further used for tuning the suspension settings, to evaluate optimum parameters for different suspension settings, which can be experimentally suggested experimentally.

6.2 Future scope of this work

Following issues can be addressed in the future course of research.

- In this thesis, the analytical expression for chassis flexibility is modeled considering the Rayleigh beam approach. This expression also includes the structural damping effect and extended to build the bondgraph model for pitch plane for a heavy vehicle. This analytical framework can be extended to modeled the chassis structure considering Timoshenko beam approach. This work is only focused to evaluate vertical dynamics of the vehicle structure. However, this work can be extended furthur to involve other dynamics, i.e., longitudinal and lateral dynamics.

- Vertical dynamics analysis has been performed considering the front, and the rear wheel assuming as simple spring element. Moreover, the analysis can be further extended to include the impact tire dynamics on commercial vehicle.

- In this work, the whole body vibration analysis has been carried out by considering 7-DOF driver model to investigate the physiological effects of the

vibrations on the human body. This study can be further extended by assuming a higher DOF occupant model to provide some extended insight.

- The vertical vibration of the sprung mass of a heavy vehicle is controlled by employing the various semi-active controllers and few newly proposed hybrid control logics. The force actuator is not reticulated in the present thesis. The scope of study can be enlarged by using actuator and other control schemes.

- In this work, optimal parameter settings have been obtained by using response surface methodology. However, multi-objective optimization considering some more factors and responses can be attempted in future.

Bondgraph Elements

A.1   Introduction

The best way to study the dynamics of a system residing in multi-energy domain is to start with a schematic diagram, which includes its important components and portrays how they are connected together. Then one can show details of each component and specify the constitutive laws governing the components and subsystems they are in. Each energy domain has its own concepts, symbolic notations and equation. However, a basic similarity exists in the common underlying energy structure.

Since the form of equations of engineering systems do not express energy structure directly, this feature cannot be observed readily from the equations. Bondgraph is an explicit graphical tool for capturing the common energy structure of systems. In the vector form, they give concise description of complex systems. Moreover, the notation of causality provides a tool not only for formulation of system equations, but also for qualitative analysis of system behavior, viz. controllability, observability, fault diagnosis, etc.

In 1959, *Paynter, (1990)* gave the revolutionary idea of portraying systems in terms of power bonds, connecting the elements of the physical system to the so called junction structures which were manifestations of the constraints. This power exchange portrait of a system is called **Bondgraph** (some prefer to write as **Bond graph**), which can be both power and information oriented. Later on, Bondgraph theory has been developed and consolidated further by many researchers *Karnopp, Margolis, and*

Rosenberg (1990), *Thoma (1990), Cellier (1991), Breedveld and Dauphin-Tanguy (1992), Gawthrop and Smith (1996), Mukherjee and Karmakar (2000) Brown (2006), Borutzky (2015), Granda (1985)* who have worked on extending this modeling technique to power hydraulics, mechanics, mechatronics, general thermodynamic systems and recently to electronics and non-energetic systems like economics and queuing theory.

Through Bondgraph approach, a physical system can be represented by symbols and lines, identifying the power flow paths. The lumped parameter elements of resistance, capacitance and inertance are interconnected in an energy conserving way by bonds and junctions resulting in a network structure. From the pictorial representation of the bondgraph, the derivation of system equations is so systematic that it can be algorithmized. The whole procedure of modeling and simulation of the system may be performed by some of the existing software e.g., **ENPORT, Camp-G, SYMBOLS, 20Sim**, **Dymola** etc.
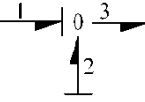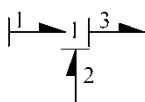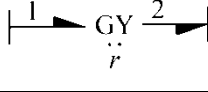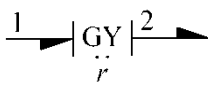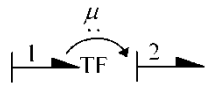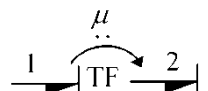
The language of bondgraphs aspires to express general class of physical systems through power interactions. The factors of power, i.e., Effort and Flow, have different interpretations in different physical domains. Yet, power can always be used as a generalized co-ordinate to model coupled systems residing in several energy domains. In bondgraphs, one needs to recognize only four groups of basic symbols, i.e., three basic one port passive elements inertance (I), capacitance (C), and resistance (R); two basic active elements source of effort (SE), and source of flow (SF); two basic two port elements gyrator (GY), and transformer (TF); and two basic junctions i.e., constant effort junction (0), and constant flow junction (1). The basic variables are effort (e), flow (f), time integral of effort (P) and the time integral of flow (Q).

212

Table A.1 gives definition of Bondgraph elements with integral causality. In a bondgraph, the assignment of power directions may be as arbitrary as fixing co-ordinate systems in classical analysis. Some of the basic concepts as presented in *Mukherjee and Karmakar (2000)* are briefed here.

A.2 Causality

Causality establishes the cause and effect relationships between the factors of power. In bondgraphs, the inputs and the outputs are characterized by the causal stroke. The causal stroke indicates the direction in which the effort signal is directed. The end of the bond that does not have a causal stroke is the end towards which the flow signal is directed. The proper causality for a storage element (I or C) is called *Integral Causality*, where the cause is integrated to generate the effect. Sometimes the causal strokes will have to be inverted, which means the constitutive relationship for the corresponding element is written as a differential equation. Genuine differential causality is not commonly encountered during system modeling except in certain cases of modeling mechanisms, robotics, etc., where link flexibilities or other aspects are neglected in the model. The occurrence of *differential causalities* in a system may indicate serious violations of principles of conservation of energy. At a 1 junction, only one bond should bring the information of flow. This uniquely causalled bond at a junction is termed as the *Strong bond*. Similarly at a 0 junction, only one bond can be stroked at the junction side. This strong bond determines the effort at the junction. The *weak bonds* are the bonds other than the strong bond.

Table A.1: Definition of Bondgraph Elements with integral causality

Type	Name	Symbol	Definition	
			Linear	**Nonlinear**
Storages	Inertance	⟶⊣ I	$e=\dfrac{dp}{dt}$ $f=(1/I)P$	$e=\dfrac{dp}{dt}$ $f=\phi_F(P)$
	Capacitance	⊢⟶ C	$e=(1/C)Q$ $f=\dfrac{dQ}{dt}$	$e=\phi_K(Q)$ $f=\dfrac{dQ}{dt}$
Dissipation	Resistance	⟶⊣R	$f=e/R$	$f=e/\phi_R$
	Resistance	⊢⟶R	$e=R*f$	$e=\phi_R*f$
Sources	Effort	SE⟶⊣	$e=e(t)$	
	Flow	SF⊢⟶	$f=f(t)$	
Junctions	Zero (0)	$\overset{1}{\longrightarrow}\,0\,\overset{3}{\longrightarrow}\,\big\vert$ $\big\vert\,2$	$e_1=e_2=e_3$ $f_1+f_2=f_3$	
	One (1)	$\overset{1}{\longrightarrow}\,1\,\overset{3}{\longrightarrow}$ 2	$f_1=f_2=f_3$ $e_1+e_2=e_3$	
Transducers (ideal)	Gyrator I	$\overset{1}{\longrightarrow}\,\text{GY}\,\overset{2}{\longrightarrow}\big\vert$ $\ddot{r}$	$e_2=r\,f_1$ $e_1=r\,f_2$	$e_2=r(x)\,f_1$ $e_1=r(x)\,f_2$
	Gyrator II	$\overset{1}{\longrightarrow}\big\vert\,\text{GY}\,\big\vert\overset{2}{\longrightarrow}$ $\ddot{r}$	$f_2=(1/r)e_1$ $f_1=(1/r)e_2$	$f_2=[1/r(x)]e_1$ $f_1=[1/r(x)]e_2$
	Transformer I	$\overset{\mu}{\overset{\cdots}{\frown}}$ $\overset{1}{\longrightarrow}\text{TF}\,\overset{2}{\longrightarrow}$	$f_2=\mu\,f_1$ $e_1=\mu e_2$	$f_2=\mu(x)\,f_1$ $e_1=\mu(x)e_2$
	Transformer II	$\overset{\mu}{\overset{\cdots}{\frown}}$ $\overset{1}{\longrightarrow}\big\vert\text{TF}\,\overset{2}{\longrightarrow}$	$e_2=(1/\mu)e_1$ $f_1=(1/\mu)f_2$	$e_2=[1/\mu(x)]e_1$ $f_1=[1/\mu(x)]f_2$
Activated Bond	Effort	$\overset{1}{\underset{e}{\longrightarrow}}\!\!\big\vert$	$f=0$	
	Flow	$\overset{1}{\underset{f}{\longrightarrow}}\!\!\big\vert$	$e=0$	
Detector	Effort, flow	$\big\vert\overset{1}{\underset{\bullet}{\longrightarrow}}$	e_1,f_1	

A.3 Activation

Some bonds in a bondgraph may be only information carriers. These bonds are not power bonds. Such bonds, where one of the factors of the power is masked are called Activated bonds. For example in a bond representing the velocity pick-up, the information of force must be masked and on the bond representing the exciter the information of the flow must be masked. A full arrow somewhere on the bonds shows that some information is allowed to pass and some information is masked. The information, which is allowed to pass may be written near that full arrow. The concept of activation is very significant to depict feedback control systems.

The term activation initially seems a misnomer. However, Paynter's idea was based on the fact that though the information of a factor of power is masked on one end, an activated bond on the other end can impart infinite power which is derived from a tank circuit used for both the measurement or actuation device (for instance, the pick-up, the amplifier and the exciter, all have external power sources).

A.4 Observers

Additional states can be added for measurement of any factor of power on a bondgraph model using the observer storage elements. A flow activated C-element would observe the time integral of flow (and consequently flow), whereas an effort activated I-element would observe the generalized momentum (and consequently effort). Activated elements are perceived as conceptual instrumentation on a model. They do not interfere in the dynamics of the system.

215

A.5   Multi and Vector Bondgraphs

When similarities in various sub-system components in the model morphology can be established, they can be represented in form of a concise notation called vector or multi bondgraphs. The dimension of the multi-bond (number of scalar bonds, it is composed of) is indicated between these parallel lines. Thus multi-bondgraphs are compact representation of large systems with identical subsystems. Since a multibond can accept only one power direction and causal orientation, all the subsystems represented by that multibond must have same power and causal structure as shown in Figure. A.1.

A.6   Fields
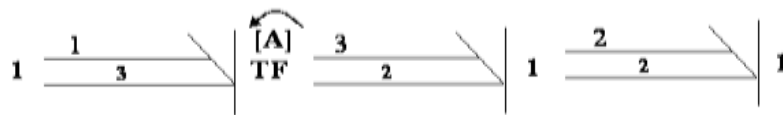
Figure A.1: Multi-bondgraph representation.

So far the external element like C, I and R were connected to a single bond like –C, -I and –R. If the parameter of the C element is any non-linear or linear function of displacement only then C element will be conservative. It will release stored energy when brought back to original state. The single port C, I and R elements may be generalized. Too start with, let us consider the multi-port generalization of element C. Whenever the efforts in a set of bonds are determined by displacement in the bonds of the same set as follows:

$$e_i = \sum_{j=1}^{n} K_{ij} Q_j \ , \ i = 1...n \tag{A.1}$$

the relation may be represented by a multi-port C element called **C Field**. Similar relationship can be established for I and R elements as well. Fields are always referred enclosed within square braces ([C], [I] and [R]).

A1.7 Description of capsule element

The dynamical system can be segmented into small groups, which is named as capsules. The description of capsule elements used in bondgraph models are presented in Table A.2.

Table A.2: Description of capsule element

Flow input ──────⟶ 1 ⊣◄──•──── SE _f1_
 	
Flow input ──────⟶ 1 ⊣◄──•──── SE _f2_
 	
SF ──────⟶ 1 ⊣──────⟶ Flow output
 	
if (_f1<_f2)
SF=f1;
else SF=f2;
	MinMax

Flow input ──────⟶ 1 ⊣◄──•──── SE _f1_
 	
Flow input ──────⟶ 1 ⊣◄──•──── SE _f2_
 	
SF ──────⟶ 1 ⊣──────⟶ Flow output
 	
if (f1>f2)
SF=f2;
else SF=f2;
	MaxMin

Formulation of Structural Damping for Infinitesimal Beam

In this formulation the vertical translation of a uniform free-free beam is considered. If the internal damping of the material is involved in the system than the strain displacement relationship or Hook's law equation can be written as *(Hagedorn, 2007)*

$$\sigma(x,t) = E\varepsilon(x,t) + \mu_I \varepsilon(x,t) \tag{B.1}$$
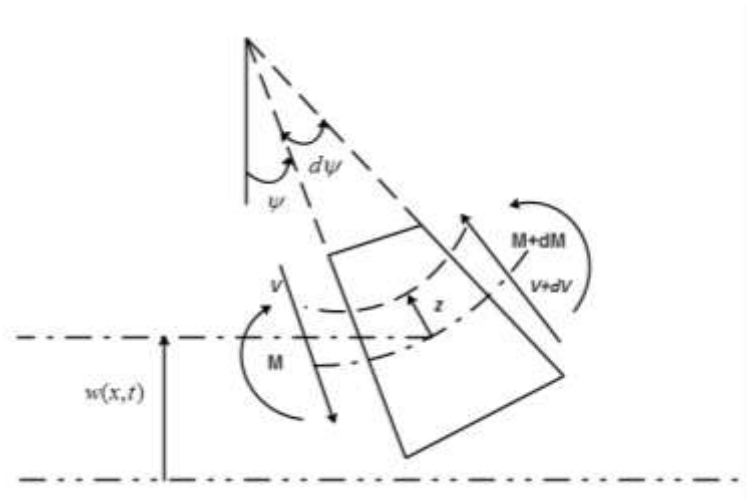
Figure B.1: Infinitesimal element of a deflected beam

The strain displacement relation at any height from the plane of the neutral fibers, which can be written as

$$\varepsilon(x,t) = \frac{zw''(x,t)}{\left[1 + w'^2(x,t)\right]^{\frac{3}{2}}} \approx -zw''(x,t) \quad \text{(Assuming } w' << 1) \tag{B.2}$$

The bending moment at any section (from Figure B.1) can be written as

$$M(x,t) = -\int_{h/2}^{-h/2} z\sigma(x,t)dA = -\big(E\varepsilon(x,t) + \mu_I\varepsilon(x,t)\big)\int_{h/2}^{-h/2} z^2 dA \qquad \text{(B.3)}$$

$$\Rightarrow \quad -\big(EIw''(x,t) + \mu_I I\dot{w}''(x,t)\big) \qquad \text{(B.4)}$$

where I is the moment of inertia cross section of beam about the neutral axis. The equation of the vertical force of an infinitesimal beam

$$(\rho A dx)\ddot{w}(x,t) = p(x,t)dx + (V+dV)\cos(\psi+d\psi) - V\cos\psi$$

or $\quad pA\ddot{w}(x,t) = p(x,t) + V' \qquad \text{(B.5)}$

The rotational dynamics of infinitesimal beam may be written as

$$((\rho I dx)\ddot{\psi} = (M+dM) - M(V+dV)\frac{dx}{2} + V\frac{dx}{2}$$

or $\quad \rho I\ddot{\psi} = M' + V \qquad \text{(B.6)}$

One may write $\psi = \dfrac{\dot{w}'(x,t)}{1+w'^2(x,t)} \approx \dot{w}'(x,t)$

Thus from the Eq (B.5) and Eq (B.6), one may have

$$\rho A\ddot{w}(x,t) - \rho I\ddot{w}''(x,t) + \mu_I I\dot{w}''''(x,t) + EIw''''(x,t) - p(x,t) = 0 \qquad \text{(B.7)}$$

Third term of Eq. (B.7) represents the structural damping or internal damping of the beam.

Appendix C
Variational Formulation for Infinitesimal Beam

This appendix gives a brief introduction to the variational formulation of dynamics of continuous systems. Consider for simplicity a one-dimensional continuous system with the field variable $w(x,t)$ which uniquely represents the configuration of the system at any time t. In the course of temporal evolution of the system, let the configurations at two time instants $t = t_1$ and $t = t_2$ be recorded as, respectively, $w(x,t_1)$ and $w(x,t_2)$. The actual path is that any infinitesimal variation over that path should leave the value of I unchanged *(Hassani, 2013)*. Now the action integral may be expressed as

$$I = \int_{t_0}^{t_1} \int_{x_0}^{x_1} \delta \mathcal{L}(...) dt dx \tag{C.1}$$

Using the extremization condition of Eq (C.1). one may obtain

$$\int_{t_0}^{t_1} \int_{x_0}^{x_1} \delta \hat{L}\left(w, w', \dot{w}, w'', t\right) dt dx = 0 \tag{C.2}$$

One may write Lagrangian density variation,

$$\delta \hat{L} = \frac{\partial \hat{L}}{\partial w} \delta w + \frac{\partial \hat{L}}{\partial \dot{w}} \delta \dot{w} + \frac{\partial \hat{L}}{\partial w'} \delta w' + \frac{\partial \hat{L}}{\partial w''} \delta w'' \tag{C.3}$$

So that, introducing eq (C.3) to eq (C.2), one may have

$$\int_{t_0}^{t_1} \int_{x_0}^{x_1} \left[\frac{\partial \hat{L}}{\partial w} \delta w + \frac{\partial \hat{L}}{\partial \dot{w}} \delta \dot{w} + \frac{\partial \hat{L}}{\partial w'} \delta w' + \frac{\partial \hat{L}}{\partial w''} \delta w'' \right] dt dx = 0 \tag{C.4}$$

The next step is to transform the integrand in Eq. (C.3) into one containing only δw, i.e one that is free of $\delta\dot{w}, \delta w', \delta w'', \delta\dot{w}'$. This can be accomplished by integration by parts, both with respect to space and time.

$$
\int_0^l \frac{\partial\hat{\mathcal{L}}}{\partial w}\delta w\Big|_{t_1}^{t_2} dx + \int_{t_0}^{t_1}\left[\frac{\partial\hat{\mathcal{L}}}{\partial w''}\delta w'' + \left\{\frac{\partial\hat{\mathcal{L}}}{\partial w'} - \frac{\partial}{\partial x}\left(\frac{\partial\hat{\mathcal{L}}}{\partial w''}\right)\right\}\delta w\right]\Big|_0^l dt +
$$

$$
\int_{t_0}^{t_1}\int_{x_0}^{x_1}\left[\frac{\partial\hat{\mathcal{L}}}{\partial w} - \frac{\partial}{\partial t}\left(\frac{\partial\hat{\mathcal{L}}}{\partial\dot{w}}\right) - \frac{\partial}{\partial x}\left(\frac{\partial\hat{\mathcal{L}}}{\partial w'}\right) + \frac{\partial^2}{\partial x^2}\left(\frac{\partial\hat{\mathcal{L}}}{\partial w''}\right) + \frac{\partial^2}{\partial x\partial t}\left(\frac{\partial\hat{\mathcal{L}}}{\partial\dot{w}'}\right)\right]\delta w\, dtdx = 0 \tag{C.5}
$$

But the vertical displacement δw is arbitrary by definition, which implies that it can be assigned values at will provide these values are compatible with the system constraint, such as geometric conditions at the end points. Letting $\delta w = \delta w' = 0$ at $x = 0$ and $x = l$. One may conclude that Eq. (C.5) can be satisfied for all values of δw in the open domain $0 < x < l$

Thus,

$$
\frac{\partial\hat{\mathcal{L}}}{\partial w} - \frac{\partial}{\partial t}\left(\frac{\partial\hat{\mathcal{L}}}{\partial\dot{w}}\right) - \frac{d}{dx}\left(\frac{\partial\hat{\mathcal{L}}}{\partial w'}\right) + \frac{\partial^2}{\partial x^2}\left(\frac{\partial\hat{\mathcal{L}}}{\partial w''}\right) + \frac{\partial^2}{\partial x\partial t}\left(\frac{\partial\hat{\mathcal{L}}}{\partial\dot{w}'}\right) = 0 \tag{C.6}
$$

Eq.(C.6) represents the *Lagrange differential equation of motion* for this continuous system and must be satisfied at every point of open domain $0 < x < l$.

$$
\frac{\partial\hat{\mathcal{L}}}{\partial w''} \equiv 0 \quad \text{or} \quad \delta w\big|_{x=0} \equiv 0 \tag{C.7a}
$$

$$
\frac{\partial\hat{\mathcal{L}}}{\partial w''}\Big|_{x=l} \equiv 0 \quad \text{or} \quad \delta w\big|_{x=l} \equiv 0 \tag{C.7b}
$$

$$
\frac{\partial\hat{\mathcal{L}}}{\partial w'} - \frac{d}{dx}\left(\frac{\partial\hat{\mathcal{L}}}{\partial w''}\right)\Big|_{x=0} = 0 \quad \text{or} \quad \delta w\big|_{x=0} \equiv 0 \tag{C.8a}
$$

$$\left. \frac{\partial \hat{L}}{\partial w'} - \frac{d}{dx}\left(\frac{\partial \hat{L}}{\partial w''} \right) \right|_{x=l} = 0 \ \text{ or } \ \left. \delta w \right|_{x=l} \equiv 0 \qquad\qquad\text{(C.8b)}$$

Eqs.(C.7-C.8) are known as the boundary conditions and only two boundary conditions must be satisfied at either end, one from condition Eq. C.7) and other from Eq.(C.8), which shows that clearly the selection is not arbitrary but it must reflect physical conditions at two ends.

Extension of Noether's Theorem

D.1 Prolongation of tangent vectors

In umbra theory, the extension of Noether's theorem may be written by using infinitesimal generators (*Olver, 2000*) of the symmetry groups, which leaves the Lagrangian invariant. The present extension is restricted to only amplitude symmetry, not involving the symmetries with dependent and independent variables. In present analysis, only amplitudes are being transformed. If the umbra-Lagrangian density admits one-parameter transformations, then the infinitesimal generators of one-parameter group of translation may be written as

$$V = s \frac{\partial}{\partial w(t,x)} + s \frac{\partial}{\partial w(\eta,x)} \tag{D.1}$$

This tangent vector is suitably prolonged (*Olver, 2000*) retaining only the relevant components of a sub-space of the jet space $J^{(3)}$; determined by the form of umbra-Lagrangian density, which may be written as

$$\begin{aligned}
pr^{(3)}V &= \xi_{w(t,x)} \frac{\partial}{\partial w(t,x)} + \xi_{\dot{w}(t,x)} \frac{\partial}{\partial \dot{w}(t,x)} + \xi_{w'(t,x)} \frac{\partial}{\partial w'(t,x)} + \xi_{\dot{w}'(t,x)} \frac{\partial}{\partial \dot{w}'(t,x)} + \\
&\xi_{w''(t,x)} \frac{\partial}{\partial w''(t,x)} + \xi_{\dot{w}''} \frac{\partial}{\partial \dot{w}''(t,x)} + \xi_{w(\eta,x)} \frac{\partial}{\partial w(\eta,x)} + \xi_{\dot{w}(\eta,x)} \frac{\partial}{\partial \dot{w}(\eta,x)} + \xi_{w'(\eta,x)} \frac{\partial}{\partial w'(\eta,x)} \\
&+\xi_{\dot{w}'(\eta,x)} \frac{\partial}{\partial \dot{w}'(\eta,x)} + \xi_{w''(\eta,x)} \frac{\partial}{\partial w''(\eta,x)} + \xi_{\dot{w}''} \frac{\partial}{\partial \dot{w}''(\eta,x)}
\end{aligned} \tag{D.2}$$

where derivatives with respect to time or umbra-time are denoted by a superscript ($\dot{}$) and derivatives with respect to space co-ordinate are denoted by ($'$). Equation (D.2)

is a 12-dimensional manifold on which this tangent vector is defined. The relations of ξ's may be written as

$$\xi_{\dot{w}(t,x)} = \frac{\partial}{\partial t}\xi_{w(t,x)} \Rightarrow \dot{\xi}_{w(t,x)}, \xi_{w'(t,x)} = \xi'_{w(t,x)}, \qquad \xi_{\dot{w}'(t,x)} = \dot{\xi}'_{w(t,x)}, \qquad \xi_{w''(t,x)} = \xi''_{w(t,x)} \qquad \text{and}$$

$\xi_{\dot{w}''(t,x)} = \dot{\xi}''_{w(t,x)}$, and relations for η variable may also be written likewise. The prolonged infinitesimal generators are composed of two parts as

$$p_r^{(3)}V = p_r^{(3)}V_\eta + p_r^{(3)}V_t \tag{D.3}$$

where $p_r^{(3)}V_\eta$ is the prolonged umbra-time component and $p_r^{(3)}V_t$ is the prolonged real-time component of the infinitesimal generators $p_r^{(3)}V$. The symmetry (invariance) condition for umbra-Lagrangian density may be expressed as

$$p_r^{(3)}V(\mathcal{L}) = 0 \tag{D.4}$$

D.2 Extended formulation of Noether's theorem for umbra-Lagrangian density

Extended formulation of Noether's theorem may be obtained by substitution of Eq. (D.3) in Eq. (D.4) and taking the limit $\eta \to t$, yields

$$\underset{\eta \to t}{Lim}\left\{ p_r^{(3)}V_\eta(\mathcal{L}) \right\} + \underset{\eta \to t}{Lim}\left\{ p_r^{(3)}V_t(\mathcal{L}) \right\} = 0 \tag{D.5}$$

The first term of the Eq. (A.5) may be given as

$$\underset{\eta \to t}{Lim}\, p_r^{(3)}V_\eta(\mathcal{L}) = \underset{\eta \to t}{Lim}\left[\begin{array}{l} \xi_{w(\eta,x)}\left(\dfrac{\partial\mathcal{L}}{\partial w(\eta,x)}\right) + \dot{\xi}_{w(\eta,x)}\left(\dfrac{\partial\mathcal{L}}{\partial\dot{w}(\eta,x)}\right) + \xi'_{w(\eta,x)}\left(\dfrac{\partial\mathcal{L}}{\partial w'(\eta,x)}\right) \\[3mm] + \dot{\xi}'_{w(\eta,x)}\left(\dfrac{\partial\mathcal{L}}{\partial\dot{w}'(\eta,x)}\right) + \xi''_{w(\eta,x)}\left(\dfrac{\partial\mathcal{L}}{\partial w''(\eta,x)}\right) + \dot{\xi}''_{w(\eta,x)}\left(\dfrac{\partial\mathcal{L}}{\partial\dot{w}''(\eta,x)}\right), \end{array} \right] \tag{D.6}$$

expanding each term with derivatives of ξ's in Eq. (D.6) yields after simplification as

$$
\underset{\eta\to t}{Lim}\, p_r^{(3)}\mathbf{V}_\eta(\mathcal{L}) = \underset{\eta\to t}{Lim}\left[
\begin{array}{l}
D_t\left\{
\begin{array}{l}
\xi_{w(\eta,x)}\left(\dfrac{\partial\mathcal{L}}{\partial\dot{w}(\eta,x)}\right) + \dfrac{\partial}{\partial x}\left(\xi_{w(\eta,x)}\left(\dfrac{\partial\mathcal{L}}{\partial\dot{w}'(\eta,x)}\right)\right) \\[3mm]
-\,\xi_{w(\eta,x)}\dfrac{\partial}{\partial x}\left(\dfrac{\partial\mathcal{L}}{\partial\dot{w}'(\eta,x)}\right)
\end{array}
\right\} \\[10mm]
+\,D_x\left\{
\begin{array}{l}
\xi_{w(\eta,x)}\left(\dfrac{\partial\mathcal{L}}{\partial w'(\eta,x)}\right) - \left(\xi_{w(\eta,x)}\dfrac{\partial}{\partial t}\left(\dfrac{\partial\mathcal{L}}{\partial\dot{w}'(\eta,x)}\right)\right) \\[3mm]
+\,\xi'_{w(\eta,x)}\left(\dfrac{\partial\mathcal{L}}{\partial w''(\eta,x)}\right) - \xi_{w(\eta,x)}\dfrac{\partial}{\partial x}\left(\dfrac{\partial\mathcal{L}}{\partial w''(\eta,x)}\right)
\end{array}
\right\}
\end{array}
\right] \qquad (D.7)
$$

where D_t and D_x are the total time and total space derivatives respectively and may be defined as

$$
D_t Z_1\!\left(t,x,w,w_x\right) = \frac{\partial Z_1}{\partial t} + \frac{\partial Z_1}{\partial w}\frac{\partial w}{\partial t} + \frac{\partial Z_2}{\partial w_x}\frac{\partial w_x}{\partial t}
$$

and $\quad D_x Z_2\!\left(t,x,w,w_x,w_{x^2}\right) = \dfrac{\partial Z_2}{\partial x} + \dfrac{\partial Z_2}{\partial w}\dfrac{\partial w}{\partial x} + \dfrac{\partial Z_2}{\partial w_x}\dfrac{\partial w_x}{\partial t} + \dfrac{\partial Z_2}{\partial w_{x^2}}\dfrac{\partial w_{x^2}}{\partial t}$

and $\quad Z_1$ and Z_2 may be given as

$$
Z_1 = \underset{\eta\to t}{Lim}\left[\xi_{w(\eta,x)}\left(\frac{\partial\mathcal{L}}{\partial\dot{w}(\eta,x)}\right) + \frac{\partial}{\partial x}\left(\xi_{w(\eta,x)}\left(\frac{\partial\mathcal{L}}{\partial\dot{w}'(\eta,x)}\right)\right) - \xi_{w(\eta,x)}\frac{\partial}{\partial x}\left(\frac{\partial\mathcal{L}}{\partial\dot{w}'(\eta,x)}\right)\right]
$$

$$
Z_2 = \underset{\eta\to t}{Lim}\left[
\begin{array}{l}
\xi_{w(\eta,x)}\left(\dfrac{\partial\mathcal{L}}{\partial w'(\eta,x)}\right) - \xi_{w(\eta,x)}\dfrac{\partial}{\partial t}\left(\dfrac{\partial\mathcal{L}}{\partial\dot{w}'(\eta,x)}\right) \\[3mm]
+\,\xi'_{w(\eta,x)}\left(\dfrac{\partial\mathcal{L}}{\partial w''(\eta,x)}\right) - \xi_{w(\eta,x)}\dfrac{\partial}{\partial x}\left(\dfrac{\partial\mathcal{L}}{\partial w''(\eta,x)}\right)
\end{array}
\right]
$$

Thus, one may re-write Eq. (D.5) as

$$
\underset{\eta\to t}{Lim}\, p_r^{(3)}\mathbf{V}_\eta\left(\mathcal{L}\right) = D_t Z_1 + D_x Z_2 \qquad (D.8)
$$

Substitution of Eq. (D.8) in Eq. (D.5) finally results in extended Noether's theorem for fields, which may be expressed as

$$D_t Z_1 + D_x Z_2 + \underset{\eta \to t}{Lim}\, p_r^{(3)} V_t \left(\mathcal{L} \right) = 0 \tag{D.9}$$

Eq.(D.9) is called as extended Noether's field equation for the umbra-Lagrangian. The first term is time derivative, second term is the space derivative or called as Noether currents (*Rastogi*, 2005), which mainly depends on the boundary conditions of fields, and the third term is an additional term called as modulatory convection term.

Basic Concept of umbra-Hamiltonian

Mathematically, the umbra-Hamiltonian (*Mukherjee, 1994; Mukherjee, 2001*) may be represented as

$$H^*\big[\boldsymbol{q}(\eta),\boldsymbol{p}(\eta),\boldsymbol{q}(t),\dot{\boldsymbol{q}}(t),t\big]=\dot{\boldsymbol{q}}(\eta)\boldsymbol{p}(\eta)-L^*\big[\boldsymbol{q}(\eta),\dot{\boldsymbol{q}}(\eta),\boldsymbol{q}(t),\dot{\boldsymbol{q}}(t),t\big]$$ (E.1)

where the umbra-momentum is $p(\eta)=\dfrac{\partial L^*}{\partial \dot{q}(\eta)}$.

The real momentum may be obtained as

$$p(t)=\underset{\eta\to t}{Lim}\frac{\partial L^*}{\partial \dot{q}(\eta)}$$

Taking total differential of Eq. (E.1), one obtains

$$dH^*=\frac{\partial H^*}{\partial p(\eta)}dp(\eta)+\frac{\partial H^*}{\partial q(\eta)}dq(\eta)+\frac{\partial H^*}{\partial q(t)}dq(t)+\frac{\partial H^*}{\partial \dot{q}(t)}d\dot{q}(t)+\frac{\partial H^*}{\partial t}dt\ ,$$

$$=\dot{q}(\eta)dp(\eta)-\frac{\partial L^*}{\partial q(\eta)}dq(\eta)-\frac{\partial L^*}{\partial q(t)}dq(t)-\frac{\partial L^*}{\partial \dot{q}(t)}d\dot{q}(t)-\frac{\partial L^*}{\partial t}dt+\left(p(\eta)-\frac{\partial L^*}{\partial \dot{q}(\eta)}\right)d\dot{q}(\eta)$$

The relations which may be derived, are

$$\dot{q}(\eta)=\frac{\partial H^*}{\partial p(\eta)}$$ (E.2)

$$\frac{\partial H^*}{\partial q(\eta)}=-\frac{\partial L^*}{\partial q(\eta)}\Rightarrow \underset{\eta\to t}{Lim}\frac{\partial H^*}{\partial q(\eta)}=-\dot{p}(t)$$ (E.3)

and the other relations obtained are

$$\frac{\partial H^*}{\partial q(t)}=-\frac{\partial L^*}{\partial q(t)}$$

$$\frac{\partial H^*}{\partial t} = -\frac{\partial L^*}{\partial t}$$

The umbra-Hamiltonian H^* is composed of two components as H_i^* and H_e^*. H_i^* is the interior Hamiltonian, which does not depend on any function of real displacement, real velocity and real time, and H_e^* is the rest of the umbra-Hamiltonian, called the exterior Hamiltonian. Thus, one may write

$$H^* = H_i^* \{q(\eta), p(\eta)\} + H_e^* \{q(\eta), p(\eta), q(t), \dot{q}(t), t\}. \tag{E.4}$$

The theorems of the umbra-Hamiltonian (*Mukherjee, 1994; Mukherjee, 2001*) are now presented.

Theorem 1

$$\underset{\eta \to t}{Lim} \left[\frac{dH^*}{d\eta} \right] = 0 \tag{E.5}$$

Proof

$$\frac{dH^*}{d\eta} = \frac{\partial H}{\partial p(\eta)} \dot{p}(\eta) + \frac{\partial H^*}{\partial q(\eta)} \dot{q}(\eta) = \dot{q}(\eta) \dot{p}(\eta) + \frac{\partial H^*}{\partial q(\eta)} \dot{q}(\eta) \tag{E.6}$$

Now taking the limit $\eta \to t$, one obtains

$$\underset{\eta \to t}{Lim} \left[\frac{dH^*}{d\eta} \right] = \underset{\eta \to t}{Lim} \left(\dot{q}(\eta) \dot{p}(\eta) \right) + \underset{\eta \to t}{Lim} \left(\frac{\partial H^*}{\partial q(\eta)} \dot{q}(\eta) \right) \tag{E.7}$$

$$= \dot{q}(t) \dot{p}(t) + \left(\underset{\eta \to t}{Lim} \frac{\partial H^*}{\partial q(\eta)} \right) \underset{\eta \to t}{Lim} \dot{q}(\eta).$$

Substitution of Eq. (E.3) gives

$$\underset{\eta \to t}{Lim}\left[\frac{dH^*}{d\eta}\right] = \dot{q}(t)\,\dot{p}(t) - \dot{p}(t)\,\dot{q}(t) = 0 \tag{E.8}$$

Theorem 2

$$\frac{dH_i^*}{dt} = -\underset{\eta \to t}{Lim}\left[\frac{dH_e^*}{d\eta}\right] \tag{E.9}$$

Proof

From theorem 1 and Eq. (E.4), one may write

$$\underset{\eta \to t}{Lim}\frac{dH_i^*\big(q(\eta), p(\eta)\big)}{d\eta} = -\underset{\eta \to t}{Lim}\left(\frac{dH_e^*}{d\eta}\right), \text{ or}$$

$$\frac{dH_i^*\big(q(t), p(t)\big)}{dt} = -\underset{\eta \to t}{Lim}\left(\frac{dH_e^*}{d\eta}\right) \tag{E.10}$$

Corollary

If, for a system, $\underset{\eta \to t}{Lim}\left[\dfrac{dH_e^*}{d\eta}\right] = 0$, then $H_i^*\big(q(t), p(t)\big)$ is a constant of motion.

Proof

It follows directly from theorem 2 that

$$\frac{dH_i^*\big(q(t), p(t)\big)}{dt} = 0 \tag{E.11}$$

Hence, $H_i^*\big(q(t), p(t)\big)$ is a constant of motion.

Integrated Controller Design for Hybrid H∞ Controllers

In Figure 4.11, block K represents the controller, an LTI model defined by a finite dimensional state space model

$$\dot{x}_K = A_K x_K + B_K y \tag{F.1}$$

$$u = C_K x_K + D_K y \tag{F.2}$$

where the coefficients A_K, B_K, C_K, D_K are to be designed. On combining the system with the controller, the block diagram in Figure. 4.11 defines a valid closed loop state space model

$$\dot{x}_{CL} = A_{CL} x_{CL} + B_{CL} w \tag{F.3}$$

$$z = C_{CL} x_{CL} + D_{CL} w \tag{F.4}$$

where

$$x_{CL} = \begin{pmatrix} x \\ x_K \end{pmatrix};$$

$$A_{CL} = \begin{pmatrix} A + B_2 D_K C_2 & B_2 C_K \\ B_K C_2 & A_K \end{pmatrix}$$

$$B_{CL} = \begin{pmatrix} B_1 + B_2 D_K D_{21} \\ D_K D_{21} \end{pmatrix}$$

$$C_{CL} = (C_1 + D_{12} D_K C_2 \quad D_{12} C_K)$$

$$D_{CL} = (D_{11} + D_{12} D_K D_{21})$$

Now for designing the coefficients of controller K, we take the closed-loop transfer function from w to z which is given by the linear fractional transformation (LFT) is (*Doyle*, 1989)

$$z = F_l(G, K)w \tag{F.5}$$

Now, the standard H∞ optimal control problem is to find all stabilizing controllers K which minimize

$$\|F_l(G, K)\|_\infty = \sup_w \bar{\sigma}(F_l(P, K)(jw)) \tag{F.6}$$

In practice, it is usually not obligatory to obtain an optimal controller for the H∞ problem, and it is often computationally (and theoretically) simpler to design a suboptimal one (i.e. one close to the optimal ones in the sense of the H∞ norm). Let min be the minimum value of $\|F_l(G, K)\|_\infty$ over all stabilizing controllers K. Then the H∞ sub-optimal control problem is: given $\gamma > \gamma_{min}$, find all stabilizing controllers K such that

$$\|F_l(G, K)\|_\infty < \gamma \tag{F.7}$$

This can be solved efficiently using the solutions of the Ricatti equations, and by reducing γ iteratively using bisection algorithm (*Doyle*, 1989), an optimal solution is approached. The algorithm is summarized below with all the simplifying assumptions.

F.1 Design of central controller

Before applying the H∞ algorithm the following assumptions are to be followed:

1. D_{12} and D_{21} have full rank,

2. $\begin{pmatrix} A - jwI & B_2 \\ C_1 & D_{12} \end{pmatrix}$ has full column rank for all w,

3. $\begin{pmatrix} A - jwI & B_1 \\ C_2 & D_{21} \end{pmatrix}$ has full row rank for all w,

4. (A, B_1) is stabilizable and (A, C_1) is detectable.

For the general control configuration of Figure 4.11 described by Eqs. (F.1-F.4), with assumptions, there exists a stabilizing controller K such that $\|F_l(G,K)\|_\infty < \gamma$ if and only if (*Ohsaku*,1999)

i. $X_\infty \geq 0$ is a solution to the algebraic Riccati equation

$$A^T X_\infty + X_\infty A + C_1^T C_1 + X_\infty (\gamma^{-2} B_1 B_1^T - B_2 B_2^T) X_\infty = 0$$

such that $\operatorname{Re} \lambda_i [A + (\gamma^{-2} B_1 B_1^T - B_2 B_2^T) X_\infty] < 0, \forall i$; and

ii. $Y_\infty \geq 0$ is a solution to the algebraic Riccati equation

$$AY_\infty + Y_\infty A^T + B_1 B_1^T + Y_\infty (\gamma^{-2} C_1^T C_1 - C_2^T C_2) Y_\infty = 0$$

such that $\operatorname{Re} \lambda_i [A + Y_\infty (\gamma^{-2} C_1^T C_1 - C_2^T C_2)] < 0, \forall i$; and

iii. $\rho(X_\infty Y_\infty) < \gamma^2$.[where $\rho(.)$ is spectral radius]

All such controllers are then given by $K = F_l(K_c, Q)$

where

$$K_c = \begin{bmatrix} A_\infty & -Z_\infty L_\infty & Z_\infty B_2 \\ F_\infty & 0 & I \\ -C_2 & I & 0 \end{bmatrix} \tag{F.8}$$

$$F_\infty = -B_2^T X_\infty, \quad L_\infty = -Y_\infty C_2^T, \quad Z_\infty = (I - \gamma^{-2} Y_\infty X_\infty)^{-1} \tag{F.9}$$

$$A_\infty = A + \gamma^{-2} B_1 B_1^T X_\infty + B_2 F_\infty + Z_\infty L_\infty C_2 \tag{F.10}$$

and Q(s) is any stable proper transfer function such that $\|Q\|_\infty < \gamma$. For Q(s) = 0, we get

$$K = K_{C_{11}} = -Z_\infty L_\infty (sI - A_\infty)^{-1} F_\infty \tag{F.11}$$

This is called the "central" controller and has the same number of states as the generalized plant G.

References

Ataei, M., Asadi, E., Goodarzi, A., Khajepour, A., Khamesee, M. B. (2017). Multi-objective optimization of a hybrid electromagnetic suspension system for ride comfort, road holding and regenerated power. *Journal of Vibration and Control*, 23(5), 782–793.

Amin, M. H. I. M., Hudha, K., Kadir, Z. A., Amer, N. H. (2015). Skyhook control for 7 DOF ride model of armored vehicle due to road disturbance. Paper presented in ASCC, 10th Asian *IEEE*.

Agostinacchio, M., Ciampa D., Olita, S. (2014) .The vibrations induced by surface irregularities in road pavements – a Matlab$^{®}$ approach. *European Transport Research Review*, 6(3), 267–275.

Alanoly, J., Sankar, S. (1988). Semi-active force generators for shock isolation. *Journal of Sound and Vibration,* 126 (1), 145-156.

Alanoly, J., Sankar, S. (1987). A new concept in semi-active vibration isolation. *Journal of Mechanisms, Transmission, and Automation in Design* (ASME), 109(2), 242-247.

Borutzky, W. (2015). Bondgraph model-based fault diagnosis of hybrid systems. *Springer International Publishing*.

Bakar, S.A.A., Samin, P.M., Jamaluddin, H., Rahman, R.A., Sulaiman, S. (2015). Semi active suspension system performance under random road profile excitations. *International Conference on Computer, Communication, and Control technology*, April 21-23, Sarawak, Malaysia.

Brown, F. T. (2006). Engineering system dynamics. *Marcel Dekker*, New York.

British standards Institution BS 6841-1987. Measurement and evaluation of human exposure to whole body mechanical vibration and repeated shock.

Blanchard, E. D. (2003). On the control aspects of semi-active suspensions for automobile applications. *M. S. Thesis*, Dept. of Mechanical Engineering, Virginia Polytechnic Institute and State University, Virginia.

Boileau, P. E., Rakheja, S. (1998). Whole body vertical biodynamic response characteristics of the seated vehicle driver. *Measurement and model development International Journal of Industrial Ergonomics* 22(6), 449-472.

Boileau, P.É., Wu, X., Rakheja, S. (1998). Definition of a range of idealized values to characterize seated body biodynamic response under vertical vibration. *Journal of Sound and Vibration*, 215(4), 841-862.

Bessinger, F. H., Cebon, D., Cole, D. J. (1995). Force control of a semi-active damper. *Journal of Vehicle System Dynamics*. 24(9), 695–723.

Breedveld, P. C. and Dauphin-Tanguy, G. (1992). Bondgraphs for engineers. North-Holland, Amsterdam.

Bahar, L.Y., Kwatny H.G. (1987). Extension of Noether's theorem to constrained non-conservative dynamical systems. *International journal of non-linear mechanics*, 22(2), 125-138.

Cai-hong, H., Jing, Z. (2010). Flexural vibration suppression of car body for high-speed passenger car based on constrained damping layers. *Journal of Traffic and Transportation Engineering*, 36-42

Cao, C. (2005). Approaches to reduce truck beaming. *Society of Automotive Engineers*, SAE Paper 2005-01-0829.

Carlbom, P. (2001) "Combining MBS with FEM for rail vehicle dynamics analysis" *Multi-body System Dynamics*, 6(3), 291-300.

Carlbom, P. (2000). Carbody in rail vehicle dynamics. *Ph.D Thesis*, Stockholm.

Carlbom, P. (2000). Carbody and passengers in rail vehicle dynamics" *Ph.D Thesis*, Royal Institute of Technology, Sweden.

Chrstos, J.P., Heydinger, G.J. (1997). Evaluation of VDANL and VDM 13Road for predicting the vehicle dynamics of a 1994 Ford tauru. *Society of Automotive Engineers*, SAE 970566.

Cellier, F.E (1991), Continuous system modeling, *Springer-Verlag*, New York.

Corbridge, C., Griffin, M. J. (1986). Vibration and comfort: Vertical and lateral motion in the range 0.5 to 5.0 Hz. *Ergonomics,* 29(2), 249-272.

Dumitriu M., Craciun, C., (2017), Modelling of structural flexibility of the railway vehicles car body, *MATEC Web of Conferences*, 112, 07007.

Dash, D. K. (2015). Over 11,000 people killed by potholes, speed breakers last year, *The Times of India Report*, (*http://timesofindia.indiatimes.com/india/Over-11000-people-killed-by-potholes-speed-breakers-last-year/articleshow/48950267.cms*).

Deprez, K., Moshoub, D., Anthonis, J., Baerdemaeker, J. De. Ramon, H. (2005). Improvement of vibrational comfort on agricultural vehicles by passive and semi-active cabin suspensions. *Computers and Electronics in Agriculture*, 49(2), 431–440.

Diana, G., Cheli, F.,Collina, A., Corradi, R., and Melzi. S., (2002). The development of a numerical model for railway vehicles comfort assessment through comparison with experimental measurements. *Vehicle System Dynamics*, 38(3), 165–183.

Diana, G., Cheli, F., Andrea, C., Corradi, R., Melzi, S. (2002). The development of a numerical model for railway vehicles comfort assessment through comparison with experimental measurements. *Vehicle. System .Dynamics,* 38(3), 165–183.

Demicd, M., Lukicd, J. (2002). Some aspects of the investigation of random vibration influence on ride comfort. *Journal of Sound and vibration,* 253(1), 109-129.

Doyle J.C., Glover K., Khargonekar P.P., Francis B.A. (1989). State space solutions to standard H2 and H∞ control problems. *IEEE Transactions on Automatic Control,* 34(8), 831–847.

Demicd, M., (1986). Physiological attitude towards influence of quasi random and repeated vertical shock vibration on human fatigue, *the Proceedings of the Second International Conference on the Combined Effects of Environments Factors* (ICCEF186), Kanazawa.

Djukic D., Vujanovic, B. (1977). Noether theory in classical mechanics. *American journal of physics*, 45, 336.

Djukic, D. (1973). A procedure for finding first integrals of mechanical systems with Gauge-variant Lagrangians. *International Journal of Non-Linear Mechanics*, 8 (5), 479-488.

Espinoza, A. A. O., Ortega, A. M. C., Martinez, J. C. T., Alcantara, D. H., Menendez, R. M. (2014). Analysis of On/Off controllers of a semi-active suspension in a CAN. *19th IFAC World Congress*, Cape Town, South Africa. Aug 24-29, 2014, 10902-10907.

Els P.S, Uys P.E, Snyman J.A, Thoresson M.J. (2006). Gradient-based approximation methods applied to the optimal design of vehicle suspension systems using computational models with severe inherent noise. *Mathematical and Computer Modelling*, 43(7-8), 787–801.

Els P.S. (2005). The applicability of ride comfort standards for off-road vehicles. *Journal of Terramechanics*, 42 (1), 47–64.

Els P.S, Uys P.E. (2003), Investigation of the applicability of the Dynamic-Q optimisation algorithm to vehicle suspension design. *Mathematical and Computer Modelling*, 37(9-10), 1029–1046.

Elbeheiry, E.M, Karnoop, D.C (1996). Optimal control of random vibration with constrained suspension deflection. *Journal of Sound and Vibration*, 189(5), 547-64.

Filippini, G., Nigro., N., Junco, S. (2010). Vehicle dynamics simulation using bondgraphs. *FCEIA*, Universidad Nacional de Rosario (UNR), Argentina.

Fischer, D., M. Börner, J Schmitt, Isermann, R. (2007). Fault detection for lateral and vertical vehicle dynamics. *Control Engineering Practice* 15 (3), 315–24.

Fairley, T. E., Griffin, M. J., (1989). The apparent mass of the seated human body: vertical vibration, *Journal of Biomechanics*, 22(2), 81-94.

Fairley, T. E., and Griffin, M. J., (1988). Predicting the discomfort caused by simultaneous vertical and fore-and-aft whole-body vibration. *Journal of Sound and vibration*, 124(1), 141-156.

Frolov, K. A. (1981). Vibration in Technics. Masinostroenie, Moscow.

Gupta, A., Rastogi, V. (2018). Computational modelling and simulation of commercial truck with road-tire interactions to evaluate ride comfort. *International Journal of Heavy Vehicle system,* 25(2), 133 – 150.

Gupta, A., Rastogi, V., (2016). Effects of various road conditions on dynamic behavior of heavy road vehicle. *Procedia Engineering*, 144, 1129–1137.

Gupta, A., Rastogi, V. (2016). Dynamic analysis and control of a full car vehicle model through bondgraphs, *International Journal of Control Theory and Applications*, 9(17), 8745-8753.

Granlund, J. (2012). Vehicle and human vibration due to road condition. *ROADEX IV* Project, EU Northern Periphery Programme.

Guglielmino, E., Sireteanu, T., Stammers, C. W., Ghita, G., Giuclea, M., (2008). Semi-active suspension control- improved vehicle ride and road friendliness. Springer-Verlag London Limited.

Goncalves, F. D., (2001). Dynamic analysis of semi-active control techniques for vehicles application, *M. S. Thesis*, Dept. of Mechanical Engineering, Virginia Polytechnic Institute and State University, Virginia.

Gawthrop, P., Smith, L. (1996), Meta modeling: bondgraphs and dynamic systems. Prentice-Hall.

Griffin, M. J., (1990). Handbook of human vibration. London: Academic Press.

Granda, J.J. (1985). Computer generation of physical system differential equations using bondgraphs. *Journal of the Franklin Institute*, 319(1–2), 243-255.

Hailong, Z., Enrong, W., Fuhong, M., Rakheja, S., Chunyi, S., (2013). Skyhook-based semi-active control of full-vehicle suspension with magneto-rheological dampers. *Chinese Journal of Mechanical Engineering*, 26(3), 498-505.

Hassani, S., (2013). Mathematical physics: A modern introduction to its foundations. *Springer international.*

Ho, C., Lang, Z.Q., Sapinski, B., and Billings, SA. (2013). Vibration isolation using nonlinear damping implemented by a feedback-controlled MR damper. *Smart Material Structures,* 22(10), 105010.

Huang Cai-hong, Zeng J. (2010). Flexural vibration suppression of car body for high-speed passenger car based on constrained damping layers*, Journal of Traffic and Transportation Engineering*. 2010 (1), 36-42.

Hagedorn, Gupta, A.D., (2007). Vibrations and waves in continuous mechanical systems. John Wiley.

Hohl GH, (1984). Ride comfort of off-road vehicle. In proceedings of the 8th international conference of the ISTVS, vol I of III Cambridge, England, August 5-11.

Ibrahim, I.M. (1995). Effect of frame flexibility on the ride vibration of heavy truck. *Journal of Computers and Structures* 58(4), 709-713.

Kashem, S. B. A., Ektesabi, M., Nagarajah, R. (2015). Comparison between different sets of suspension parameters and introduction of new modified skyhook control strategy incorporating varying road condition. *Vehicle System Dynamics*, 50(7), 1173-1190.

Kong, Y. S., Omar, M. Z., Chua, L. B., Abdullah, S., (2014). Ride quality assessment of bus suspension system through modal frequency response approach. *Advance Mechanical Engineering*, 269721, 17.

Ke, C., Jie, G., (2010), Simulation of vehicle ride comfort based on VPG. Proc. - 3rd Int. Conf. Intell. Networks Intell. Syst. ICINIS 2010, 323–326.

Kiencke, U. and Dai, A. (2007). Observation of lateral vehicle dynamics. *Control Eng. Practice.* 5(8), 1145-1150.

Kargarnovin, M.H., Younesian, D., Thompson, D., Jones, C., (2005), Ride comfort of high-speed trains travelling over railway bridges. *Vehicle System Dynamics*, 43(3), 173-197.

Kim, J.H., Yim, H.J. (1994). Influence of chassis flexibility on dynamic behavior of engine mount systems. SAE Paper, 942269.

Karnopp, D.C, Margolis, D.L, Rosenberg, R.C (1990). System dynamics: A unified Approach. *Wiley publications*.

Karnopp, D. C., (1990). Design principles for vibration control systems using semi-active dampers. *Journal of Dynamic Systems, Measurement, and Control,* 112,448-455.

Karnopp, D. C., Crosby, M. J., Harwood, R. A., (1974). Vibration control using semi-active force generators. *Journal of Engineering for Industry*, 96 (2), 619-626.

Liang C. Chung, Chaiang Chi-Feng (2006). A study on biodynamic models of seated human subjects exposed to vertical vibration. *International Journal of Industrial Ergonomics*, 36(10), 869-890.

Liu, Y., Waters, T. P., Brennan, M. J., (2005). A comparison of semi-active damping control strategies for vibration isolation of harmonic disturbances. *Journal of Sound and Vibration* 280(1-2), 21-39.

Lin, L. and Corina, S. (2005). On the impact of cargo weight, vehicle parameters, and terrain characteristics on the prediction of traction for off-road vehicles. *Journal of Terramechanics* 44(3), 221–238.

Lin, Y., Xin, L., Yang, C., Zou, Z. (2001). Study on dynamic response of train excited by the irregularity of track on the high speed railway bridge. *Journal of vibration and shock*, 3, 47–49.

Lewis, C. H., Griffin M. J. (1996). The transmission of vibration to the occupants of a car seat with a suspended back-rest. *Journal of Automobile Engineering,* 210(3), 199-207.

Lozia, Z. (1991). Analysis of vehicle behaviour during lane change manoeuvre on an uneven road surface. *Vehicle system dynamics*, 20(sup-1), 417-431.

Leatherwood, J. D., Dempsey, T. K., Clevenson, S. A. (1980). A design tool for estimating passenger ride discomfort within complex ride environments. *Human Factors*, 22, 291-312.

Mohajer, N., Abdi, H., Nelson, K., Nahavandi, S. (2017). On the simulation-based objective estimation of road vehicle ride comfort. Mechatronic (ICM) International conference, IEEE, 978-1-5090-4538-9/17, 159-165.

Mitra, A., Patil, M., Banerjee, N. (2014). Optimization of vehicle suspension parameters for ride comfort based on RSM. *Journal of the Institution of Engineers (India): Series C*, 96 (2), 165-173.

Mukherjee, A., Rastogi, V., Das Gupta, A., (2011). Revisiting umbra Lagrangian Hamiltonian mechanics: Its variational foundation and extension of Noether's theorem and Poincare-cartan integral. *International Journal of Non linear mechanics*, 46(5), 745-757.

Mukherjee, A., Rastogi, V., Das Gupta, A., (2009). Extension of Lagrangian-Hamiltonian mechanics for continuous systems: Investigation of dynamics of a one-dimensional internally damped rotor driven through a dissipative coupling. *Non-linear Dynamics*, Springer, 58 (1), 107-127.

Mukherjee, A., Rastogi, V., Das Gupta, A., (2007). A study of a bi-symmetric electro-mechanical system through umbra Lagrangian generated by bondgraphs, *Simulation*, 83(9), 611-630.

Mukherjee, A., Rastogi, V., Dasgupta, A., (2006). Invariants of motion for asymmetric systems with gauge-transformed umbra-Lagrangian generated by bondgraph. *Simulation,* 82(4), 207-226.

Mukherjee A., Samantaray A.K. (2006). SYMBOLS- Shakti user's manual. High-tech consultants, STEP, Indian Institute of technology, Kharagpur, India.

Mukherjee, A., Rastogi, V. and Dasgupta, A. (2005). A procedure for finding invariants of motions for general class of unsymmetric systems with gauge-variant umbra-lagrangian generated by bondgraphs. *International Conference on Bondgraph Modeling and Simulation* (ICBGM), 2005, 11-16.

Marzaband, J., Goodarz, A., Zohoor, H., Hojjat, Y. (2004). Stochastic optimal preview control of a vehicle suspension. *Journal of Sound and vibration*, 275(3-5), 973-990.

Margolis, D., Shim, T. (2001). A bondgraph model incorporating sensors, actuators, and vehicle dynamics for developing controllers for vehicle safety. *Journal of the Franklin Institute,* 338 (1), 21-34.

Ma, X.Q., Wang, E.R., Rakheja, S., and Su, C.Y., (2002). Modeling hysteretic characteristics of MR fluid damper and model validation. *Proceedings of the 41st IEEE Conference on Decision and Control*, Las Vegas, NV, December 2002.

Mukherjee, A. (2001). The issue of invariants of motion for general class of symmetric systems through bondgraph and umbra-Lagrangian. *Proc. of Int. Conf. of Bondgraph Modelling and Simulation ICBGM'01*, 33(1), 295-304.

Montgomery, D. C. (2001). Design and analysis of experiments. New York: John Wiley.

Mastinu, G., Gobbi, M. (2001). Analytical description and optimization of the dynamic behaviour of passively suspended road vehicles. *Journal of sound and vibration*, 245(3), 457-48.

Mukherjee, A., Karmakar, R. (2000). Modelling and simulation of engineering system through bondgraph. *Narosa publishing House*, New Delhi.

Mukherjee, A., Karmakar, R., Samantaray, A. K. (1999). Modelling of basic induction motors and source loading in rotor-motor system with regenerative force field. *Simulation Practice of Theory*, 7(5-6), 563-576.

Mansfield, N. J., Lunstrog, R. M, (1999). Models of apparent mass of the seated human body exposed to horizontal whole body vibration. *Aviation, Space and Environmental Medicine* 70(12), 1162-1172.

Mukherjee, A., Samantaray, A.K. (1997). Umbra-Lagrange's equations through bondgraphs. *Proceedings of International Conference on Bondgraph Modeling and Simulation* (ICBGM), Phoenix, Arizona, USA, 168-174.

Mechanical vibration and shock- evaluation of human exposure to whole body vibration (1997), part-I: general requirement ISO 2631-1. *The international organization for standardization*, 15.

Mukherjee, A. (1994). Junction structures of bondgraph theory from analytical mechanics viewpoint. *Proc. of CISS-1st Conference of International Simulation Societies*. Zurich, Switzerland, 661-666.

Margolis, D., Edeal, D. (1990). Towards an understanding of beaming in large trucks. *Journal of commercial vehicles*, 99(2), 952-959.

Margolis, D., Edeal, D. (1989), Modelling and control of large flexible frame vehicles using bondgraphs. *Journal of commercial vehicles*, 98(2), 605-611.

Michelberger, P., Keresztes, A.,Boker, J., and Varlaki, P. (1984), Dynamic modelling of commercial road vehicle structures from test data. *Society of Automotive Engineers*, SAE Paper 845120.

Mierovitch, L. (1980). Computational methods in structural dynamics. *Springer Science & Business Media*.

Miwa, T., (1967). Evaluation methods for vibration effects Part I: measurements of the solid and equal sensation contours of whole body vibration for vertical and fore and aft vibrations. *Industrial Health*, 5, 183-205.

Nguyen, Q. H., Choi, S. B. (2009). Optimal design of MR shock absorber and application to vehicle suspension. *Smart Materials Structure*, 18(3), 035012.

Nishiyama, S., Uesugi, N. (2000). Research on vibration characteristics between human body and seat, steering wheel, and pedals (Effects of seat position on ride comfort). *Journal of Sound and vibration*, 236(1), 1-21.

Olver, PJ. (2000). Applications of lie groups to differential equations" *Springer international*.

Oborne, D. J., Heath, T. O., Boarer, P. (1981). Human response to whole body vibration. *Ergonomics,* 34(1), 127-160.

Paddan, G. S., Griffin, M. J., (1994). Transmission of roll and pitch seat vibration to the head. *Ergonomics*, 37(9), 1513-1531.

Parsons, K. C., Griffin, M. J., (1988). Whole-body vibration perception thresholds. *Journal of Sound and vibration.* 121(2), 237-258.

Patil, M. K, Palanichamy, M.S., Ghista, D.N., (1977). Dynamic response of human body seated on a tractor and effectiveness of suspension systems. SAE 770932, 755-792.

Paynter, H. M. (1960). Analysis and design of engineering systems. *M. I. T. Press*, Cambridge.

Raj R., A., Shrivastava, S., Trikhande, M. W., (2015). Modelling and analysis of skyhook and fuzzy logic controls in semi-active Suspension System. *International Conference on Industrial Instrumentation and Control* (ICIC), College of Engineering Pune, India.

Reza-Kashyzadeh, Kazem, Mohammad Jafar Ostad-Ahmad-Ghorabi, Alireza Arghavan (2014). Investigating the Effect of road roughness on automotive component. *Engineering Failure Analysis*, 41, 96–107.

Rideout, D.G. (2012). Simulating coupled longitudinal, pitch and bounce dynamics of trucks with flexible frames. *Modern Mechanical Engineering*, 2(4), 176-189.

Road Accidents in India 2013, Government of India, Ministry of Road Transport and Highways, Transport Research Wing, New Delhi, August 2014.

Road Accidents in India 2012, Government of India, Ministry of Road Transport and Highways, Transport Research Wing, New Delhi, June 2013.

Rideout, D., Khan, M. T., (2010). Flexible truck modeling and investigation of coupling between rigid and flexible dynamics. *Proceeding of ICBGM*, Orlando.

Rastogi, V. (2005). Extension of Lagrangian-Hamiltonian mechanics, study of symmetries and invariants. *Ph.D thesis*, IIT Kharagpur, India.

Strecker, Z., Mazůrek, I., Roupec, J., Klapka, M., (2015). Influence of MR damper response time on semi-active suspension control efficiency, *Meccanica*, 50(8), 1949-1959.

Strydom, A., Els, P.S., (2014). The applicability of hybrid control to a small off-Road vehicle without a differential, *Proceedings of ASME*, International Design Engineering Technical Conferences & Computers and Information in Engineering Conference (IDETC/CIE), August 17-20, 2014, Buffalo, New York.

Stine, J.S., Bridget, C. H, Sean N. B, Eric, T.D. (2010). Analysing the influence of median cross-section design on highway safety using vehicle dynamics simulations. *Accident Analysis and Prevention*, 42 (6), 1769-1777.

Shamsi, A., Choupani, N., (2008). Continuous and discontinuous shock absorber control through skyhook strategy in semi-active suspension system (4-DOF model), *International Journal of Mechanical, Aerospace, Industrial, Mechatronic and Manufacturing Engineering,* 2(5), 697-701.

Schandl, G., Lugner, P., Benatzky, C., (2007). Comfort enhancement by an active vibration reduction system for a flexible railway car body. *Vehicle System Dynamics*. 45 (9), 835-847.

Spencer, B.F., Dyke, S.J., Sain, M.K., Carlson, J.D. (1996). Phenomenological model for a magneto-rheological Damper. *Journal of Engineering Mechanics*. ASCE. 123(3), 230-252.

Tomioka, T., Takigami T., Aida, K., (2017). Experimental investigations on the damping effect due to passengers on flexural vibrations of railway vehicle car body and basic studies on the mimicry of the effect with simple substitution. *Vehicle System Dynamics*, 55(7), 995-1011.

Tomioko, T., Takigami, T., (2015). Experimental and numerical study on the effect due to passengers on flexural vibrations in railway vehicle car bodies. *Journal of Sound and Vibration*, 343, 1-19.

Teng, T. L, Chang, F., Liu, Y.S., Peng, C.P., (2008). Analysis of dynamic response of vehicle occupant in frontal crash using multi-body dynamics method. *Mathematical and Computer Modelling,* 48 (11-12), 1724–36.

Tomioka, T., Takigami, T., Suzuki, Y. (2006). Numerical analysis of three-dimensional flexural vibration of railway vehicle car body. *Vehicle System Dynamics*. 44(Supp-1), 272–285.

Tamboli, J.A, Joshi, S.G. (1999). Optimum design of a passive suspension system of a vehicle subjected to actual random road excitations. *Journal of sound and vibration*, 219(2), 193-205.

Thoma, J. U. (1990), Simulation by Bondgraphs: Introduction to a graphical Method, Springer Verlag, Berlin, New York.

Uys, P. E., Els, P. S., Thoresson, M., (2007), Suspension settings for optimal ride comfort of off-road vehicles travelling on roads with different roughness and speeds, *Journal of Terramechanics*, 44(2), 163–175.

Vujanovic, B., Jones, S. E., (1989*).* Variational methods in non-conservative phenomena, Academic press, Boston.

Vujanovic, B., (1978). Conservation laws of dynamical systems via d'Alembert's principle. *International Journal of Nonlinear Mechanics*, 13(3), 185-197.

Wilder, D., Magnusson, M. L., Fenwick, J., Pope, M., (1994). The effect of posture and seat suspension design on discomfort and back muscle fatigue during simulated truck driving. *Applied Ergonomics*, 25(2), 66-76.

Yang, Y.B., Lin, C.L., Yau, J.D., Chang, D.W., (2004). Mechanism of resonance and cancellation for train-induces vibrations on bridges with elastic bearings. *Journal of Sound vibration*, 269(1-2), 345-360.

Yoon. I., Hac, A. (1995). Semi active suspension with adaptive capability. *Journal of Sound and vibration*, 180(3), 475-492.

Zhou, J., Goodall, R., Ren, L., Zhang, H., (2009). Flexural vibration suppression of car body for high-speed passenger car based on constrained damping layers, *Part F: Journal of Railway Transport*, 223.

Zhou, J., Goodall, A., Ren, L., Zhang, H. (2009). Influences of car body vertical flexibility on ride quality of passenger railway vehicles. *Part F: Journal .Rail and Rapid Transit*, 2009, 223.

Publication from the Present Work

International Journal

1. **Ashish Gupta**, Vikas Rastogi (2018) "Computational modelling and simulation of commercial truck with road-tire interactions to evaluate ride comfort" *International Journal of Heavy Vehicle system", 25*(2).

2. **Ashish Gupta**, Vikas Rastogi (2016) "Dynamic Analysis and Control of a Full Car Vehicle Model through Bond Graphs", *International Journal of Control Theory and Applications*, 9(17).

3. **Ashish Gupta**, Vikas Rastogi (2016) "Effects of Various Road Conditions on Dynamic Behaviour of Heavy Road Vehicle" *Procedia Engineering*, 144.

4. **Ashish Gupta**, Vikas Rastogi "Modeling and simulation of various semi active control strategies for road vehicles through bond graphs" *Transactions of the Society for Modeling and Simulation* (**communicated**).

5. **Ashish Gupta**, Vikas Rastogi "Development of Hybrid Control Algorithm for Improvement of performance of Semi-Active Suspension System" *World Journal of Modelling and simulation* (**minor revision submitted)**

International Conferences

1. **Ashish Gupta,** Vikas Rastogi "Recent advancement in semi active suspension control strategies", presented in NFEST 2018 (January 08-11, 2018), New Delhi.